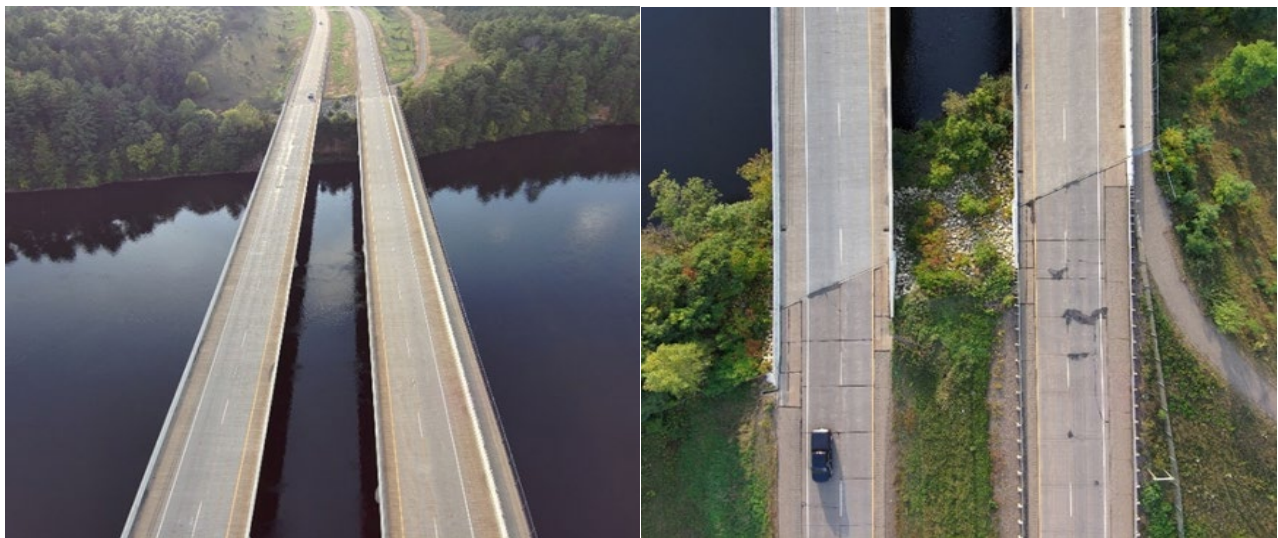


Traffic Disruption-free Bridge Inspection Initiative with Robotic Systems



September 2025
Final Report

Project number TR202004/TPF-5(462)
MoDOT Research Report number cmr 25-011

PREPARED BY:

Genda Chen

Zhenhua Shi

Son Nguyen

Mohammad Hossein Afsharmovahed

Peter Damilola Ogunjinmi

Ying Zhuo

Missouri University of Science and Technology

PREPARED FOR:

Missouri Department of Transportation

Construction and Materials Division, Research Section

Technical Report Documentation Page

1. Report No. cmr 25-011	2. Government Accession No.	3. Recipient's Catalog No.	
4. Title and Subtitle Traffic Disruption-free Bridge Inspection Initiative with Robotic Systems		5. Report Date July 2025 Published: September 2025	
		6. Performing Organization Code	
7. Author(s) Genda Chen, https://orcid.org/0000-0002-0658-4356 , Zhenhua Shi Son Nguyen Mohammad Hossein Afsharmovahed Peter Damilola Ogunjinmi Ying Zhuo		8. Performing Organization Report No.	
9. Performing Organization Name and Address Center for Intelligent Infrastructure Missouri University of Science and Technology 1401 N. Pine Street, Rolla, MO 65401		10. Work Unit No. (TRAIS)	
		11. Contract or Grant No. MoDOT project #TR202004/TPF-5(462)	
12. Sponsoring Agency Name and Address Missouri Department of Transportation (SPR-B) 1617 Missouri Blvd. Jefferson City, MO 65109		13. Type of Report and Period Covered Final Report (August 2019-July 2025)	
		14. Sponsoring Agency Code	
15. Supplementary Notes Conducted in cooperation with the U.S. Department of Transportation, Federal Highway Administration. MoDOT research reports are available in the Innovation Library at https://www.modot.org/research-publications .			
16. Abstract The current practice of bridge inspection requires the use of snoopers trucks and, when parked on bridges, the control of passing traffic, thus causing an operation safety concern for both passengers and inspectors. It also leads to inherently subjective and qualitative results. This pooled-fund study aims to develop case studies on the deployment and performance of Bridge Inspection Robot Deployment Systems (BIRDS) developed in the INSPIRE University Transportation Center for faster, safer, cheaper, and more quantitative bridge inspection with minimum impact on traffic flow. To this endeavor, an automated bridge preservation framework was envisioned to integrate advanced robotics, remote sensing, and nondestructive testing into the practice of visual inspection and associated maintenance. By evaluating the advanced technologies at 59 bridges in diverse types, age groups, and geographical locations, the best practices of the technologies were summarized in inspection protocols and guidelines using commercial drones, structural crawlers, and custom-built hybrid uncrewed vehicles. Vision-based instance segmentation via machine learning efficiently and effectively detected, located, and quantified weld defects in steel bridges, including cracks, debonding, and cavity, in real time. Topside and underside deck inspections were compared to ensure the reliability of traffic disruption-free bridge inspection from the underside of the bridge deck. By combining flying, traversing, and crawling capabilities, the award-winning invention - BIRDS offered a versatile robotic solution that addressed the limitations of commercial drone technologies. Its ability to seamlessly transition between aerial and ground-based inspection modes ensured a comprehensive coverage of bridge structures. This innovation enabled both global visual monitoring and local detailed inspection using remote sensing (e.g., microscope imager and laser scanner) and nondestructive testing (e.g., ultrasonic metal thickness gauge) for the detection and quantification of bridge surface and substrate defects. Since a limited type and number of defects were observed from the selected bridges, more bridges should be inspected to collect big data required in machine learning to develop decision-making support tools toward data-driven bridge asset management.			
17. Key Words Bridge inspection, Robotic platform, Remote sensing, In-situ sensing, Nondestructive testing, Machine learning, 3D reconstruction		18. Distribution Statement No restrictions. This document is available through the National Technical Information Service, Springfield, VA 22161.	
19. Security Classification (of this report) Unclassified	20. Security Classification (of this page) Unclassified	21. No. of Pages 158	22. Price

Traffic Disruption-free Bridge Inspection Initiative with Robotic Systems

By

Genda Chen,
Zhenhua Shi,
Son Nguyen,
Mohammad Hossein Afsharmovahed,
Peter Damilola Ogunjinmi, and
Ying Zhuo

Missouri University of Science and Technology

Prepared for
Missouri Department of Transportation

July 2025

Final Report

TR202004, FHWA Pooled Fund TPF-5(395), S064101S

Copyright

Authors herein are responsible for the authenticity of their materials and for obtaining written permissions from publishers or individuals who own the copyright to any previously published or copyrighted material used herein.

Disclaimer

The contents of this report reflect the views of the author(s) who is (are) responsible for the facts and accuracy of the data presented herein. The contents do not necessarily reflect the official views or policies of the Missouri Department of Transportation or the Federal Highway Administration. This report does not constitute a standard, specification, or regulation.

Acknowledgments

Financial support for the pooled-fund study No. TPF-5(395) is provided by New York, Virginia, Wisconsin, Georgia, Missouri, Texas, and California State Departments of Transportation under Award No. TR202004. This study was coordinated by Ms. Jennifer Harper from Missouri Department of Transportation.

Financial support for the Tier 1 INSPIRE University Transportation Center led by Missouri S&T (<http://inspire-utc.mst.edu>) is provided by the U.S. Department of Transportation, Office of the Assistant Secretary for Research and Technology (USDOT/OST-R) under Grant No. 69A3551747126.

Thanks are extended to Drs. Taruta Ghosh Mondal, Haibin Zhang, Woubishet Z. Taffese, and Ritesh Sharma at Missouri S&T and Derek Lepper from Missouri Department of Transportation for their participation in bridge inspections.

Table of Contents

Executive Summary.....	1
CHAPTER 1. INTRODUCTION	4
1.1 Goals and Objectives.....	4
1.2 Organization of This Report	5
CHAPTER 2. A VISION OF AUTOMATED BRIDGE PRESERVATION	6
2.1 A Framework of Integrated NDE, Sensing, and Visual Inspection	6
2.2 Performance Metrics of the Integrated System of Systems.....	11
2.2.1 NDE for Corroded Member Thickness through Ultrasonic Measurement.....	11
2.2.2 Probability of Corrosion Detection Using Fe-C Coated LPFG Sensors	12
2.2.3 Visual Inspection of Tested Samples in Corrosive Environments.....	15
2.3 Impact of NDE, Sensing, and Visual Inspection Integration	15
CHAPTER 3. SELECTION OF BRIDGES TO BE INSPECTED	16
3.1 Selection Process of Highway Bridges	16
3.2 California Bridge Selection.....	20
3.3 Georgia Bridge Selection.....	20
3.4 Missouri Bridge Selection	21
3.5 New York Bridge Selection.....	22
3.6 Texas Bridge Selection	22
3.7 Virginia Bridge Selection	23
3.8 Wisconsin Bridge Selection.....	24
3.9 Summary of Bridges Selected for Inspection.....	24
CHAPTER 4. UNCREWED VEHICLES AND SENSING Systems	28
4.1 Commercial Uncrewed Aerial Systems.....	28
4.2 Custom-built Uncrewed Aerial Systems	29
4.2.1 Mechanical Engaging Mechanism in BridgeBot Protocol III.....	30
4.2.2 Magnetic Engaging Mechanism in BridgeBot Protocol IV	32
4.2.3 Structural Crawlers for Nondestructive Testing.....	32
4.3 Automated Vision-based Weld Inspection	34
4.3.1 YOLO-based Defect Detection on Magnified RGB Imagery.....	34
4.3.2 3D Laser Scanning	36
CHAPTER 5. BRIDGE DECK NONDESTRUCTIVE TESTING	39

5.1 Bridge Conditions and Nondestructive Testing	39
5.2 Data Acquisition and Processing for GPR, IE, and USW.....	41
5.3 Microwave 3D SAR Bridge Imaging.....	45
5.4 Concluding Remarks.....	47
CHAPTER 6. CASE STUDIES ON REPRESENTATIVE BRIDGES.....	48
6.1 Georgia Highway Bridges	48
6.2 Missouri Highway Bridges.....	51
6.3 Texas Highway Bridges.....	58
6.4 Virginia Highway Bridges	61
6.5 Wisconsin Highway Bridges	65
6.6 Automated vs. Manual Inspection of Highway Bridges.....	67
6.6.1 AASHTO Manual for Bridge Element Inspection	67
6.6.2 Manual Inspection	69
6.6.3 Defect Identification and Quantification from Automated Inspection	71
6.6.4 Pros and Cons of Automated and Manual Inspections	76
6.7 BridgeBot and Crawler Tests on Real-world Bridges	77
6.7.1 Short-span Highway Bridges	78
6.7.2 Long-span River-crossing Bridges	81
6.8 Underwater Inspection Using Remotely Operated Sonar Imaging	85
6.8.1 Remotely Operated Vehicles	85
6.8.2 Swimming Pool and Field Tests	87
6.8.3 3D Point Cloud Data Processing to Detect Bridge Scour	89
CHAPTER 7. INSPECTION PROTOCOLS AND GUIDELINES	92
7.1 Pre-inspection Preparation	92
7.1.1 UAV and Sensor/Camera Selection	92
7.1.2 UAV Flight Planning	92
7.1.3 Legacy Data Review and Documentation	94
7.1.4 Inspection Checklist	95
7.2 During-inspection Execution at Bridge Sites.....	96
7.2.1 Responsibilities of Team Members	96
7.2.2 GPS Station Setup	97
7.2.3 Navigation and Flight Control Logging.....	97
7.2.4 Meteorological Condition and Sensor Operation Logging	97

7.2.5 File Management	97
7.3 Post-inspection Processing	98
7.3.1 Statistical Analysis	98
7.3.2 Data Management	99
7.3.3 Software Evaluation	101
CHAPTER 8. CONCLUSIONS AND RECOMMENDATIONS	102
8.1 Conclusions Drawn from Field Tests	102
8.2 Recommendations and Future Research	104
References	105
Appendix A: Visual/Manual Inspection Reports	109
Appendix B: Excerpt of the 2019 Manual for Bridge Element Inspection	134

List of Tables

Table 1. State Grouping by Highway Bridge Type.....	17
Table 2. Key Nine Wisconsin Bridge Candidates in Each Age Group.....	19
Table 3. California: Prestressed Concrete Girder Bridges.....	25
Table 4. Georgia: Prestressed Concrete Girder Bridges	25
Table 5. Missouri: Prestressed Concrete Girder Bridges	26
Table 6. Missouri: Steel Girder Bridges.....	26
Table 7. New York: Steel Girder Bridges	26
Table 8. Texas: Prestressed Concrete Girder Bridges.....	27
Table 9. Virginia: Steel Girder Bridges	27
Table 10. Wisconsin: Steel Girder Bridges	27
Table 11. Primary Features of Five Commercial UASs.....	29
Table 12. Bridge Condition State Classes.....	68
Table 13. Bridge Elements Categorization.....	68
Table 14. Service Environment Categorization in Bridge Inspection.....	68
Table 15. Illustrative Examples of Defect Determination and CS Assignment	72
Table 16. Clustering Methods for 3D Point Cloud Segmentation.....	90
Table 17. Example Responsibilities of Team Members During Bridge Inspection	96

List of Figures

Figure 1. A Framework of Robot-Assisted Inspection and Maintenance	7
Figure 2. Corroded RC Slab and its Corresponding Microwave Image (25.4 mm = 1 in)	8
Figure 3. The Operation Principle of a Synthetic Aperture Radar	8
Figure 4. A Fe-C Coated LPFG Sensor Based on Gr/AgNW	9
Figure 5. Packaged Sensing System for Corrosion, Strain, and Temperature Measurement	10
Figure 6. LPFG Wavelength and Mass Loss of Fe-C Layer, Tube, and Rebar ($1 \mu\text{A}/\text{cm}^2 = 6.45 \mu\text{A}/\text{in}^2$, $1 \text{ nm} = 3.94 \times 10^{-8} \text{ in}$).....	10
Figure 7. An A1207 Ultrasonic Thickness Gauge	11
Figure 8. Wavelength-mass Loss Curves of Fe-C Coated LPFG Corrosion Sensors.....	13
Figure 9. POD Plot with a 95% Lower Confidence Bound Following a Normal Distribution	13
Figure 10. Detectable Mass Losses a_{90} and $a_{90/95}$ at Various Detection Thresholds.....	14
Figure 11. Test Specimen and Corrosion Effects	15
Figure 12. Geographical Distribution of Seven Participating States.....	18
Figure 13. United States National Highway System	18
Figure 14. Bridge Candidates in California: (a) All, and (b) Nine in Each Age Group.....	20
Figure 15. Bridge Candidates in Georgia: (a) All, and (b) Nine in Each Age Group	21
Figure 16 Prestressed Bridge Candidates in Missouri: (a) All, and (b) Nine in Each Age Group ..	21
Figure 17 Steel Bridge Candidates in Missouri: (a) All, (b) Nine in Each Age Group	22
Figure 18. Bridge Candidates in New York: (a) All, and (b) Nine in Each Age Group.....	22
Figure 19. Bridge Candidates in Texas: (a) All, (b) Nine in Each Age Group	23
Figure 20. Bridge Candidates in Virginia: (a) All, and (b) Nine in Each Age Group.....	23
Figure 21. Bridge Candidates in Wisconsin: (a) All, and (b) Nine in Each Age Group.....	24
Figure 22. Screenshot of the Selected Bridges on the Google Map	25
Figure 23. Mobile Test Facility: (a) 12-Seat Van, and (b) Test Equipment in the Van	28
Figure 24. A Suite of Commercial Drones	28
Figure 25. A Complete BridgeBot Prototype III System.....	31
Figure 26. Mechanical Hanging Mechanism with Gravity-Supported Wheels.....	31
Figure 27. Magnetic Attracting Mechanism with Ackermann Steering	32
Figure 28. Microscope Crawler for Detailed Visual Inspection	33
Figure 29. Ultrasonic Gauge Crawler for Metal Thickness Measurement.....	33
Figure 30. Three Variants (Nano, Small, and Medium) of the YOLOv11 Model.....	35
Figure 31. Workflow of the Client Machine.....	35
Figure 32. Crawler Operation for Image Data Collection	35
Figure 33. Performance of the YOLOv11 Nano Model for Detection and Segmentation	36
Figure 34. High- and Low-Resolution 3D Laser Scanning	37
Figure 35. Laser Scanning to Record Point Cloud for 3D Surface Reconstruction	38
Figure 36. The Pedestrian Bridge on Missouri S&T Campus as a Testbed	39
Figure 37. Various Types of Deterioration in the Pedestrian Bridge	40
Figure 38. GPR Data Acquisition	41
Figure 39. IE Data Acquisition	42
Figure 40. GPR and IE Test Direction Relative to the Rebar Position	42

Figure 41. GPR Parallel Profiles (left) and Possible Detected Reinforcement (right) of the Top Surface Section Using the 2.5 GHz Frequency Antenna	42
Figure 42. Processed GPR Output Showing Top and Bottom Rebar Mats	43
Figure 43. Processed PSPA Output Showing the USV and IE Results	43
Figure 44. Topside Deck Survey: (a) USV and (b) IE Variation Map.....	44
Figure 45. Underside Deck Survey: (a) USV and (b) IE Variation Map.....	45
Figure 46. SAR Image of Underside Deck Corresponding to Damage Areas	46
Figure 47. SAR Image of a Section of the Topside of the Bridge	47
Figure 48. Georgia Bridge 5700510 (Phantom 4)	49
Figure 49. Georgia Bridge 5700510 (Nikon)	49
Figure 50. Georgia Bridge 5700510 (Elios 2).....	50
Figure 51. Georgia Bridge 5700510 (FLIR)	51
Figure 52. Point Cloud for Georgia Bridge 5700510 from Headwall (unit: m, 1 m = 3.28 ft).....	51
Figure 53. Missouri Steel Bridge A4988 (Parrot Anafi)	52
Figure 54. Missouri Steel Bridge A4988 (Nikon)	52
Figure 55. Missouri Steel Bridge A4988 (Elios 2)	53
Figure 56. Missouri Steel Bridge A4988 (FLIR).....	54
Figure 57. Point Cloud for MO A4988 from Headwall (unit: m, 1 m = 3.28 ft).....	55
Figure 58. Missouri Prestressed Concrete Bridge A5805 (Phantom 4)	55
Figure 59. Missouri Prestressed Concrete Bridge A5805 (Nikon)	56
Figure 60. Missouri Prestressed Concrete Bridge A5805 (Elios 2).....	56
Figure 61. Missouri Prestressed Concrete Bridge A5805 (FLIR)	57
Figure 62. Point Cloud for Missouri Bridge A5805 from Headwall (unit: m, 1 m = 3.28 ft)	57
Figure 63. Texas Bridge 151630002405167 (Phantom 4).....	58
Figure 64. Texas Bridge 151630002405167 (Nikon)	59
Figure 65. Texas Bridge 151630002405167 (Elios 2)	59
Figure 66. Texas Bridge 151630002405167 (FLIR).....	60
Figure 67. Point Cloud for Texas Bridge 151630002405167 from Headwall (unit: m, 1 m = 3.28 ft)	60
Figure 68. Virginia Bridge 11562 (Skydio 2).....	61
Figure 69. Virginia Bridge 11562 (Nikon).....	62
Figure 70. Virginia Bridge 11562 (Elios 2)	63
Figure 71. Virginia Bridge 11562 (FLIR).....	63
Figure 72. 3D Reconstruction of the Virginia Bridge No. 29171.....	64
Figure 73. Hyperspectral Image for VA 11562.....	64
Figure 74. Point Cloud for VA 11562 from Headwall (unit: m, 1 m = 3.28 ft)	65
Figure 75. Wisconsin Bridge B090209 (Skydio 2).....	65
Figure 76. Wisconsin Bridge B090209 (Nikon).....	66
Figure 77. Wisconsin Bridge B090209 (Elios 2).....	66
Figure 78. Wisconsin Bridge B090209 (FLIR)	67
Figure 79. Point Cloud for Wisconsin Bridge B090209 from Headwall (unit: m, 1 m = 3.28 ft) ...	67
Figure 80. Research and Professional Inspection Teams.....	69
Figure 81. Manual Inspection of Highway Bridges	70

Figure 82. Bridge A4188 Frames vs. AASHTO Reference Photos for Coating Deterioration and Steel Connection Corrosion Assessment (25.4 mm = 1 in).....	73
Figure 83. Bridge A4351 Frames vs. AASHTO Reference Photos for Concrete Spalling and Rebar Corrosion Assessment (25.4 mm = 1 in)	74
Figure 84. Bridge A4982 Frames vs. AASHTO Reference Photos for Concrete Spalling and Leaching Assessment (25.4 mm = 1 in).....	75
Figure 85. Bridge A4988 Frames vs. AASHTO Reference Photos for Concrete Leaching and Steel Corrosion Assessment (25.4 mm = 1 in)	76
Figure 86. Hanging Mechanism for Robotic Inspection of Prestressed Concrete Girders	78
Figure 87. Hexacopter Testing on the 10 th Street Bridge in Rolla, MO	79
Figure 88. Hexacopter Testing on the Rubidoux Creek Bridge in Waynesville, MO.....	79
Figure 89. Protective Box Drone Testing on the 10 th Street Bridge in Rolla, MO.....	80
Figure 90. Protective Box Drone Testing on the Rubidoux Creek Bridge in Waynesville, MO.....	80
Figure 91. RGB Imaging on the Rubidoux Creek Bridge in Waynesville, MO	81
Figure 92. Hybrid Drone and Crawler Maneuvering along Steel I-beams on the Bill Emerson Memorial Cable-Stayed Bridge in Cape Girardeau, MO	82
Figure 93. Crawler Access to Narrow Spaces for Weld Connection Inspection	83
Figure 94. Crawler Access to a Potentially Corroded Area via Microscopic View	83
Figure 95. Crawler Access to the Bridge Support Area.....	84
Figure 96. Automated Nondestructive Testing on the Web of a Steel Girder	85
Figure 97. Remotely Operated Vehicles	86
Figure 98. Field Test of the Integrated USV System in a Lake	87
Figure 99. Test Setup and Remote Operation for Underwater Inspection	88
Figure 100. Testing on the Blueboat Control System under Different Payloads.....	88
Figure 101. 3D Point Cloud Showing Scouring and Exposure of the Footing	89
Figure 102. Connectivity-Based Clustering of Bridge Elements with a Max_neighbor Value of: (a) 10, and (b) 15	91
Figure 103. Robot-Assisted Bridge Inspection Tactics	93
Figure 104. Autonomous Flight Path with Sensor-Triggered Polygons (DJI M600).....	94
Figure 105. Robot-Assisted Bridge Inspection Preparation Checklist	95

List of Abbreviations and Acronyms

23 CFR 420	Code of Federal Regulations, Title 23, Part 420
AASHTO	American Association of State Highway and Transportation Officials
ACS	Acoustic Control Systems
ADE	Agency Developed Elements
ASCE	American Society of Civil Engineers
ASPRS	American Society for Photogrammetry and Remote Sensing
ASR	Alkali-Silica Reaction
ASTM	American Society for Testing and Materials
ATC	Air Traffic Control
BIRDS	Bridge Inspection Robot Deployment System
BME	Bridge Management Elements
BMS	Bridge Management Systems
COCO	Common Objects in Context
CoRe	Commonly Recognized
CS	Condition State
DEM	Digital Elevation Model
DOF	Degrees of Freedom
DOT	Department of Transportation
EDM	Electrical Discharge Machining
EM	Electromagnetic
FAA	Federal Aviation Administration
FHWA	Federal Highway Administration
FLIR	Forward Looking Infrared
FPS	Frame Per Second
GPR	Ground Penetrating Radar
GPS	Global Positioning System
GSSI	Geophysical Survey System Inc.
GUI	Graphical User Interface
HRNet	High Resolution Network
IE	Impact Echo
IoU	Intersection over Union
LED	Light Emitting Diode
LiDAR	Light and Detection Range
Li-ion	Lithium Ion
LiPo	Lithium Polymer
LPFG	Long Period Fiber Grating
LTBP	Long Term Bridge Performance
MP	Megapixels
NBE	National Bridge Elements
NBI	National Bridge Inventory
NBIS	National Bridge Inventory Standards
NDE	Nondestructive Evaluation

NDT	Nondestructive Testing
NTL	National Transportation Library
NUC	Next Unit of Computing
OPUS	Online Positioning User Service
PIC	Pilot in Command
POD	Probability of Detection
PSPA	Portable Seismic Property Analyzer
RC	Reinforced Concrete
RGB	Red Green Blue
RMSE	Root Mean Square Error
ROSA P	Repository & Open Science Access Portal
ROV	Remotely Operated Vehicle
RPM	Random Parameter Model
SAR	Synthetic Aperture Radar
SEM	Scanning Electron Microscope
SHM	Structural Health Monitoring
SODAD	Size of Damage/Deterioration at Detection
UAS	Uncrewed Aerial System
UAV	Uncrewed Aerial Vehicle
USV	Uncrewed Surface Vessel
USW	Ultrasonic Surface Waves
UUV	Uncrewed Underwater Vehicle
VNA	Vector Network Analyzer
VNIR	Visible Near Infrared
VO	Visual Observer
YOLO	You Only Look Once

EXECUTIVE SUMMARY

The primary purpose of bridge inspection is to ensure that structures are safe for the travelling public. Since the inception of National Bridge Inspection Standards (NBIS), most updates have been made when new lessons are learned from bridge failures over time. In recent years, however, inspection data has been increasingly used to support a more proactive approach of asset management so that bridge structures are not only safe but can also be maintained with a minimal lifecycle cost. This broadening of inspection scope requires a significant shift in practice from fully visual inspection to partially visual inspection supplemented with remote sensing, nondestructive evaluation, and structural health monitoring. These emerging technologies enable the implementation of objective decision-making processes in asset management and the understanding of infrastructure resilience.

The current practice of bridge inspection requires the use of snoopers trucks and, when parked on bridges, the control of ongoing traffic. It causes an operation safety concern for both passengers and inspectors. Due to different educations, experiences, judgements, and physical conditions of the inspectors, the manual inspection leads to inherently subjective and qualitative results. The goals of this pooled-fund initiative are to engage closely with the state Departments of Transportation (DOTs) and leverage the INSPIRE University Transportation Center resources to develop case studies, protocols, and guidelines. These documents can be potentially adopted by state DOTs for bridge inspection with a minimum adverse impact on the traffic. In this study, automated bridge preservation is envisioned to integrate advanced robotics, remote sensing, and nondestructive testing into the practice of visual inspection and associated maintenance.

The alternative robotic technology, referred to as Bridge Inspection Robot Deployment Systems (BIRDS), received a U.S. patent issued in 2025 and won the 2025 American Society of Civil Engineers (ASCE) Charles Pankow Award for Innovation. The award selection committee cited that “BIRDS is revolutionizing bridge inspection, leveraging latest technology in drones and AI.” The BIRDS is a unique mobile test facility that enables big data collection from elevated bridge structures both in air and under water. By inventing effective engaging mechanisms with key bridge elements, such as I-shaped girders, the BIRDS ultimately provides safe access to both superstructure and substructure for close-distance inspection and NDT.

BIRDS represents an integration of uncrewed aerial vehicles, structural crawlers, hybrid uncrewed vehicles, remote sensing, nondestructive testing, and computational intelligence. By combining flying, traversing, and crawling capabilities, this invention offers a versatile robotic solution that addresses the limitations of commercial drone technologies in terms of consistent illumination, stationary measurement, precise positioning, and automated data collection for more quantifiable results. Its ability to seamlessly transition between aerial and ground-based inspection modes ensures a comprehensive coverage of bridge structures, enabling both global visual monitoring and local detailed inspection. Local inspection uses remote sensing (e.g., microscopic imager and laser scanner) and nondestructive testing (e.g., ultrasonic metal thickness gauge and impact echo) for the detection and quantification of bridge surface and substrate defects. Vision-based instance segmentation via machine learning can efficiently and

effectively provide real-time detection, location, and quantification of weld defects in steel bridges, including cracks, debonding, and cavity.

By evaluating the advanced technologies at 59 bridges in diverse types, age groups, and geographical locations, the best practices of the technologies are summarized in inspection protocols and guidelines using commercial drones, structural crawlers, and hybrid uncrewed vehicles. Bridge inspection protocols and guidelines are presented in three parts: pre-inspection preparation, during-inspection execution, and post-inspection processing. The type and number of defects observed from the 59 selected bridges in three age groups (15-20, 25-30, and 35-40 years) are limited. Observed deterioration and damage include concrete cracks, concrete spalling, concrete delamination, rebar exposure, steel corrosion, and steel member buckling.

Complementary commercial drones (e.g., DJI M600, Elios 3, Parrot Anafi, Phantom 4, and Skydio 2) can provide a comprehensive inspection of bridges: above-deck, below-deck, and side. For instance, DJI M600 equipped with LiDAR, thermal, and hyperspectral sensors is safe to fly above the bridge at an altitude of 30-50 m. Elios 3 can help effectively inspect the underside of a bridge deck in a GPS-denied, poor lighting, confined space between parallel girders. The remaining drones can be used interchangeably for bridge side and above-deck inspection. Manual photographing with a high-resolution camera (or binocular) may supplement drones in robot-inaccessible areas.

A pre-defined autonomous flight path can improve consistency and efficiency in drone operation. For example, a heavy-duty drone (e.g., DJI M600) can complete the above-deck inspection of a bridge in 20-30 min regardless of the bridge length. This feature is especially attractive for long-span bridges spanning over rivers. Below-deck inspection time of a lightweight drone (e.g., Skydio 2) depends on the length and number of girders, and the accessibility of bridges. Although comparable in time for short-span bridges, the robotic operation is advantageous over its corresponding manual operation in visual inspection. The robotic inspection with multimodal sensors eliminates bridge access challenges and traffic control, improves inspection comprehensiveness for surface and subsurface defects, enhances inspection objectivity and quantification, and extends the usefulness of inspection reports in developing maintenance strategies. Specifically, robot-assisted bridge inspection enables an automated execution of the entire inspection process from data collection through machine learning for bridge elements of interest to defect identification and quantification, thus assisting in the implementation of more comprehensive inspection methods as prescribed in the 2019 AASHTO *Manual for Bridge Element Inspection*. For long-span bridges, the robotic solution is substantially more efficient than the visual inspection. To attract no or minimum attention of passing traffic for operation safety, drones are flown along bridge sides, if image resolution of the entire bridge is sufficient for vision-based inspection.

Complementary remote sensing technologies are applied to achieve multiple objectives. High-resolution RGB images are informative of any bridge surface defects in terms of color, texture, and pattern. Thermal images are effective in revealing substrate defects such as delamination when taken above bridge decks during the heating process (e.g., 10 am – 2 pm) in a sunny day or

when taken from bridge decks (both topside and underside) during the cooling process (e.g., after sundown). Hyperspectral images can shed light on the type of materials used in bridge construction and chemical marks left on the surface of bridge decks. Images and point cloud data can be fused into the 3D reconstruction of bridges toward a digital transformation of bridge asset management. For example, when LiDAR point cloud data is fused with RGB and thermal images, geo-referenced surface features and subsurface indicators (e.g., delamination and void) can be efficiently inspected anywhere and anytime by anyone.

Nondestructive testing can effectively detect near-end rebar conditions in concrete bridge decks but fails to locate far-end rebar into concrete up to 7-7/8 in (20 cm) thick due to signal scattering in heterogeneous concrete. For example, a test on the topside deck surface results in inconclusive findings on the condition of bottom rebar. As such, inspecting from the underside of decks is necessary for structural safety in addition to reducing disruption to the traffic. The results from nondestructive testing such as microwave imaging, impact echo, and ultrasonic surface waves are indicative of the presence of defects but tend to be less quantifiable.

Although the advanced robotic, sensing, and nondestructive testing technologies have been demonstrated to provide a unique dataset at the 59 bridge sites, their translation for practical adoption and implementation is just beginning. Further testing at the bridge sites is warranted to exploit all implementation challenges and, more importantly, extract diverse types of defects using artificial intelligence and quantify their uncertainty in statistical analysis. Since a limited type and number of defects are observed from the in-service bridges, it is recommended that more bridges be inspected and evaluated to collect big data required in machine learning to develop decision-making support tools toward data-driven bridge asset management. Multitask machine learning taking spatiotemporal characteristics into account should be further developed to implement physical constraints and engineering knowledge so that multiple types of defects can be classified both efficiently and effectively.

CHAPTER 1. INTRODUCTION

Bridge inspection often requires the use of heavy lifting and access equipment, thus increasing operation time and direct costs. When access to the inspected area must be made from bridge decks, the indirect costs associated with road closures multiply. In such a case, travelers are frustrated with traffic congestion and both the travelers and inspectors are subject to safety concerns on high volume highways. Moreover, visual inspection is subjective and inconsistent to various degrees, depending on inspectors' education, experience, judgement, and physical conditions. It is thus of economic, psychological, and social importance to develop an alternative platform for faster, safer, cheaper, and more consistent bridge inspection that has little or no impact on traffic flow.

Sponsored by the U.S. Department of Transportation, Office of the Assistant Secretary for Research and Technology (USDOT/OST-R), the 2016-2024 INSPIRE University Transportation Center (<https://inspire-utc.mst.edu>) at Missouri University of Science and Technology focused on the development of advanced technologies to aid bridge inspectors in informed decision-making on load posting and maintenance strategies. Specifically, structural crawlers, uncrewed aerial vehicles (UAVs), and their hybrid vehicles provide a mobile platform for in-depth inspection of elevated bridges. A special multimodal uncrewed vehicle, named Bridge Inspection Robot Deployment System (BIRDS), is developed to combine both the driving capability of crawlers and the flying capability of UAVs into one system for bridge inspection.

At the INSPIRE Center, microwave imaging is developed to assess concrete delamination of reinforced concrete (RC) bridges. Together with impact echo, impact sounding, and infrared imaging, they provide a suite of measurement tools and methods for the nondestructive evaluation (NDE) of structural damage and deterioration in RC bridges. Hyperspectral imaging is developed to assess the coating integrity and corrosion of steel bridges with various coatings. Laser scanning and microscopic imaging are developed to evaluate the surface defects of welded steel connections. An ultrasonic testing device is introduced to measure the thickness of corroded steel members. Innovative sensors such as UAV-based smart rocks for scour monitoring and integrated point and distributed optical fiber systems for strain and corrosion monitoring provide mission-critical data at strategic locations, such as the maximum scour depth, corrosion-induced steel mass loss, and live load induced strains to normalize the NDE data taken as needed over time.

In this study, the BIRDS and associated remote sensing and in-situ sensing technologies are evaluated and demonstrated at bridge sites. The inspection data collected from these technologies, the best-practice experience with these tools at bridge sites, and the lessons learned from this project including both technical and administrative aspects are summarized in this report.

1.1 Goals and Objectives

The goals of this pooled-fund initiative are to engage closely with several state Departments of

Transportation (DOTs) and leverage the INSPIRE Center resources to develop case studies, protocols, and guidelines. These documents can be potentially adopted by state DOTs for bridge inspection without adversely impacting the traffic. The initiative involves the integration, field demonstration and documentation of a robotic system (BIRDS) of structural crawlers, UAVs, NDE devices, sensors, and data analytics tools. The objectives of this initiative include:

- Development of inspection/operation protocols for several types of bridges with the robotic system integrated into the current practice of visual inspection,
- Comparison and correlation of bridge deck inspections from the top and bottom of decks to understand the reliability of traffic disruption-free bridge inspection from the underside of decks,
- Design and technical guidelines of measurement devices on a robotic platform for the detection of surface and internal damage/deterioration in structural elements, and for the change in lateral support of foundations,
- Data fusion and analytics of measurements that are taken from various imaging and sensing systems for consistency and reliability, and
- Development of best practices on bridge inspection using the robotic system.

1.2 Organization of This Report

This report is organized as follows. Chapter 1 states the challenges of bridge inspection and the goals and objectives of this pooled-fund initiative. Chapter 2 introduces a vision of automated bridge preservation that integrates NDE, sensing, visual inspection, and aerial manipulation in bridge inspection and maintenance. Chapter 3 presents the selection process of bridges to be inspected as the focus of this pooled-fund initiative. Chapter 4 describes the operation of multimodal uncrewed vehicles and sensing systems. Chapter 5 presents the correlation of comparative topside and underside deck inspections. Chapter 6 presents the case studies on representative bridges highlighting remote sensing, aerial NDE, and visual inspection. Chapter 7 summarizes the inspection protocols and guidelines based on this study. Chapter 8 provides a list of conclusions and recommendations.

CHAPTER 2. A VISION OF AUTOMATED BRIDGE PRESERVATION

Planned, monitored, and evaluated preventive maintenance (or protection) preserves transportation systems for extended service life (or for minimum disruption in the aftermath of extreme events). Highways and railways traverse elevated bridges or buried tunnels. Access to these structures can be difficult, dangerous, and disruptive. Their inspection and maintenance require the use of heavy lifting equipment (e.g., boom trucks) and access equipment (e.g., snooper trucks). Hands-on inspection required by National Bridge Inspection Standards (NBIS) for fracture critical members is particularly challenging in elevated steel bridges. More importantly, visual inspection is labor intensive and subjective, often resulting in inconsistent bridge element ratings. Deploying an alternative platform for field inspection and maintenance using uncrewed systems (autonomous or remotely controlled aerial vehicles, structure crawlers or mobile robots), sensors, and NDE devices replace current disadvantages with enhanced access, less risk and labor, consistent measurements and recording, and reliable element ratings.

The primary goal of bridge inspection is to ensure that structures are safe for the travelling public. Since the inception of the NBIS, most updates to the NBIS have been made when new lessons are learned from bridge failures over time. However, in recent years, inspection data are increasingly being used to support a more proactive approach of asset management such that bridge preservation enables structures that are not only safe but also can be maintained in a manner that minimizes life-cycle costs. This broadening of inspection scope requires a significant shift in practice from fully visual inspection to partially visual inspection supplemented with advanced technologies such as remote sensing, NDE, and structural health monitoring (SHM). These technologies enable the implementation of objective decision-making processes in asset management and the understanding of infrastructure resilience.

At the same time, multimodal uncrewed aerial systems continue to advance to the stage that they can dispatch crawling robots to install sensors on bridge elements and conduct nondestructive tests remotely. Furthermore, in-situ sensing, remote sensing, and nondestructive testing enable the quantification of various defects in bridges according to the latest *Manual for Bridge Element Inspection* (AASHTO, 2019). It is thus imperative to develop a strategy to integrate the advanced technologies into the current practice of visual inspection.

2.1 A Framework of Integrated NDE, Sensing, and Visual Inspection

With the further advent of emerging technologies, a robot-assisted inspection and maintenance strategy is achievable by integrating NDE devices, in-situ sensors, and remote sensing images for visual inspection into a robotic manipulation platform. Figure 1 shows a vision of how advanced technologies can be integrated into various bridge tasks in inspection and maintenance phases.

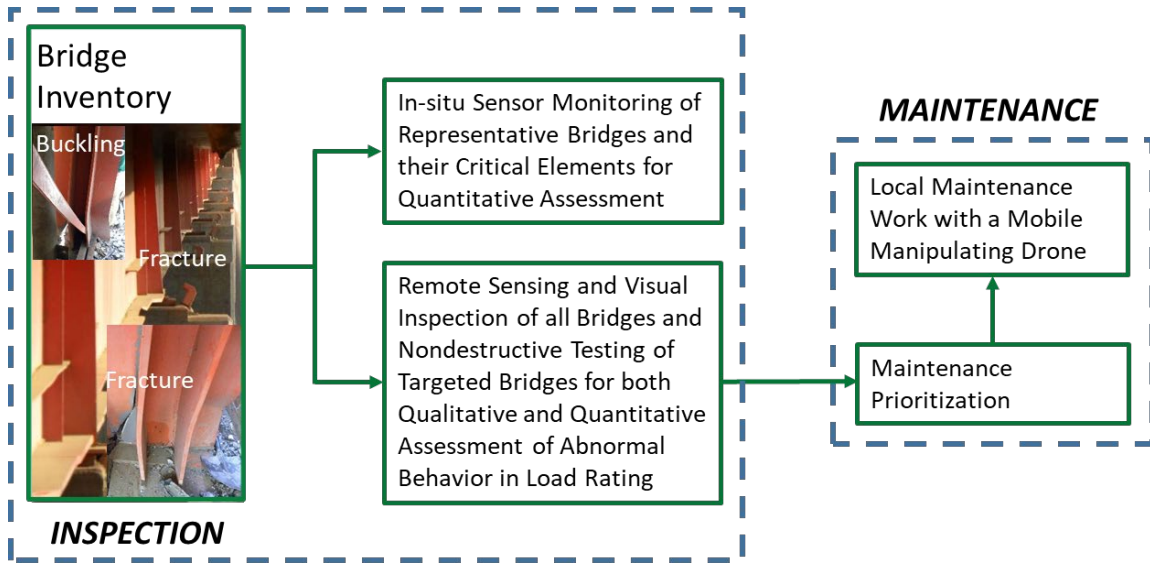


Figure 1. A Framework of Robot-Assisted Inspection and Maintenance

Bridges are subject to various deterioration and damage mechanisms over their lifecycles. Corrosion of steel in concrete is an electrochemical process of metals due to chloride ingress, carbonation, and the presence of moisture and oxygen. Alkali-Silica Reaction (ASR) is a damaging chemical reaction in concrete that leads to deterioration, primarily due to the expansive force of the reaction product. Under an extreme event such as an earthquake, the built-up steel girder as illustrated in Figure 1 experiences the buckling of diagonal braces, fracture of web plates and weld connections, and displacement of lateral brackets. While some of these deterioration and damage outcomes are visible, many are invisible to human eyes. For visible defects and damaging elements, images from remote sensing and visual inspection are meaningful in engineering practices. For invisible defects and damage, in-situ sensors and nondestructive testing are required to provide insights on structural behaviors and support informed decision-making.

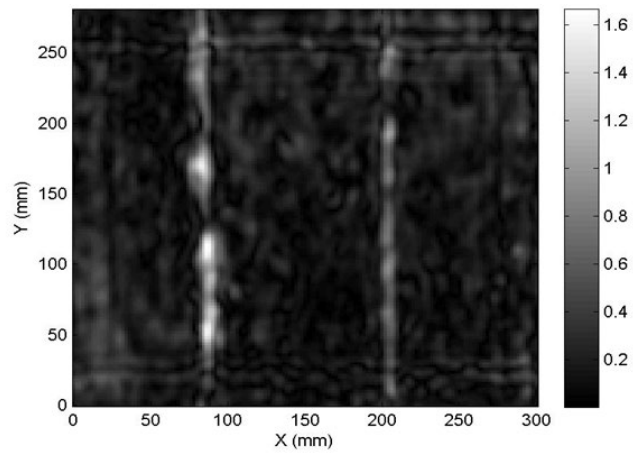
As indicated in Figure 1 in the inspection phase, in-situ sensors are installed on the limited critical elements of representative bridges to quantify their behaviors under external stressors. Rapid visual inspection and drone-based remote sensing can be used to screen the general conditions of all bridges among which targeted bridges are rated through qualitative and quantitative assessment by prescribing special nondestructive and load testing. The findings and results from the complementary and comprehensive condition assessment of bridges enable the development of prioritized maintenance strategies. For maintenance tasks in a small area, a mobile manipulating drone may be prescribed for aerial actuation without setting up any scaffold to access the rehabilitated and repaired area. The robot-assisted, streamlined, integrated inspection and maintenance strategy will be both efficient and effective. Its field operation will also be safe and dependable.

To demonstrate the roles of NDE and sensing in data-driven decision-making, microwave imaging and corrosion sensing technologies are compared for the assessment of steel rebar corrosion conditions in RC slabs (Liu et al., 2020). Figure 2 shows a RC slab of 12 in × 12 in (300 mm × 300

mm) in plan size. The concrete was made of cement, sand, and water, with a water-to-cement ratio of 0.55 and a sand-to-cement ratio of 2.81. It was reinforced by two rebar placed in parallel.



(a) Corroded specimen



(b) Microwave image on rebar corrosion

Figure 2. Corroded RC Slab and its Corresponding Microwave Image (25.4 mm = 1 in)

Synthetic Aperture Radar (SAR) as a microwave imaging technology is illustrated in Figure 3. It uses the motion of an antenna over a target area to create high-resolution images, synthesizing a larger antenna from the motion. This allows SAR to achieve finer spatial resolution than traditional radar systems, enabling detailed imaging on the RC slab specimen. For an optimal corrosion detection performance of a SAR system, many parameters should be investigated, including the frequency band selected, the corrosion process, the concrete cover, and the concrete dielectric constant that is related to the water-to-cement (w/c) ratio of the concrete. For the corroded RC slab, the microwave image as presented in Figure 2(b) indicates the presence of rebar corrosion as the rebar size clearly changes along its length. The non-uniform cross section of the rebar is a result of corrosion tests in the aggressive NaCl solution. However, the rebar image does not allow the determination of how much steel mass has been lost. In this case, the microwave technology provides a qualitative assessment of corrosion condition.

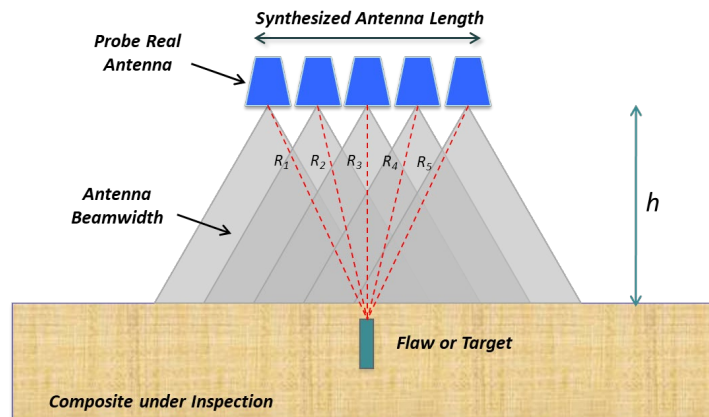


Figure 3. The Operation Principle of a Synthetic Aperture Radar

Fe-C coated long-period fiber gratings (LPFG) as a corrosion sensing technology is illustrated in Figure 4(a). The Fe-C coated LPFG corrosion sensor is composed of three co-axial layers (Guo and Chen, 2021): an innermost LPFG, a middle conductive composite of graphene (Gr) and silver nanowire (AgNW), and an outmost Fe-C layer. The bare LPFG is fabricated with a CO₂ laser on single-mode optical fibers (Corning SMF28e⁺). The Gr/AgNW layer is prepared by growing Gr on a thin copper sheet and strengthened by AgNW fibers before it is wrapped around the LPFG sensor. By applying electricity, the middle layer is used to electroplate the Fe-C layer. The final product, a Fe-C coated LPFG sensor as illustrated in Figure 4(b), can be used for corrosion monitoring since the corrosion of the Fe-C layer changes the refractive index of the coatings outside the LPFG.

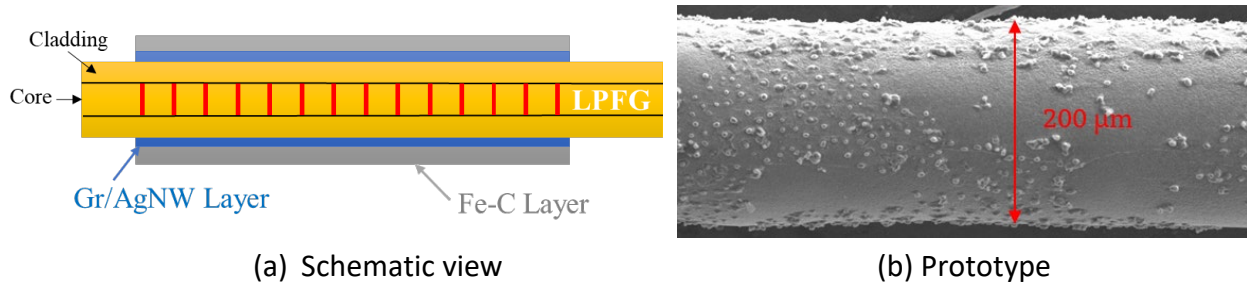


Figure 4. A Fe-C Coated LPFG Sensor Based on Gr/AgNW

The Fe-C layer as shown in Figure 4(b) is approximately 0.0015 in (37.5 μm) thick as the standard LPFG sensor is 0.005 in (125 μm) in diameter. It is corroded in days and thus good to provide corrosion rates in its service lifespan. To understand long-term corrosion behavior in steel structures, the Fe-C coated LPFG sensors are encapsulated in coaxial steel tubes with predetermined wall thickness for three threshold corrosion levels of engineering interest (e.g., in years). Steel tubes are extracted from rebar using Electrical Discharge Machining (EDM) to ensure that the chemical composition of the steel tube matches precisely with that of the rebar. Consequently, the corrosion process of the tube can accurately represent the performance of the rebar in a corrosive environment.

Figure 5(a) presents a schematic view of three 2 in (5 cm) -long, 0.01 in (0.25 mm) thick, coaxial steel tubes with 0.1, 0.157, 0.217 in (2.5, 4.0, and 5.5 mm) in outer diameter, respectively. The wall thickness of each tube is designed to control the corrosion penetration life of the steel tube. Three Fe-C coated LPFG corrosion sensors and two LPFG sensors are deployed. One Fe-C coated LPFG sensor inside each tube is used for corrosion rate measurement and the two LPFG sensors inside the small tube are for strain and temperature measurement to help decouple the effects of strain, temperature, and corrosion on the fiber optic sensors. The packaged sensing system is attached to a rebar sample as shown in Figure 5(b) for corrosion, temperature, and strain tests (Guo and Chen, 2021).

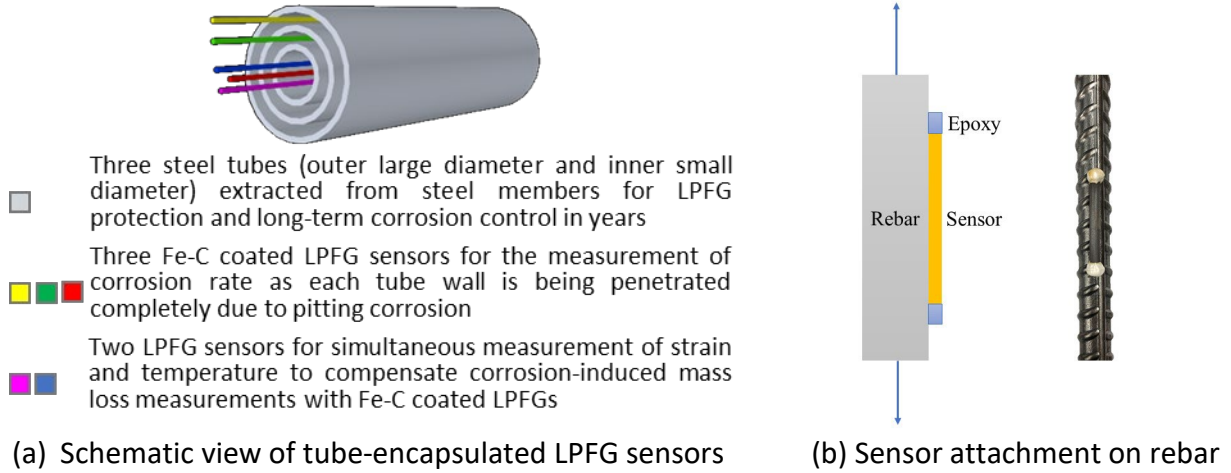


Figure 5. Packaged Sensing System for Corrosion, Strain, and Temperature Measurement

The packaged sensor as shown in Figure 5(b) was tested in 3.5 w.t % NaCl solution to understand the mass loss correlation between the sensor and the rebar. Three current densities, 3226, 2581, and 1935 $\mu\text{A}/\text{in}^2$ (500, 400 and 300 $\mu\text{A}/\text{cm}^2$), were applied on the rebar samples to accelerate the process of corrosion. Figure 6(a) shows three linear correlations of the mass losses between a corroded steel tube and a corroded rebar. Once a tube wall is penetrated, the Fe-C coated LPFG sensor inside the tube starts to corrode. Figure 6(b) presents calibration curves of the wavelength and transmission of a Fe-C coated LPFG sensor as a function of Fe-C mass loss over time. It is clearly observed that mass loss occurs in two corrosion stages. The wavelength-mass loss calibration curve consists of two straight lines. Stage I is associated with the pitting corrosion along weak paths of the Fe-C layer until it is completely penetrated by the NaCl solution. Stage II spreads the isolated pitting corrosion spots laterally until they are fully connected at an accelerated rate. Once measured in practical applications, the wavelength of a Fe-C LPFG sensor can be converted to its corresponding mass loss in the Fe-C layer or corrosion rate in each time. As such, corrosion sensors provide a tool for quantitative assessment.

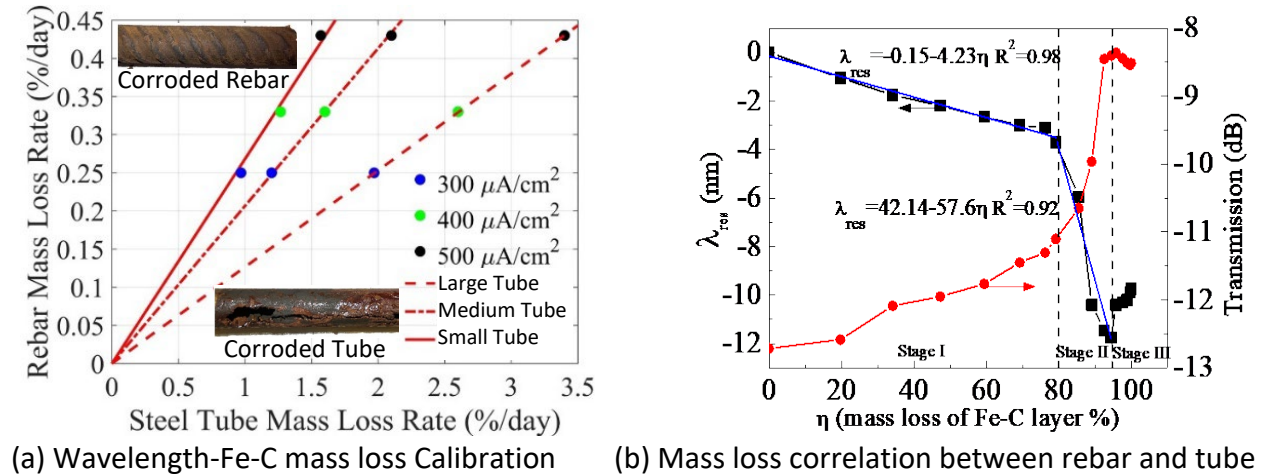


Figure 6. LPFG Wavelength and Mass Loss of Fe-C Layer, Tube, and Rebar ($1 \mu\text{A}/\text{cm}^2 = 6.45 \mu\text{A}/\text{in}^2$, $1 \text{ nm} = 3.94 \times 10^{-8} \text{ in}$)

2.2 Performance Metrics of the Integrated System of Systems

A system of steel rebar, three steel tubes, and three Fe-C coated LPFG sensors, as shown in Figure 5, was further explored to demonstrate the integrated NDE, sensing, and visual inspection capability in evaluating the corrosion condition of the system. Some NDE technologies such as microwave imaging, ground penetrating radar, ultrasonic surface waves, and impact echo tend to provide qualitative condition assessment of RC slabs, which are efficient to cover a large test area. An ultrasonic thickness gauge as one of other NDE technologies does provide quantitative metal thickness.

2.2.1 NDE for Corroded Member Thickness through Ultrasonic Measurement

Figure 7 shows the A1207 PenGauge that is designed to combine the instrument and transducer into a single package (ACS, 2025). Such a design affords true single-hand operation and provides a very capable, yet simple-to-use device. Its features and benefits include:

- Hot-pluggable built-in exchangeable 7 MHz dual-crystal probe for all standard applications or optional 4 MHz single-crystal probe for extending measurement range
- Measurement range from 0.028 to 5.91 in (0.7 to 150 mm) depending on material and surface
- Built-in Bluetooth module for communication and real-time display of digital measurements and A-Scans of the signals to the screen of a smartphone or a tablet PC



Figure 7. An A1207 Ultrasonic Thickness Gauge

2.2.2 Probability of Corrosion Detection Using Fe-C Coated LPFG Sensors

The measurement capability of Fe-C coated LPFG corrosion sensors has been shown in Figure 6(b). Its association with parent steel members such as rebar has also been delineated clearly in Figure 6(a). In practical applications, the maximum corrosion-induced mass loss that any inspection may miss is closely related to the quantifiable condition state assigned to bridge elements (AASHTO, 2019). The probability of detection (POD) has been developed as described in the Department of Defense Handbook MIL-HDBK-1823A (Annis, 2009) and applied in NDE for material defects. NDE datasets were collected from various locations independently over time and thus were analyzed statistically by assuming the independence of the collected data.

However, SHM differs from NDE in that an in-situ sensor is deployed at a fixed location and takes flaw data from one test setup and sensing system at the same location over time. The data points collected are inherently dependent, which has been neglected in the SHM community. To quantify the reliability of sensor data, statistically viable laboratory performance and successful field operation must be demonstrated. Key to sensor evaluation is the method to enable the POD analysis in civil infrastructure based on a wealth set of sensor data.

When applied to in-situ sensors for the measurement of flaw sizes, such as fatigue-induced crack length and corrosion-induced mass loss, the validity and reliability of the traditional POD method in the MIL-HDBK-1823A is unknown. As part of the INSPIRE Center project, two POD methods called size-of-damage/deterioration-at-detection (SODAD) and random parameter model (RPM) for sensor data and their associated reliability assessment for detectable flaw sizes were evaluated by Zhuo et al. (2024) based on the prior work (Meeker et al., 2019).

Figure 8 presents the wavelength shifts as the mass losses of ten Fe-C coated LPFG sensors change over time in a log-log scale. The shaded area represents the POD at a corresponding mass loss. The wavelength shift increases with the accumulated mass loss of the Fe-C coating and the relationship between them is nearly linear as indicated in Figure 6(b) in corrosion phase I or II. The linear regression curve of each set of data from one sensor is also shown in Figure 8 with a coefficient of determination exceeding $R^2=0.92$.

The SODAD method is detailed here. It gives the mass loss when the wavelength shift crosses a detection threshold of 2 nm in wavelength shift. The distribution of the SODAD values is difficult to decide due to a limited sample size of the SODAD values. To understand the robustness of the SODAD method, Weibull, lognormal, normal, and largest extreme value distributions were considered to evaluate their effects on the POD estimation. The only difference between the four probability plots is the scale of axes. If the points in a probability plot appear linear for a particular distribution, the distribution can be verified to be consistent with the data (Meeker et al., 2021). Zhuo et al. (2024) found that the 90% POD (a_{90}) values of all four distributions are close to 38% and different distributions have negligible effect on a_{90} . However, the 90% POD at 95% confidence level or $a_{90/95}$ values of the four distributions range from 47% to 58%. The distribution of SODAD values has a significant effect on $a_{90/95}$. With the normal distribution, the POD plot is presented in Figure 9 with $a_{90}=37.57\%$ and $a_{90/95}=47.30\%$.

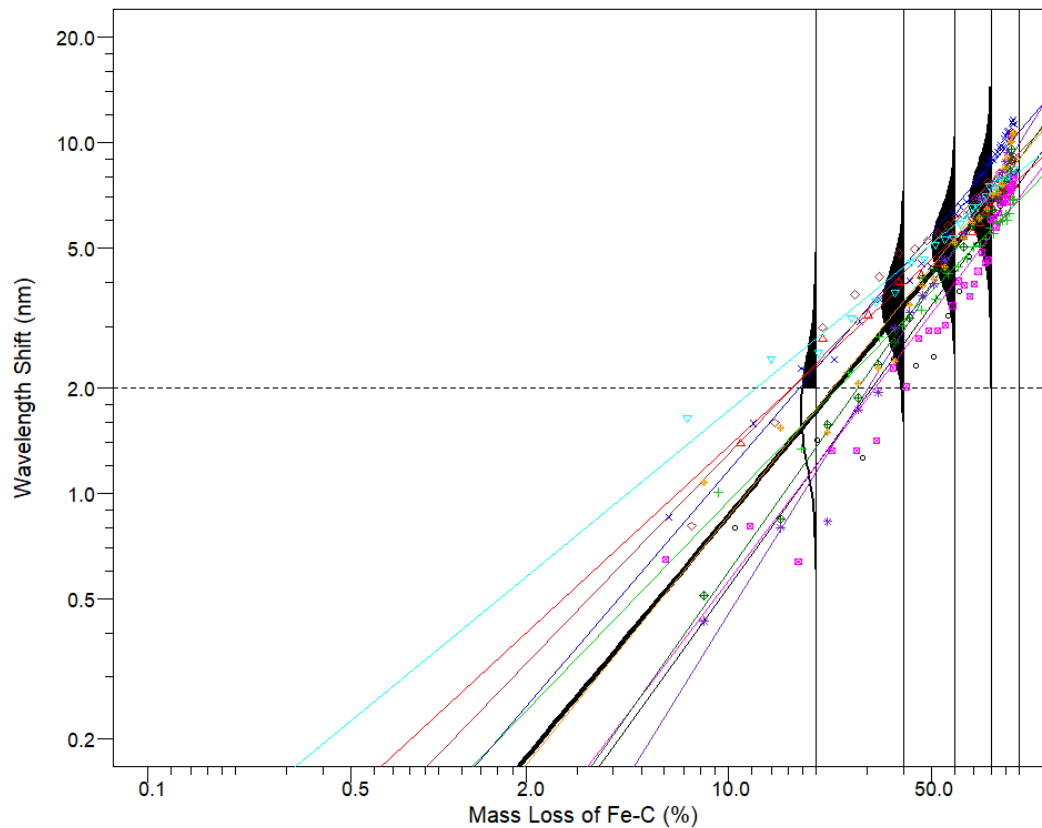


Figure 8. Wavelength-mass Loss Curves of Fe-C Coated LPFG Corrosion Sensors

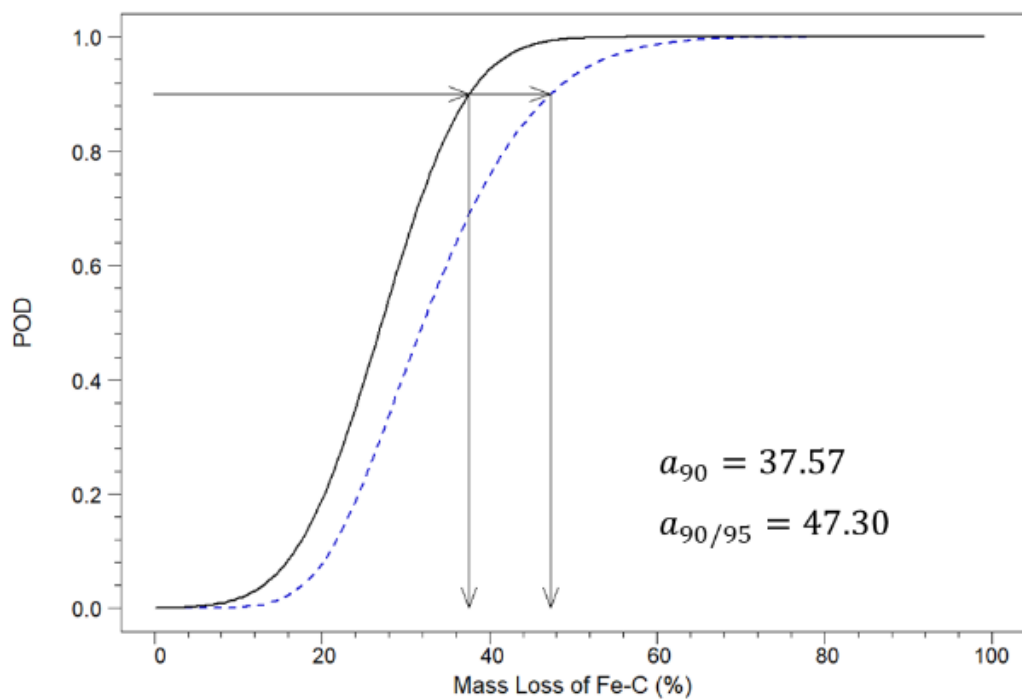


Figure 9. POD Plot with a 95% Lower Confidence Bound Following a Normal Distribution

To understand the POD sensitivity to the detection threshold, a_{90} , and $a_{90/95}$ are calculated for a detection threshold of 0.5 to 3.5 nm using three methods: Traditional, SODAD, and RPM. Their POD results are compared in Figure 10, in which the lower shaded bar represents a_{90} values while the upper blank bar represents the difference between $a_{90/95}$ and a_{90} values.

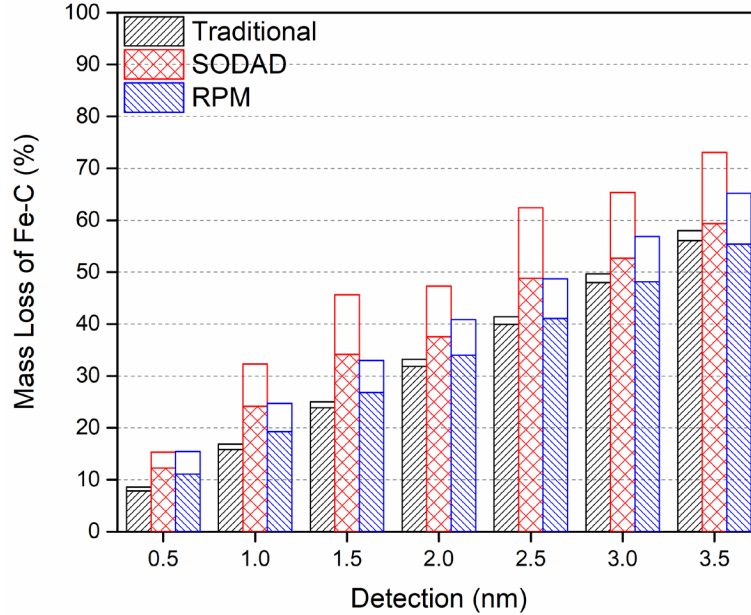


Figure 10. Detectable Mass Losses a_{90} and $a_{90/95}$ at Various Detection Thresholds

When the detection threshold is 2.0 nm, the a_{90} values of the three methods are comparable, but the $a_{90/95}$ values are quite different. For the traditional method, $a_{90/95}$ is much lower than the other two methods. This is because corrosion test data used in the traditional method are assumed temporally independent while they are correlated. Though the traditional method can be applied, the calculation results may be overconfident. Considering that $a_{90/95}$ with the normal distribution is the smallest among the four distribution assumptions, the traditional method is nonconservative. For example, when the detection threshold is set to 2.0 nm, the traditional method gives a detectable mass loss $a_{90/95}$ of approximately 33% while the SODAD and the RPM methods can only claim to have confidently detected 47% and 41% in mass loss. Therefore, a mass loss at 40% is considered as a true positive detection for the traditional method while it is a false positive detection based on the SODAD and RPM methods. In addition, the $a_{90/95}$ value of the RPM method is smaller than the SODAD method based on the normal distribution. The RPM method is more robust since it uses all the data set, while the SODAD method only uses 10 points. Compared to the SODAD method, the RPM method provides results that are more consistent with the traditional method. Even so, the traditional method remains unconservative.

The normalized mass loss η can be converted to an equivalent corrosion depth of a Fe-C coating ring with inside radius and thickness of 0.0025 in (62.5 μm) and 0.0015 in (37.5 μm), respectively, when uniform corrosion in peripheral direction of the Fe-C coated LPFG sensor is assumed. Corresponding to $a_{90}=37.57\%$ and $a_{90/95}=47.30\%$, the equivalent corrosion depths are 0.00048 in (12.2 μm) and 0.000614 in (15.6 μm), respectively.

2.2.3 Visual Inspection of Tested Samples in Corrosive Environments

Visual inspection remains an effective means to understand the condition state of bridge elements as visualized graphically in the *Manual for Bridge Element Inspection* (AASHTO, 2019). Even for the rebar corroded in laboratory tests as shown in Figure 11, visual inspection is critically important to verify test data and help interpret the experimental findings in a specific laboratory. For example, by comparing the rebar sample before and after significant corrosion, a pattern of indicated corrosion areas in terms of ribs and valleys of the deformed rebar can be visually observed. A close examination on the corroded steel tubes for surface irregularity such as cracks and holes can verify their complete penetration in a corrosive environment.

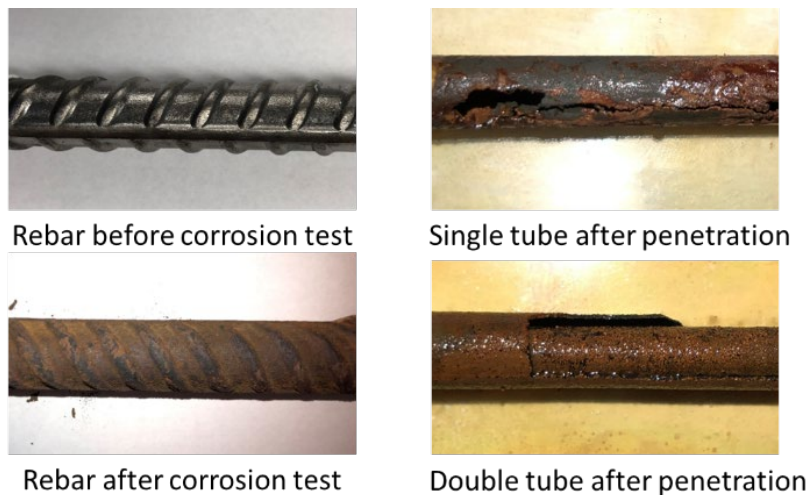


Figure 11. Test Specimen and Corrosion Effects

2.3 Impact of NDE, Sensing, and Visual Inspection Integration

The presentations and discussion in Section 2.2.1-2.2.3 highlight the capabilities of individual components: NDE, sensing, and visual inspection. These capabilities are complementary to each other. They can be integrated to enable an in-depth comprehensive understanding and quantification of defects and damage in a cost-effective way. In the example of steel rebar and tube-encapsulated Fe-C coated LPFG sensors, the ultrasonic metal thickness measurement provides evidence for corrosion solution penetration through the wall of steel tubes as visually observed on their surface. The onset of the wall penetration corroborates with the shift in wavelength of the encapsulated Fe-C coated LPFG sensor. The wavelength shift indicates the beginning and growth of corrosion in the Fe-C layer, which can be further verified from surface morphology of the sensor by visually examining scanning electron microscope (SEM) images.

CHAPTER 3. SELECTION OF BRIDGES TO BE INSPECTED

A selection protocol of bridges was developed to enable comparison and contrast between manual and automated visual inspections and/or between visual inspection and NDE. The main parameters considered in this selection included span length, bridge type, years of service, accessibility, and importance. For example, long-span bridges with limited accessibility may require intensive in-depth inspection using advanced technologies, while short-span bridges with easy access may have the minimum advantage (e.g., efficiency) of robotic inspection as the time required to travel to a remote bridge site may be predominant. Other specific criteria included state owned bridges, maximum span length from 32.8 to 164 ft (10 to 50 m), two to four lanes, average daily traffic of less than 50,000, and less than 50 years of service. The bridges within the Long-Term Bridge Performance (LTBP) database were of particular interest for potential comparison with the data collected under the LTBP program.

To ensure their difference and importance of deterioration, three age groups were determined: 15-20 years, 25-30 years, and 35-40 years. Two common girder materials were chosen: prestressed concrete and steel girder bridges. They were clustered in convenient locations for work efficiency. A total of 72 highway bridges were selected, including 18 bridges (9 for prestressed concrete bridges, and 9 for steel bridges) in the state of Missouri due to their proximity to Missouri S&T, and 9 bridges in each state of Wisconsin, Georgia, Virginia, Texas, New York, and California. Due to drone operation restrictions and coordination challenges, the bridges selected in California and New York were not yet tested to date. This makes the total number of 54 highway bridges inspected during this pooled-fund initiative.

In addition, a pedestrian bridge on Missouri S&T campus was used to compare the effectiveness of NDE technologies for inspection from the top and bottom of the bridge deck. The Bill Emerson Memorial Cable-stayed Bridge over the Mississippi River in Cape Girardeau, MO, was selected to evaluate the operability of the robotic platform on river-crossing bridges. The eight-span, 10th Street Bridge in Rolla, MO, supporting a four-lane road crossing over a railroad track and two local streets was also selected for drone and crawler test and evaluation due to its proximity to the Missouri S&T campus. The I-44 Rubidoux Creek Bridge in Waynesville, MO, and the US63 Gasconade River Bridge in Venna, MO, were tested for scour effects on their foundation.

3.1 Selection Process of Highway Bridges

When selecting bridge candidates for inspection, several factors were considered to narrow down a large pool of candidates present in the National Bridge Inventory (NBI) for each participating state. The first factor considered in the selection process was that the respective State Highway Agency be the owner of the structure and responsible for maintenance. This corresponded with items 21 (Maintenance Responsibility) and 22 (Ownership) in the NBI. For both items, the “Recording and Coding Guide for the Structure Inventory and Appraisal of the Nation’s Bridges” provided by the Federal Highway Administration (FHWA) uses a value of “1” to indicate that the respective State Highway Agency is responsible. This factor was considered to avoid the need to involve additional parties in the approval process of field tests.

After removing bridges that did not meet the requirements for ownership and maintenance, the next factor considered was the service type of the structure. In the data provided by the NBI, item 42A recorded the service use of the structure. Per the guide provided by the FHWA, structures with values of 1 and 5 were selected for further consideration as they provide Highway and Highway-pedestrian service, respectively. Limiting the structures to the two service values allowed for more consistent data to be gathered from a smaller sample of structures. Following the consideration of service type, recorded values for culvert structures were removed from the selection pool. If the recorded value for item 62 in the NBI was not an N, the structure was considered a culvert. The removal of culverts from the selection pool was done as they are not representative of typical bridges within the state roadway network systems considered.

To provide a rich test dataset, bridges that have two or more spans were selected from the NBI database except in the state of California when the number of candidates as suggested by the LTBP Program was limited. The remaining structures were sorted by their material type. If the recorded value for item 43A was a 3 or 4, the structure was steel whereas a 5 or 6 indicated that the structure was made of prestressed concrete.

To enable statistical comparison, the nine highway bridges selected from each state were focused on one type of structural material, either steel girder or prestressed concrete (PC) girder. The participating state DOTs were divided into the two groups based on their remaining bridge type and regional climate. The grouping of these states can be seen in Table 1.

Table 1. State Grouping by Highway Bridge Type

Steel Girder	Prestressed Concrete (PC) Girder
New York	California
Virginia	Georgia
Wisconsin	Texas
Missouri	Missouri

Figure 12 provides an overview of the geographical distribution of seven participating states. The states of New York, Virginia, and Wisconsin were in one group of steel girder bridges due to their access to steel mills in the east coast and their common steel corrosion issues. The states of California, Georgia, and Texas were in another group of prestressed concrete girder bridges as these states have a dominated number of PC bridges. The state of Missouri was in both groups of material, totaling 18 bridges, as it is the closest to the headquarters of INSPIRE University Transportation Center at Missouri S&T.

The nine selected candidates for each material type were divided evenly into three age groups of 15-20 years, 25-30 years, and 35-40 years. The three bridges in each age group represented the minimum number to discuss inspection results in a statistical sense according to the American Society for Testing and Materials Standards (ASTM, 2021; 2022). Data collected from these aged bridges provided representative defects for a better understanding of bridge performance over extended periods.

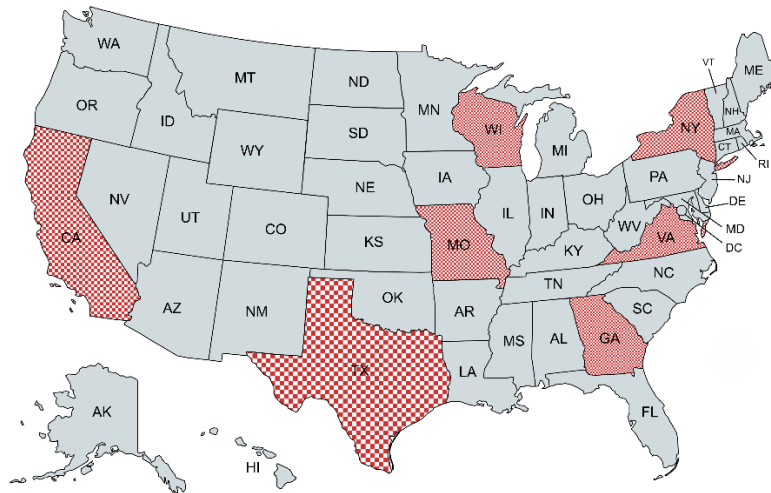


Figure 12. Geographical Distribution of Seven Participating States

During the selection process, three sets of nine potential bridges were considered for each type of material in each state. The nine bridges in each set were further narrowed down to three bridges in each age group. An effort was made to ensure that the selected bridges in each state were geographically close. This was done to allow for cost-effective data collection as travel time between the locations can be reduced significantly by selecting bridges in clusters where possible. Figure 13 highlights the U.S. National Highway System as recognized by the FHWA and provides an idea of the ease of accessibility that was experienced when traveling to these locations. As an example, the nine bridges in each age group in the state of Wisconsin (state code 55) were highlighted by color-shaded cells in an excel sheet as seen in Table 2 where key information about the bridge candidates can be found.



Figure 13. United States National Highway System

Table 2. Key Nine Wisconsin Bridge Candidates in Each Age Group

STATE_CODE	STRUCTURE_NUMBER	ROUTE_NUMBER	COUNTY_CODE	FEATURES_DESC_006A	LAT_016	LONG_017	YEAR_BUILT	TRAFFIC_LANES	ADT_029	YEAR_ADT	Lat_real	Long_real	SPAN
55	'B53021700000000'	90	105	'''LRD COLLEY RD'''	42303673	88585300	2004	2	24800	2016	42.5102	88.98139	3
55	'B53021600000000'	90	105	'''LRD COLLEY ROAD'''	42303785	88585365	2003	3	25300	2016	42.51051	88.98157	3
55	'B32020200030000'	14	63	'''MISSISSIPPI RIVER'''	43482786	91152484	2004	2	6600	2016	43.80774	91.2569	6
55	'B32020200010000'	14	63	'''MISSISSIPPI RIVER / S R'''	43483312	91154788	2004	2	6600	2016	43.8092	91.2633	4
55	'B70021000000000'	0	139	'''IH 41'''	44124164	88283358	2001	2	3500	2017	44.2116	88.4760	3
55	'B18017300000000'	12	35	'''USH 53'''	44474160	91272220	2005	6	26500	2016	44.7949	91.4562	2
55	'B09021800000000'	29	17	'''USH 53'''	44532987	91245403	2004	2	10700	2016	44.8916	91.4150	2
55	'B09020900000000'	29	17	'''CHIPPEWA RIVER'''	44535545	91271698	2005	2	6500	2016	44.8987	91.4547	4
55	'B09023500000000'	178	17	'''CHIPPEWA RIVER'''	44563300	91212160	2000	2	5400	2016	44.9425	91.3560	5
55	'B44015700000000'	41	87	'''STH 96'''	44162400	88280000	1992	3	38550	2017	44.2733	88.4667	2
55	'B44013000000000'	41	87	'''IH 41'''	44175442	88212261	1993	2	7400	2018	44.2985	88.3563	2
55	'B70011000000000'	0	139	'''USH 10-STH 441'''	44133002	88263877	1990	2	5900	2018	44.2250	88.4441	2
55	'B32014300000000'	0	63	'''USH 53-STH 35'''	43571705	91164891	1992	2	590	2016	43.9547	91.2803	2
55	'B44013200000000'	0	87	'''IH 41'''	44175090	88211207	1992	2	3100	2017	44.2975	88.3534	3
55	'B32013700000000'	0	63	'''USH 53'''	43552415	91143015	1990	2	9100	2017	43.9234	91.2417	2
55	'B08003100000000'	114	15	'''USH 10'''	44122601	88200015	1993	2	9900	2018	44.2072	88.3334	2
55	'B13038300000000'	18	25	'''SUGAR RIVER'''	42591235	89342362	1991	2	11300	2016	42.9868	89.5732	3
55	'B13038600000000'	51	25	'''LRD TAYLOR ST'''	43011245	89175835	1992	2	10100	2016	43.0201	89.2995	3
55	'B32005600000000'	53	63	'''IH 90'''	43522527	91123388	1984	3	16400	2017	43.8737	91.2094	2
55	'B25002300000000'	0	49	'''USH 151'''	42573541	90062424	1980	2	270	2016	42.9598	90.1067	2
55	'B13030400000000'	78	25	'''USH 18-USH 151'''	43000521	89453740	1984	3	2200	2016	43.0014	89.7604	2
55	'B32008200000000'	14	63	'''PAMMEL CREEK/BNSF RR'''	43454407	91122869	1981	4	29000	2017	43.7622	91.2080	4
55	'B32009800000000'	16	63	'''BNSF RR'''	43492270	91125953	1981	4	37000	2017	43.8230	91.2165	3
55	'B70009100030000'	21	139	'''FOX RIVER'''	44020329	88334535	1982	4	19600	2017	44.0342	88.5626	2
55	'B70009100010000'	21	139	'''FOX RIVER'''	44020342	88335207	1982	4	19600	2017	44.0343	88.5645	2
55	'B44007500000000'	0	87	'''LRD W WATER ST'''	44151394	88241937	1980	4	14000	2017	44.2539	88.4054	11
55	'B44008800000000'	187	87	'''SHIOC RIVER'''	44274356	88340214	1981	2	1400	2018	44.4621	88.5673	3

Note: the STRUCTURE_NUMBER in red color indicates a bridge both in the NBI and LTBP databases. The white, green, and blue shading cells represent the ages of considered bridges in 15-20, 25-30, and 35-40 years, respectively, at the time of selection.

The latitude and longitude coordinates (LAT_016 and LONG_017 in Table 2) in the NBI database are expressed in 'Degree Minutes Seconds'. They must be converted to the format of 'Decimal Degrees' (Lat_real and Long_real in Table 2) when accessing the google map. Before inputting the coordinate in the google map, a minus sign should be added to the longitudinal coordinate since the bridges are in the Western Hemisphere. Bridge selection in individual states is discussed further in Section 3.2-3.8.

3.2 California Bridge Selection

In the state of California, all bridge candidates were prestressed concrete girders as indicated in Table 1 and presented in Figure 14(a). The short-listed bridge candidates were clustered in the northern region of the state to reduce travel costs. The locations of these bridges can be viewed in Figure 14(b). Mapping these bridge locations with major roads in the state, the short-listed candidate bridges in three age groups can be reached via Interstate 5, 80, and various state routes.

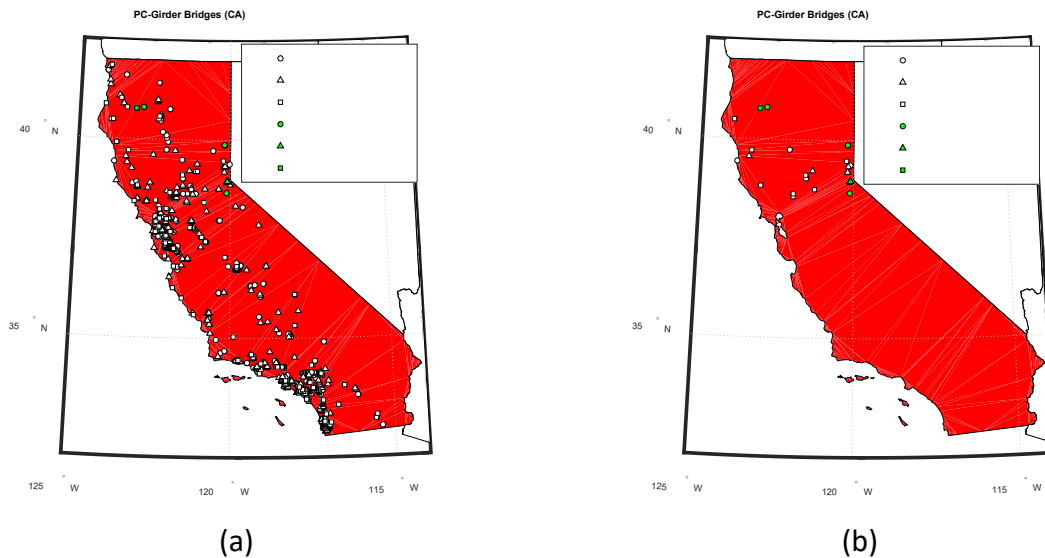


Figure 14. Bridge Candidates in California: (a) All, and (b) Nine in Each Age Group

3.3 Georgia Bridge Selection

In the state of Georgia, all bridge candidates were prestressed concrete girders as indicated in Table 1 and presented in Figure 15(a). The short-listed three age groups were clustered in the west region of Atlanta. The locations of these bridges can be viewed in Figure 15(b). According to the state highway map, the short-listed candidate bridges in three age groups can be accessed via Interstate 20, 75, and various state routes.

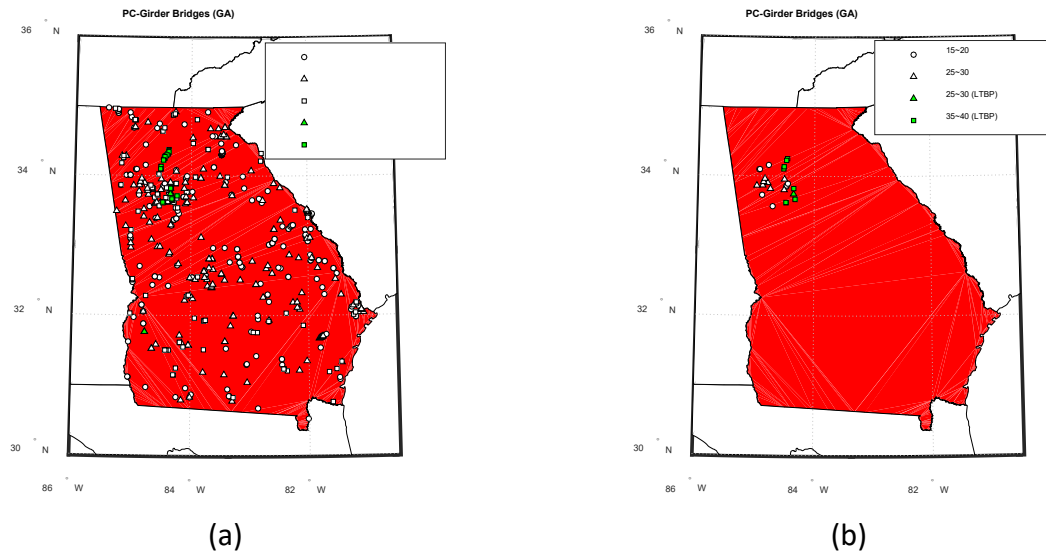


Figure 15. Bridge Candidates in Georgia: (a) All, and (b) Nine in Each Age Group

3.4 Missouri Bridge Selection

In the state of Missouri, both prestressed concrete girder bridges and steel girder bridges were considered as candidates as indicated in Table 1 and presented in Figure 16(a) and Figure 17(a), respectively. The short-listed three sets representing prestressed concrete and steel girder bridges are shown in Figure 16(b) and Figure 17(b), respectively. For both types of candidate girder bridges, the first set was located around Kansas City. The second set was located near Jefferson City. The third set was located west of the St. Louis area along Interstates 44 and 70. Comparing these bridge sites with major highway corridors in the state, the short-listed candidate bridges in three age groups can be accessed via Interstates 44, 70, and various state routes.

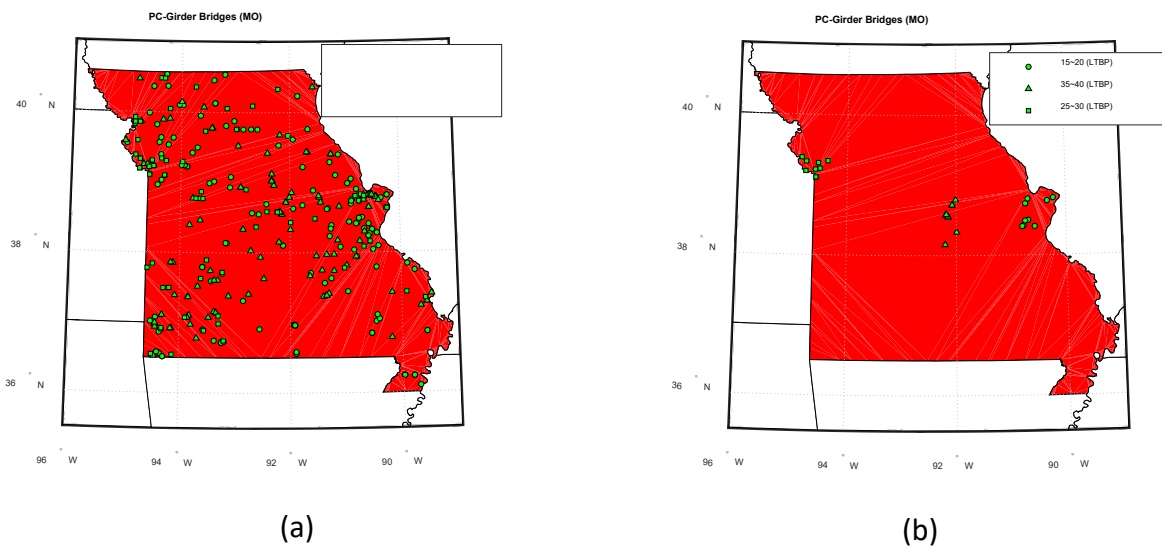


Figure 16 Prestressed Bridge Candidates in Missouri: (a) All, and (b) Nine in Each Age Group

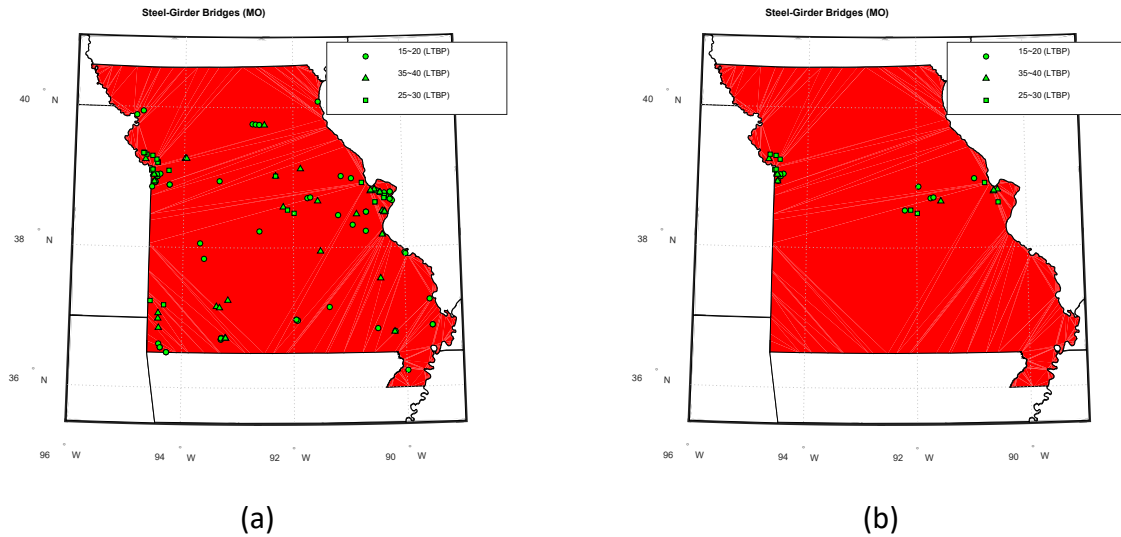


Figure 17 Steel Bridge Candidates in Missouri: (a) All, (b) Nine in Each Age Group

3.5 New York Bridge Selection

In the state of New York, all bridge candidates were steel girders as indicated in Table 1 and presented in Figure 18(a). The short-listed three sets were clustered and distributed across the state. The first and second sets were near Binghamton, and the third set was towards Rochester. The locations of these bridges can be viewed in Figure 18(b). The short-listed candidate bridges in three age groups can be reached via Interstates 86, 90, 390, and various state routes.

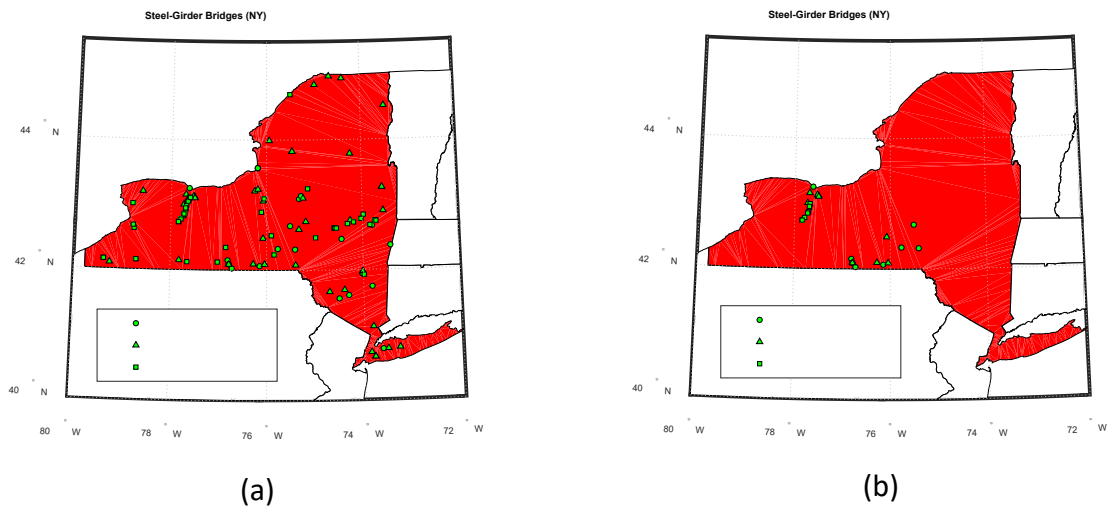


Figure 18. Bridge Candidates in New York: (a) All, and (b) Nine in Each Age Group

3.6 Texas Bridge Selection

In the state of Texas, all bridge candidates were prestressed concrete girders as shown in Table 1 and presented in Figure 19(a). The short-listed three sets were contained to the eastern portion

of the state with the first set being north of the Dallas-Fort Worth, the second between Dallas and Austin, and the third near north of the San Antonio. The locations of these bridges can be viewed in Figure 19(b). The short-listed candidate bridges in three age groups can be accessed via Interstate 35 and various state routes.

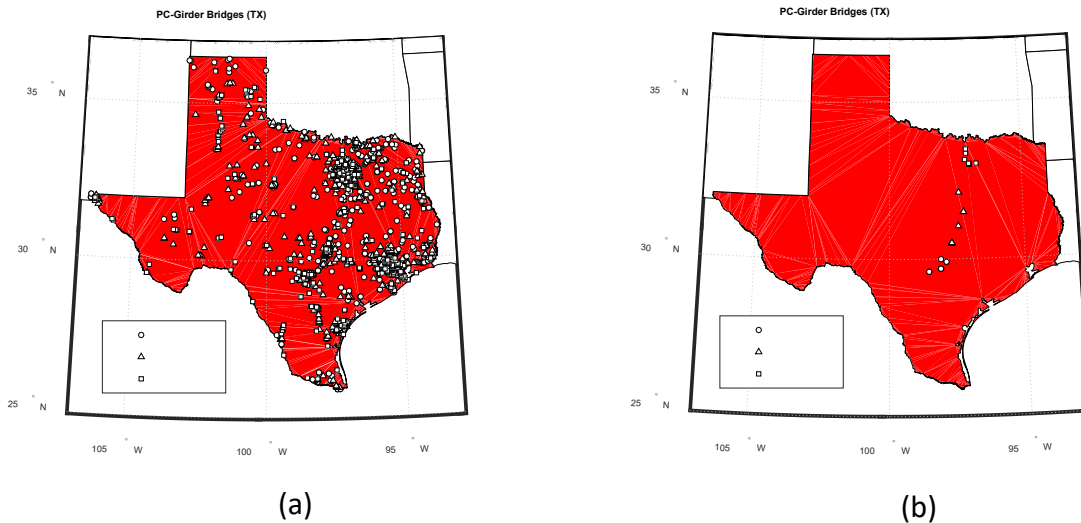


Figure 19. Bridge Candidates in Texas: (a) All, (b) Nine in Each Age Group

3.7 Virginia Bridge Selection

In the state of Virginia, all bridge candidates were steel girders as indicated in Table 1 and presented in Figure 20(a). The short-listed three sets further considered were clustered across the state with the first set near the western region of the state just outside of the Washington D.C. area, the second set around Roanoke, and the third in the west region of Emporia. The locations of these bridges can be viewed in Figure 20(b). According to the state highway map, the short-listed bridge sets outside Roanoke and Emporia can be accessed via Interstates 81 and 85, respectively, and various state routes while the selected bridge set outside the Washington D.C. can be accessed via Interstates 66, 95, and various state routes.

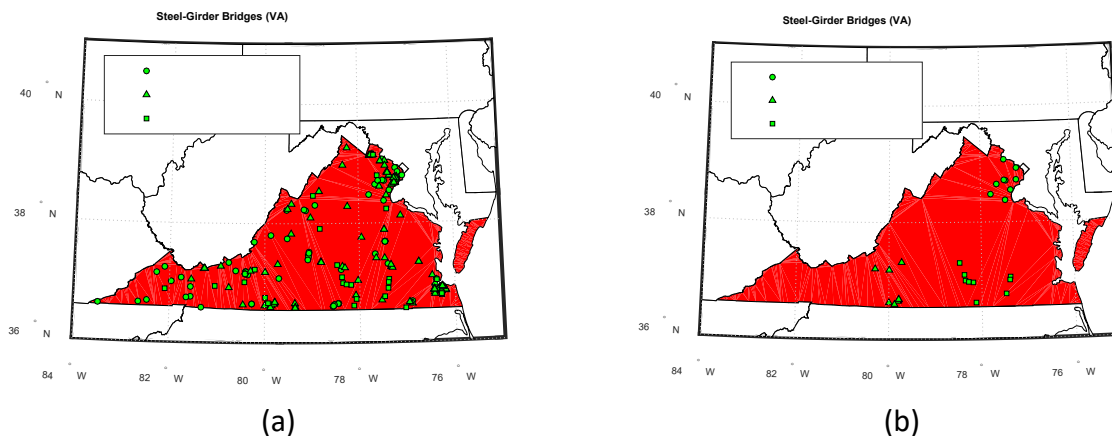


Figure 20. Bridge Candidates in Virginia: (a) All, and (b) Nine in Each Age Group

3.8 Wisconsin Bridge Selection

In the state of Wisconsin, all bridge candidates were steel girders as indicated in Table 1 and presented in Figure 21(a). The short-listed bridges were clustered and distributed across the state. The three sets in age group are located around Oshkosh, southern and western part of the state. The locations of the short-listed bridges can be viewed in Figure 21(b). The selected bridges can be accessed via Interstates 41, 90, and 94 and various state routes.

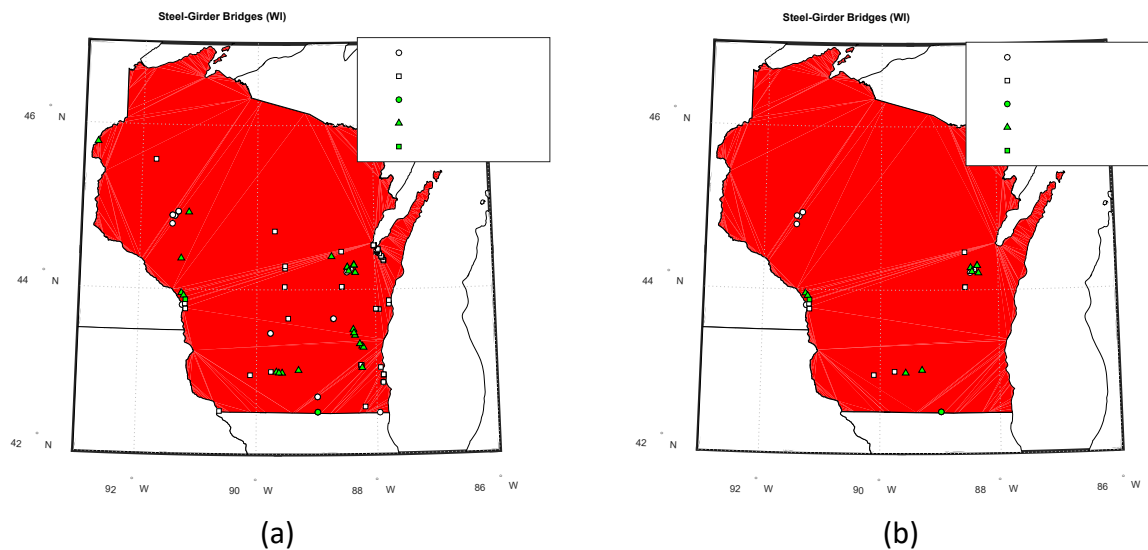


Figure 21. Bridge Candidates in Wisconsin: (a) All, and (b) Nine in Each Age Group

3.9 Summary of Bridges Selected for Inspection

To finalize the bridge selection, nine bridge candidates in each age group were shared with their owner to collaboratively narrow down to three bridges. All the selected bridges are marked in balloon symbols on the Google map with a screenshot presented in Figure 22. Note the red balloons represent overpasses in the state of Missouri, where extra care must be exercised to watch for ongoing traffic underneath the bridges during field inspections. Tables 3-10 summarize the selected nine bridges in three age groups for each state in an alphabetical order except 18 bridges in the state of Missouri. Note some older bridges were included in the states of Texas in Table 8 and Wisconsin in Table 10 due to their limited number of bridges that could be clustered in that group.

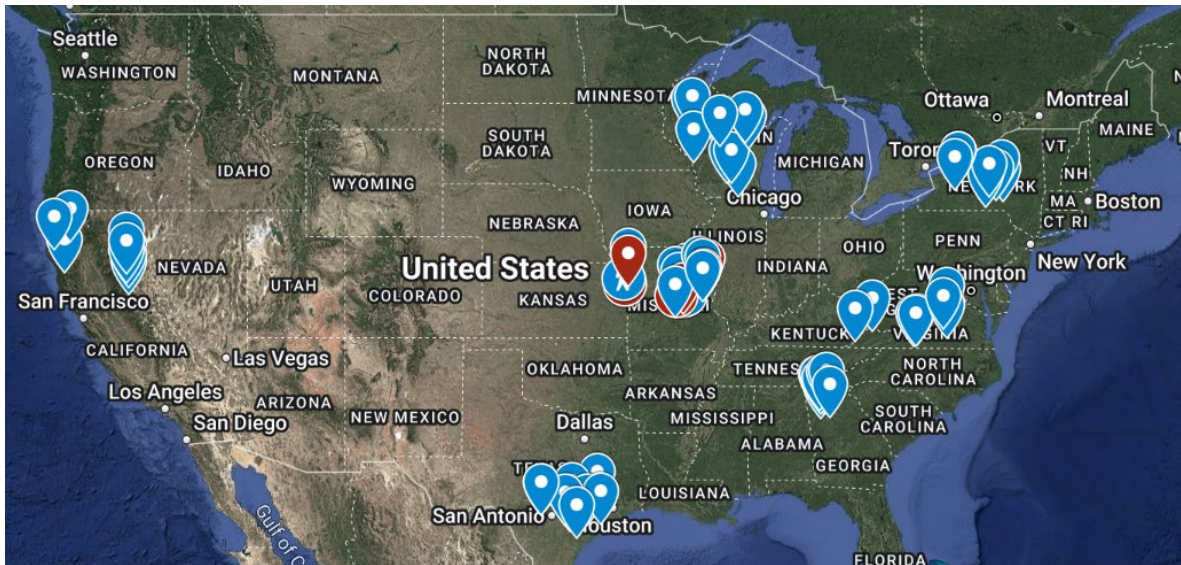


Figure 22. Screenshot of the Selected Bridges on the Google Map

Table 3. California: Prestressed Concrete Girder Bridges

State	Structure Number	Year Built	Age Group	Main Span Material
California	050011	1984	35-40	Prestressed Concrete Continuous
California	040094	1984	35-40	Prestressed Concrete Continuous
California	130009	1982	35-40	Prestressed Concrete Continuous
California	250103	1991	25-30	Prestressed Concrete
California	100293	1995	25-30	Prestressed Concrete Continuous
California	190032	1990	25-30	Prestressed Concrete Continuous
California	260049	2002	15-20	Prestressed Concrete Continuous
California	090072	2000	15-20	Prestressed Concrete
California	170013	2004	15-20	Prestressed Concrete

Table 4. Georgia: Prestressed Concrete Girder Bridges

State	Structure Number	Year Built	Age Group	Main Span Material
Georgia	5700450	1982	35-40	Prestressed Concrete
Georgia	5700510	1982	35-40	Prestressed Concrete
Georgia	8902880	1984	35-40	Prestressed Concrete
Georgia	6702120	1995	25-30	Prestressed Concrete
Georgia	22300360	1992	25-30	Prestressed Concrete
Georgia	22300390	1993	25-30	Prestressed Concrete
Georgia	12153000	2000	15-20	Prestressed Concrete
Georgia	1551150	2004	15-20	Prestressed Concrete
Georgia	1551170	2005	15-20	Prestressed Concrete

Table 5. Missouri: Prestressed Concrete Girder Bridges

State	Structure Number	Year Built	Age Group	Main Span Material
Missouri	2774	1983	35-40	Prestressed Concrete Continuous
Missouri	2815	1981	35-40	Prestressed Concrete Continuous
Missouri	3443	1985	35-40	Prestressed Concrete Continuous
Missouri	2898	1992	25-30	Prestressed Concrete Continuous
Missouri	3995	1993	25-30	Prestressed Concrete Continuous
Missouri	4057	1992	25-30	Prestressed Concrete Continuous
Missouri	29015	2004	15-20	Prestressed Concrete Continuous
Missouri	29166	2002	15-20	Prestressed Concrete Continuous
Missouri	30322	2005	15-20	Prestressed Concrete Continuous

Table 6. Missouri: Steel Girder Bridges

State	Structure Number	Year Built	Age Group	Main Span Material
Missouri	3412	1985	35-40	Steel Continuous
Missouri	3425	1984	35-40	Steel Continuous
Missouri	3558	1984	35-40	Steel Continuous
Missouri	3870	1995	25-30	Steel Continuous
Missouri	4038	1995	25-30	Steel
Missouri	4202	1994	25-30	Steel Continuous
Missouri	12003	2001	15-20	Steel Continuous
Missouri	30522	2004	15-20	Steel Continuous
Missouri	30523	2004	15-20	Steel Continuous

Table 7. New York: Steel Girder Bridges

State	Structure Number	Year Built	Age Group	Main Span Material
New York	1070311	1980	35-40	Steel Continuous
New York	1070312	1980	35-40	Steel Continuous
New York	1071740	1982	35-40	Steel Continuous
New York	1012930	1993	25-30	Steel Continuous
New York	1043390	1995	25-30	Steel Continuous
New York	3312530	1995	25-30	Steel Continuous
New York	1003860	2002	15-20	Steel Continuous
New York	1030730	2002	15-20	Steel Continuous
New York	1024810	2000	15-20	Steel Continuous

Table 8. Texas: Prestressed Concrete Girder Bridges

State	Structure Number	Year Built	Age Group	Main Span Material
Texas	161290034804011	1930	80-90	Prestressed Concrete
Texas	131210008903010	1930	80-90	Prestressed Concrete
Texas	151630002405068	1939	80-90	Prestressed Concrete
Texas	130080040805019	1961	50-60	Prestressed Concrete
Texas	131580017904069	1971	50-60	Prestressed Concrete
Texas	151630002405167	1983	35-40	Prestressed Concrete
Texas	161960037102076	1985	35-40	Prestressed Concrete
Texas	130900034701010	1988	30-35	Prestressed Concrete
Texas	160890AA0134001	1990	25-30	Prestressed Concrete

Table 9. Virginia: Steel Girder Bridges

State	Structure Number	Year Built	Age Group	Main Span Material
Virginia	11562	1981	35-40	Steel
Virginia	11563	1981	35-40	Steel Continuous
Virginia	14005	1981	35-40	Steel
Virginia	23537	1992	25-30	Steel Continuous
Virginia	23672	1993	25-30	Steel
Virginia	24414	1995	25-30	Steel Continuous
Virginia	25607	2001	15-20	Steel Continuous
Virginia	26791	2005	15-20	Steel Continuous
Virginia	29171	2005	15-20	Steel

Table 10. Wisconsin: Steel Girder Bridges

State	Structure Number	Year Built	Age Group	Main Span Material
Wisconsin	B320082	1981	35-40	Steel Continuous
Wisconsin	B440075	1980	35-40	Steel Continuous
Wisconsin	B440088	1981	35-40	Steel Continuous
Wisconsin	B130383	1991	25-30	Steel Continuous
Wisconsin	B130386	1992	25-30	Steel Continuous
Wisconsin	B710018	1962	50-60	Steel Continuous
Wisconsin	B530216	2003	15-20	Steel Continuous
Wisconsin	B090209	2005	15-20	Steel Continuous
Wisconsin	B090235	2000	15-20	Steel Continuous

CHAPTER 4. UNCREWED VEHICLES AND SENSING SYSTEMS

A mobile test facility, referred to as Bridge Inspection Robot Deployment System (BIRDS), was developed to support a crew of two-to-four inspectors, a robotic system, remote sensing, and NDE devices at bridge sites. The BIRDS was housed in a 12-seat Nissan van as illustrated in Figure 23(a). The front five seats of the van were kept in place for crew members and the remaining seats were removed to make space for test equipment as illustrated in Figure 23(b). The robotic system included commercial drones, structural crawlers, and their combinations tailored to make bridge inspection both efficient and effective. These robotic vehicles are equipped with multiple remote sensing and NDE devices, such as microscopic imager and laser scanner.



Figure 23. Mobile Test Facility: (a) 12-Seat Van, and (b) Test Equipment in the Van

4.1 Commercial Uncrewed Aerial Systems

The commercial part of the BIRDS included an uncrewed aerial system (UAS) of commercial drones such as Skydio 2+ (Skydio, 2025), Elios 3 (Flyability, 2025), Parrot Anafi (Parrot, 2025), and DJI Phantom 4 (DJI, 2025), and custom-designed vehicles such as Headwall-integrated DJI M600 (Headwall, 2025) and Geodetic-integrated DJI M600 (Geodetics, 2025), as illustrated in Figure 24. These robots are equipped with multimodal remote sensing systems including RGB cameras, infrared cameras, hyperspectral cameras, and Light and Detection Range (LiDAR) scanners. RGB, infrared, and hyperspectral images provide information about surface textures and colors, substrate defects, and surface material chemical species, respectively. LiDAR provides a 3D point cloud with geospatial information.

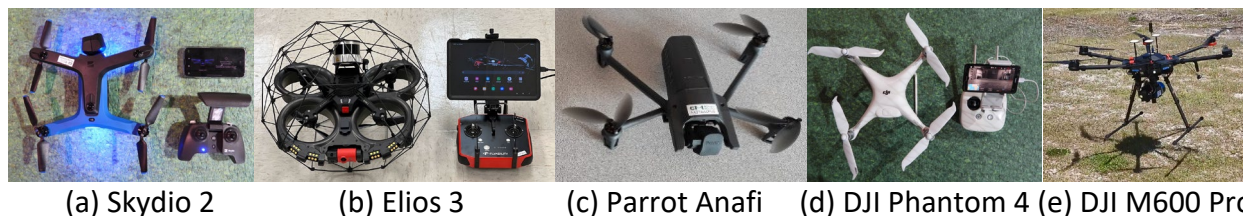


Figure 24. A Suite of Commercial Drones

A suite of heterogeneous UASs is required to support a complete inspection due to limited onboard sensor type and resolution, flight time, illumination capability, collision-tolerance, maneuverability, and reliability. They are also required for backup operations when some vehicles malfunction unexpectedly at bridge sites. In addition, supplementary cameras are needed for crowded areas that drones are unable to access. Table 11 summarizes the primary features of five UASs: Skydio 2+, Elios 3, Parrot Anafi, DJI Phantom 4, and DJI M600 Pro.

Table 11. Primary Features of Five Commercial UASs

UAS	Gimbal Range	Video/Image	Flight Time	Illumination	Obstacle/Collision
Skydio 2+	-110° to +45°	4K UHD/60fps, 12 MP	27 min	No	Obstacle Avoidance
Elios 3	-90° to +90°	4K/30fps, 12MP (4:3)	10 min	10/16K Lumens	Collision-Tolerant
Parrot Anafi	-90° to +90°	4K UHD/30fps, 21MP	25 min	No	None
DJI Phantom 4	-90° to +30°	4K UHD/25fps, 12 MP	28 min	No	None
DJI M600 with FLIR Duo Pro R640	-90° (fixed)	640×512/30fps, 19 mm, FOV 56°×45°	18 min (5.5 kg payload)	No	None

4.2 Custom-built Uncrewed Aerial Systems

During bridge inspections, commercial drones equipped with cameras are often faced with challenges to produce high-quality imagery due to poor light condition, windy operation environment, collision-preventive distance, and physical accessibility through dense tree branches. They are difficult, if not impossible, to support nondestructive testing on bridge structures. Additionally, flying a drone above a bridge is distracting to passing traffic, a potential concern of safety.

To enable steady measurement, consistent illumination, and extended operation time, a unique robotic system of the BIRDS was designed to combine the flying capability of drones and the traversing capability of crawlers into a hybrid uncrewed vehicle called BridgeBot. This hybrid flying and traversing system can aid in the inspection of both steel and concrete girder bridges. In the past six years, the envisioned BridgeBot has evolved through the test and evaluation of four prototypes (I-IV) for improved structural, mechanical, electronic, and control systems. Prototypes I and II were mainly tested in the laboratory to understand the feasibility of hybrid flying and traversing operation (Reven et al., 2019). Prototypes III and IV were tested and evaluated for components and system performance both in the laboratory and in real-world field conditions. Following is a brief description of Prototypes III and IV and their equipped sensing functions.

BridgeBot III introduced a gravity-support hanging mechanism that provided a guided one-dimensional traversing movement along both steel and concrete girders ‘like a railway track for trains.’ BridgeBot IV used a magnetic attracting mechanism that provided two-dimensional traversing movement on the bottom flange of a steel girder ‘like a highway lane for cars.’ Both BridgeBot III and IV can launch a palm-size, magnet-wheeled, structural crawler off a metal ramp for detailed inspection on steel weld cracks and other defects such as corrosion. The passive engaging mechanisms of both BridgeBot III and IV on a bridge girder do not require power once the BridgeBot is in traversing mode along the girder. This design does not only conserve battery power but also provides additional stability and safety against unexpected disturbances such as wind gusts, uneven cross sections, and sudden illumination changes for vision-based vehicle control.

I-shaped girders are made of steel and normal or prestressed concrete with a bottom flange width ranging from 10 to 24 in (25.4 to 61.0 cm). Inspecting the underside of bridge decks is efficient for gravity-induced cracks and leakage-induced corrosion deterioration in close distance. To facilitate this process, a robot is required to fly around and contact each individual girder. Such a robot can traverse along the girder to gather both visual and physical data as needed. This necessitates a mechanism that allows the robot to engage with and disengage from the girder, in addition to serving as a traversing module.

A common platform of BridgeBot weighed less than 4 kg; it was tested and evaluated on girder bridges for visual inspection and NDE testing. While it can fly for about eight minutes only, BridgeBot can traverse for more than 60 minutes along bridge girders. The resolution of an image from a GoPro Hero11 camera installed on the BridgeBot is 5.9×10^{-4} in (0.015 mm) when taken at 11.8 in (0.3 m) distance or 4.6×10^{-4} in (0.14 mm) at a girder spacing of 9 ft (2.75 m). This level of pixel resolution is sufficient for the detection of any structural features on the bridge surface. The BridgeBot recently received the 2025 American Society of Civil Engineers (ASCE) Charles Pankow Award for Innovation. The award committee cites that the innovation is revolutionizing bridge inspection.

4.2.1 Mechanical Engaging Mechanism in BridgeBot Protocol III

Figure 25 shows a complete system of BridgeBot Prototype III. Figure 25(a) illustrates the hybrid vehicle with aerial and ground traversing functions. The system incorporates a hybrid drone capable of both flying and traversing using an I-shaped girder. This dual-function design allows the drone to transition seamlessly between aerial operations and ground-based traversal. Additionally, the drone includes an integrated launching station for deploying a crawler robot, enabling effective deployment across diverse terrains. Figure 25(b) illustrates a ground control station for operation and monitoring. The system features a ground control station designed to oversee and manage both the hybrid drone and the crawler robot through video feeds and wireless communication. This station allows for real-time monitoring and control of both units, ensuring synchronized operations and efficient task execution beyond the visual line of sight.

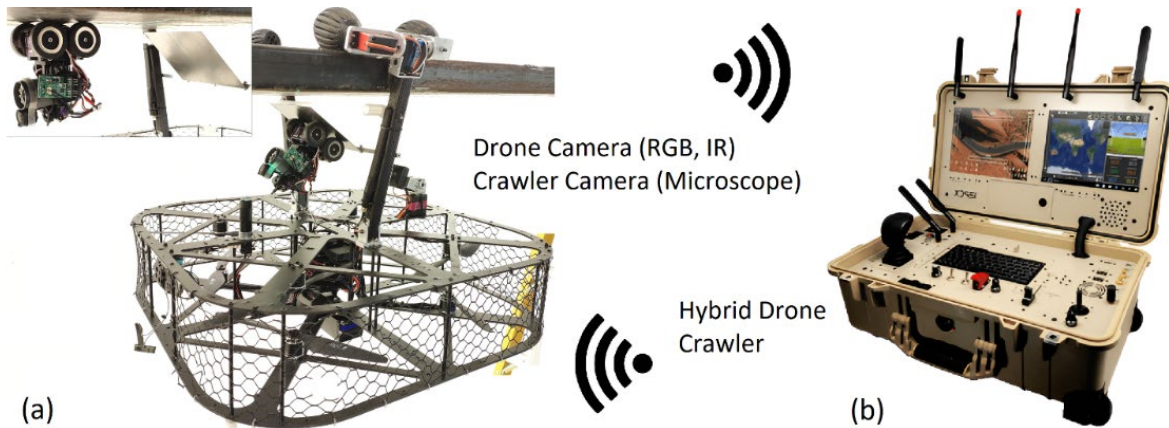


Figure 25. A Complete BridgeBot Prototype III System

Prototype III, as illustrated in Figure 26, introduced a hanging mechanism of four gravity-support elastic wheels designed to operate on both steel and concrete girders with widths ranging from 10 to 24 in (25.4 to 61.0 cm). This mechanism has two degrees-of-freedom (2DOF): one DOF for engagement with the girder and another DOF for traversing along the girder length. It consists of two hanging arms, each having two elastic wheels. The two wheels at the end of one hanging arm are rotated by an engaging servo and one of the two wheels is controlled by a moving motor for traversing along the girder. The servo motors as actuators were chosen for their precision and reliability. The main frame is constructed from a combination of carbon fiber and aluminum, providing an optimal balance of strength and light weight.

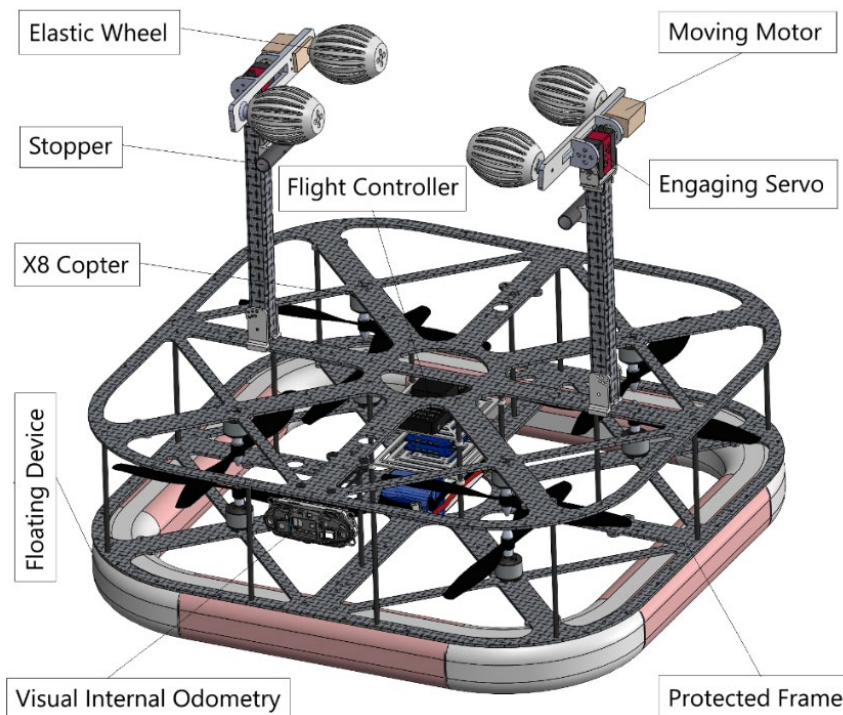


Figure 26. Mechanical Hanging Mechanism with Gravity-Supported Wheels

4.2.2 Magnetic Engaging Mechanism in BridgeBot Protocol IV

As discussed in Section 4.2.1, the mechanical hanging mechanism in Prototype III must be adjusted to ensure that the arm spacing fits into the width of the bottom flange of a bridge girder. Prototype IV features a size-independent hanging mechanism based on magnetic forces induced by magnetic wheels. Figure 27 shows an overview of a magnet-wheeled BridgeBot. Four magnetic wheels can be adhered to the bottom flange of a steel girder during inspection at close distance.

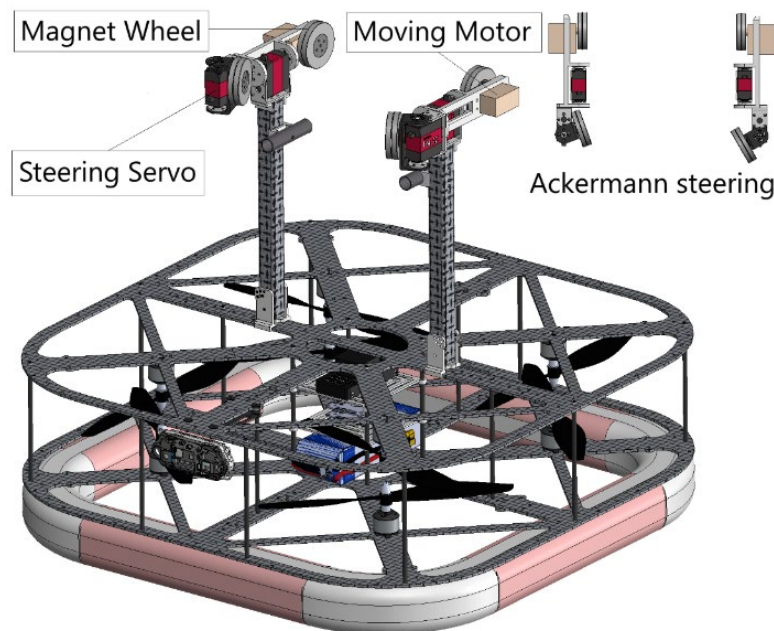


Figure 27. Magnetic Attracting Mechanism with Ackermann Steering

4.2.3 Structural Crawlers for Nondestructive Testing

A compact magnetic-wheeled crawler robot, measuring $3.15 \times 3.15 \times 3.15$ in ($80 \times 80 \times 80$ mm), was developed for detailed inspection tasks on steel structures. As shown in Figure 28, the robot was equipped with both an RGB camera and a microscopic imager, along with an integrated LED lighting system to facilitate operation in low-light conditions. Designed for high mobility, the crawler can navigate over complex geometries commonly found in steel bridge structures, including internal and external corners, narrow edges, and areas obstructed by bolts and nuts. This capability enables the robot to access previously unreachable or hazardous zones, particularly critical inspection points such as joints and connectors. The camera system is mounted on a 2-DOF pan-tilt mechanism, providing flexible visual coverage and enabling the robot to monitor its surroundings during transitions and while performing inspection tasks. The microscopic imager offers up to 500 \times magnification, enabling high-resolution imaging for the detection of fatigue cracks and other micro-defects. The imager's zoom and focus functions are motorized for precise adjustment.

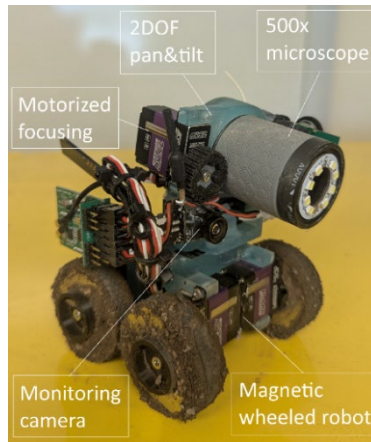


Figure 28. Microscope Crawler for Detailed Visual Inspection

The compact robot can be remotely operated at a distance of up to 328 ft (100 m), even in environments with limited line-of-sight communication due to structural interferences. It is powered by a 450 mAh lithium-polymer (LiPo) battery, providing approximately 10 min of continuous operation under the current design specifications. Notably, the crawler was designed to be deployed from a hybrid drone platform, enabling aerial delivery and placement onto steel surfaces in otherwise inaccessible or dangerous inspection environments.

Another magnetic-wheeled crawler, measuring $4 \times 4 \times 6$ in ($105 \times 105 \times 150$ mm), was equipped with a 4-DOF manipulator designed for the physical inspection of steel bridge structures. As shown in Figure 29, the robot was remotely operated from a ground station. Locomotion and manipulator articulation were controlled via a 2-DOF joystick and a twin 4-DOF haptic sensor. This configuration offered both simplicity and flexibility in sensor deployment. The magnetic robot was powered by a lithium-ion (Li-ion) battery, enabling operational autonomy for up to 20 min. A 4K camera was mounted at the end-effector of the manipulator, providing a comprehensive view of both the surrounding environment and the inspection area. The system can accommodate various sensing payloads up to 0.44 lb. (200 g), allowing for customizable configurations tailored to specific inspection tasks. Additionally, the robot can be deployed from a hybrid aerial drone, enhancing its accessibility in challenging environments.

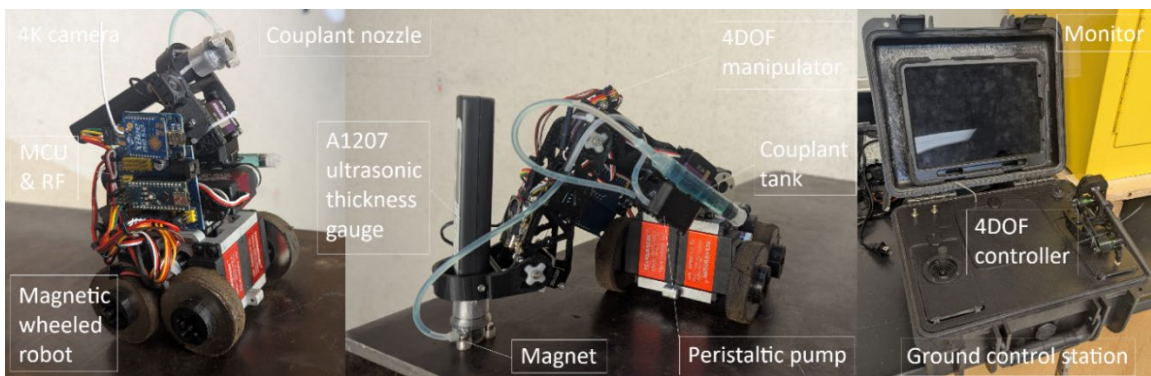


Figure 29. Ultrasonic Gauge Crawler for Metal Thickness Measurement

As an example, the robot was equipped with a payload of A1207 ultrasonic thickness gauge. This sensor required the use of an ultrasound gel to ensure effective acoustic coupling with the inspection surface. The ultrasound gel delivery system comprised a reservoir tank, a peristaltic pump, a silicone tube, and a specially designed nozzle. The nozzle encased the sensor probe and was magnetically equipped to maintain steady contact with the metallic surface. The sensor was mounted on the manipulator via a flexible linkage, which compensated for minor positioning inaccuracies caused by manipulator movement, thus enabling accurate readings.

4.3 Automated Vision-based Weld Inspection

To demonstrate the application of crawlers, an automated, AI-based inspection system was developed for weld inspection in steel bridges. The system employed a magnetic wheel-based crawler equipped with a microscopic imager that streamed real-time video for defect detection or a 3D laser scanner for accurate defect size estimation. The integrated sensing systems ensured that weld defects in steel bridges had been inspected both efficiently and effectively.

4.3.1 YOLO-based Defect Detection on Magnified RGB Imagery

Six steel weld samples were fabricated with each containing three types of weld defects: debonding, cracking, and cavity. Debonding represents a lack of fusion between a weld and its base metal. Cracking is a process of material fracture within the weld in heat-affected zones. Cavity describes a void or space resulting from gas bubbles trapped in the weld metal due to contaminants or improper shielding. For cavities in a material, the term of porosity is often used.

A microscopic imager was used to capture thousands of images among which 741 high-resolution images of the weld samples were chosen for the processing and analysis steps. Images were recorded from varying angles, distances, and lighting conditions to simulate diverse inspection environments and increased dataset variability. The collected images were imported into the Roboflow platform (Roboflow, 2025) for an efficient manual annotation of defects into three categories. The dataset was augmented through techniques such as rotation, flipping, and resizing, increasing the total image count, and enhancing model robustness. After preprocessing, the expanded image dataset was split into 70% for training, 10% for validation, and 20% for testing sets.

The You Only Look Once (YOLO) v11 model (Khanam and Hussain, 2024), pretrained on the Common Objects in Context (COCO) dataset, was fine-tuned using the transfer learning technique on the annotated weld dataset. As shown in Figure 30, three variants of the YOLOv11 model, named Nano, Small, and Medium, were tested. All three models can predict the weld defects accurately. Among them, the Nano model was selected for deployment due to its optimal tradeoff between accuracy and inference speed, making it suitable for edge devices. The trained model was deployed on a NVIDIA Jetson computer as a remote processing unit. The client machine received the video stream, extracted video frames, applied YOLOv11 inference, and displayed results in real time. Figure 31 illustrates the workflow of the client machine.

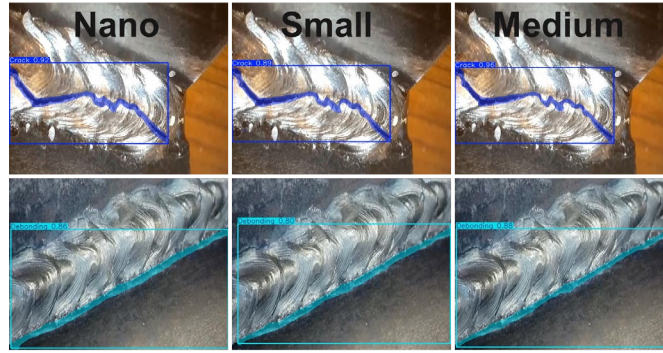


Figure 30. Three Variants (Nano, Small, and Medium) of the YOLOv11 Model

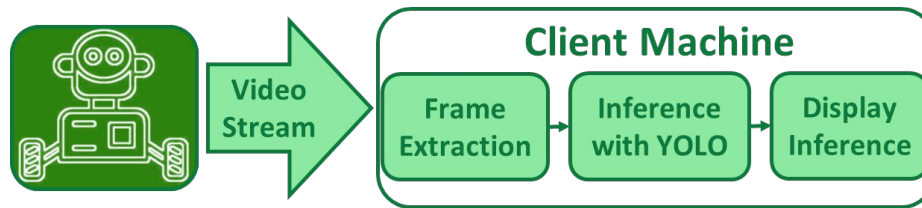
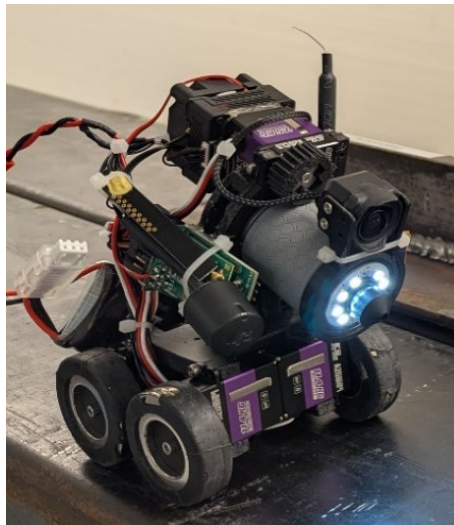
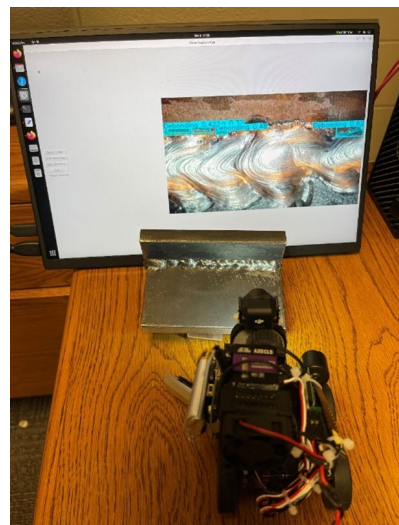


Figure 31. Workflow of the Client Machine

The magnet-wheeled crawler equipped with the microscope imager streamed videos through an antenna with a local Wi-Fi network to the client machine. The wireless connection enables real-time monitoring and defect detection in inspector-inaccessible areas. Figure 32 shows the climbing robot used to collect imagery, which was an early version of the design shown in Figure 28.



(a) Climbing robot



(b) Weld detection system

Figure 32. Crawler Operation for Image Data Collection

The deployed system demonstrated high detection accuracy, enabled by the microscopic resolution of the input images. The YOLOv11 Nano model accurately segmented and detected

weld defects in real time, providing immediate feedback to the operator. The real-time workflow from video capture to defect display ensured efficient and safe weld inspection without requiring manual probing or close-range human access. Figure 33 presents the Mean Average Precision (mAP50) calculated at an Intersection over Union (IoU) threshold of 0.50 to quantify the performance (accuracy) of YOLOv11 Nano model for detection and segmentation. The mAP50 increases with the number of training cycle (Epoch) with a complete training dataset and approaches to 0.83 and 0.76, respectively, after approximately 50 epochs. These confidence levels of performance are reasonable in applications. Table 12 demonstrates the AI model prediction for different defect types on the RGB images taken by the microscopic imager.

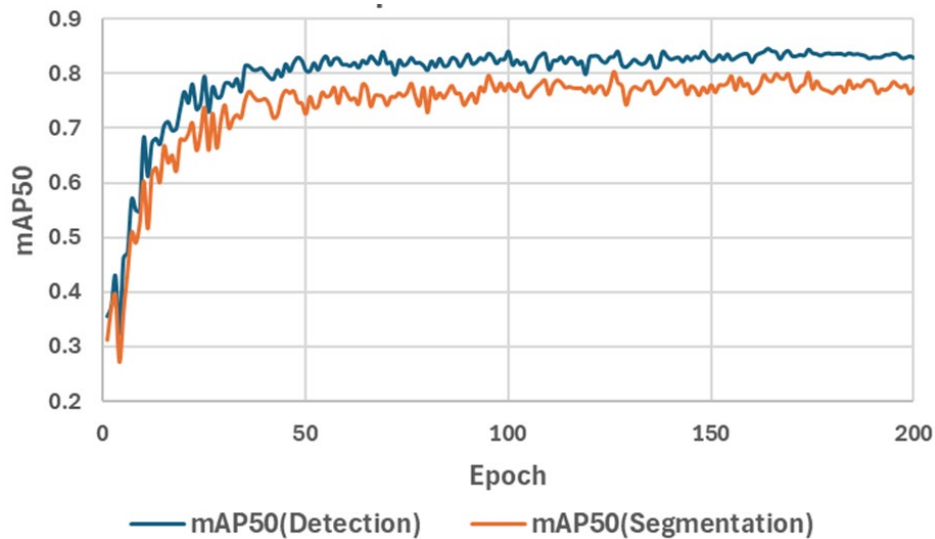

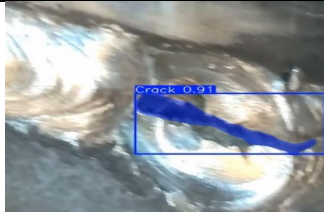



Figure 33. Performance of the YOLOv11 Nano Model for Detection and Segmentation

Table 12. Weld Defect Detection Results from Microscopic Images

Defect	Cavity	Cracking	Debonding
AI Prediction			

4.3.2 3D Laser Scanning

Two 2D/3D laser scanners were used for accurate defect size estimation. First, the Micro-Epsilon scanCONTROL 3060-50/BL (Micro-Epsilon, 2025), as shown in Figure 34(a), is a high precision 2D/3D laser line scanner that uses a blue laser to capture detailed surface profiles of objects. It projects a laser line onto the target and records the reflected light using a high-speed sensor to generate accurate measurements in the X (width) and Z (depth) directions. By moving the sensor (or object) and capturing successive profiles, it reconstructs full 3D shapes along the Y-axis. It supports the RS422 encoder input for precise synchronization with motion, making it ideal for

measuring welds, surface defects, and geometric dimensions in industrial and research settings. For real-time applications, an encoder should be integrated into the scanning system to accurately assign the distance between each scanned slice in real time. If real-time detection is not required and the moving speed of the Micro-Epsilon scanner remains constant, the Y-axis (or any other axis) can also be manually scaled as needed. The high-resolution sensor matrix offers a resolution of 2,048 points with an ultimate point distance of just 12 μm , which is sufficient for an accurate measurement of fine surface features, such as hairline cracks for structural durability inspection in corrosive environments.

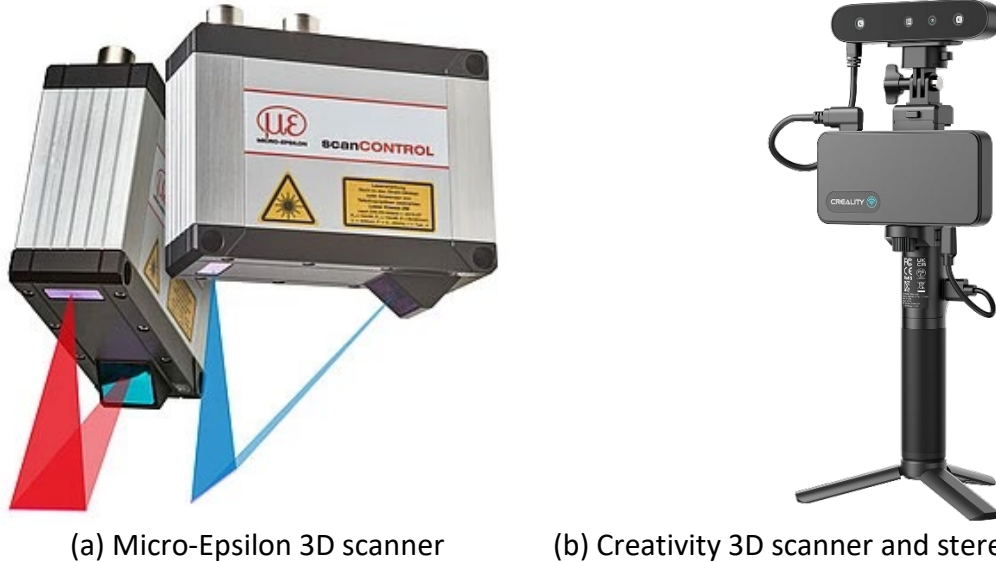
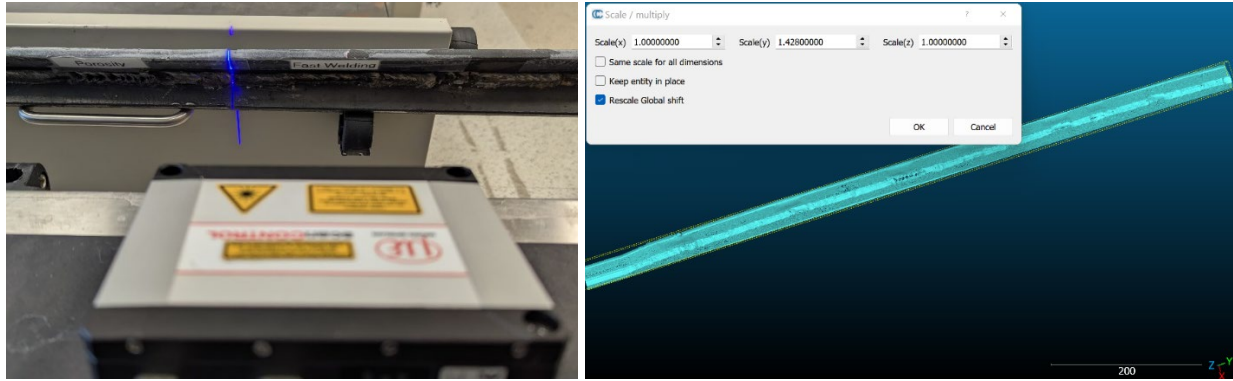


Figure 34. High- and Low-Resolution 3D Laser Scanning

Second, the SR-Scan Ferret Pro 3D scanner (CREALITY, 2025), as shown in Figure 34(b), consists of a scanner head, a wireless bridge, a power bank handle, a phone holder, and various cables and accessories. The scanner itself utilizes a high-resolution 2-megapixel color camera and a 3D imaging specific chip for efficient data capture. It can scan a size of 6-80 in (150-2000 mm) at a point distance of 0.006 in (0.16 mm) up to 30 fps. It can register features as small as 0.004 in (0.1 mm). This level of accuracy is suitable for structural safety inspection as a concrete crack that has structural implications likely exceeds 0.016 in (0.4 mm) in width.

To collect data, the scanCONTROL 3060-50/BL (and the SR-Scan Ferret Pro 3D scanner) was placed on a conveyor to keep scanning distance and speed consistent. The laser scanner captured slices of point clouds in the form of parallel vertical lines, which accumulated over time to form the sample's longitudinal dimension along the Y-axis. As a result, the Y-axis scale depended on the speed of the conveyor. Figure 35(a, b) illustrates the laser scanning and the point cloud scaling in CloudCompare (CloudCompare, 2025). While the X-axis and Z-axis do not require any scaling, the Y-axis associated with the moving speed of the laser scanner is scaled by calculating the sample length and its scanned 3D point cloud length as demonstrated in Figure 35(b).



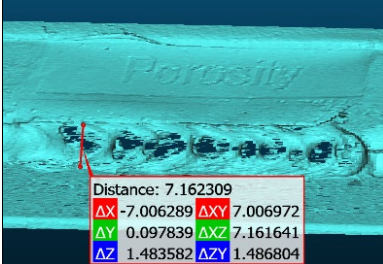

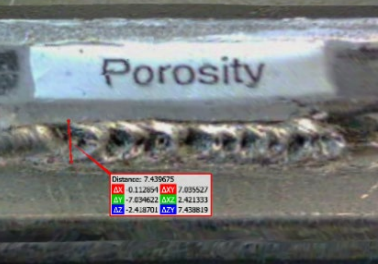
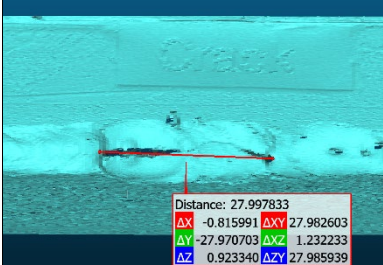

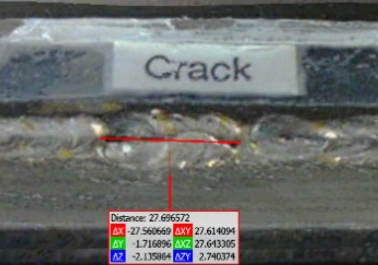
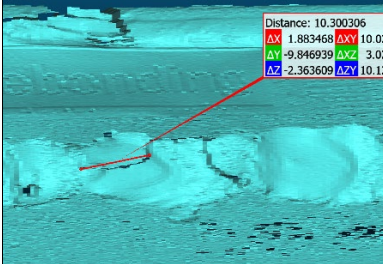

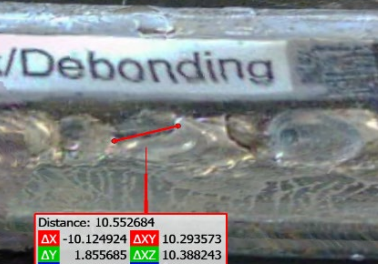
(a) A blue laser line on the weld surface

(b) Point cloud along the Y direction

Figure 35. Laser Scanning to Record Point Cloud for 3D Surface Reconstruction

Table 13 compares defect size measurements from the scanCONTROL 3060-50/BL (monochrome point cloud), the SR-Scan Ferret Pro 3D scanner (colored point cloud), and a measure tape. It can be observed from Table 13 that the defect size measurements from the two scanners are consistent with their ground truths in every direction. The maximum difference in cavity, cracking and debonding measurements from the monochrome and colored point clouds is 3.7%. Note that the defect labels on the sample are clearly seen in the monochrome point cloud.

Table 13. Detected Defects from Point Cloud and Ground Truth Measurements

Defect	Monochrome Point Cloud	Ground Truth	Colored Point Cloud
Cavity			
Cracking			
Debonding			

CHAPTER 5. BRIDGE DECK NONDESTRUCTIVE TESTING

Due to gravity, deterioration on the bottom surface of a bridge deck (a structural safety issue) is equally if not more important than that on the top surface (an operation safety concern). Inspections above and below a pedestrian bridge deck on Missouri S&T campus were compared to understand their correlation or complementary nature. NDE techniques applied to the pedestrian bridge included ultrasonic surface waves (USW), impact echo (IE), ground penetrating radar (GPR), and microwave synthetic aperture radar (SAR).

5.1 Bridge Conditions and Nondestructive Testing

Figure 36 shows an overall view and condition of the pedestrian bridge on the Missouri S&T campus. The pedestrian bridge is located between the Computer Science Building and the Engineering Research Laboratory on campus. Built 50 years ago, the bridge deck is 94 ft (28.6 m) long, 11 ft (3.45 m) wide, and 7 to 12 in (18 to 30 cm) thick.

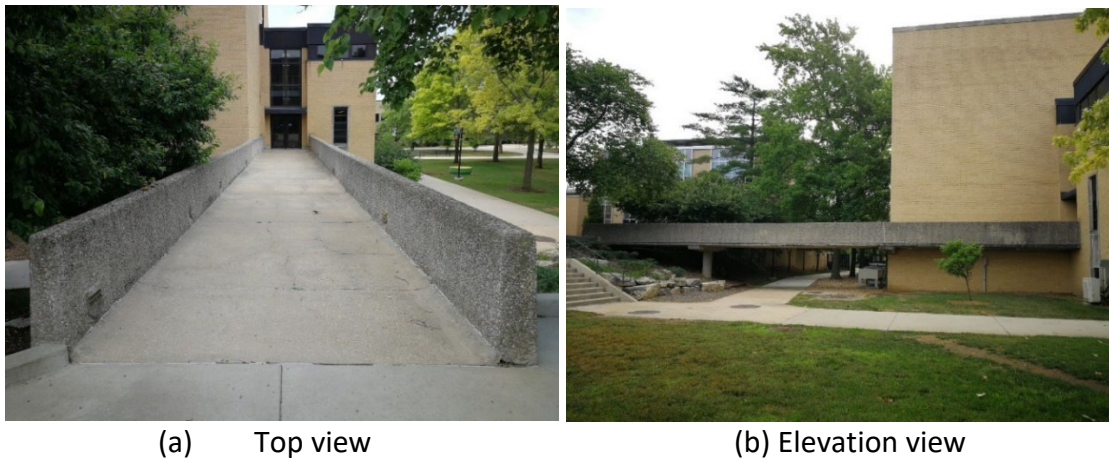


Figure 36. The Pedestrian Bridge on Missouri S&T Campus as a Testbed

Figure 37 presents a close-up view of the deterioration on the pedestrian bridge. Delamination, rebar exposure, rebar corrosion, deck cracking on the top, and deck leaching on the bottom can be noticed. The deterioration of the test bridge is likely a result of decades of rain and spreading salts to prevent deck icing during cold winters. These events permeated salty water into the bridge deck, thus causing corrosion of rebar and subsequently delamination, cracks and spalling of concrete. Although not documented, deck resurfacing in the past was observed on the bridge top surface to remediate the water permeation problem. However, the deterioration remains an ongoing slow process.

The pedestrian bridge was used for nondestructive testing (Alhaj et al., 2019). An area of approximately 10×9 ft (3.05×2.74 m) was surveyed using GPR, IE, USW, and SAR imaging methods at the bridge surfaces of the RC bridge deck for condition assessment. This study was conducted to investigate the effectiveness of nondestructive testing (NDT) methods from the topside and underside of the bridge deck.

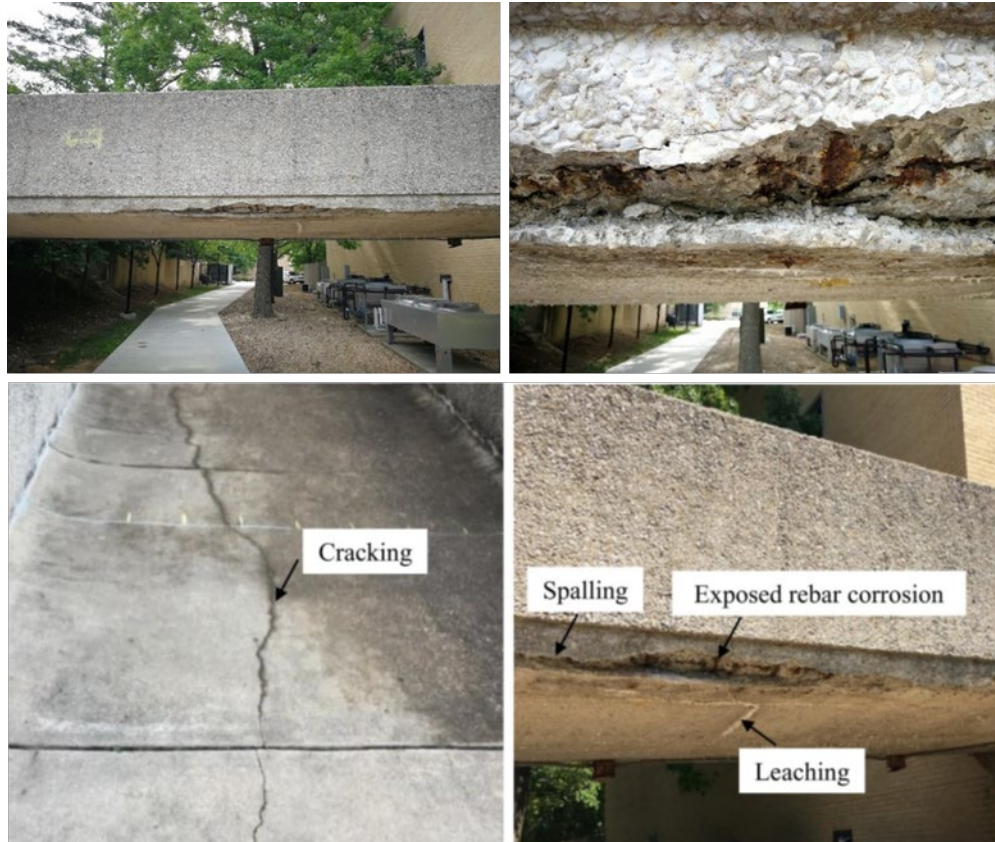


Figure 37. Various Types of Deterioration in the Pedestrian Bridge

GPR is a geophysics method used widely in bridge evaluations. GPR depends on the transmission and receiving of electromagnetic (EM) waves that propagate through subsurface materials. The reflected EM signals are recorded and then used to detect some embedded features (e.g., delamination and rebar corrosion) based on the changes of electrical conductivity and dielectric properties of the transmitted materials. Furthermore, GPR responds to the presence of saline moisture and can be used to determine the relative concrete condition by identifying areas where there is low to high concrete deterioration. Data interpretation can help determine relative concrete condition to good (no deterioration), fair (moderate deterioration), or poor (extensive deterioration) (Sneed et al., 2014; Anderson and Li, 2014).

IE and USW are also used widely in bridge evaluations. They are based on transmitting and receiving acoustic waves propagating through a uniform medium using a portable seismic property analyzer (PSPA) device. The USW method can measure the variations of Young's Modulus of concrete along the bridge deck and the IE method can measure depth to possible embedded defects in concrete along the bridge deck. Both USW and IE provide information about the concrete quality of the bridge deck (Gucunski et al., 2008; Nazarian, 1984).

Microwave signals can propagate through dielectric materials such as concrete and be reflected by voids, delamination, and steel reinforcing bars. The reflected microwave signals are affected by contrast in materials' dielectric properties which are further affected by moisture, ionic

solution, and corrosion by-products. Acquired microwave reflection data, on a two-dimensional (2D) grid, is then used to form a graphical representation of the interior structure in the form of image slices corresponding to different depths. One powerful method for forming such images is the wideband SAR imaging technique. The principle of microwave SAR imaging techniques, specifically for NDE applications, has been well studied and previously documented. Commonly, a wideband microwave transceiver and antenna, capable of measuring the phase-calibrated reflection coefficient, is used to scan a bridge element surface following a 2D (planar) grid. The collected reflected data (referenced to the aperture of the antenna) is then processed to produce high-resolution 3D images of an object (Ghasr et al., 2014; 2016; Case et al., 2012). The resulting image resolution depends on the overall scanned area dimension, the wavelength inside the materials, and the depth inside the materials (or distance from the antenna) (Case et al., 2012; Zoughi, 2018). Higher frequencies and higher dielectric permittivity both result in shorter wavelengths and therefore SAR images with higher resolution (Case et al., 2012; Bao et al., 2017).

5.2 Data Acquisition and Processing for GPR, IE, and USW

GPR data were acquired using a Geophysical Survey System, Inc. (GSSI) with 1.6 and 2.5 GHz antennas. GPR profile spacing was 1 ft (30.5 cm) along a predetermined section of 10 ft \times 9 ft (3.05 m \times 2.74 m) on the top and bottom surfaces of the bridge deck as shown in Figures 38, 40, and 41 (Alhaj et al., 2019). Furthermore, USW and IE data were acquired using the PSPA device with one impact transmitter and two receivers (Sensor 1 near the transmitter and Sensor 2 away from the transmitter). PSPA profile spacing was 1 ft (30.5 cm) along the same predetermined section of 10 ft \times 9 ft (3.05 m \times 2.74 m) on the top and bottom of the bridge deck as shown in Figures 39 and 40. GPR data as shown in Figure 42 were processed using Radan 7 (GSSI) and plotted using Surfer 10 (Golden Software). The GPR data cannot detect the presence of the bottom layer of rebar due to significant energy dissipation and wave dispersion through the heterogeneous concrete material. USW and IE data as shown in Figure 43 were processed using the PSPA device and plotted using Surfer 10.



Figure 38. GPR Data Acquisition



Figure 39. IE Data Acquisition

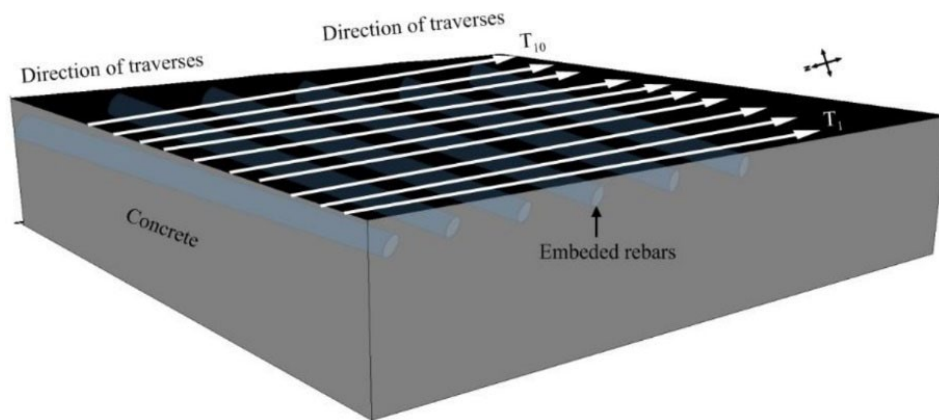


Figure 40. GPR and IE Test Direction Relative to the Rebar Position

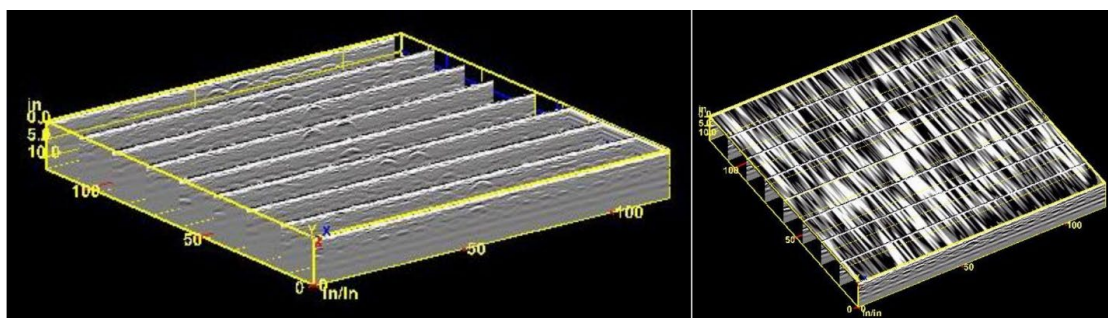


Figure 41. GPR Parallel Profiles (left) and Possible Detected Reinforcement (right) of the Top Surface Section Using the 2.5 GHz Frequency Antenna

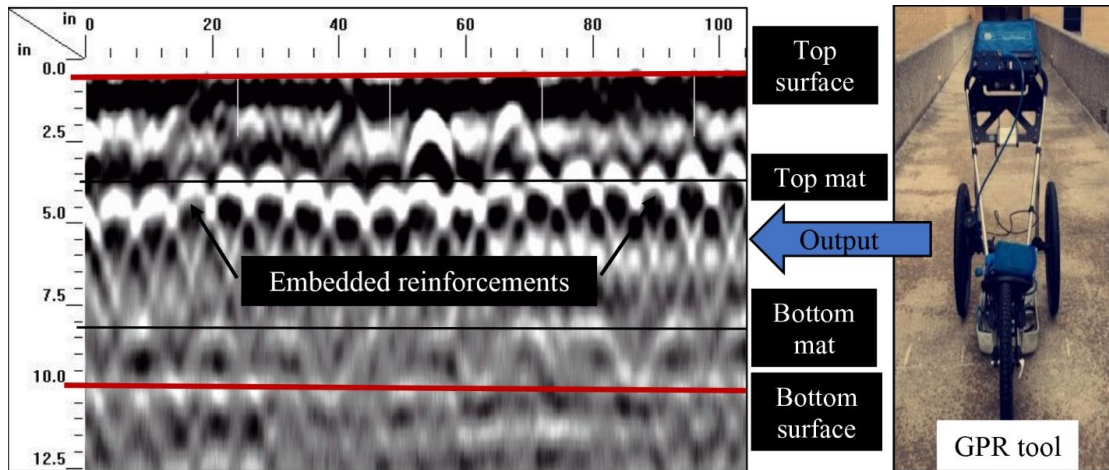


Figure 42. Processed GPR Output Showing Top and Bottom Rebar Mats

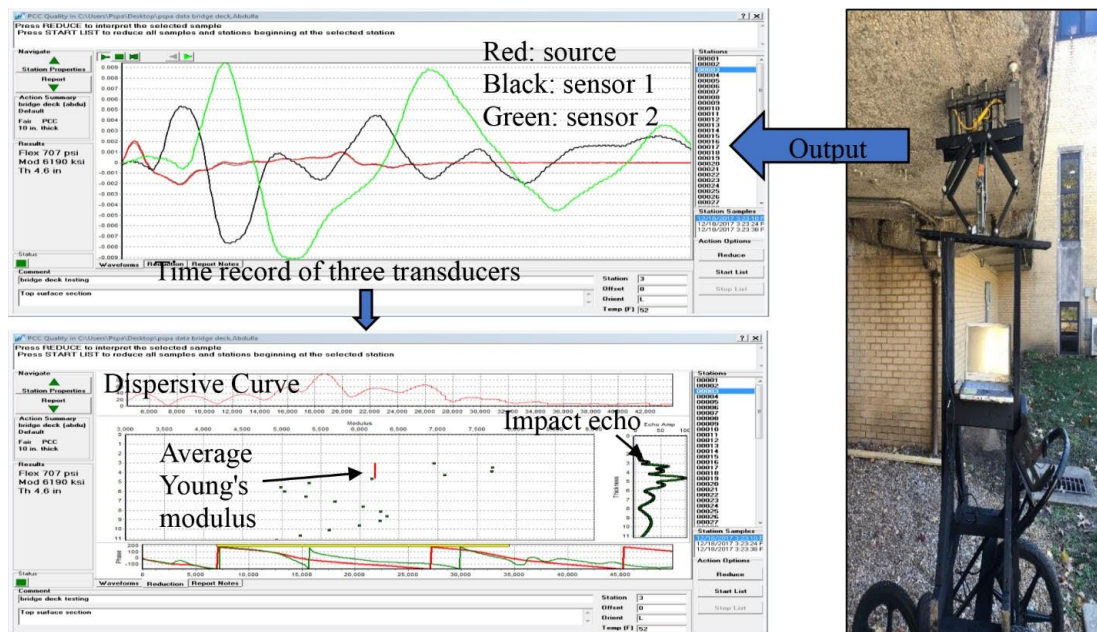
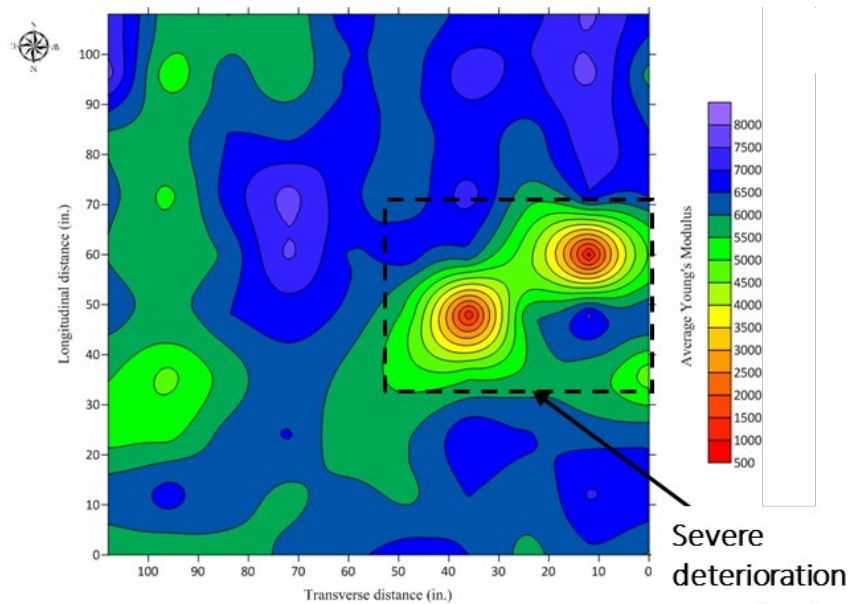


Figure 43. Processed PSPA Output Showing the USW and IE Results

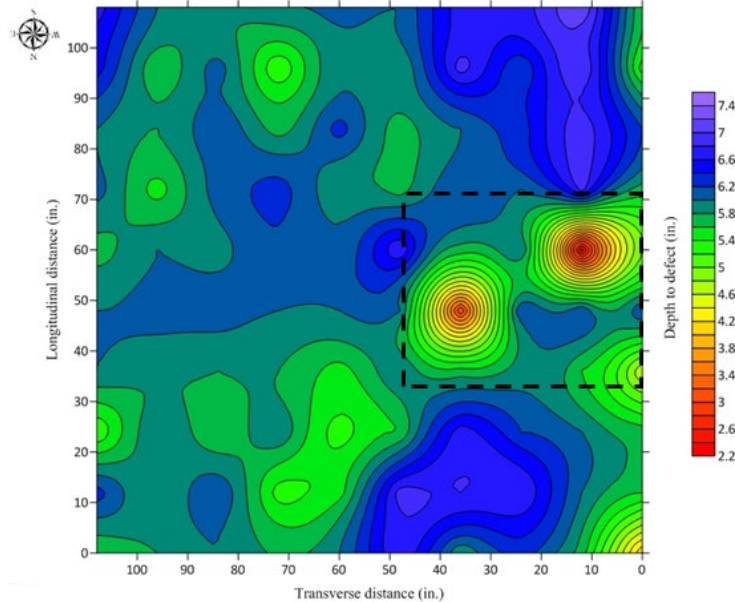
The significant inconsistency in apparent depth to the top layer of embedded concrete reinforcement, as illustrated in Figure 42, was observed due to the irregular reinforcement mat, including the potential addition of reinforcement placed during the rehabilitation/repair project. These uncertain factors made the GPR data interpretation a challenge in the bridge deck assessment. As such, further GPR results are not presented in this report.

Figures 44 and 45 present the USW and IE variation maps from the topside and underside surveys of the bridge deck, respectively. The dashed box indicates significant deterioration while the solid box represents the location of visually observed exposed rebar and concrete spalling. The two methods (USW and IE) showed corresponding results from the topside and underside deck

surveys. At the top section as shown in Figure 44, areas of high deterioration indicated by a low range of average Young's Modulus, less than 2901 ksi (20 GPa), and a high range of depth to defects 2 – 5 in (5.1-12.5 cm). At the bottom section as shown in Figure 45, areas of high deterioration indicated by a low range of average Young's Modulus, less than 2901 ksi (20 GPa), and a high range of depth to defects 2 – 4 in (5.1-10.2 cm). An extensive deterioration area was observed approximately at the western part of the bottom section near the exposed reinforcement corrosion area.



(a) Average Young's Modulus (USV)



(b) Depth to defects (IE)

Figure 44. Topside Deck Survey: (a) USV and (b) IE Variation Map

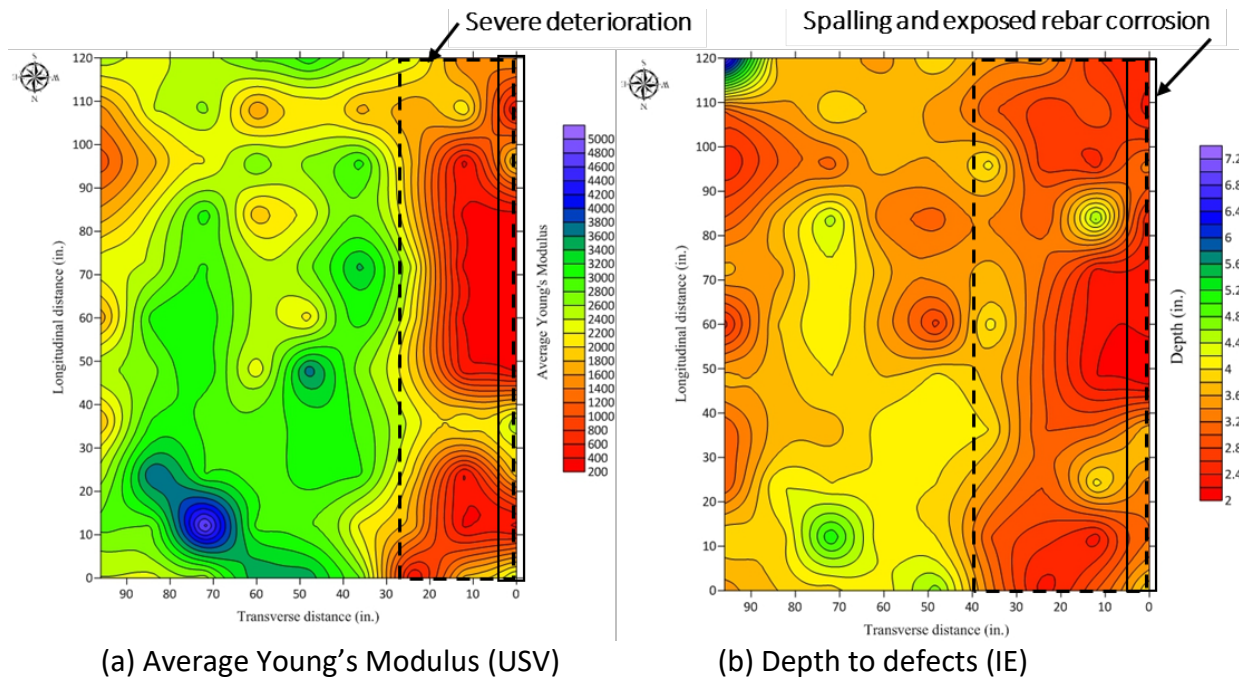


Figure 45. Underside Deck Survey: (a) USV and (b) IE Variation Map

5.3 Microwave 3D SAR Bridge Imaging

The middle section of this bridge was manually scanned using a wideband horn antenna connected to a field-portable vector network analyzer (VNA). Custom-made software programs on a PC read the data from the VNA as it measured the reflection coefficient across a frequency band of 1 to 4 GHz (matching the specifications of the antenna). These measurements were conducted on a 2D measurement grid with 4 in (10 cm) spacing. The antenna, which had an aperture of approximately 9 × 7 in (230 × 180 mm), was manually moved across this grid. However, an optimally designed robotic automated scanning platform can also be used along with antenna arrays to speed up the data collection process and to reach inaccessible areas (Ghaser et al., 2017). The collected data were then processed using the SAR algorithm to form 3D images. Two-dimensional (2D) image slices at depths of interest were then produced. Figure 46 shows the image produced from the underside of the bridge and focused on a depth of 1.57 in (40 mm) inside the concrete (closely corresponding to the location of rebar). This image shows more severe delamination near the edge of the bridge and its extent and spread towards the middle section of the bridge. Also visible in this image are two indications near X = 20 in (500 mm): one which corresponds to a location in the concrete with signs of deterioration and another which does not correspond to any visible distress. This latter indication may correspond to a void, pocket of high moisture, or an unknown embedded structure (e.g., drainage pipe) inside the bridge, which can be verified with additional testing or better yet with destructive testing.

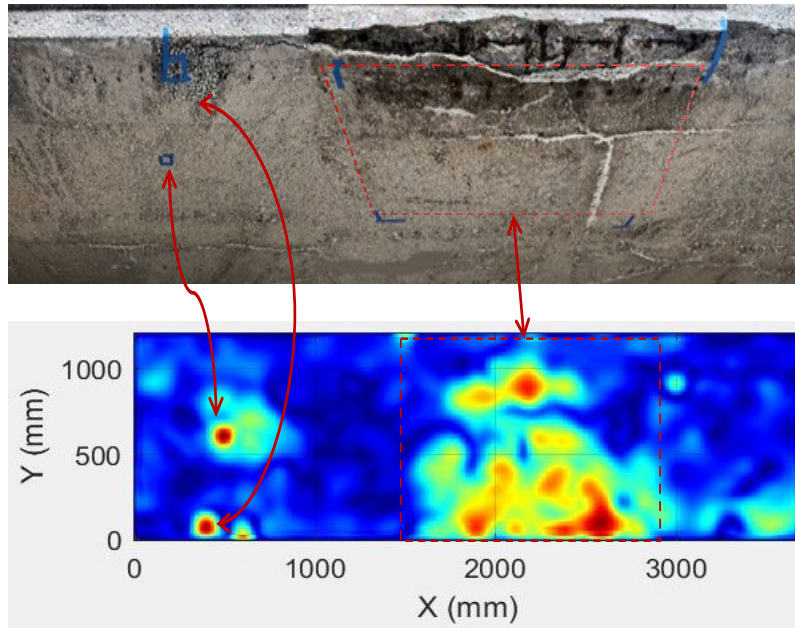


Figure 46. SAR Image of Underside Deck Corresponding to Damage Areas

Another scan was performed on the top side of the bridge deck, as shown in Figure 47, corresponding to a depth of approximately 3.15 in (80 mm) inside the concrete. Due to the repair and resurfacing work, the exact depth of the first rebar layer could not be ascertained. It was uncertain whether additional rebar mesh was placed on top of the original top rebar layer. The image in Figure 47 shows indications of degradation in multiple areas of the bridge. These can be due to rebar corrosion and concrete delamination or features in the bridge deck from the repair work conducted in the past.

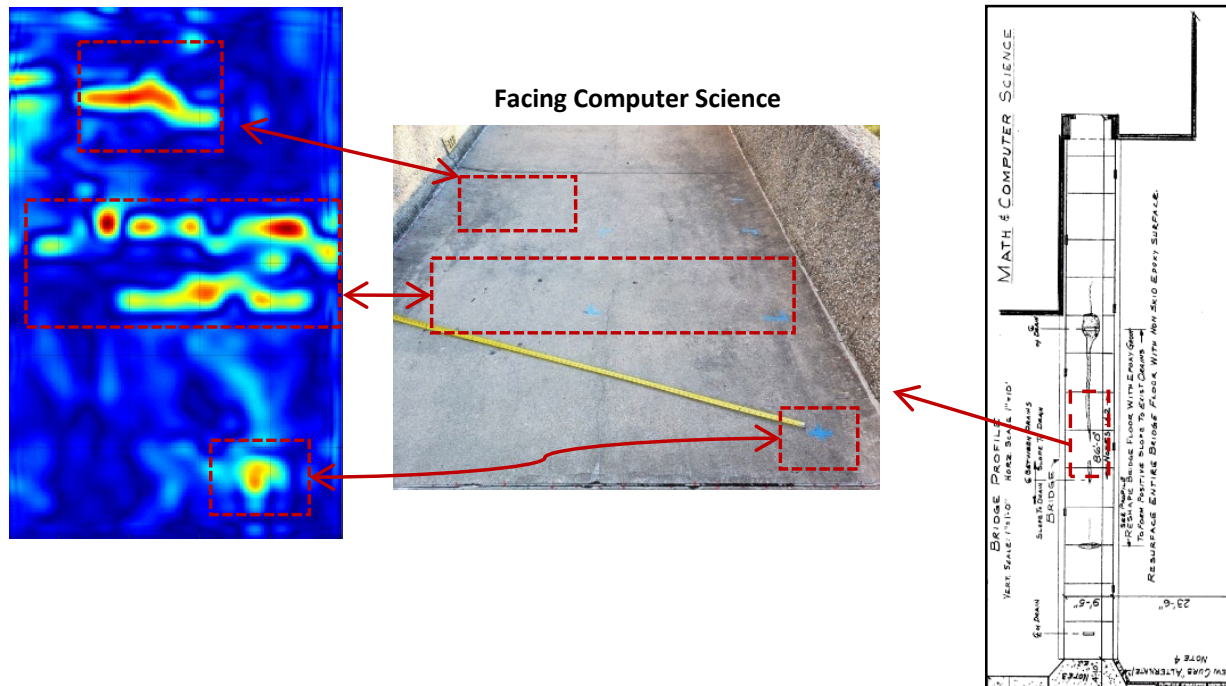


Figure 47. SAR Image of a Section of the Topside of the Bridge

5.4 Concluding Remarks

The findings on the pedestrian bridge are summarized as follows:

- Due to energy dissipation and wave dispersion through heterogeneous concrete materials, a GPR survey on the top surface of the bridge deck cannot detect structural condition deterioration such as concrete delamination and steel rebar corrosion on the underside of the deck. Considering a significant inconsistency in the apparent depth of embedded top-layer reinforcement, GPR data from the top surface of the bridge deck were difficult to interpret for the overall bridge deck integrity assessment.
- USW and IE were used to determine concrete quality of the bridge deck by estimating the Modulus of elasticity and depth to embedded defects, respectively. The west part of the bottom section dominated by a lower-than-average Young's Modulus and high depth to defects corresponds to the exposed corroded rebars area. This pilot study indicated that the bottom surface surveying may be effectively implemented in the bridge deck assessment.
- On the other hand, microwave 3D SAR imaging has shown potential in detecting steel corrosion and delamination in concrete structures. A section of the bridge was scanned from the top and bottom and the results showed indications of the extent of delamination and other damage inside the bridge. However, follow-up NDTs and destructive tests (as part of future planned repairs) may shed additional light on the feasibility of microwave SAR imaging for in-field inspection of bridges.

CHAPTER 6. CASE STUDIES ON REPRESENTATIVE BRIDGES

To date, 54 of the 72 selected bridges in the states of Missouri, Wisconsin, Georgia, Virginia, and Texas were inspected (Shi et al., 2023). The remaining bridges in New York and California were not visited due to UAS flight restrictions and coordination challenges. A Phantom 4 or Skydio 2 drone equipped with a RGB camera was used to inspect the side of the bridge and the topside of the bridge deck. An Elios 2 drone equipped with a RGB camera was used to inspect the underside of the bridge deck, especially in confined channels between bridge girders for close-up inspection. A Headwall DJI M600 drone equipped with both FLIR infrared and hyperspectral cameras was used to scan subsurface delamination and surface chemical species. A Nikon camera was used to inspect drone-inaccessible and high-priority areas. Drone inaccessible scenarios include tree branches and bushes that become obstacles for drone flight near bridge spans, high-water level conditions, tight flying spaces, and other unsuitable flying conditions due to severe weather (high wind, high-humidity, and extreme temperatures) or a dusty environment.

In this chapter, representative RGB, thermal, hyperspectral, and LiDAR data from different UAVs are presented first. They are followed by a comparison between automated and manual inspections. The last two sections highlight how INSPIRE Center's BIRDS mobile test facility produces unique datasets both in air and under water at highway and river-crossing bridges.

6.1 Georgia Highway Bridges

This subsection presents the representative inspection data for Georgia state bridge 5700510 in the age group of 35-40 years. Figure 48 shows RGB images taken from the Phantom 4. It can be observed that cracks appear on the roadway near the approach spans and the outside of the exterior girders are painted. Figure 49 shows images from the Nikon camera for high-priority inspection areas. Minor spalling, rebar exposure, and drainage water marks can be noticed at the bridge caps. This is further revealed by Elios 2, as shown in Figure 50. Both the inside of the exterior girders and interior girders appear uncoated. Figure 51 shows thermal images from the FLIR camera. The cracks can be noticed on the road before the bridge approach spans. The main bridge span does not reveal noticeable delamination. Figure 52 shows the point cloud explored as one of the digitization approaches for virtual bridge asset management.





(c)



(d)

Figure 48. Georgia Bridge 5700510 (Phantom 4)



(a)



(b)



(c)



(d)

Figure 49. Georgia Bridge 5700510 (Nikon)

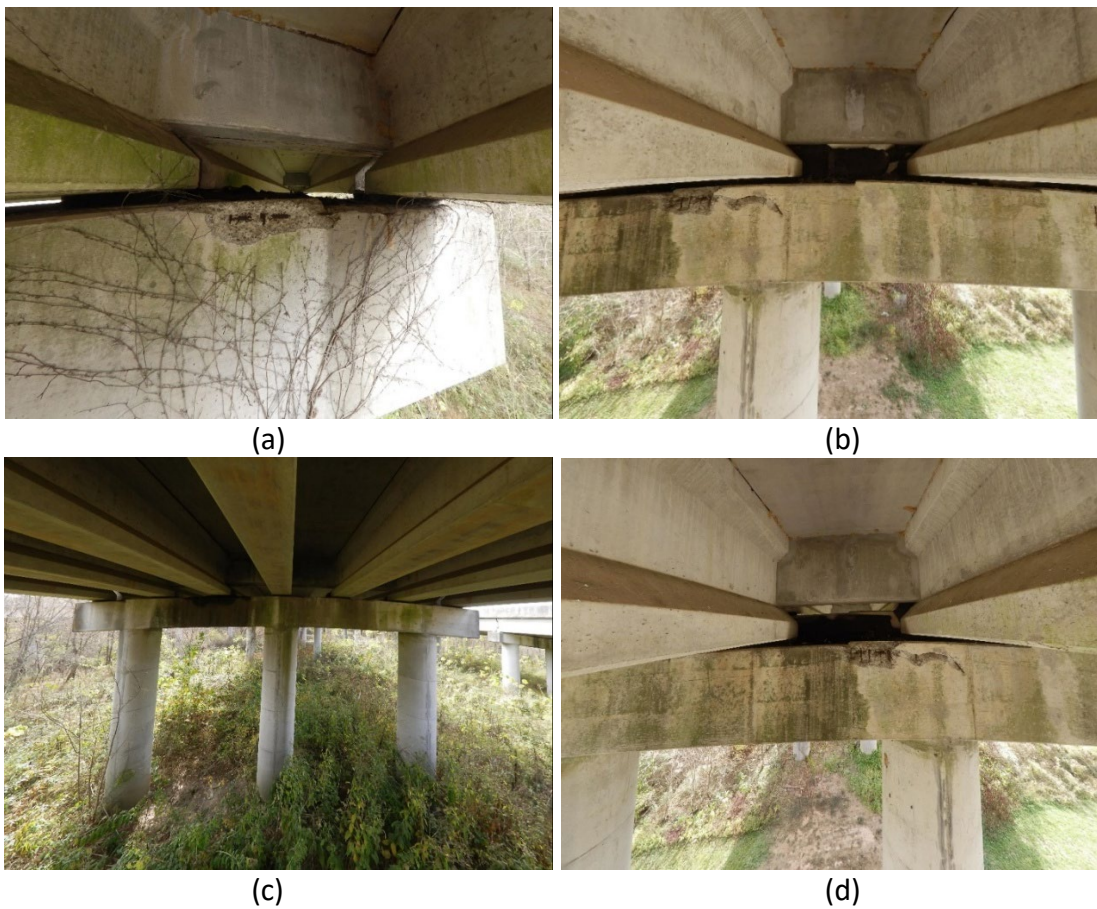
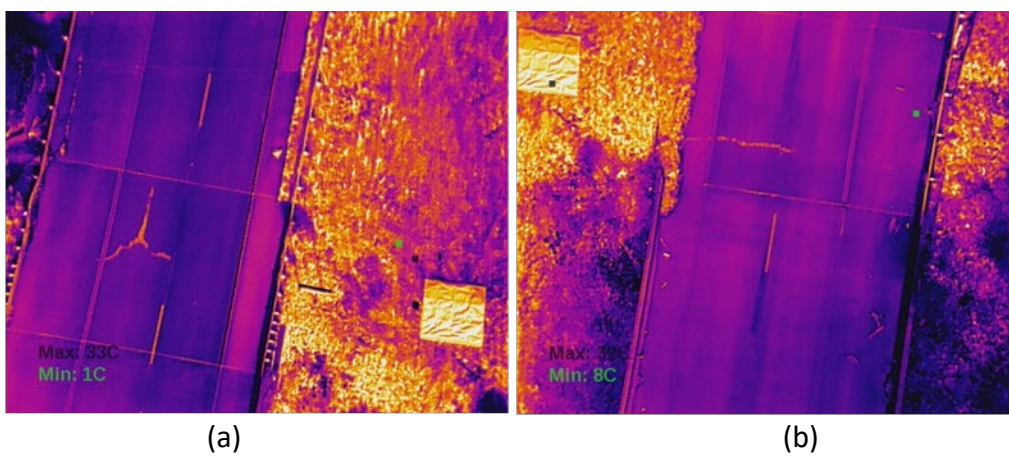


Figure 50. Georgia Bridge 5700510 (Elios 2)



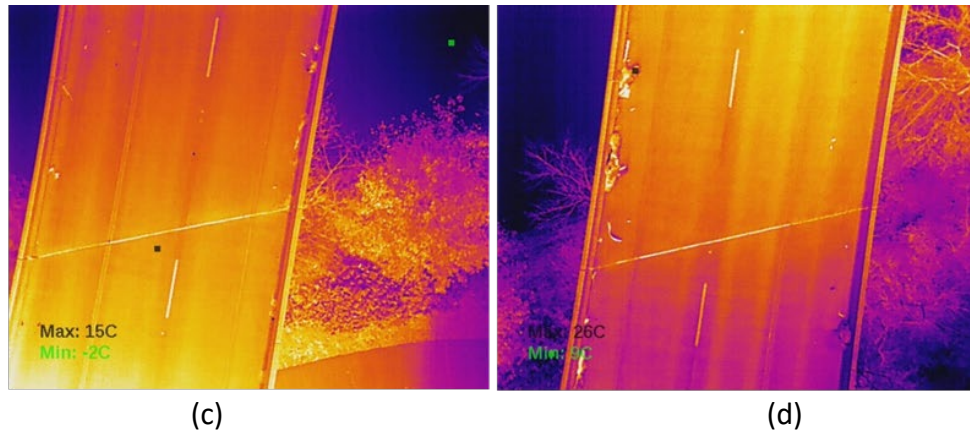


Figure 51. Georgia Bridge 5700510 (FLIR)

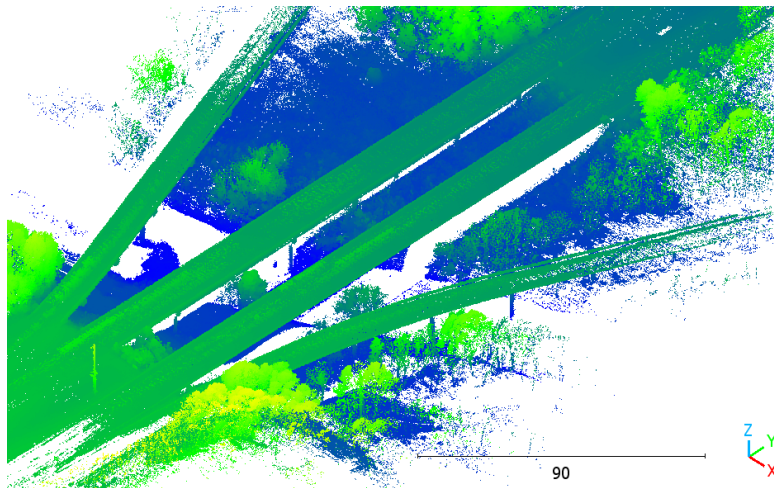


Figure 52. Point Cloud for Georgia Bridge 5700510 from Headwall (unit: m, 1 m = 3.28 ft)

6.2 Missouri Highway Bridges

This subsection presents the representative results of two Missouri bridges: a steel bridge (A4988) and a prestressed concrete girder bridge (A5805). Figure 53 shows images of the steel bridge A4988 taken from the Parrot Anafi drone, while Figure 54 shows images taken from the Nikon camera. This bridge in the age group of 15-20 years is in good condition. Figure 55 shows images taken from the Elios 2 drone with no major damage observed at the time of the inspection. Figure 56 shows the thermal images taken from the FLIR camera. Joints and road surface patches can be clearly noticed before the approach spans. No major damage is noticed for the deck of the main spans.





(c)



(d)

Figure 53. Missouri Steel Bridge A4988 (Parrot Anafi)



(a)



(b)



(c)



(d)

Figure 54. Missouri Steel Bridge A4988 (Nikon)



(a)



(b)

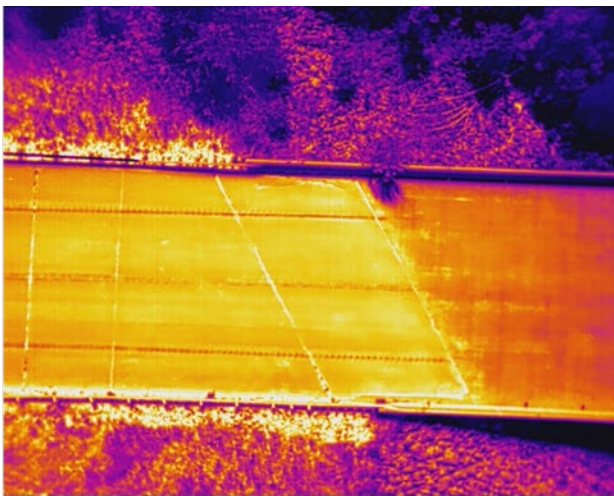


(c)

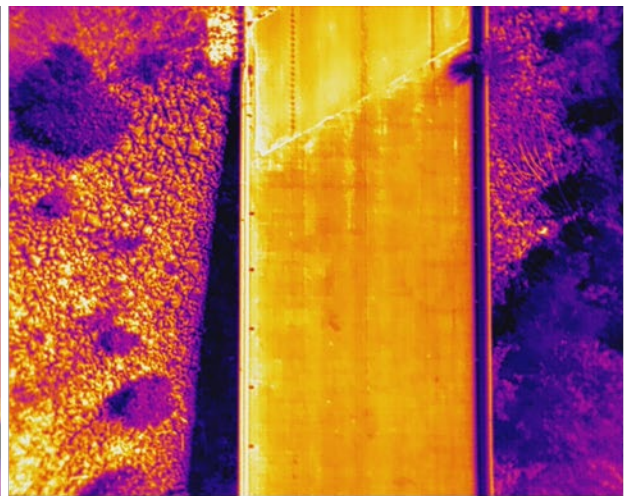


(d)

Figure 55. Missouri Steel Bridge A4988 (Elios 2)



(a)



(b)

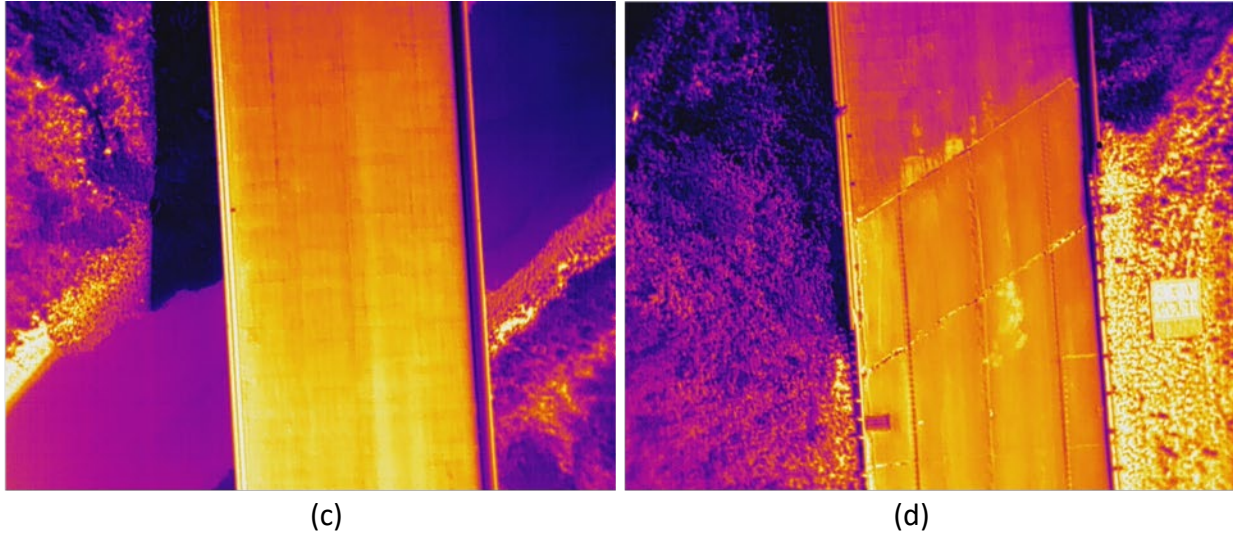
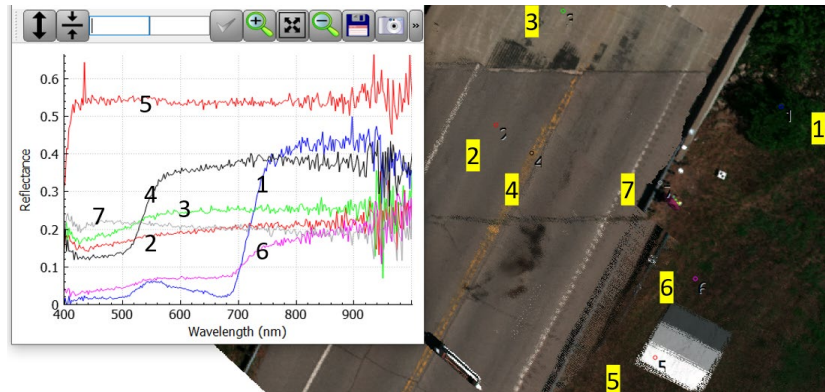
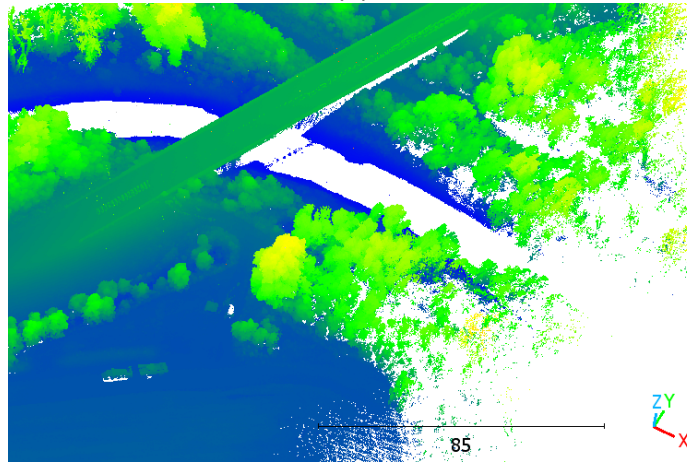


Figure 56. Missouri Steel Bridge A4988 (FLIR)

A Hyperspectral image contains continuous spectral information for each pixel of the image and is typically useful for discrimination and characterization of similar colors. The data is stored in a 3-dimensional (2 spatial dimension + 1 spectral dimension) hypercube that consists of a stack of images with wavelength information of the pixel. Figure 57 (a) shows a hyperspectral image taken from the Headwall's Visible Near Infrared (VNIR) hyperspectral camera with a wavelength of $1.57 \times 10^{-5} - 3.94 \times 10^{-5}$ in (400-1000 nm) for Missouri bridge No. A4988. It can be noticed that hyperspectral images have continuous spectral information at each pixel. Seven points are picked from the image to demonstrate their distinctive spectra. The spectrum jumps near 2.83×10^{-5} in (720 nm) at the vegetation area of point 1 and around 2.13×10^{-5} in (540 nm) at the solid yellow traffic line of point 4. At the white tarp of point 5, the spectrum shows the highest reflectance starting from 1.81×10^{-5} in (460 nm). The two different road surface materials also show quite different reflectance. The darker asphalt (point 2) shows the lower reflectance compared to the lighter color concrete area (point 3). The bluish guard rail of point 7 shows a gradual decrease from 1.81×10^{-5} in (460 nm) to 3.94×10^{-5} in (1000 nm). The rusty area of point 6 for exposed ground soil shows a general increase from 2.68×10^{-5} in (680 nm) to 3.15×10^{-5} in (800 nm). Figure 57(b) shows the generated point cloud from the Headwall LiDAR sensor, which serves as an intermediate step to digitize bridge assets for anywhere and anytime virtual inspection by anyone authorized to access.



(a)



(b)

Figure 57. Point Cloud for MO A4988 from Headwall (unit: m, 1 m = 3.28 ft)

For Missouri bridge A5805 in the age group of 15-20 years, Figures 58-60 present representative images taken from the Phantom 4 drone, the Nikon camera, and the Elios 2 drone. They show no indication of deterioration or damage. Figure 61 shows several thermal images taken above the bridge deck from the FLIR camera. The joints near the approach can be clearly noticed. The main bridge deck shows no key issues. Figure 62 shows the point cloud generated for bridge A5805 explored to digitize bridge assets.



Figure 58. Missouri Prestressed Concrete Bridge A5805 (Phantom 4)

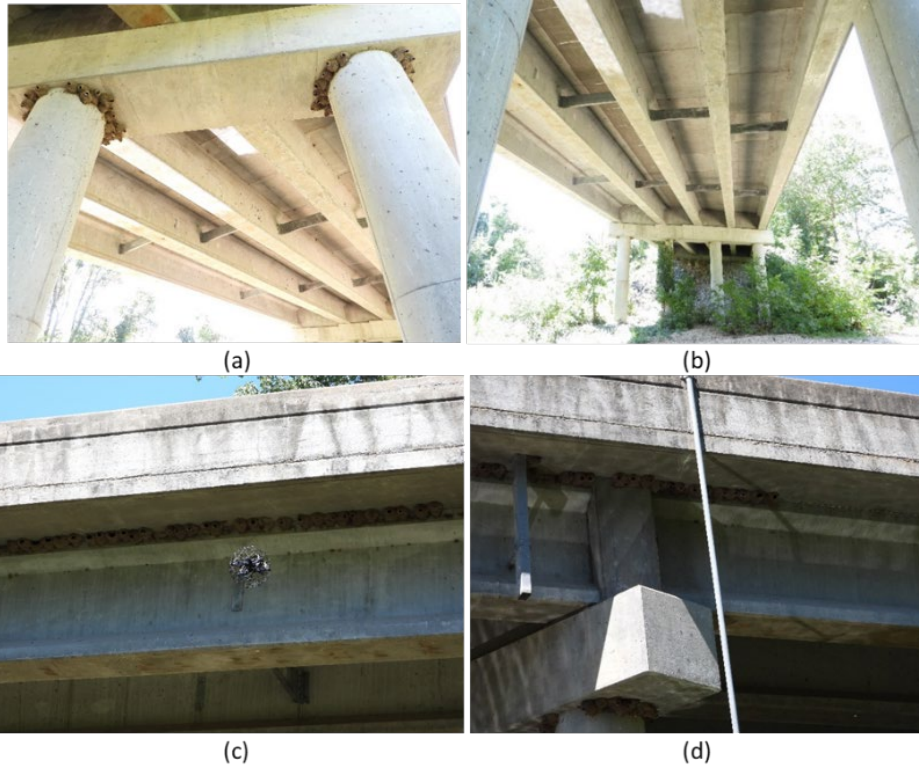


Figure 59. Missouri Prestressed Concrete Bridge A5805 (Nikon)

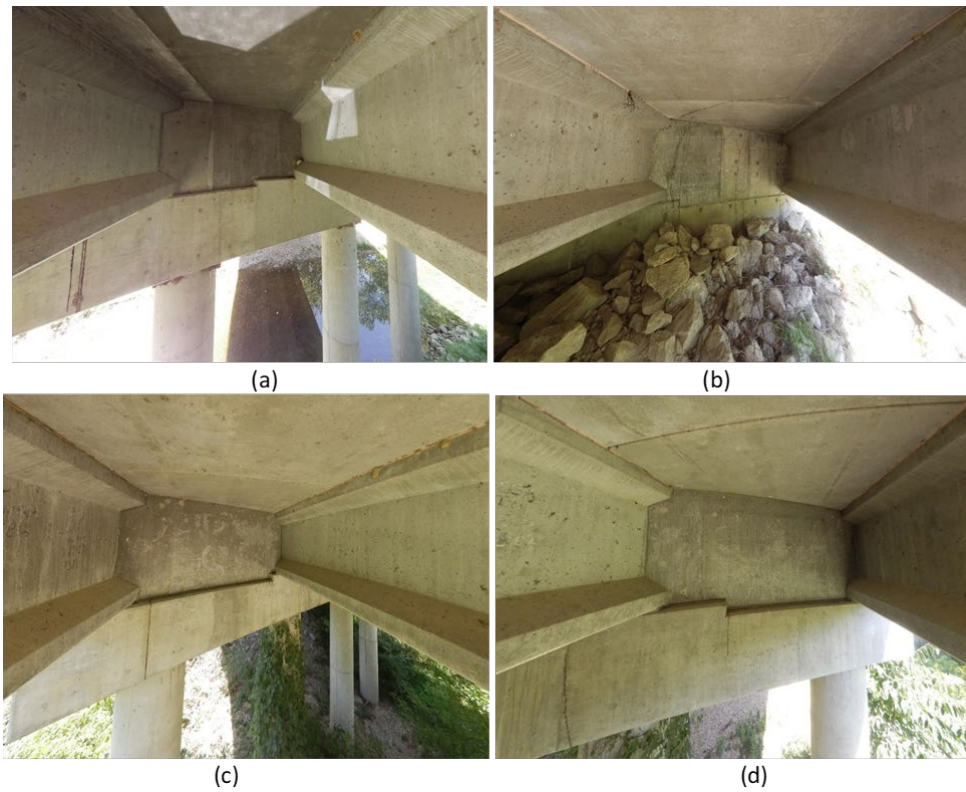


Figure 60. Missouri Prestressed Concrete Bridge A5805 (Elios 2)

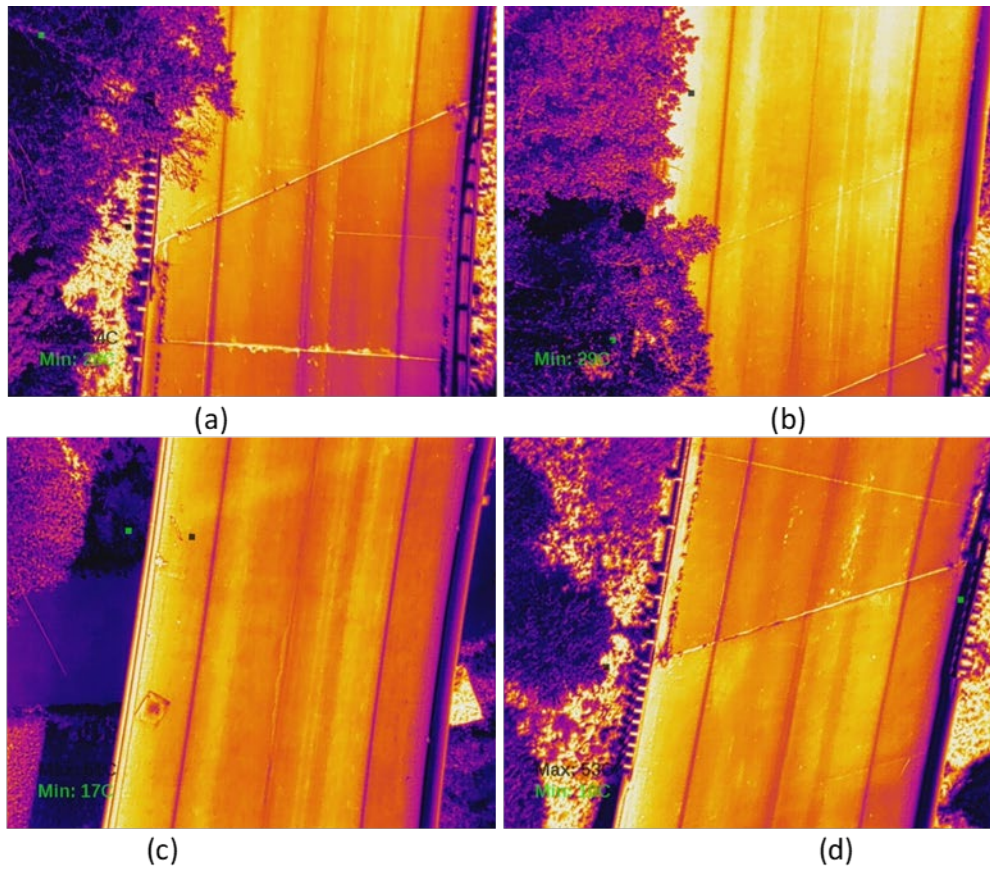


Figure 61. Missouri Prestressed Concrete Bridge A5805 (FLIR)

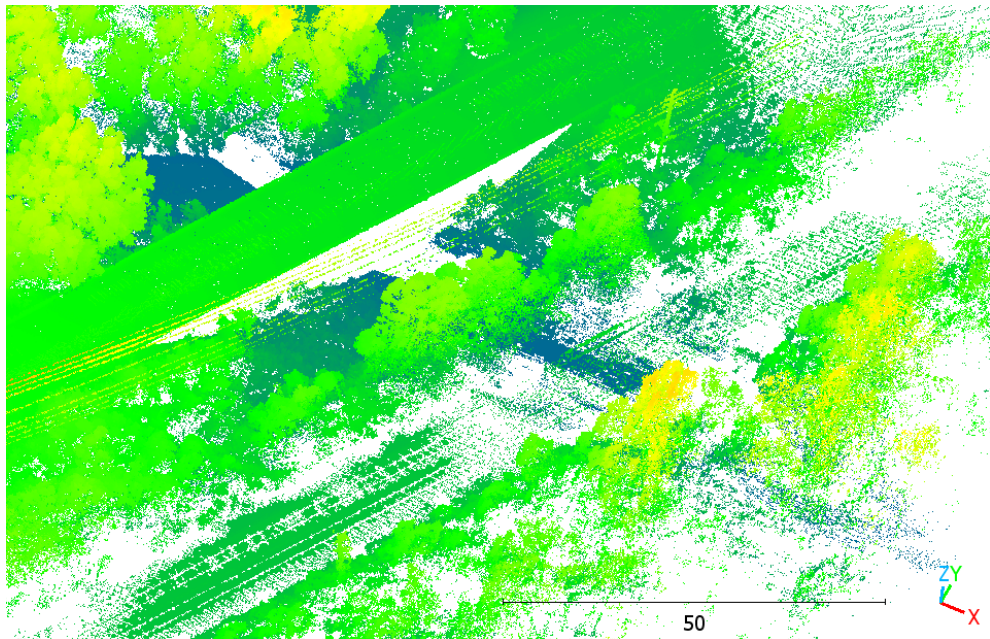


Figure 62. Point Cloud for Missouri Bridge A5805 from Headwall (unit: m, 1 m = 3.28 ft)

6.3 Texas Highway Bridges

This subsection presents example inspection results for Texas bridge 151630002405167 in the age range of 35-40 years. The presented bridge example is a composite bridge with both pre-stressed concrete spans and steel girder spans. Figure 63 shows representative images from the Phantom 4. Some bridge deck surface abrasion can be noticed. Heavy corrosion can also be observed on the girders, especially at the supports. As shown in Figure 64, images from the Nikon camera reveal scouring around foundations of the bridge columns and rain drainage marks at the bridge caps. Misalignment of the deck and bridge cap can also be noticed. Figure 65 shows images taken from the Elios 2, further revealing the drainage issues at the joints. Figure 66 presents thermal images from the FLIR camera. The rough surface and boundary corrugated marks can be clearly noticed. Figure 67 shows the point cloud generated for the bridge as one of the digitization processes of bridge assets.

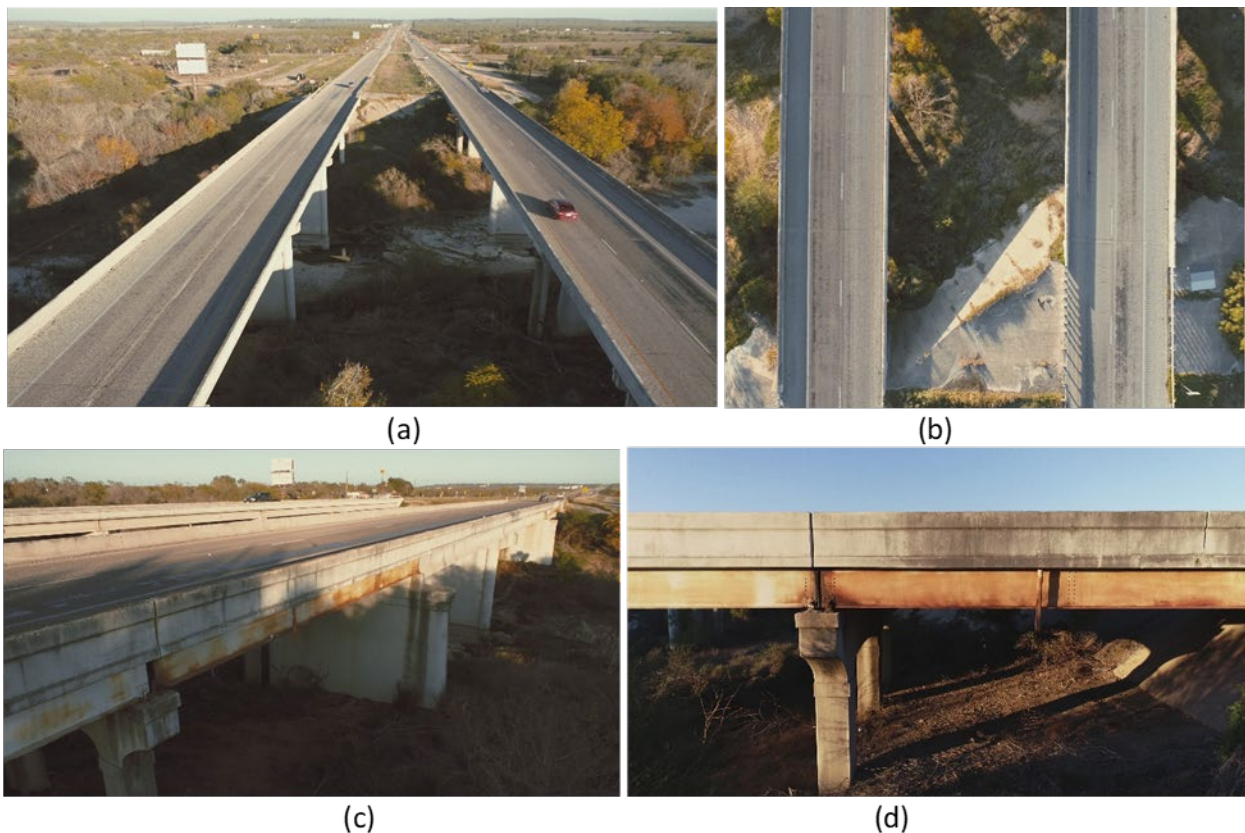


Figure 63. Texas Bridge 151630002405167 (Phantom 4)



(a)



(b)



(c)



(d)

Figure 64. Texas Bridge 151630002405167 (Nikon)



(a)



(b)

Figure 65. Texas Bridge 151630002405167 (Elios 2)

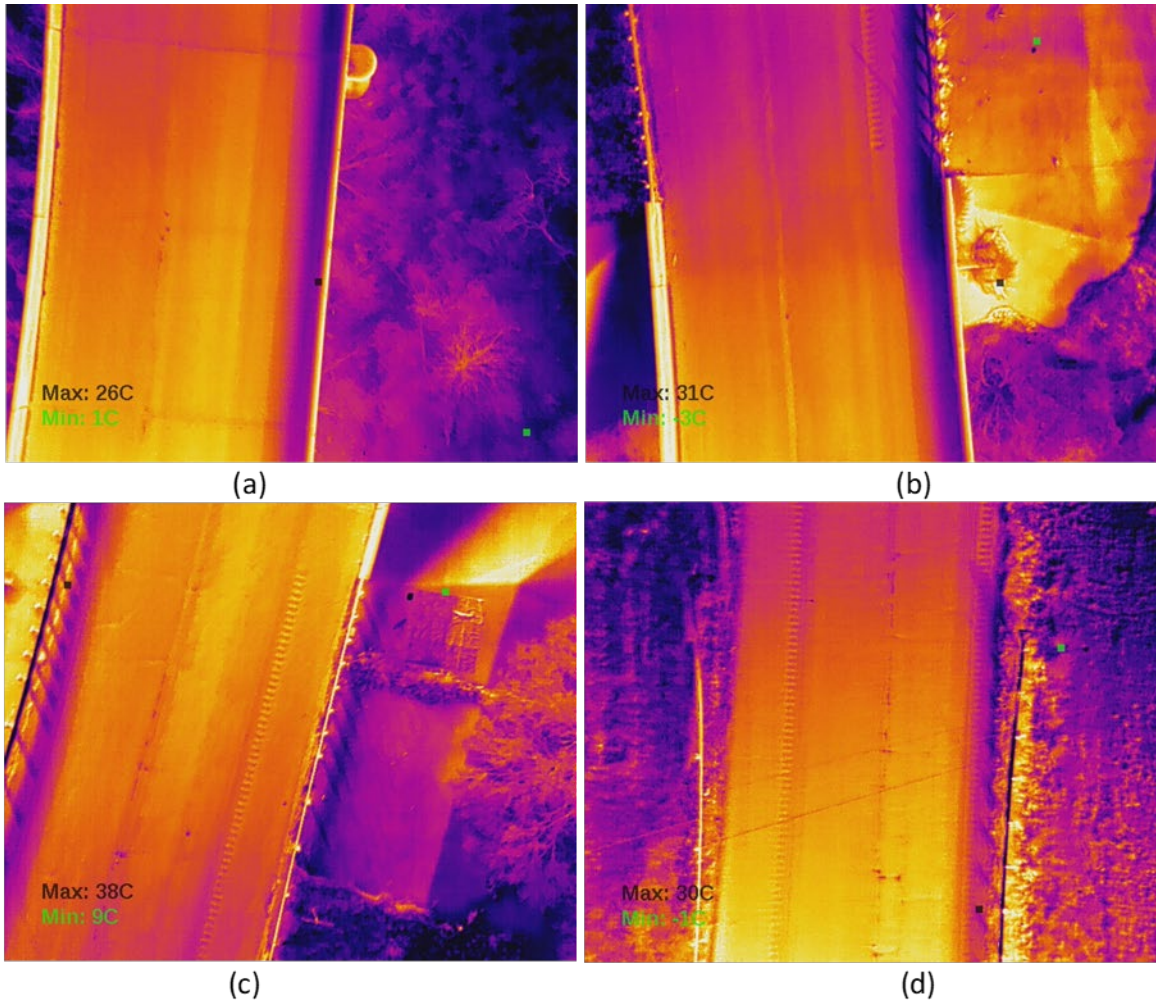


Figure 66. Texas Bridge 151630002405167 (FLIR)

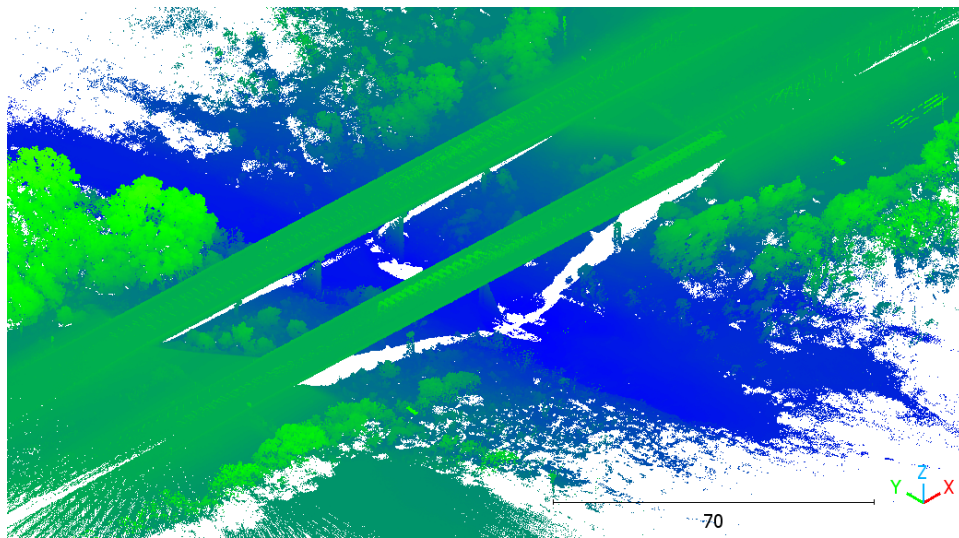


Figure 67. Point Cloud for Texas Bridge 151630002405167 from Headwall (unit: m, 1 m = 3.28 ft)

6.4 Virginia Highway Bridges

This subsection presents the inspection results for Virginia bridge 11562 in the age group of 35-40 years. Figure 68 presents some of the images taken from the Skydio 2. Specifically, Figure 68(a) shows the overall top view of the bridge with surface changes noticed at the approach spans. Figure 68(b-d) shows the side view of the bridge with corrosion at the support and the middle part of the exterior steel girders, where only partial painting remains near the support. Figure 68(e) shows a 3D model of the bridge generated from Agisoft using individual images and videos. The 3D model enables an overview of the entire bridge from any perspective, potentially enabling virtual inspection of the bridge anywhere and anytime by anyone authorized to access.

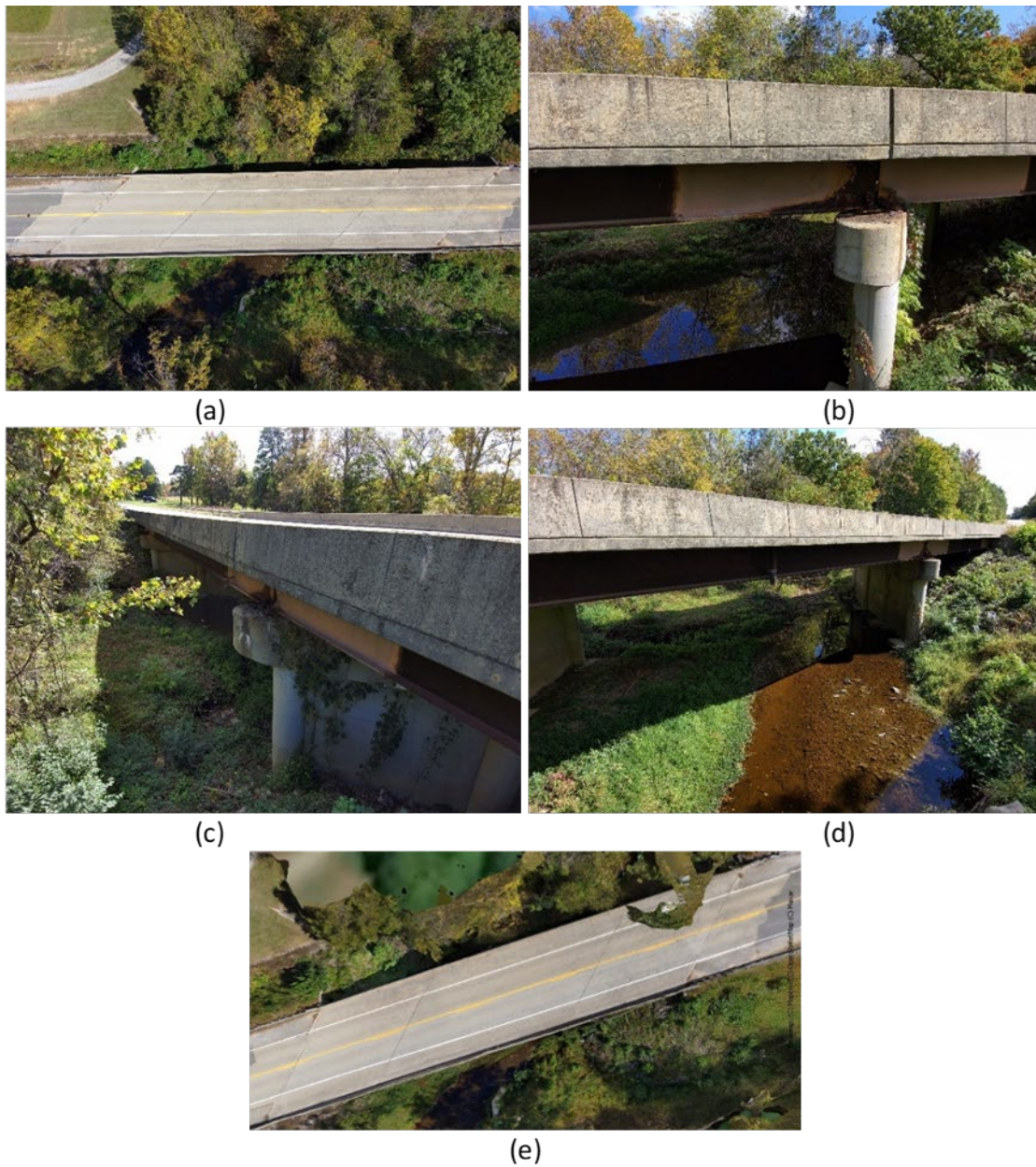


Figure 68. Virginia Bridge 11562 (Skydio 2)

Figure 69 shows images taken from the Nikon camera. Corrosion issues and deterioration at the support can be noticed clearly. Spreading of the corrosion on the steel girders can also be noticed, which is consistent with the observations from the Skydio 2 and the Elios 2. Figure 70 shows images taken from the Elios 2. These images further reveal the corrosion issue at the supports, and the drainage issue at the concrete caps which may be a cause for the corrosion. Corrosion patterns can be noticed at the steel girders. The inner side of the exterior girder shows good condition of the paint, while interior girders show rust at the mid-span. In general, bridge supports present a consistent corrosion issue. Figure 71 presents a 3D thermal model of the bridge generated from individual thermal images using photogrammetry. Such a 3D thermal model enables an overview of the bridge from any angle in top view as the DJI M600 drone collects data above the bridge only. Major patch issues and asphalt surface changes can be noticed at the approach spans. Note that thermal imaging is effective for subsurface delamination, but it requires a temperature change. The best time would be 10 am – 2 pm with sunny conditions for rising temperature data collection and after sundown for decreasing temperature data collection.

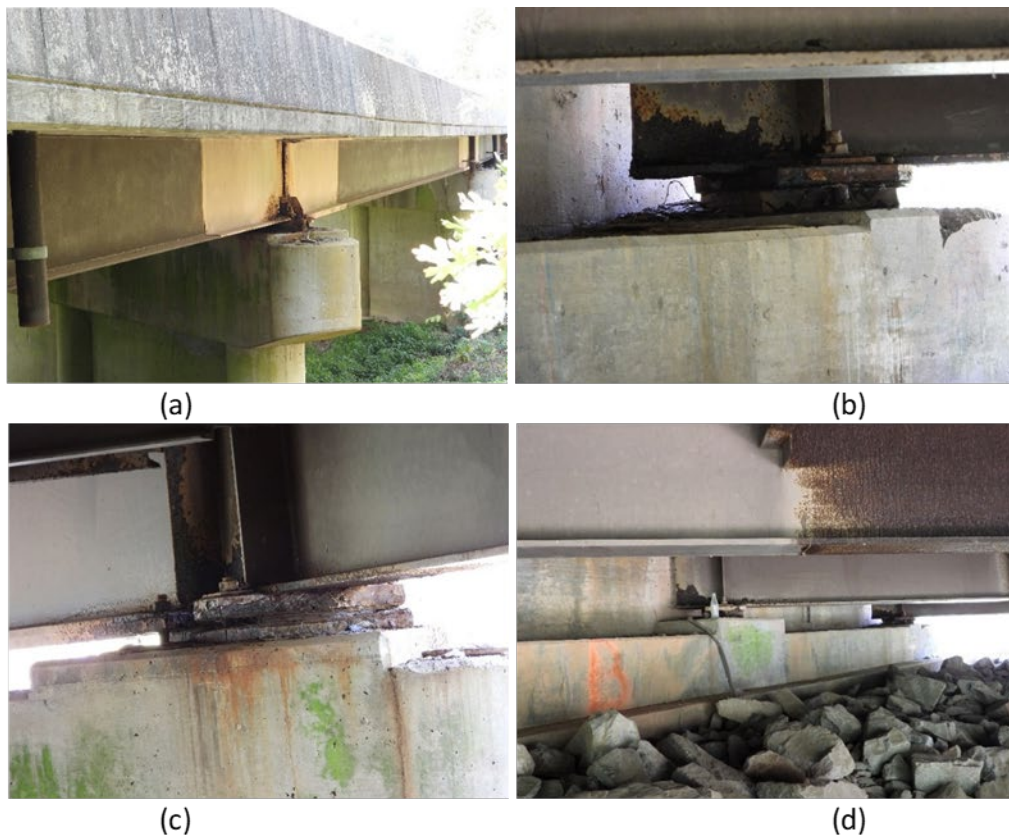


Figure 69. Virginia Bridge 11562 (Nikon)



Figure 70. Virginia Bridge 11562 (Elios 2)

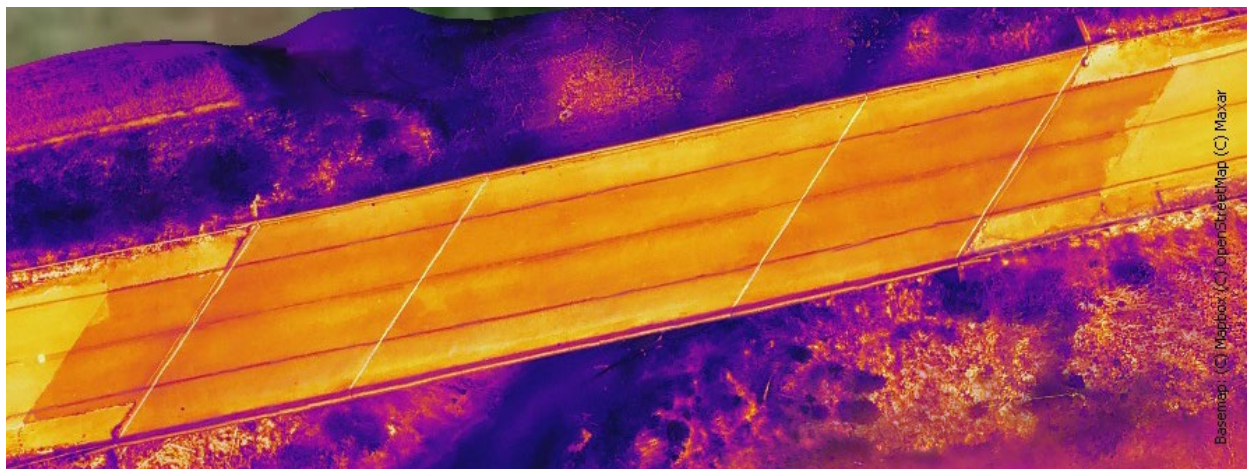


Figure 71. Virginia Bridge 11562 (FLIR)

Figure 72 presents the reconstructed 3D model of bridge No. 29171 in Agisoft software from videos recorded by the Skydio 2 drone. This reconstruction is limited to the top view of the bridge as it is a challenge to collect data upward underneath the bridge deck.



Figure 72. 3D Reconstruction of the Virginia Bridge No. 29171

As shown in Figure 57(a) for the Missouri bridge, Figure 73 presents the hyperspectral image at one end of the bridge taken from Headwall's VNIR hyperspectral sensor for Virginia bridge No. 11562. Similar observations can be made from seven points on the roadway and its surrounding. Figure 74 shows the point cloud generated from the Headwall drone, which is explored as one of the approaches to digitize bridge assets for long term bridge health monitoring studies.

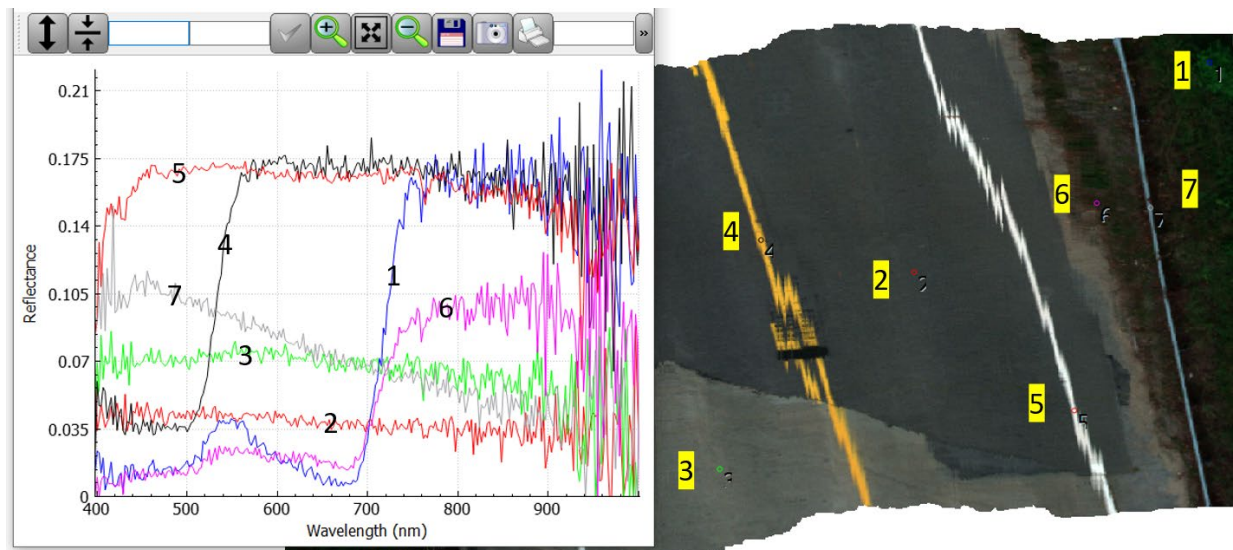


Figure 73. Hyperspectral Image for VA 11562

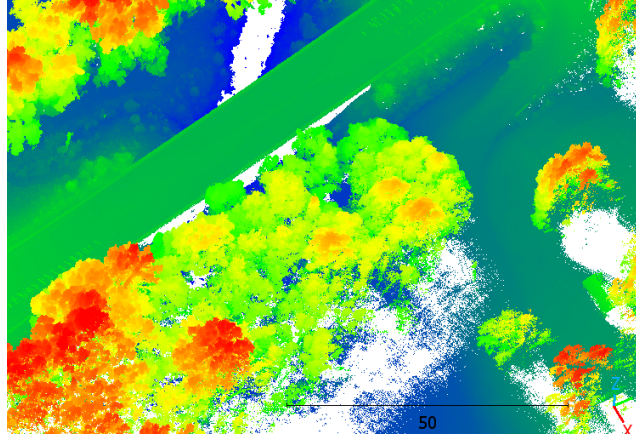


Figure 74. Point Cloud for VA 11562 from Headwall (unit: m, 1 m = 3.28 ft)

6.5 Wisconsin Highway Bridges

This subsection presents the representative data for Wisconsin state bridge B090209 in the age range of 15-20 years. Overall, the bridge is in good condition except minor corrosion at the approach span support, cracks at the abutment, and dense roadway cracks before the approach spans. Figure 75 presents an overview (top view) of the bridge deck and approach slab with noticeable cracks. Figure 76 presents close-up views underneath the bridge from the Nikon camera on the ground. It includes the Elios 2 drone in the upward view. The flashlight on the Elios 2 drone provides sufficient lighting for inspecting the girder channels with dim lighting conditions. A part of the steel girder appears unpainted. Figure 77 shows additional close-up views on the underside of the bridge deck and cross frame taken from the Elios 2 drone. Figure 78 shows several FLIR thermal images. Along with regular RGB images, the cracks and construction joints before the approach spans can be clearly noticed in the thermal images. Figure 79 shows the point cloud of Wisconsin bridge B090209.

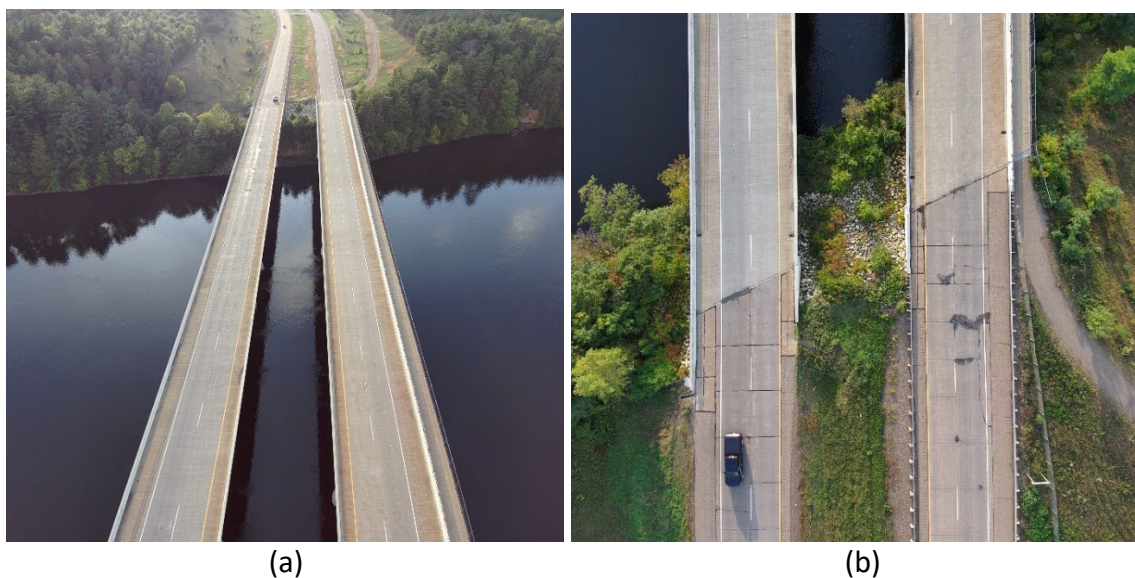
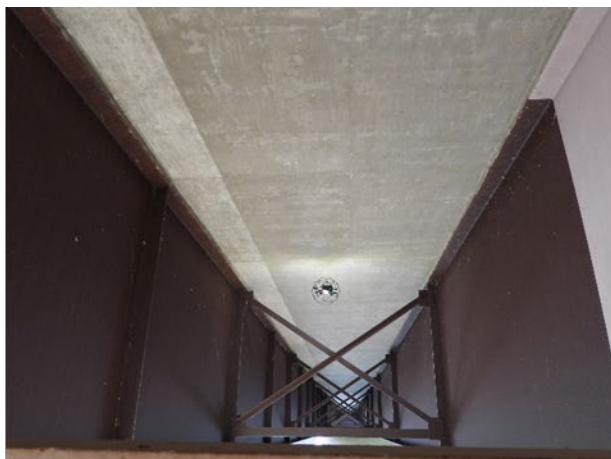
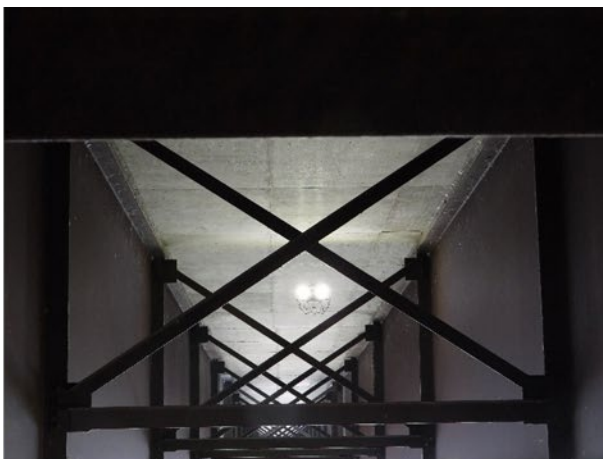


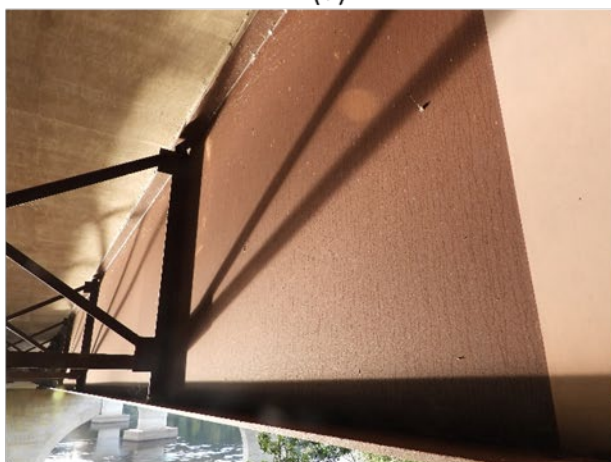
Figure 75. Wisconsin Bridge B090209 (Skydio 2)



(a)



(b)



(c)



(d)

Figure 76. Wisconsin Bridge B090209 (Nikon)



(a)



(b)

Figure 77. Wisconsin Bridge B090209 (Elios 2)

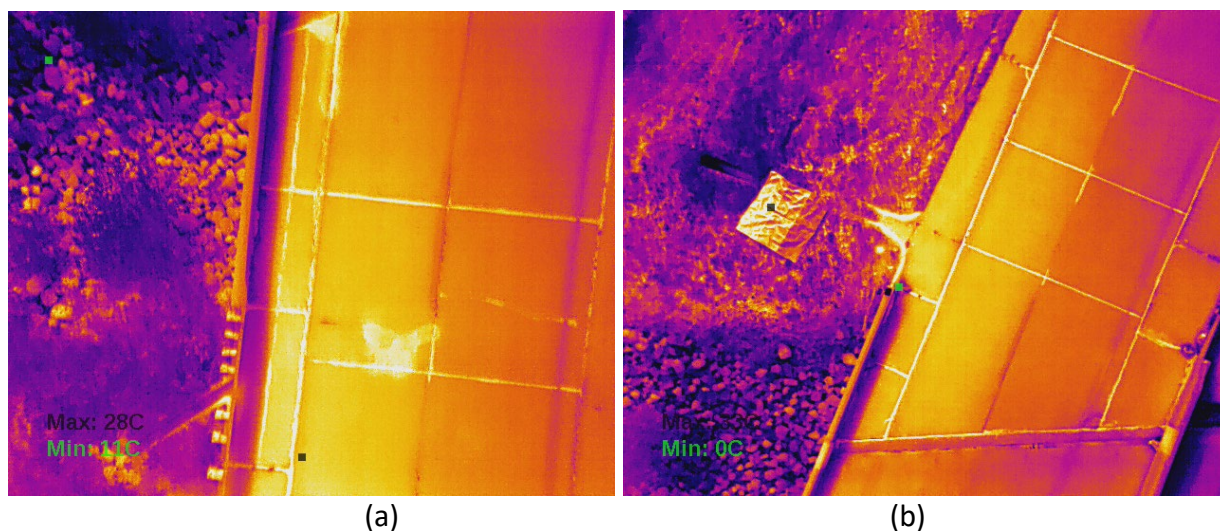


Figure 78. Wisconsin Bridge B090209 (FLIR)

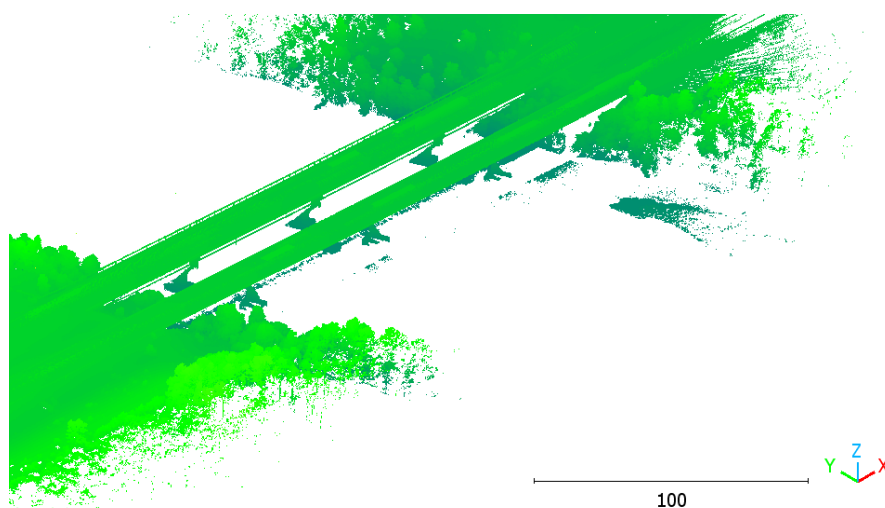


Figure 79. Point Cloud for Wisconsin Bridge B090209 from Headwall (unit: m, 1 m = 3.28 ft)

6.6 Automated vs. Manual Inspection of Highway Bridges

Section 6.1-6.5 presents example automated inspections of bridges using UASs. To have a comparative study in terms of inspection efficiency, data quality, and finding reporting, corresponding manual inspections of some of the selected highway bridges are reported in this subsection.

6.6.1 AASHTO Manual for Bridge Element Inspection

The American Association of State Highway and Transportation Officials (AASHTO)' *Manual for Bridge Element Inspection* (AASHTO, 2019) is referenced in this study. The guidelines and referenced photos to help define four condition states of each key defect are summarized in Appendix B. Manual inspection typically relies on simple tools such as laser (or tape) measures and binoculars. Although the *Manual* provides crack pattern and crack width measurement

guidelines by simply estimating their area and length, it remains difficult to quantify the damage with great efficiency and consistency in practice. However, the *Manual* does provide standardized terminologies that may be integrated into advanced robotic inspections. The condition state (CS) of a bridge can be categorized into four groups as listed in Table 12.

Table 12. Bridge Condition State Classes

Condition State (CS)	CS 1	CS 2	CS 3	CS 4
Description	Good	Fair	Poor	Severe

AASHTO Commonly Recognized (CoRe) Structural Elements include National Bridge Elements (NBE) and Bridge Management Elements (BME), as shown in Table 13. NBE covers primary load-carrying members, such as the deck and slabs, superstructure, substructure, and culverts as defined in FHWA's Recording and Coding Guide for the Structure Inventory and Appraisal of the Nation's Bridges. Additional elements included in this category are bridge railings and bearings.

Table 13. Bridge Elements Categorization

Element Type	National Bridge Elements (NBE)	Bridge Management Elements (BME)	Agency-Developed Elements (ADE)
Specific Elements	Deck and Slabs, Superstructure, Substructure, Culvert, Railings, Bearings	Joints, Approach slabs, Wearing surfaces, Protective coating systems, Deck/slab protection systems	Sub-elements of NBE and BME, ADE without any tie to NBE and BME - ID 800+

In an inspection report, the inspector may describe the elements (pieces of the bridge) and their quantities, severity of the defects, and the service environment. The inspector would record the predominant environmental factor affecting an element. Table 14 presents four types of service environments:

- Traffic volumes and truck movements
- Exposure to water, road salt, and other corrosive materials
- Condition of protective and water proofing systems
- Temperature extremes, either from nature or human activity

Table 14. Service Environment Categorization in Bridge Inspection

Environment	Description
Benign	Neither environmental factors nor operating practices, mitigated by the presence of highly effective protective systems
Low	No adverse influence, lessened by the application of effective protective system
Moderate	Quite normal changes, considered typical by the agency
Severe	Contributes to the rapid decline in the condition of the element

For agencies utilizing Bridge Management Systems (BMSs), the appropriate element defects and environments should be recorded for use in deterioration modeling. Units should be associated with the elements. For example, scour defects are reported individually for columns and per linear feet for pier walls.

For multiple defects operating in the same defined space, the inspector may report the defect in the most severe condition state or report all defects, in which case the total in each condition state reported for the parent element will not include overlapping defects.

For materials or elements that are not defined, the inspector may use judgment to select the closest element or use the “other” element type. For undefined conditions, the inspector may use a general description of the condition state to determine the appropriate condition.

Elements with a portion of all the quantity in Condition State 4 often have load capacity implications that warrant a structural review. A structural review may include a study of field inspection notes and photographs and as-built plans, or analysis as deemed appropriate to evaluate the performance of the element.

6.6.2 Manual Inspection

A manual inspection of three highway bridges in Callaway County, MO, was conducted together with Missouri Department of Transportation Engineers as indicated by the group activities shown in Figure 80. Bridge A4982 (Structure No. 30522 in Table 6) crossing the Tavern Creek, built in 2004, is a 3-span continuous steel-girder bridge, with a length of 240 ft (73.15 m) and a width of 40 ft (12.19 m). Bridge A4988 (Structure No. 30523 in Table 6) crossing the Logan Creek, built in 2004, is a 4-span continuous steel-girder bridge, with a total length of 359 ft (109.4 m) and a width of 40 ft (12.19 m). Bridge A3450 (Structure No. 2898 in Table 5) overpassing the County Road 436, built in 1992, is a 3-span prestressed concrete girder bridge, with a total length of 196 ft (59.74 m) and a width of 48 ft (14.63 m). This effort does not only provide guidance to the development of robotic inspections but also provides a comparison basis with the pros and cons of automated inspections using UASs.



Figure 80. Research and Professional Inspection Teams

For each bridge, the manual inspection started with taking pictures of the bridge deck (top view) and the abutments and bents of the bridge for documentation purposes. Inspectors then walked through the abutments, girders, columns, and bents to check any abnormalities such as loose bolts and excessive deformation. Referring to the previous report, the inspectors took photos of any significant newly developed deterioration, measured the crack width by using a crack gauge or a filler if needed, and documented the new findings and measurements on an inspection report. For bridges that are high and difficult to access for visual inspection, a snooper truck is required to access various critical areas for visual inspection in practice.

Figure 81 presents several images of a manual inspection. They show the inspector walking underneath the bridge for deck, girder, and column inspection, explaining bridge column cracks to be visually inspected, and walking along the riverbank checking bridge bents and columns.



Figure 81. Manual Inspection of Highway Bridges

Overall, the visual inspection covered the entire bridge surface although remote inspection at distances could make it difficult to observe visual features. It identified the location, orientation, and type of defects such as bank/channel erosion, steel corrosion, cracks, leaching, riprap erosion, and concrete spalling. The severity of the defects was specified using descriptive words such as minor, moderate, few, light, random, heavy, many, and fine. Laser and tape distance measures and crack width measurements can also be done on accessible elements during a rapid

walk-through visual inspection. The complete visual inspection reports of the three Missouri bridges A4982, A4988, and A3450 are enclosed in Appendix A.

6.6.3 Defect Identification and Quantification from Automated Inspection

Automated inspection allows a direct identification and determination of defects from machine learning through bridge element segmentation and defect classification. The frames including the bridge element and defect of interest are extracted from an inspection video. The defects are then quantified in size and location. Lastly, the condition state (CS) of the bridge elements is assigned according to the *Manual of Bridge Element Inspection* (AASHTO, 2019) by comparing the extracted images with the referenced photos, as shown in Appendix B. This semi-autonomous approach as detailed below includes three steps: (1) defect identification from machine learning, (2) defect quantification in computer software, and (3) CS assignment of bridge elements.

In the first step, an artificial intelligence (AI) model is trained on a dataset of bridge images. All the images are labeled (annotated) for two defect types and five element types (bearing, railing, deck, superstructure, and substructure) based on the AASHTO *Manual*. The two defect types are Defect 1 for cracking and efflorescence due to their similar visual effects, and Defect 2 for corrosion, connection, effectiveness, and oxide film degradation due to their close relations. The AI modeling starts with a convolutional neural network, called high-resolution network (HRNet) (Wang, 2021), using a general dataset available in the open literature. It is then fine-tuned using a bridge-specific dataset, which includes approximately 100 images from the 2009 China and Chile earthquakes (Yen et al., 2011a; 2011b), 200 images from bridges located in different states in the U.S., and 400 photos from online sources. Once trained, the model is used to analyze new images and create image masks to show both the elements and defects of interest. A separate Python script extracts the frames including defects and elements of interest from an inspection video so that the AI model can run inference on the frames. This process preserves an exact time of the frames during the inspection.


In the second step, the Elios 3 drone's software, Inspector, is used to measure the defects that the AI model has identified in the frames extracted by the Python script. This measurement feature is attributed to Elios 3's camera distance sensor. The Inspector software's measurement tool finds a specific frame corresponding to the AI-identified exact time when a defect appears in a recorded video. It is then used to measure the defect dimensions. As noted in Flyability's Elios 3 documentation, the camera's optical axis should be perpendicular to the flat surface showing elements and defects of interest to ensure the measurement error is below 10%. Otherwise, the online measurement tool is unavailable, especially when the video is recorded with sudden changes in illumination, background contrast, and drone speed.

In the final step, the guidelines and corresponding illustrative photos in the AASHTO *Manual* are referenced to assign a CS for each specific defect and element. Note that one of the three bridges manually inspected, A3450 overpass, is not evaluated for defect quantification due to safety concerns with underpass traffic when flying with the Elios 3 drone. Instead, representative defects from Missouri bridge A4188 and A4351 (Structure No. 3425 and 3558 in Table 6) near

Jefferson City, MO, and A5805 (Structure No. 29015 in Table 5) near St. Louis, MO, are included to ensure that the defect quantification method is applicable to multiple bridges.

Table 15 lists various types of defects in different bridge elements and CS (i.e., condition states) of the bridge elements. These results are obtained following the above three-step approach. As mentioned before, the bridge elements are segmented and the defects on the bridge elements are classified using the AI model. The identified defects are then quantified in the Inspector software coming with the Elios 3 drone. The condition states are finally determined by comparing the identified defects in the frames extracted from an inspection video with the reference photos in the *AASHTO Manual*. Note that Table 15 is for illustrative purposes only. It does not include a complete CS assessment of all types of defects in all bridge elements of each bridge. These examples demonstrate the effectiveness and efficiency of the proposed automated inspection.

Table 15. Illustrative Examples of Defect Determination and CS Assignment

Bridge No.	Defect Type	Defect Detection from Machine Learning	Defect Quantification in the Inspector Software	CS Assignment
A4188	Connection			CS2
A4351	Effectiveness			CS2
A4351	Effectiveness			CS2
A4982	Corrosion			CS2
A5805	Cracking and Efflorescence			CS1

The current AI model developed in this study was limited to detecting two specific types of defects related to cracking (Defect 1) and corrosion (Defect 2). It is not applicable to other types of defects such as concrete spalling and rebar exposure. Therefore, bridge elements and defects are manually extracted from an inspection video to demonstrate the automated inspection feature for other defects, as summarized in Table 15. In this case, the CS assignment process is detailed by a side-by-side comparison of the extracted frame and the referenced photo (AASHTO, 2019).

Figure 82(a) shows the corrosion issue at the bolted connection part of bridge A4188 near Jefferson City, MO. The top beam flange showed a corrosion area of approximately 4.53×17.1 in (115×433 mm), while the bottom flange showed an area of approximately 13.4×39.9 in (341×1010 mm). This corrosion condition may be classified into CS2, in reference to the AASHTO *Manual* as shown in Figure 82(b).

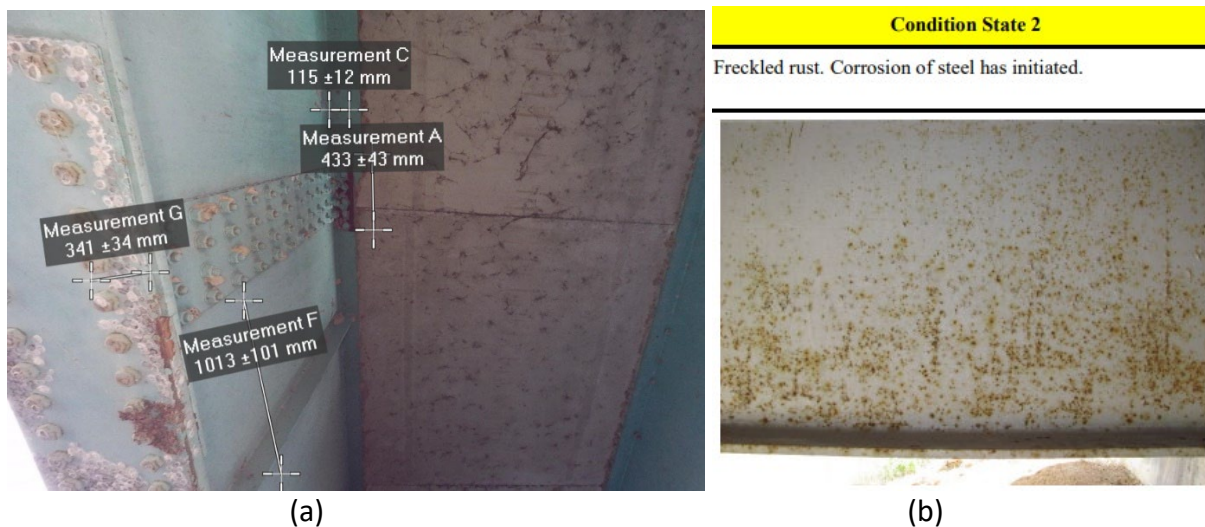


Figure 82. Bridge A4188 Frames vs. AASHTO Reference Photos for Coating Deterioration and Steel Connection Corrosion Assessment (25.4 mm = 1 in)

Figure 83 shows a severe spalling with exposed rebar on a cap beam of bridge A4351 near Jefferson City, MO. The spalling area was measured to have approximately 29.3×80.3 in (745×2040 mm). Rebar exposure also revealed the spacing of approximately 4.72×7.09 in (120×180 mm) in the middle section. Comparing to the AASHTO reference as shown in Figure 83(b), the defect may be classified into CS3.

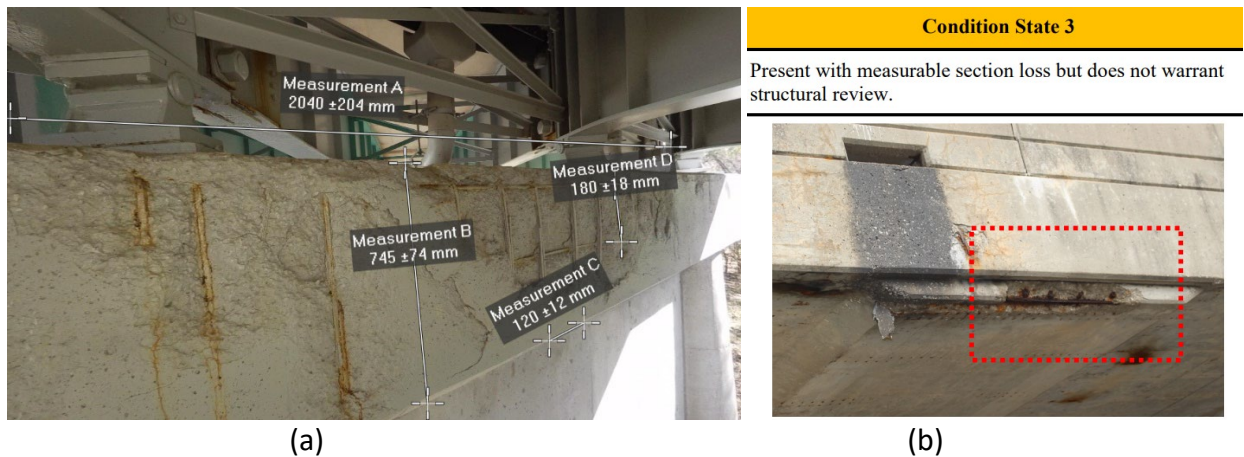
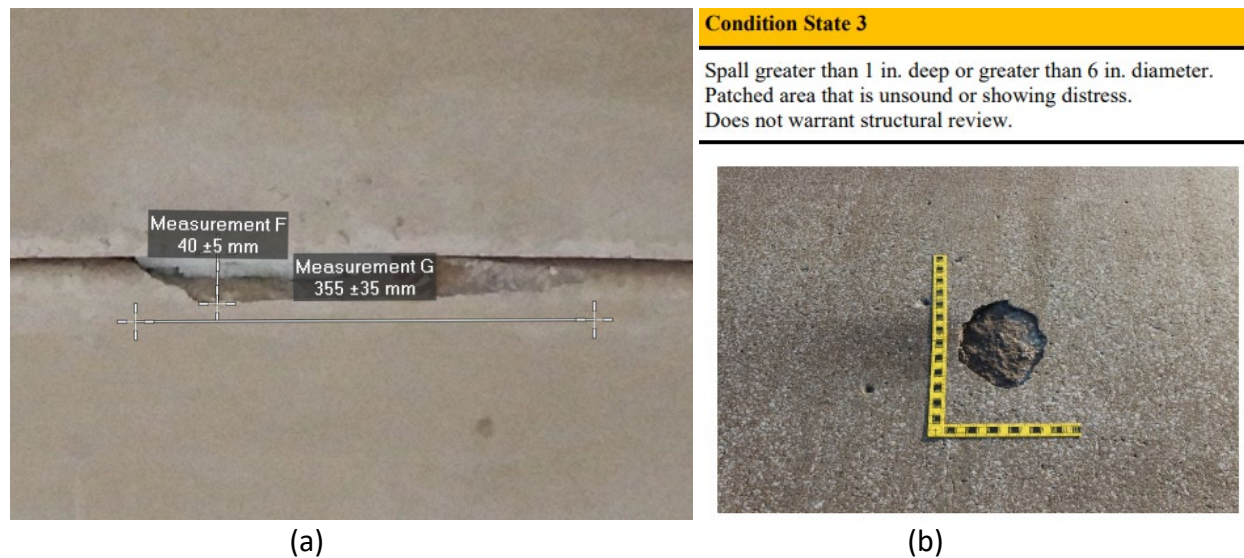


Figure 83. Bridge A4351 Frames vs. AASHTO Reference Photos for Concrete Spalling and Rebar Corrosion Assessment (25.4 mm = 1 in)

Figure 84 compares the video frames of bridge A4982, including notable defects, with reference photos in the AASHTO *Manual* (AASHTO, 2019) to assign appropriate CS of the bridge elements. Specifically, Figure 84(a) shows the measurement of a spalling area, sizing approximately 1.57 × 14 in (40 × 355 mm), on the underside of the bridge deck. This spalling condition may be categorized into CS2 to CS3 in reference to the excerpted photos from the AASHTO *Manual*, as shown in Figure 84(b). Figure 84(c) shows a 26 in (661 mm)-long leaching trace on the bridge abutment, which may be categorized into CS1 compared to the reference photo in Figure 84(d).





(c)

Boundary Image CS 1-2



(d)

Figure 84. Bridge A4982 Frames vs. AASHTO Reference Photos for Concrete Spalling and Leaching Assessment (25.4 mm = 1 in)

Figure 85 shows sample defect measurements for bridge A4988. Specifically, Figure 85(a) shows a leaching area of approximately 37.9×38.0 in (962×964 mm) at the abutment of bridge A4988. Compared to the AASHTO reference as shown in Figure 85(b), the defect may be classified into CS2. Figure 85(c) shows the corrosion of a rectangular steel plate sizing 3.23×12.2 in (82×310 mm). Compared to the AASHTO reference as shown in Figure 85(d), the corrosion condition may be classified into CS2. However, further verification is required as the color alone is insufficient to draw a definitive conclusion on the degree of deterioration.



(a)

Boundary Image CS 2-3



(b)

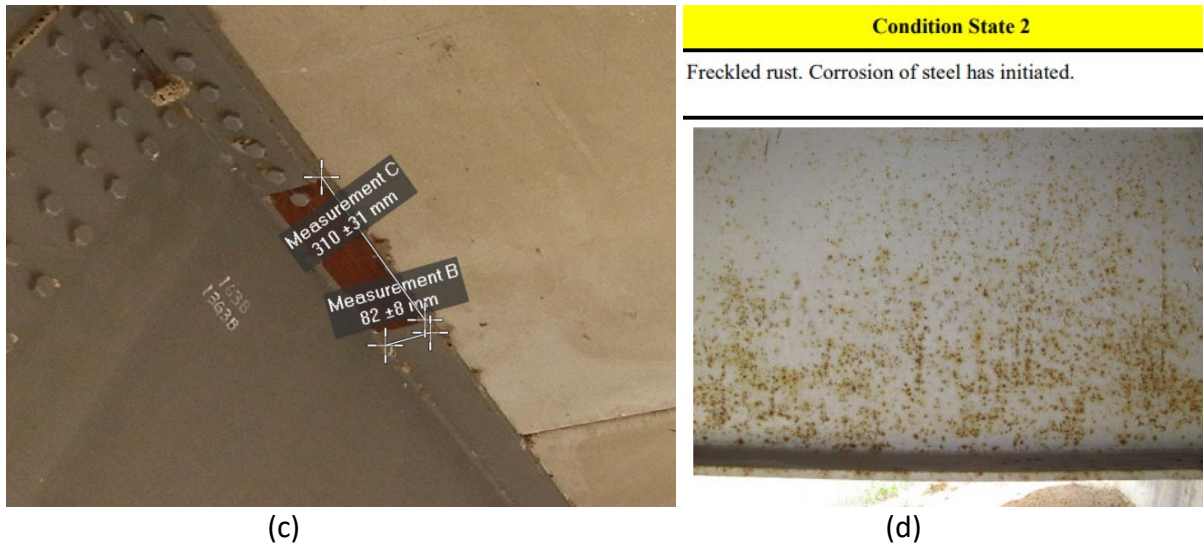


Figure 85. Bridge A4988 Frames vs. AASHTO Reference Photos for Concrete Leaching and Steel Corrosion Assessment (25.4 mm = 1 in)

6.6.4 Pros and Cons of Automated and Manual Inspections

The visual/manual inspection is compared with the automated inspection in terms of accessibility, comprehensiveness, time, quantification, reporting, and usefulness. Each attribute is briefly described below.

6.6.4.1 Accessibility and Traffic Control

For high-elevation or river-crossing bridges, visual inspection requires the use of a snoop truck to access all bridge elements. When accessed from bridge decks, traffic control is required to ensure safety. On the other hand, drones, crawlers, and their hybrid uncrewed vehicles provide a mobile platform to access otherwise inaccessible areas during inspection. Whenever access trucks are required in the conventional visual inspection, an alternative robotic inspection is advantageous in terms of inspection effort and cost.

6.6.4.2 Coverage and Comprehensiveness

Each inspector represents the most sophisticated intelligent system with unique characteristics helping streamline an inspection process from data acquisition and analytics to inference. Versatile and adaptive to environmental circumstances, the inspector can remotely cover every inch of bridge element surfaces during inspection but is unable to see features beyond the visible range (e.g., infrared range). Most importantly, the inspector cannot see any defect in the subsurface of bridges. On the other hand, a robot equipped with an array of sensors can access areas inaccessible to the inspector for high-resolution imaging and nondestructive testing. The robot can collect a consistent set of big data from the visible to infrared range from bridges, enabling the detection of both surface and subsurface defects. The robot can also archive the bridge's surroundings such as bank and channel profiles for the understanding of river hydraulics. While the manual inspection is more complete in terms of surface coverage, the automated inspection is generally more comprehensive in finding all types of defects.

6.6.4.3 Operation Time

The time required to complete a visual inspection of bridges largely depends on bridge deck area, bridge height, bridge deterioration, and ease of access to bridge elements. For example, for river-crossing bridges, inspectors will have to climb back on top of the bridge and walk over to inspect the other half of the bridge. For high-elevated spans, inspectors may have difficulty seeing all bridge elements clearly with the naked eye, as shown in Figure 81(a, c). For easy-to-access highway bridges, it takes approximately 30 minutes to complete a visual inspection of a 3- or 4-span bridge (e.g., A4982, A4988, and A3450) without requiring a snoop truck and associated traffic control. This level of inspection time is close to the time required for robotic inspection, including drone setup, drone operation, and imaging with 80% image overlapping to ensure satisfactory coverage of the bridge surface. Even though the robotic inspection may save some time, the saving in inspection time is negligible when compared with the time required to drive to a remote bridge site. However, for long-span bridges, the robotic inspection expects to be substantially more efficient than the manual inspection.

6.6.4.4 Objectivity and Quantification

Depending on their characteristics such as education and training, inspection experience, and physical conditions including eyesight and fitness, inspectors may perceive defects and judge their structural implications in a slightly different way. The unique characteristics may thus result in subjective visual observations and conclusions to various degrees. On the other hand, robots follow operation commands to execute tasks precisely and output results consistently. Machine learning can be used to segment bridge elements of interest and classify defects in the bridge elements from recorded videos and sensing data. Automated identification and quantification of bridge elements and associated defects would further enhance bridge inspection objectivity. They are promising in data-driven classification of condition states according to the *Manual for Bridge Element Inspection* (AASHTO, 2019).

6.6.4.5 Reporting and Usefulness

An annual manual inspection of a bridge is completed after visual observations, field notes, and straightforward measurements as appropriate have been translated into a standard final inspection report, as exemplified in Appendix A for three Missouri bridges A4982, A4988, and A3450. Although the location, type, and orientation of key defects in a bridge are recorded, the severity of defects is often documented in descriptive terms. However, a robotic inspection enables an automated process of generating a final inspection report and, more importantly, streamlines an entire bridge preservation process from inspection to maintenance strategy development. In doing so, inspection results and findings do not only provide a nation-wide basis for federal fund allocation for bridge preservation but also ensure the operational and structural safety of bridges through proper maintenance.

6.7 BridgeBot and Crawler Tests on Real-world Bridges

A variety of hybrid flying, traversing, and crawling vehicles, as discussed in Section 4.2, were tested and demonstrated for their performance at bridge sites. These performance indicators

included mobility, accessibility, quality, and efficiency.

6.7.1 Short-span Highway Bridges

The mechanical mechanism of the BridgeBot III prototype was designed for all types of girder bridges. As illustrated in Figure 86, the prototype was used to inspect a PC-girder bridge located near Freeburg, MO. The hybrid drone equipped with cameras, moved along the girder to inspect the girder and its surrounding from installed cameras.



Figure 86. Hanging Mechanism for Robotic Inspection of Prestressed Concrete Girders

As shown in Figure 86, the hybrid drone was tested for its ability to traverse along a PC girder with a bottom flange width of 17 in (43 cm). The drone was engaged with the girder using a clamping mechanism, which allows stable movement along the structure. The clamping system was manually adjustable to accommodate variations in girder size. The platform was equipped with elastic wheels capable of handling rough surfaces and overcoming small obstacles commonly found in inspection environments. Additionally, the drone was equipped with a RGB camera that provides both close-up views for inspecting the underside of the girder and downward views for terrain monitoring beneath the bridge, such as riverbank and channel erosion. This system was designed to be modulated and can support additional payloads for aerial NDT, such as a manipulator arm integrated with an ultrasonic array sensor for detecting internal voids in concrete, a ground-penetrating radar for rebar monitoring, or sensors for assessing crack depth.

As demonstrated in Figure 87, the initial tests of the mechanical hanging mechanism were carried out on the eight-span, 10th Street Bridge in Rolla, MO, supporting a four-lane road crossing over a railroad track and two local streets. The girder size on this bridge measured 12 in (30.5 cm)

wide, providing a suitable real-world environment for evaluating the BridgeBot's ability to engage with and inspect bridge structures. During these tests, the BridgeBot performed as expected, with its functionality closely mirroring the results observed in controlled environments. The system can hover, navigate, and engage with the girder, demonstrating its ability to operate efficiently in real-world conditions.



Figure 87. Hexacopter Testing on the 10th Street Bridge in Rolla, MO

Following the successful tests on the 10th Street Bridge, additional tests were conducted at the I-44 Rubidoux Creek Bridge in Waynesville, MO, as shown in Figure 88. The test of this wide bridge presented a distinct set of challenges, including variations in girder design and environmental factors such as wind and lighting conditions. These tests provided valuable insights into BridgeBot's ability to adapt to diverse bridge types and real-world conditions, further refining its functionality. The data collected from both test sites were instrumental in fine-tuning the BridgeBot's systems and ensuring its reliability for bridge inspections and other structural assessment tasks.

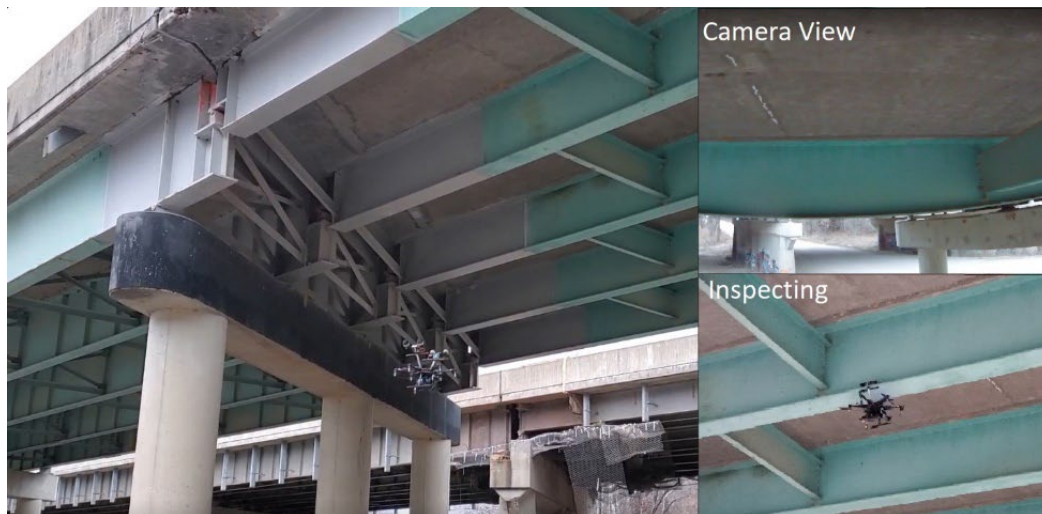


Figure 88. Hexacopter Testing on the Rubidoux Creek Bridge in Waynesville, MO

Extensive testing of the BridgeBot with a protective frame was carried out on several bridges, including the 10th Street Bridge in Rolla, MO, as shown in Figure 89, and the Rubidoux Creek Bridge in Waynesville, MO, as shown in Figure 86. During these tests, BridgeBot successfully

collected RGB and thermal visual data as illustrated in Figure 90, demonstrating its capability to perform in real-world conditions. As demonstrated in Figure 91 for RGB imaging, these tests further validated BridgeBot's performance and highlighted its potential for efficient and reliable bridge inspections, both in terms of stability and data quality.



Figure 89. Protective Box Drone Testing on the 10th Street Bridge in Rolla, MO

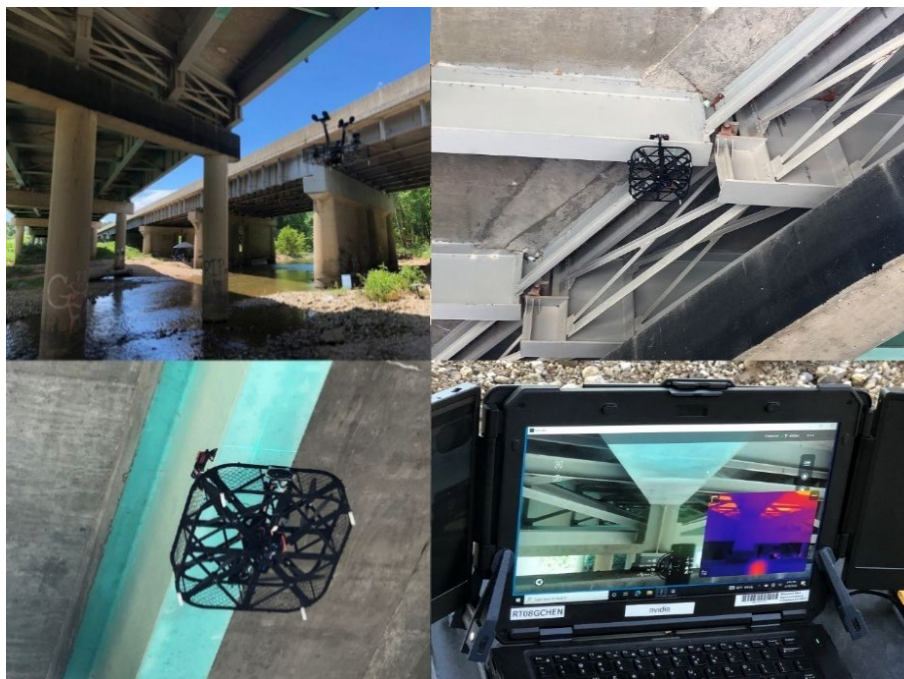


Figure 90. Protective Box Drone Testing on the Rubidoux Creek Bridge in Waynesville, MO



Figure 91. RGB Imaging on the Rubidoux Creek Bridge in Waynesville, MO

6.7.2 Long-span River-crossing Bridges

The magnetic attracting mechanism of BridgeBot Prototype IV was tested on the Bill Emerson Memorial Cable-stayed Bridge in Cape Girardeau, MO, to demonstrate how the hybrid vehicle launched a crawler for local defect detection and aerial NDT. The field tests were focused on the Missouri side span, 468 ft (143 m) long, with a significantly varying bottom flange width up to 24 in (61 cm) making the operation of BridgeBot Prototype III with a mechanical hanging mechanism a challenge. This series of Prototype IV field tests in real-world conditions provided valuable insights into BridgeBot's functionality and reliability.

As demonstrated in Figure 92, a miniature magnetic-wheeled crawler robot was launched from a hybrid aerial platform - BridgeBot Prototype IV. Specifically, the hybrid drone traversed on the bottom flange of the longitudinal steel girder and launched a crawler that transitioned from the bottom flange to the web of the girder for bolted connection inspection, as shown in Figure 92(a). The hybrid drone then traversed along the transverse floor beam and launched the crawler to inspect the crossing longitudinal stringer made of corrugated steel, approximately 12 in (30.5 cm) tall, as shown in Figure 92(b). The flange or web thickness of the utility stringer, 0.2 in (5 mm) only, posed a challenge for needed attaching magnetic force and navigation. The transition from the web to the flange was successful as illustrated in Figure 92(b).



(a) Longitudinal steel girder



(b) Transverse floor beam and longitudinal stringer

Figure 92. Hybrid Drone and Crawler Maneuvering along Steel I-beams on the Bill Emerson Memorial Cable-Stayed Bridge in Cape Girardeau, MO

As demonstrated in Figure 93, the crawler successfully maneuvered through the crowded space in bridge anchorages. The crawler maintained stable contact with the longitudinal girder and traversed continuously across the structural surface. The robot's mobility system enabled sharp transitions on narrow flanges while preserving inspection capabilities. These tests verified the effectiveness of the proposed drone-crawler cooperation for accessing and inspecting hard-to-reach infrastructure components, such as the anchorage area consisting of steel girder, pin, stiffener plates, and weld connections, without requiring human intervention in hazardous environments. The test results as shown in Figure 93 validated the integration of aerial delivery and ground inspection into a unified robotic system, paving the way for advanced automated bridge preservation in sensor installation, NDT, visual inspection, and local maintenance.

As shown in Figure 94, a microscopic imager was used to inspect the bolt connection where bird nests and rust were observed in detail from magnified images. Similarly, the functions of the crawler for bolt and nut inspection and the anchorage area examination were illustrated in Figure 95. While not observable by the operator, the crawler provided a beyond-the-visual-line-of-sight view of rust on the web of the steel girder in Figure 95(b). The presence of trapped water may contribute to rusty conditions.



Figure 93. Crawler Access to Narrow Spaces for Weld Connection Inspection



Figure 94. Crawler Access to a Potentially Corroded Area via Microscopic View



(a) The bolt and nut assembly



(b) Transverse stiffeners at the end of steel girder

Figure 95. Crawler Access to the Bridge Support Area

As demonstrated in Figure 96, an aerial NDT was conducted on the longitudinal steel girder using a structural crawler. The crawler was equipped with an ultrasonic metal thickness measurement device. During operation, the crawler halted at the target inspection site, then the pumping system dispensed the ultrasonic gel, and finally the manipulator deployed the ultrasonic sensor for thickness measurement. The camera view from the crawler included the sensor to help the crawler navigate through the bolt area as shown in Figure 96(a). Once the ultrasonic device was in place, its readings on the thickness of the web of the longitudinal girder were displayed on the screen as illustrated in Figure 96(b).



(a) Crawler navigation around the bolted connection area



(b) Web thickness measurements and readings at two designated points

Figure 96. Automated Nondestructive Testing on the Web of a Steel Girder

6.8 Underwater Inspection Using Remotely Operated Sonar Imaging

Underwater acoustic imaging has emerged as a pivotal technology for bridge inspectors, enhancing the efficiency and safety of underwater operation. Traditional methods, such as visual inspection and tactile examination, face challenges in the underwater environment due to limited visibility. Consequently, modern inspections increasingly incorporate acoustic imaging techniques on remotely operated vehicles, which provide detailed insights into the condition of submerged structures and surrounding environments.

6.8.1 Remotely Operated Vehicles

To support underwater inspection, two types of remotely operated vehicles (ROV) were developed: (1) a modified BlueROV2, referred to as Uncrewed Underwater Vehicle (UUV) as shown in Figure 97(a), and (2) a modified BlueBoat, referred to as Uncrewed Surface Vessel (USV) as shown in Figure 97(b). For the first ROV or UUV, the original BlueROV2 was expanded vertically

to create more space to accommodate a BV5000 Sonar and other accessories. The UUV was tested in the Hydraulics Laboratory at Missouri S&T to determine the optimum parameters for maintaining control of the robotic system underwater. Ballast weights were added to or removed from the base of the ROV2 as required to ensure balance of the system. The fine-tuned UUV was equipped with a BV5000 sonar to obtain detailed scour data around bridge piers. The optimization and field test performance of the UUV were referred to in Ogunjinmi et al. (2024).

For the second ROV or USV, the BlueBoat employed BlueOS as the onboard operating system and ArduRover as the vehicle control software. It had five main types of motion: manual control with a joystick, automatic waypoint navigation, guided click-to-navigate, position hold, and return home if the connection is lost, all of which are done through QGroundControl. To achieve this, the boat used a Raspberry Pi 4 as the onboard computer including a quad-core 64-bit processor, 4GB RAM, USB 3.0 and 2.0 ports, Gigabit Ethernet, and two micro-HDMI ports. The Raspberry Pi 4 supported Bluetooth 5.0, 2.4 and 5.0 GHz wireless communication, and 4k dual display. Moreover, the boat computer was connected to a GPS and a navigator flight controller, which has an IMU, barometer, and ADC sensors. The base station worked as a Wi-Fi access point that hosted a 2.4GHz network, allowing the ground computer to connect to the boat. With a 36 Wh (Watt-hour) internal battery capacity, the base station can operate for 6-8 hours.



(a) Modified BlueROV2



(b) Original BlueBoat



(c) BV5000 Sonar

Figure 97. Remotely Operated Vehicles

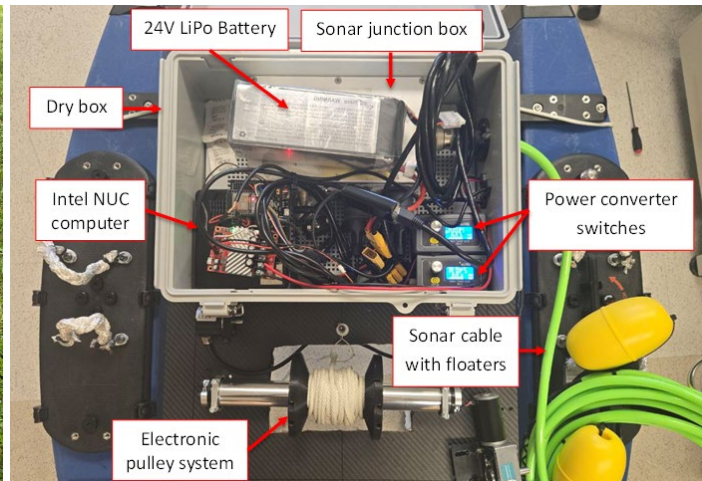
This section is focused on the implementation of the USV with two specific objectives: (1) integrate a BV5000 sonar into the modified BlueBoat (or USV) to enable 3D reconstruction of underwater bridge piers, and (2) test and evaluate the USV system for underwater acoustic imaging and scour evaluation. Implementation challenges include cable management, electronics overheating, and robot stability in strong currents. The BV5000 sonar as shown in Figure 97(c) has the following technical specifications:

- ✓ Operating frequency = 1.35 MHz
- ✓ Field of view = $42^\circ \times 1^\circ$
- ✓ Beam width = $1^\circ \times 1^\circ$
- ✓ 256 beams
- ✓ Optimal range: 3.28 – 66 ft (1 – 20 m)
- ✓ Range resolution: 0.59 in (1.5 cm)

Figure 98(a) shows an integrated USV system of the BlueBoat, the BV5000 sonar, a waterproof electronics box on a raised composite platform, an antenna, and several buoys. To enable sonar imaging, a miniature computer (Intel NUC) is installed on the BlueBoat and wired to the BV5000 sonar. The BlueBoat is controlled by a computer at the base station via wireless communication using a sailing controller that manages propulsion and steering mechanisms for precise navigation. Driven by two M200 motors, the propulsion system consists of multiple independently controlled units, enabling the vehicle to move in various orientations (pitch, yaw, roll) and directions (heave, surge, sway). This flexibility is crucial for navigating a complex water environment and maintaining stability during operation. Figure 98(b) shows the watertight electronics box that houses the portable NUC computer, a sonar junction box, a 24V 200Ah rechargeable LiPo battery, and DC-AC power converter switches. The Intel NUC computer runs on windows 11 OS with Intel Core i7 1.10 GHz, 64GB RAM, and 1TB storage space. It is connected to the sonar headbox and communicates directly with the laptop computer at the base station for remote data collection and visualization. When fully charged, a 24V battery can power the sonar, the NUC computer, and the pulley system for 3 hours.



(a) The integrated USV system



(b) Inside the dry box

Figure 98. Field Test of the Integrated USV System in a Lake

6.8.2 Swimming Pool and Field Tests

As demonstrated in Figure 99, the USV system was set up and tested on a windy day in a lake. The operator at the base station monitored real-time information of the lake bottom through the 3D sonar mounted on the BlueBoat. The integrated USV can perform various autonomous tasks on water. Its design incorporated features that enhance stability and maneuverability, making it suitable for river channel inspection and payload delivery.



Figure 99. Test Setup and Remote Operation for Underwater Inspection

The BV5000 sonar can generate 3D point clouds of underwater structures by mechanically rotating the sonar head through a pan and tilt attachment. Data collection in the field was managed through complementary Proscan software. At the project site, the generated point cloud data were viewed and manipulated in the Blueviewer software for zooming, rotation, and other visualization adjustments. During the post-processing, the point cloud can be cleaned, optimized, and registered (also known as stitching) using the QuickStitch software.

During the development of the integrated USV system, the robotic deployment design was tested in Missouri S&T's swimming pool on April 8, 2025, to evaluate its stability and maneuverability in realistic field conditions. As shown in Figure 100, the robot was submerged into the water by adding a bucket of weights and navigated through the pool.

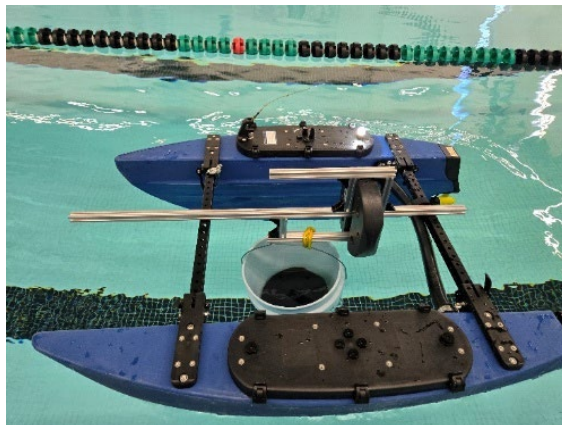


Figure 100. Testing on the Blueboat Control System under Different Payloads

To achieve optimal stability against water current while maintaining the ease of operation, the payload capacity of the BlueBoat was calibrated. The BlueBoat was then modified and equipped with a BV5000 sonar in a final USV system, as illustrated in Figure 98(a). Finally, the USV system was tested at bridge sites to obtain detailed scouring data around bridge piers. The steps involved in the field test are summarized below:

1. Place the integrated USV equipped with the BV5000 sonar in a shallow river.
2. Navigate the USV towards a bridge pier of interest with the onboard controller.
3. Through the electric pulling system, lower the BV5000 sonar down to the riverbed within 5-10 ft (1.5 – 3.0 m) distance from the pier and ensure that the sonar stand on a base plate remains stable and vertical by adding pan and tilt using the onboard electric winch.
4. Check the remote connectivity between the sonar and the laptop computer within the ProScan software GUI and return the pan and tilt to its home position.
5. With the sonar head at the home position, run a 360° spherical scan or single scan as needed while aiming the target at an appropriate tilt angle (+15°, -15°, +45°, -45°).
6. At the completion of scanning, visualize the point cloud data (in “.xyz” and “.son” formats) in the Blueviewer software GUI.
7. Lift the sonar and move the USV to the next stop and repeat Steps 1-6 until the underwater structure is fully scanned.

6.8.3 3D Point Cloud Data Processing to Detect Bridge Scour

This section presents an illustrative case of riverbed scanning and scour evaluation at Interstate I-44 over the Roubidoux Creek, Waynesville, MO. Figure 101 shows the combined 3D point cloud data obtained from several scans using the BV5000 sonar. It can be observed that the bridge footings are exposed due to scouring. A machine learning approach is developed to detect and segment columns and footings as discussed below.

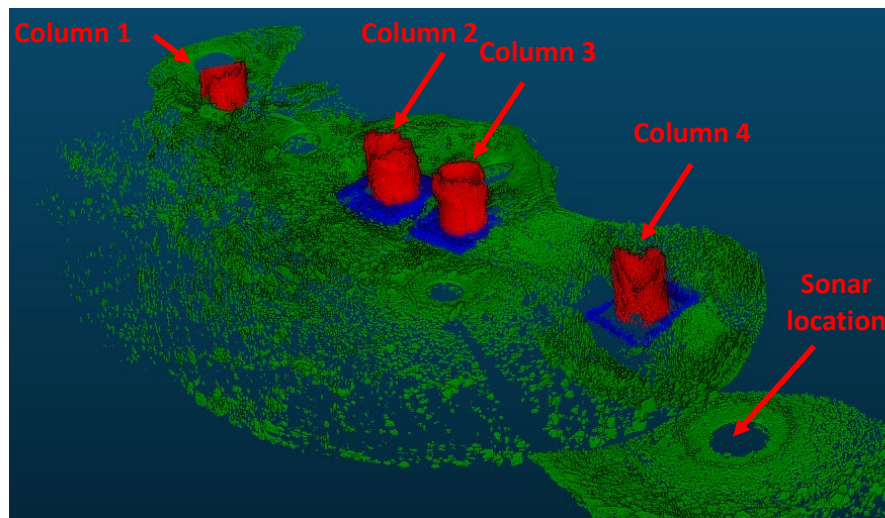


Figure 101. 3D Point Cloud Showing Scouring and Exposure of the Footing

Clustering is an unsupervised machine learning method. It can separate data into subgroups, or clusters, without requiring labeled examples. It produces segmented groups of data points that can serve as a basis for further tasks such as feature extraction, classification, and 3D modeling. This study is focused on three clustering approaches based on centroid, density, and connectivity (Poux, 2025). Their best practices and key characteristics are summarized in Table 16. Following is a detailed presentation of the connectivity-based approach as it leads to the best segmentation results of columns and footings.

Table 16. Clustering Methods for 3D Point Cloud Segmentation

Clustering	Best use cases	Common algorithms	Key characteristics
Centroid-based	Uniform geometric distributions, compact spatial structures, urban infrastructure mapping	k-means	Maintains fixed number of clusters and spherical cluster shapes, changes with outliers significantly
Density-based	Irregular point distributions, noisy environments, complex geological surveys	Density-based spatial clustering of applications with noise	Adapts to nonlinear shapes, handles noise effectively, captures local density variations
Connectivity-based	Nested spatial relationships, multiscale analysis, architectural and forest canopy mapping	Connected components	Reveals hierarchical structures with no predefined cluster number, preserves spatial semantics

The point connectivity-based clustering approach is to build a graph from the point cloud and then detect connected components within the graph. Each connected component represents a distinct cluster. In a graph-based point cloud segmentation, the size of the graph reflects the density of connections based on the chosen “*radius*” and the “*max neighbors*” parameter. These parameters must be carefully selected for optimal results. On one hand, a small radius leads to very localized connections, often producing small and fragmented clusters. On the other hand, a large radius results in broader connections, which can cause distinct objects to merge into a single cluster, especially when objects are clogged in crowded spaces. Choosing the best radius depends heavily on the characteristics of the specific dataset. The “*max neighbors*” parameter serves as both a computational and topological regularization control, restricting the number of connections each node can have and thus preventing the graph from becoming overly complex. Setting the value too low may break apart meaningful spatial relationships, while setting it too high can introduce noise and diminish the graph’s ability to distinguish between different structures. Finding the optimal value typically involves iterative experimentation, considering the unique geometry of the point cloud and the goals of the analysis. Carefully tuning this parameter is essential for creating robust and generalizable algorithms in spatial data analysis.

Each connected component in the point cloud graph analysis can be interpreted as a potential object. By detecting these components, we can segment the point cloud into meaningful clusters. The segmentation results obtained from the connectivity-based clustering on the bridge point cloud data, as shown in Figure 101, is presented in Figure 102 corresponding to two *max neighbors*’ values. In practical applications, the segmentation results corresponding to different *max neighbors*’ values may be averaged to improve the clustering robustness. Once the columns and footings are identified and segmented, their surrounding scour hole can be detected from the original 3D point cloud using a Delaunay triangulation.



**Figure 102. Connectivity-Based Clustering of Bridge Elements with a Max_neighbor Value of:
(a) 10, and (b) 15**

CHAPTER 7. INSPECTION PROTOCOLS AND GUIDELINES

This chapter aims to develop the protocols and guidelines for disruption-free bridge inspection using robot-assisted remote sensing, in-situ sensing, nondestructive testing, and visual examination. Best practices from multiple field visits (Shi et al., 2023) are summarized in the automated bridge inspection guidelines (Chen et al., 2024).

7.1 Pre-inspection Preparation

To facilitate automated bridge inspection, UAV and sensing systems should be selected appropriately. Immediately before an inspection, metadata such as bridge drawings and legacy data from previous inspection reports should be reviewed and documented, based upon which a UAV flight mission plan is developed.

7.1.1 UAV and Sensor/Camera Selection

UAV-based inspection platforms include light and heavy UAVs equipped with different combinations of visible, infrared, and hyperspectral cameras (sensors), as displayed in Figure 24. Light UAVs are equipped with one sensor (e.g., RGB imaging) by manufacturers with a few exceptions with two sensors (e.g., RGB and thermal imaging). Heavy UAVs may include more sensors for a comprehensive, reliable bridge inspection using data fusion techniques. A few UAVs are collision-tolerant or collision-avoidable during navigation.

7.1.2 UAV Flight Planning

To understand the progression of deterioration, bridge inspection should be geo-referenced to make data and results comparable over time. This requires the development of a UAV flight protocol for bridge inspection. Such a protocol includes:

- Flight paths at various levels of inspection using visible, thermal, and hyperspectral imagery and a LiDAR point cloud on the elements of a bridge, and
- National bridge elements inspected for defect types as described in the *AASHTO Manual for Bridge Element Inspection* (AASHTO, 2019).

The longitude and latitude coordinates of a bridge should be clearly specified. These coordinates help locate a permanent survey marker, if available, that is often cast in the wingwall or abutment near the bridge name plate. They are also used to check pertinent FAA airspace requirements for the operation of UAV surrounding restricted areas.

The main purpose of a bridge safety inspection is to document any change in bridge condition from the last inspection. The UAV flight paths should cover all significant bridge elements and defects at three levels of inspection as illustrated in Figure 103:

- 1 Screening Inspection. Inspectors drive/walk around the bridge, when accessible, or fly a light UAV equipped with RGB and infrared cameras at a standoff distance of 5-10 ft (1.5 - 3.0 m). The range of standoff distance lies between twice and quadruple the diameter of propellers for negligible ceiling and near-wall effects of most quadcopters, hexacopters,

and octocopters (Conyers, 2019). Depending on the wind speed during flight, this distance range also makes average pilots feel comfortable operating drones.

- 2 Probing Inspection. Inspectors fly a light UAV in the areas of interest at a standoff distance of less than 5 ft (1.5 m) or operate a hybrid robot attached to a girder for near-surface imaging. The inspectors may choose to fly a heavy UAV with multimodal imaging and LiDAR scanning functions at a standoff distance of 10-15 ft (3.0-4.6 m). Underwater inspection to understand bridge foundation scour should be conducted using a sonar device for developing a 3D point cloud of potential exposed foundations or a smart rock positioning system for the determination of maximum scour depth.
- 3 Verifying Inspection. Severe damage/defects determined during the probing inspection should be verified by inspectors based on visual inspection using augmented reality or nondestructive evaluation. If available, surface-attached and embedded sensors provide in-situ data for the confirmation of inspection results. Depending on the interest and in-house capability, interactive robot-assisted nondestructive testing can be conducted during the Probing Inspection.

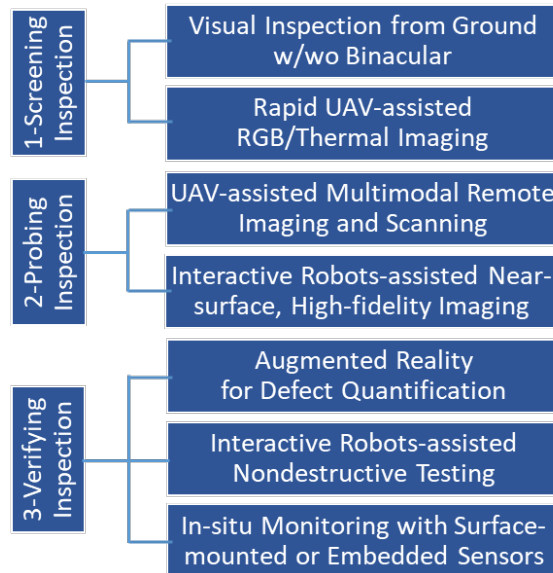


Figure 103. Robot-Assisted Bridge Inspection Tactics

Coordination about a bridge inspection should be well prepared prior to UAS operation. Besides coordination with state Departments of Transportation (DOTs) and compliance with Federal Aviation Administration (FAA) regulations (FAA, 2024), flight mission planning involves flight crew formation, flight path planning, and emergency plan establishment. Special permission from the Air Traffic Control (ATC) is required to inspect a bridge located outside a Class G airspace. A UAS flight crew should consist of at least a remote pilot in command (PIC) and a visual observer (VO). The PIC must complete recurrent training every 24 months and receive a remote pilot certificate. All UASs must be registered with the FAA when operated under the Part 107 Category. An emergency plan should be developed to minimize any injury or property damage. In the event of a severe injury to any person, loss of consciousness, or damage to any property greater than \$500 to repair or replace (whichever is lower), an accident report must be filed to the FAA (2024).

Figure 104 shows a flight path of a DJI M600 drone prepared in UgCS (2025). The flight path of 16 waypoints should be along the side of the bridge deck to minimize direct flight over the traffic and maintain a constant standoff distance of the camera facing the bridge façade. A factor of safety (e.g., 1.5) is recommended when determining a flight height due to inaccuracy in the digital elevation model referenced in the software. A flight height in the range of 98 – 164 ft (30 – 50 m) AGL at a flight speed of 3.36 mph (1.5 m/s) is recommended to avoid typical obstacles such as trees, powerlines, and utility poles. The blueish lines in Figure 104 indicate where a hyperspectral sensor is triggered, outside of which the sensor remains inactive. The total flight time for the DJI M600 drone should stay within 15 min to ensure a safe landing in a sufficient remaining time.



Figure 104. Autonomous Flight Path with Sensor-Triggered Polygons (DJI M600)

Due to its low wind tolerance, Elios 2 should fly underneath a bridge deck through a channel between two adjacent girders. Its collision-tolerance cage makes it easy to navigate through narrow spaces. When it reaches the end of a span or the end of the entire bridge, the drone is maneuvered into an adjacent channel between two girders and flown in the opposite direction. A hand-held camera should be used in drone-inaccessible areas such as tree and bush obstacles, dusty areas, tight space areas, and high-water level conditions.

7.1.3 Legacy Data Review and Documentation

Prior visual inspection reports and as-built drawings of the bridge should be reviewed and saved in a portable device that is available during the field inspection. The quality of legacy data, which is prepared to support field inspection, is measured by their structured organization, comprehensiveness, and quantitative nature. Prior visual inspection reports should be reorganized to categorize the condition states of bridge elements according to the *Manual for Bridge Element Inspection* (AASHTO, 2019). For each element, several types of defects are listed and color-coded by importance for reference during the inspection. Each type of defect should be quantified to an extent practically feasible. Descriptions of bridge elements and defects (condition states) should be brief and informative. The engineering drawings corresponding to the areas of abnormal defects should be retrieved for spatial references, object identifications, and geometric dimensions. The engineering drawings and prior structural deterioration information should be easily accessible in the middle of the field inspection. It should be prepared by an inspection crew specifically assigned to the bridge. Otherwise, the crew members should review the information thoroughly prior to their departure for the field inspection.

7.1.4 Inspection Checklist

Prior to each bridge site visit, all types of equipment and tools should be prepared to ensure success of the bridge inspection at a remote site. Figure 105 shows a checklist of the test equipment and setup tools and includes test records such as environmental and atmospheric conditions during the bridge inspection. For safety and productivity, a typical inspection crew consists of three people: a team leader and two members. The team leader is responsible for final decisions whenever disagreements arise among the inspectors. During the field operation, the team leader assigns specific roles to the inspectors. The team leader and the inspectors are referred to as Pilot in Command (PIC) and Visual Observers in the context of UAS operation.

Day:		Date:					
Bridge ID & Location							
Inspection Date							
Pilot-in-command (PIC)							
Visual Observer 1 (VO1)							
Visual Observer 2 (VO2)							
iG4		Point Description	Instrument Height		Start Time	End Time	
Meteorological Data Recorded Every Hour	Index\Time	Start Time []					End Time []
	Wind Gust (mph)						
	Temperature (F)						
	Humidity (%)						
	Pressure (inHg, relative)						
	Light (W/M ²)						
Items		Check	Items		Check	MISC Items	
Binocular		<input checked="" type="checkbox"/>	Flight Mission Planning & Uploading		<input type="checkbox"/>	Tape Measure	
Camera & Tripod		<input type="checkbox"/>	GNSS Receiver iG4		<input type="checkbox"/>	Tarps	
Canopy		<input type="checkbox"/>	Ice Box		<input type="checkbox"/>	Traction Boards/ Tire Chains	
Cellphone for Hotspot		<input type="checkbox"/>	MicroSD & Hard Drive Clearance		<input type="checkbox"/>	Traffic Cones	
Chairs		<input type="checkbox"/>	Napkin & Hand Sanitizer		<input type="checkbox"/>	UAS/Pilot Permits	
Charge All Batteries		<input type="checkbox"/>	PPE: Glasses & Hard Hats		<input type="checkbox"/>	Vests	
Drones	ANAFI Parrot <input type="checkbox"/> Elios2 <input type="checkbox"/> Geodetic M600 <input type="checkbox"/> Headwall M600 <input type="checkbox"/> Phantom4 <input type="checkbox"/> Skydio2 <input type="checkbox"/>	<input type="checkbox"/>	RT09 Computer & Hard Drive		<input type="checkbox"/>	Walkie-Talkie	
Extension Cord		<input type="checkbox"/>	Strobe Light		<input type="checkbox"/>	Water & Food	
First Aid Kit		<input type="checkbox"/>	Tables		<input type="checkbox"/>	Weather Station & Pipe Holder	

Figure 105. Robot-Assisted Bridge Inspection Preparation Checklist

7.2 During-inspection Execution at Bridge Sites

Inspection tasks should be documented with an identification of the bridge number, the type of bridge, the year built, and inspection date and time. They should be clearly described for easy understanding by third parties. These tasks include responsibility clarification, GPS station setup, navigation and flight control logging, sensor operation condition logging, weather condition logging, and file management.

7.2.1 Responsibilities of Team Members

Table 17 summarizes example responsibilities of the PIC, VO1, and VO2 during a bridge inspection. Specific tasks should be assigned to inspection team members according to needs and their skill sets. Pre-developed flight paths should be reviewed and modified as needed upon arrival at the bridge site. Review items include any potential changes of bridge elements and configurations made after the original construction or undocumented rehabilitation tasks, and any potential difference in the site conditions which naturally evolved over time.

Table 17. Example Responsibilities of Team Members During Bridge Inspection

Items	Pilot in Command (PIC)	Visual Observer 1 (VO1)	Visual Observer 2 (VO2)
Arrival	<ul style="list-style-type: none">• Identify focused areas and decompose a flight plan as needed.• Mark the flight plan on engineering drawings.• Define flight routes (.json) and the areas of interest (.kml).	<ul style="list-style-type: none">• Set up a weather station and record arrival time.• Set up an operation base station under a canopy in hot weather.• Set up markers, tarps, and ice buckets.	<ul style="list-style-type: none">• Set up tripods, chairs, tables, cameras, an iG4 ground station and a canopy as needed.• Connect electric extension cords to the van and table.
Flight operation	<ul style="list-style-type: none">• Calibrate Parrot Anafi drone for imaging.• Calibrate Flyability Elios 3 drone under < 10 mph (4.5 m/s) wind.• Collect hyperspectral and thermal images using DJI M600 drone.	<ul style="list-style-type: none">• Assist with drone calibration and record weather conditions every 30 min.• Provide safety watch to ensure safe operation.• Start/stop infrared and hyperspectral cameras.	<ul style="list-style-type: none">• Copy and rename data files to hard drives for storage.
Departure	<ul style="list-style-type: none">• Pack and load drones and mark off returned items on the checklist.• Load retrieved items and mark off returned items on the checklist.• Check for missing items and complete the return checklist.	<ul style="list-style-type: none">• Pack and load drones and mark off returned items on the checklist.• Move and load retrieved items and mark off returned items.• Check all items on the return checklist.	<ul style="list-style-type: none">• Retrieve tripods, chairs, tables, cameras, markers, extension cords, the iG4 station, the canopy, ice buckets, markers, and tarps.• Record time and weather.

7.2.2 GPS Station Setup

Upon arrival at a bridge site, a minimum of one GPS station (e.g., iG4) should be set on a tripod at approximately 5 ft (1.5 m) above ground and kept still until the bridge inspection is completed. The accuracy for GPS should be 0.4 in (1 cm) or less. The GPS data is uploaded to an open site Online Positioning User Service (OPUS) website for iG4 station coordinate correction. For bridges with a permanent reference station, the GPS station may be related to the given coordinates in the OPUS from the National Geodetic Survey. The Federal Highway Administration (FHWA) long-term bridge performance (LTBP) program hosts certain bridge location data for potential verification.

7.2.3 Navigation and Flight Control Logging

The flight status and surrounding conditions should be logged into a document for each flight. The document should be named consistently in the file management system for easy reference at the bridge site. During drone calibration and operation, the flight status includes any correction factors and disruptions, including battery runout and replacement. Surrounding conditions related to the flight include obstacles' height, density, surface light reflectivity (e.g., concrete vs. steel), and distance to the bridge. Obstacles to flight at a bridge site includes trees, power transmission poles, overpass/underpass bridges, and nearby buildings.

7.2.4 Meteorological Condition and Sensor Operation Logging

A portable weather station should be set up at a bridge site to record meteorological conditions during inspection. Such a station should include a minimum of temperature, moisture, wind speed and attack angle, and sunlight condition (sunny, partly sunny, cloudy, and light raining). The brand and model of each device should be documented in the inspection report.

The drone-assisted remote sensing and nondestructive testing should be documented. This documentation should include any sensor calibration done at bridge sites and incomplete data collection due to reasons such as camera battery runout, improper parameter setup, and insufficient illumination condition.

7.2.5 File Management

A military-grade rugged laptop computer should be dedicated to field tests. Files from each field inspection should be organized and stored in structured folders to ensure their unique and consistent designations. Each file, for example XYZ, can be traced intuitively through a sequence of key information including the inspection date, the bridge owner, the bridge number, the UAS platform, and the sensor. An example file path is designated by .../InspectionDate/BridgeOwner/BridgeNumber/UASPlatform/Sensor/XYZ.

A file folder is created for easy reference on each field inspection. The name of a folder can be the same as the state bridge designation prefixed by two-letter state and territory abbreviation (e.g., MO) and field test date (mmddyyyy). For example, 02222021_MO_3995 indicates data and information collected from the field tests of Missouri bridge no. 3995 on February 22, 2021. For

inventory purposes, sketches and notes on defect numbers and locations taken during the screening inspection should be kept in the main folder as metadata together with engineering drawings marked on site.

Inside each main folder, data should be organized such that anyone can understand and use the data without ambiguity. First, subfolders should be created for several types of UAS platforms, for example, Parrot_Anafi, Flyability_Elios3, DJI_Phantom4, Headwall_DJI_M600, Geodetic_DJI_M600, and No_UAV (i.e., manual inspection with a handheld device). Inside each subfolder, data is structured by the type of sensors (e.g., Sony4k, FLIR_Duo_R640, VLP-16, and Headwall_NanoHyperspec for visual, infrared, light detection and ranging, and hyperspectral cameras) used for data collection. Sensors such as those on the Elios 2 are accompanied by a log file associated with sensor operation; these types of files must be saved under the same subfolder so that thermal images can be viewed using software (Inspector 3.0). When on-site calibration of a sensor is required, the collected data should be saved under the subfolder of that sensor.

Due to a wide range of variations in bridges, drones, and sensors, data and file management should be refined as needed at bridge sites, to ensure a unique path of each set of information for easy reference and smooth data postprocessing. For example, a Headwall_DJI_M600 drone records data from its GPS antenna in addition to the FLIR-Duo-R640 thermal camera and the Headwall_NanoHyperspec camera. Multiple flight paths may be required for long-span bridges.

At the end of each inspection day, data files should be copied from the laptop computer to two external hard drives and a pre-defined cloud system (Google Drive, One Drive, etc.) through a stable internet connection. Once it is confirmed the data files on the external drive and the cloud system were properly transferred, the data on the laptop computer can be deleted to clear space for the next day of inspection. Depending on data size, internet speed, and cybersecurity concern, data uploading to the cloud system should be done after each inspection trip. Two hard copies of the field inspection data are kept for records with redundancy. Any deletion of the two copies must be approved by pertinent program directors.

7.3 Post-inspection Processing

Quality control in inspection is related to the specific locations of interest. The data collected from a UAV-based multimodal sensing system must be accurate enough to be useful in practice. The data should be validated against ground truths through statistical analysis.

7.3.1 Statistical Analysis

The UAS-based inspection data after in-field rapid extraction from imagery via deep learning algorithms should be analyzed further and compared with their respective ground truths. The mean and standard deviation of the inspection and ground truth data are determined to understand their difference in average value and variation. The root-mean-square error (RMSE) between the inspection data and ground truth is also determined to support decision-making on

whether the inspection data meets the quality requirements in these standards. The coefficient of correlation between the inspection data and the ground truth should exceed 0.85.

Both hardware and software approaches can be used to assess the condition states of bridge elements. They are respectively implemented for the determination of critical parameters (e.g., crack width) and for the automatic extraction of useful information and data (including crack width) from videos. The hardware approach to extract data for element condition assessment involves the use of a camera and a structured light projector (e.g., Intel Depth Camera SR300 and D435) to determine crack widths directly from an image. The software approach to extract data through 3D bridge reconstruction is two-fold, active and passive. LiDAR is one of the most widely used active sensors for object detection. Passive image-based 3D reconstruction requires a balance of sensor cost and data resolution. Stereo vision is a popular passive method for obtaining 3D data and then processing two images captured with slightly different perspectives. Individual bridge elements and deterioration can be detected from 3D model reconstruction using software such as Agisoft Metashape with AI technologies.

During laboratory tests, multiple samples can be prepared following a proper experimental design to collect a set of data for statistical analysis. During field inspections, however, there is only one ground truth data sample from an aging bridge available for each type of element defect. This is mainly because bridges are designed and built by different teams according to distinctive design codes that evolve over time, and they experience various degrees of deterioration over time under various loading and environmental conditions. In this case, two strategies can be used to supplement sample data for statistical analysis:

1. Weakly-correlated samples can be collected for one type of defect from one bridge. Take the width of a flexural crack as an example. The lengths of cracks are often observed in the multiple elements of a bridge. Using the maximum crack width at one flexural crack as a reference, the crack widths from other cracks on various bridge elements can be scaled up, depending on the bending moments applied at respective sections.
2. Samples from multiple bridges that were designed and built with the same procedure and process along the same transportation corridor (similar traffic and environmental conditions) can be collected for statistical analysis. The statistics of maximum crack widths collected from all the bridges are analyzed and compared to understand the confidence level of any prediction used for comparison with the inspection data. While the sample data collected this way is uncorrelated, they are likely to have a larger variation than that using the first strategy due to additional changes in traffic and environmental conditions.

7.3.2 Data Management

Inspection data should be processed and well documented before they are archived for future uses. To facilitate data preservation and sharing, the collected data should be managed to ensure their widest applications possible in engineering services, research projects, and education initiatives. Data management may cover sensor data assimilation, metadata reporting, and data standards and curation.

7.3.2.1 Sensor Data Assimilation

Several types of sensor data and their integration in computational models for bridge condition evaluation toward data-driven bridge asset management should be documented. Sensor data is collected from remote sensing (i.e., drone-based hyperspectral, RGB, thermal, and LiDAR imagery), in-situ sensing, and NDT. Hyperspectral and RGB images can be used to evaluate material types (e.g., concrete vs. asphalt pavements), surface colors (e.g., corrosion products), and surface textures (e.g., cracks), which are indicative of corrosion products and surface defects. Thermography can be used to detect temperature variations and subsurface defects such as concrete delamination in bridge decks. LiDAR point clouds can be used to create high-fidelity 3D reconstruction of bridges to enable virtual inspection on a digital twin platform when fused with RGB and thermal images. In-situ sensors such as distributed coaxial cable sensors for crack width and long-period fiber gratings for corrosion-induced mass loss (Guo and Chen, 2021) can be used as ground truths in machine learning and model validation. NDT data such as reinforcement bar distribution in concrete, crack depth, and electrical resistivity can be used to examine material deterioration and structural element degradation in local areas.

The 3D reconstruction of bridges (and digital twins in the future) can be developed not only to keep track of their lifecycle asset management records (e.g., retrofit and rehabilitation tasks) but also to demonstrate computational model updating and deterioration progression in near real-time as needed. The digital twin fused with RGB images and LiDAR point clouds can also serve as a mapping tool for guiding flight-mission planning for future inspection. The computational models used include finite element model, computer vision model, and computational intelligence (AI algorithms and models).

7.3.2.2 Metadata Reporting

Metadata includes bridge drawings, 3D models, scripts and codes in machine learning algorithms, meeting notes, and publications. The as-built drawings of bridges used to facilitate field inspection should be organized and documented together with field notes and sketches taken during the inspection. The 3D models should be documented to include design assumptions, general methodology, operation procedures, result validations, and application limitations. Presentation slides and readme files for various data sources should be developed to ensure that the curated data are easy to understand by a third party. Virtual meetings to get ready for field inspections should be recorded pending participants' consent; the recorded videos should be curated and archived for the public when deemed necessary. Technical publications that summarize inspection data and results should be documented for future references.

Specifically, metadata should be stored on a portable device (e.g., tablet or laptop) prior to and during each field inspection, and organized for final archival during post processing. Metadata includes the inspected bridge, inspection date/time, robotic platform, multimodal sensing system, and operation condition such as illumination, wind, in-field reference, image quality, and other important notes.

7.3.2.3 Data Standards and Curation

Imagery and videos taken from various cameras and scanners should follow American Society for Photogrammetry and Remote Sensing (ASPRS) Standards or other equivalent guidelines to ensure quality. All simulation, raw and processed experimental data should be prepared and/or summarized according to ASCE journal standards due to their wide acceptance among potential users in civil engineering. Most of the data should be presented in the format of text descriptions, tables, graphs, images, and videos. Engineering drawings should be saved in PDF format. Big data should be partitioned in a logical order as documented in readme files.

Sensor data and metadata should be authenticated, archived, retrieved, and preserved by a certified entity and data repository such as the Scholars' Mine at Missouri S&T. Such a repository should conform to the core characteristics of a trustworthy data repository by the U.S. Department of Transportation (USDOT) CoreTrustSeal Certification that Missouri S&T received in April 2018.

7.3.3 Software Evaluation

Image processing software should be evaluated to quantify the effects of UAV flight speed, frames per second (fps), sensor calibration, and illumination variation on orthophoto data quality and digital elevation model. Compared with Agisoft and EnsoMOSAIC software, Pix4UAV 3D and Menci APS can perform camera self-calibration. Considering the 3D reconstruction accuracy and configurability, GPU support and price, Agisoft is attractive to research groups and advanced users, and Pix4UAV 3D for commercial uses.

Pix4UAV 3D is the most stable, UAS specific software package; but it lacks enhanced functionality or adaptive integration. It requires the second least amount of processing time and performs at comparable or higher accuracy. It does not require knowledge in photogrammetry to operate and offers bulk secondary "Pix4UAV Desktop Rapid" licenses (GPU enabled and limited batch processing capacity) for quick turnaround data validation at bridge sites.

Agisoft has the least number of photogrammetric components, calculates comprehensive internal camera calibration parameters, and offers substantial data export options/formats with batch and scripting capability. It requires the most processing time and performs at comparable to lower accuracy. It does not require knowledge in photogrammetry to operate but is deeply ingrained in 3D modeling from still photographs and requires considerable trial and error to derive the best practices of use.

CHAPTER 8. CONCLUSIONS AND RECOMMENDATIONS

The pooled-fund study developed a framework of automated bridge preservation, introduced advanced robotic, sensing, and NDT technologies, demonstrated their applicability in bridge inspection, and documented their performance at 59 bridge sites. Compared to the current visual inspection practices, the more quantifiable inspection findings and results based on the proposed advanced technologies can be used directly to develop cost-effective maintenance strategies. They can thus streamline the inspection-to-maintenance process in data-driven bridge asset management. The best practices learned from this study will have a profound impact on bridge inspection and maintenance.

8.1 Conclusions Drawn from Field Tests

Based on extensive field experiments, the following conclusions can be drawn:

- A framework of automated bridge preservation is developed to integrate advanced robotic, sensing, and NDT technologies into the visual inspections currently used. While sensing systems always provide quantitative measurements, visual inspection and NDT results are mostly qualitative to the assessment of material deterioration and structural behavior. Their integration is promising in delivering a comprehensive solution in bridge inspection and maintenance.
- BIRDS is a unique mobile test facility that enables big data collection from elevated bridge structures both in air and under water. By inventing effective engaging mechanisms with key bridge elements, such as I-shaped girders, the BIRDS ultimately provides safe access to both superstructure and substructure for close-distance inspection and NDT; it overcomes environmental and operational variation challenges with commercial drones for consistent data acquisition and thus high-quality condition assessment, thus revolutionizing the inspection of bridges.
- By combining flying, traversing, and crawler-launching capabilities, Missouri S&T's invention – BIRDS (BridgeBot specifically) offers a versatile robotic solution that addresses the limitations of commercial drone technologies. Its ability to seamlessly transition between aerial and ground-based inspection modes ensures a comprehensive coverage of bridge structures, enabling both global visual monitoring and local detailed inspection. Local inspection uses remote sensing (e.g., microscopic imager and laser scanner) and NDT (e.g., ultrasonic metal thickness gauge and impact echo) for the detection and quantification of bridge surface and sub-surface defects. For example, vision-based instance segmentation via machine learning can efficiently and effectively provide real-time detection, location, and quantification of weld defects in steel bridges, including cracks, debonding, and cavity.
- NDT is ineffective to detect deep rebar conditions in concrete bridge decks thicker than 8 in (20 cm) due to signal scattering in heterogeneous concrete. For example, a test on the topside deck surface results in inconclusive findings on the condition of bottom rebar. As such, inspecting from the underside of decks is necessary for structural safety in addition to reducing disruption to the traffic. The results from NDT such as microwave imaging,

impact echo, and ultrasonic surface waves are indicative of the presence of defects but tend to be less quantifiable.

- Complementary commercial drones (e.g., DJI M600, Elios 3, Parraot Anafi, Phantom 4, and Skydio 2) can provide a comprehensive inspection of bridges in three parts: above-deck, below-deck, and side. For instance, a DJI M600 equipped with LiDAR, thermal, and hyperspectral sensors is safe to fly above the bridge and provide all types of remote sensing data. The Elios 3 can help effectively inspect the underside of a bridge deck in a GPS-denied, poorly lit, and confined space between parallel girders. The remaining drones can be used interchangeably for bridge side and above-deck inspections. Manual operation with a high-resolution camera (or binocular) may supplement the robotic operation in robot-inaccessible areas.
- The type and number of defects observed from the 59 selected bridges in three age groups (15-20, 25-30, and 35-40 years) are limited. Observed deterioration and damage include concrete cracks, concrete spalling, concrete delamination, rebar exposure, and steel corrosion.
- Bridge inspection protocols and guidelines represent the best practices accumulated from evaluating the 59 bridges over five years. They are presented in three phases: pre-inspection preparation, during-inspection execution, and post-inspection processing.
- To collect high-quality data without affecting the passing traffic, drones are operated at an altitude of 98 – 164 ft (30-50 m) along bridge sides if image resolution is sufficient for vision-based inspection. Direct flight over the traffic is minimized for operation safety.
- A pre-defined autonomous flight path can improve consistency and efficiency in drone operation. For example, a heavy-duty drone (e.g., DJI M600) can complete the above-deck inspection of a bridge in 20-30 min regardless of the bridge length. This feature is especially attractive for long-span bridges. The time required to complete the under-deck inspection of a bridge using a lightweight drone (e.g., Skydio 2) depends on the length and number of girders and the accessibility of bridges.
- Robot-assisted bridge inspection enables an automated execution of the entire inspection process from data collection through machine learning for bridge elements of interest to defect identification and quantification, thus assisting in the implementation of more comprehensive inspection methods as prescribed in the 2019 AASHTO *Manual for Bridge Element Inspection*.
- Although comparable in time for short-span bridges, the robotic operation is advantageous over its corresponding manual operation in visual inspection. The robotic inspection with multimodal sensors eliminates bridge access challenges and traffic control, improves inspection comprehensiveness for surface and subsurface defects, enhances inspection objectivity and quantification, and extends the usefulness of inspection reports in developing maintenance strategies. For long-span bridges, the robotic solution is also significantly more efficient than the visual inspection.
- Complementary remote sensing technologies are applied to achieve multiple objectives. High-resolution RGB images effectively reveal bridge surface defects in terms of color, texture, and pattern. Thermal images are effective in revealing substrate defects such as delamination when taken above bridge decks during the heating process (e.g., 10 am – 2

pm) on a sunny day or when taken from bridge decks during the cooling process (e.g., after sundown). Hyperspectral images can shed light on the type of materials used in bridge construction and chemical marks left on the surface of bridge decks.

- The 3D reconstruction of bridges is a critical step in a digital transformation of bridge asset management. When a LiDAR point cloud is fused with RGB and thermal images, geo-referenced surface features and subsurface indicators (e.g., delamination and void) can be virtually inspected anywhere and anytime by anyone authorized for access.

8.2 Recommendations and Future Research

- Although the advanced robotic, sensing, and NDT technologies have been demonstrated to be unique in data collection, their translation for practical adoption and implementation is just beginning. Further testing at the 59 bridge sites is warranted to exploit all implementation challenges and, more importantly, extract several types of defects using artificial intelligence and quantify their uncertainty in statistical analysis.
- Since a limited type and number of defects are observed in the 59 in-service bridges, more bridges should be inspected and evaluated to collect the big data required in machine learning to develop decision-making support tools toward data-driven bridge asset management.
- While promising, sonar point clouds should be further analyzed to accurately segment objects, such as columns and footings, and calculate useful quantities around bridge foundations, such as scour hole volume and depth.
- Future research is needed to fuse LiDAR point cloud data with RGB and thermal images to enable a virtual inspection of geo-referenced digital bridge twins for multiple defects. To this endeavor, pre-defining autonomous flight paths hinging on physical constraints and 3D reconstruction requirements should be developed for consistent bridge side and deck underside inspection.
- Multitask machine learning taking spatiotemporal characteristics into account should be further developed to implement physical constraints and engineering knowledge so that multiple types of defects can be classified both efficiently and effectively.
- The ultrasonic thickness gauge has been demonstrated to be efficient and effective in measuring the web and flange thicknesses of cleaned weathering steel girders (e.g., ASTM A709 Grade 50W) on the 22-years-old Bill Emerson Cable-stayed Bridge over the Mississippi River. However, how the surface of severely corroded steel should be mechanically brushed or laser cleaned warrant further investigations on real-world bridges. Weathering steel as a specialized type of high-strength, low-alloy steel is characterized by its rust-like patina in a corrosive environment. The patina forms naturally over time. When severely corroded, the surface of the weathering steel with its signature warm, earthy tones may become rough, affecting the contact condition with the ultrasonic gauge.

REFERENCES

- AASHTO. 2019. *Manual for Bridge Element Inspection*, including 2022 and 2024 interim revisions. American Association of State Highway and Transportation Officials (AASHTO), Washington, DC. Accessed June 6, 2025. <https://aashtojournal.transportation.org/aashto-publishes-new-manual-for-bridge-element-inspection/>.
- Alhaj, Abdullah, Qu, Hongya, Zhang, Haibin, Chen, Genda, Anderson, Neil Lennart, and Torgashov, Evgeniy V. 2019. "Evaluations of Multiple Nondestructive Techniques on Top and Bottom Surfaces of a Reinforced Concrete Bridge Deck." 9th International Conference on Structural Health Monitoring of Intelligent Infrastructure (SHMII-9). Accessed June 6, 2025. https://scholarsmine.mst.edu/civarc_enveng_facwork/1746/.
- ACS. n.d. *Acoustic Control Systems* – ACS Group. Accessed May 30, 2025. <https://acs-international.com/product/pengauge/>.
- ASTM. 2021. *Standard Test Method for Compressive Strength of Cylindrical Concrete Specimens*. American Society for Testing and Materials, Committee C09 on Concrete and Concrete Aggregates. ASTM International, Accessed May 6, 2025. https://store.astm.org/c0039_c0039m-20.html.
- ASTM. 2022. *Standard Test Method for Flexural Strength of Concrete (Using Simple Beam with Third-Point Loading)*. American Society for Testing and Materials, ASTM C78/C78M-22, Accessed May 6, 2025. https://store.astm.org/c0078_c0078m-22.html.
- Anderson, Neil, and Li, Mengxing. 2014. "Testing and Assessment of Portable Seismic Property Analyzer." Final Report No. NUTC R297. Center for Transportation Infrastructure and Safety. Missouri University of Science and Technology. Accessed June 6, 2025. <https://transportation.mst.edu/media/research/transportation/documents/R297%20Final%20Report.pdf>.
- Annis C. 2009. *Nondestructive Evaluation System Reliability Assessment Department of Defense Handbook*. MIL-HDBK-1823A. Wright-Patterson AFB, USA. 2009. <https://statistical-engineering.com/wp-content/uploads/2017/10/MIL-HDBK-1823A2009.pdf>.
- Bao, Yi, Ghasr, Mohammad Tayeb, Ying, Kuang, Chen, Genda, and Zoughi, Reza. 2017. "Microwave Synthetic Aperture Radar Imaging for Nondestructive Evaluation of Mechanically Stabilized Earth Walls." *Materials Evaluation*, 75(2): 177-184. https://www.researchgate.net/publication/313215570_Microwave_Synthetic_Aperture_Radar_Imaging_for_Nondestructive_Evaluation_of_Mechanically_Stabilized_Earth_Walls.
- Case, Joseph T., Ghasr, Mohammad Tayeb, and Zoughi, Reza. 2012. "Optimum 2-D Nonuniform Spatial Sampling for Microwave SAR-based NDE Imaging Systems." *IEEE Transactions on Instrumentation and Measurement* 61.11. 2012: 3072-3083. Accessed May 6, 2025. <https://doi.org/10.1109/TIM.2012.2203732>.
- Chen, Genda, Taffese, Woubishet Z., Sharma, Ritesh, and Shi, Zhenhua. 2024. *QA/QC Guidelines on Drone-based Remote Sensing for Bridge Element Inspection*. Final Project Report No. INSPIRE-025, Submitted to the U.S. Department of Transportation by INSpecting and Preserving Infrastructure through Robotic Exploration (INSPIRE) University Transportation Center, Missouri University of Science and Technology. Accessed June 6, 2025. https://scholarsmine.mst.edu/cgi/viewcontent.cgi?article=1000&context=project_im-4.
- CloudCompare. n.d. Accessed June 6, 2025. <https://www.danielgm.net/cc/>.

- Conyers, Stephen A. 2019. *Empirical Evaluation of Ground, Ceiling, and Wall Effect for Small-scale Rotorcraft*. Ph.D. Dissertation submitted to the Graduate Faculty of the University of Denver. Accessed May 6, 2025. <https://digitalcommons.du.edu/etd/1570/>.
- CREALITY. n.d. Accessed July 30, 2025. <https://store.creality.com/products/cr-scan-ferret-pro-3d-scanner>.
- DJI. n.d. Accessed May 14, 2025. <https://www.dji.com/support/product/matrice600-pro>.
- FAA. n.d. *UAS Homepage, Federal Aviation Administration*. Accessed March 12, 2024. <https://www.faa.gov/uas/>.
- Flyability. n.d. Accessed May 14, 2025. <https://www.flyability.com/elios-3>.
- Geodetics. n.d. Accessed May 14, 2025. <https://geodetics.com/>.
- Ghasr, Mohammad Tayeb, Case, Joseph T., and Zoughi, Reza. 2014. "Novel Reflectometer for Millimeter-wave 3-D Holographic Imaging." *IEEE Transactions on Instrumentation and Measurement* 63(5): 1328-1336. Accessed May 6, 2025. <https://ieeexplore.ieee.org/document/6718120>.
- Ghasr, Mohammad Tayeb, Horst, Matthew J., Dvorsky, Matthew R., and Zoughi, Reza. 2016. "Wideband Microwave Camera for Real-time 3-D Imaging." *IEEE Transactions on Antennas and Propagation* 65(1): 258-268. Accessed May 6, 2025. <https://ieeexplore.ieee.org/document/7747447>.
- Gucunski, Nenad, Slabaugh, Greg, Wang, Zhe, Fang, Tong, and Maher, Ali. 2008. "Impact Echo Data from Bridge Deck Testing: Visualization and Interpretation." *Transportation research record* 2050(1): 111-121. Accessed May 6, 2025. <https://journals.sagepub.com/doi/abs/10.3141/2050-11>.
- Guo, Chuanrui, and Chen, Genda. 2021. "A Corrosion Threshold-controllable Sensing System of Fe-C Coated Long Period Fiber Gratings for Life-cycle Mass Loss Measurement of Steel Bars with Strain and Temperature Compensation." *Smart Structures and Systems, An International Journal* 28(4): 443-453. Accessed May 6, 2025. <https://doi.org/10.12989/sss.2021.28.4.443>.
- Headwall. n.d. Accessed May 14, 2025. <https://headwallphotonics.com/>.
- Khanam, Rahima, and Hussain, Muhammad. 2024. *Yolov11: An Overview of the Key Architectural Enhancements*. Accessed June 6, 2025. <https://doi.org/10.48550/arXiv.2410.17725>.
- Liu, Chao, Al Qaseer, Mohammad T., and Zoughi, Reza. 2020. *Microwave Camera for Concrete Delamination and Steel Corrosion Detection*. Final Project Report No. INSPIRE-006, Submitted to the U.S. Department of Transportation by INSpecting and Preserving Infrastructure through Robotic Exploration (INSPIRE) University Transportation Center, Missouri University of Science and Technology. Accessed May 6, 2025. https://scholarsmine.mst.edu/project_sn-4/1/.
- Meeker, William, Roach, Dennis, and Kessler, Seth. 2019. "Statistical Methods for Probability of Detection in Structural Health Monitoring." 2019 International Workshop on Structural Health Monitoring, Stanford, CA. <https://doi.org/10.12783/shm2019/32095>.
- Meeker, William Q., Escobar, Luis A., and Pascual, Francis G. 2021. *Statistical Methods for Reliability Data*. John Wiley & Sons. Accessed June 6, 2025. <https://www.wiley.com/en-us/Statistical+Methods+for+Reliability+Data%2C+2nd+Edition-p-9781118115459>.
- Micro-Epsilon. n.d. Accessed June 6, 2025. <https://www.micro-epsilon.com>.
- Nazarian, Soheil. 1984. In Situ Determination of Elastic Moduli of Soil Deposits and Pavement Systems by Spectral-Analysis-of-Surface-Waves Method (Shear Velocity, Propagation,

- Liquefaction, Non-Destructive, Earthquake). Final Project Report No. FHWA/TX-87/46+437-2. The University of Texas at Austin. Accessed June 6. <https://library.ctr.utexas.edu/digitized/texasarchive/phase2/437-2.pdf>.
- Ogunjinmi, Peter, Nguyen, Son, and Chen, Genda, 2024. *Robot-Assisted Underwater Acoustic Imaging for Bridge Scour Inspection*. Final Project Report No. INSPIRE-015, Submitted to the U.S. Department of Transportation by INSpecting and Preserving Infrastructure through Robotic Exploration (INSPIRE) University Transportation Center, Missouri University of Science and Technology. Accessed June 6, 2025. https://scholarsmine.mst.edu/cgi/viewcontent.cgi?article=1000&context=project_as-8.
- Parrot. n.d. Accessed May 14, 2025. <https://www.parrot.com/en/drones/anafi>.
- PCI. n.d. *Prestressed Concrete Institute*, Chicago, IL. Accessed November 30, 2024. https://www.pci.org/PCI_Docs/Design_Resources/Transportation_Resources/AASHTO%20I%20Beams.pdf.
- Poux, Florent. 2025. *3D Data Science with Python: Building Accurate Digital Environments with 3D Point Cloud Workflows*. 1st Ed. O'Reilly Media ISBN: 9781098161330. Accessed May 6, 2025. <https://www.oreilly.com/library/view/3d-data-science/9781098161323/>.
- Reven, Alec M., Fritsche, Clayton A., and Chen, Genda. 2019. "Unmanned Aerial and Traversing Robot as Mobile Platform for Bridge Inspections." 9th International Conference on Structural Health Monitoring of Intelligent Infrastructure (SHMII-9). Accessed June 6, 2025. <https://scholarsmine.mst.edu/>.
- Roboflow. n.d. Accessed June 2025. <https://roboflow.com/>.
- Shi, Zhenhua, Zhang, Haibin, Ghosh Mondal, Tarutal, Hartnagel, Bryan A., and Chen, Genda. 2023. "A Streamlining Remote Sensing and Digitalization Process for Bridge Inspection." 2023 International Workshop on Structural Health Monitoring. Accessed May 6, 2025. <https://www.destechpub.com/product/structural-health-monitoring-2023/>.
- Skydio. n.d. Accessed June 4, 2025. <https://shop.skydio.com/>.
- Sneed, Lesley, Anderson, Neil, and Torgashov, Evgeniy. 2014. Nondestructive Evaluation of MoDOT Bridge Decks—Pilot Study: Bridge A1187. Final Project Report No. cmr14-010. Missouri Department of Transportation. Research, Development and Technology Division. Accessed June 6, 2025. <https://rosap.nrl.bts.gov/view/dot/27135>.
- UgCS. n.d. *Homepage*. Accessed May 14, 2025. <https://www.ugcs.com/>.
- Wang, Jingdong, Sun, Ke, Cheng, Tianheng, Jiang, Borui, Deng, Chaorui, and Zhao, Yang. 2021. "Deep High-Resolution Representation Learning for Visual Recognition." IEEE Transaction on Pattern Analysis and Machine Intelligence 43(10): 3349–3364. Accessed July 31, 2025. <https://doi.org/10.1109/TPAMI.2020.2983686>.
- Yen, Wen-Huei Phillip, Chen, Genda, Yashinsky, Mark, Hashash, Youssef, Holub Curtis, Wang, Kehai, and Guo, Xiaodong. 2011a. China Earthquake Reconnaissance Report: Performance of Transportation Structures During the May 12, 2008, M7.9 Wenchuan Earthquake. Final Report No. FHWA-HRT-11-029, Federal Highway Administration. Accessed July 29, 2025. <https://www.fhwa.dot.gov/publications/research/infrastructure/structures/11029/index.cfm>.
- Yen, Wen-Huei Phillip, Chen, Genda, Buckle, Ian, Allen, Tony, Alzamora, Daniel, Ger, Jeffrey, and Arias, Juan G. 2011b. Post-Earthquake Reconnaissance Report on Transportation Infrastructure: Impact of the February 27, 2010, Offshore Maule Earthquake in Chile. Final


Report No. FHWA-HRT-11-030, Federal Highway Administration. Accessed July 29, 2025.
<https://www.fhwa.dot.gov/publications/research/infrastructure/structures/11030/index.cfm>.

Zhuo, Ying, Ma, Pengfei, Guo, Chuanrui, and Chen, Genda. 2023. "Probability of Detection for Corrosion-induced Steel Mass Loss Using Fe–C Coated LPFG Sensors." *Structural Health Monitoring* 23(6): 3705-3718. Accessed June 6, 2025.
<https://doi.org/10.1177/14759217241227229>.

Zoughi, Reza. 2018. "Microwave and Millimeter Wave Nondestructive Testing Principles." *Materials Evaluation* 76(8): 1063-1069. Accessed June 6, 2025.
<https://source.asnt.org/microwave-and-millimeter-wave-nondestructive-testing-principles/1>.

APPENDIX A: VISUAL/MANUAL INSPECTION REPORTS

Visual inspections of three Missouri bridges A4982, A4988, and A3450 were conducted on May 31, 2025, by Missouri Department of Transportation. The findings were summarized in inspection reports and shared with the research team. Following is a presentation of the three complete inspection reports as references for evaluation of the proposed automated bridge inspection.

	Missouri Department of Transportation State Bridge Inspection Report				July 01, 2025 7:17:54AM
COUNTY: CALLAWAY	DISTRICT: CD	CLASS: STATBR	FED-ID: 30522	BRIDGE: A4982	
STRUCTURE POSTING					
APPROVED CATEGORY: S-1 Ton 1:		NO POSTING REQUIRED Ton 2:		Ton 3:	
COMMENTS:					
FIELD CATEGORY: S-1 Ton 1:		NO POSTING REQUIRED Ton 2:		Ton 3:	PROBLEM:
COMMENTS:				PROBLEM DIRECTION:	
GENERAL COMMENTS/MAJOR RATED ITEMS					
GENERAL COMMENTS: (BOWDEJ1, 04/26/2007)--(65'-110'-65') CONT COMP PL GDR SPANS					
[ITEM 58] DECK: 7-GOOD CONDITION RATING : 01/03/2017		COMMENTS: (TRAMPA, 01/03/2017)--MANY REFLECT T-CR W/MINOR LE;			
[ITEM 59] SUPER: 8-VERY GOOD CONDITION RATING : 01/29/2007		COMMENTS: (OTTINM, 11/20/2012)--MINOR ABUT DIAPH CRACKS			
[ITEM 60] SUB: 8-VERY GOOD CONDITION RATING : 02/27/2025		COMMENTS: (GREENA2, 02/23/2023)--NO DEFECIENCIES NOTED. (LEPPED1, 02/27/2025)--FEW CRACKS IN BENTS AND ABUT			
[ITEM 61] BANK/CHANNEL: 7-MINOR DAMAGE RATING : 02/15/2017		COMMENTS: (STEGEC, 02/15/2017)--BIG SWEEPING CURVE UPSTREAM - LINED WITH RIPRAP - STABLE IN 2016 SOME MINOR EROSION DOWNSTREAM IN 2016			
[ITEM 113] SCOUR: 8-STABLE FOR CALCULATED RATING : 09/23/2004 EVALUATION TYPE :		COMMENTS:			
[ITEM 71] WATERWAY ADEQUACY: ABOVE FLOOD ELEVATIONS RATING : 09/23/2004		COMMENTS:			
[ITEM 72] APPRRDWY ALIGNMENT: 8-VERYGOOD RATING : 09/23/2004		COMMENTS:			
RAILING AND APPROACH PAVEMENT COMPONENTS AND RATINGS					
[ITEM 36A] BRIDGE RAILING RATING: MEETS CURRENT STANDARDS-1 RATING : 05/23/2004		COMMENTS:			
MATERIAL REINFORCED CONCRETE	CONSTRUCTION SAFETY BARRIER CURB	DIRECTION BOTH	COMMENTS		
[ITEM 36B] TRANSITION RAILING RATING: MEETS CURRENT STANDARDS-1 RATING : 05/23/2004		COMMENTS:			
MATERIAL GALVANIZED STEEL	CONSTRUCTION THRIE BEAM TO W-BEAM	DIRECTION ALL	COMMENTS		
[ITEM 36C] APPROACH RAILING RATING: MEETS CURRENT STANDARDS-1 RATING : 05/23/2004		COMMENTS:			
MATERIAL GALVANIZED STEEL	CONSTRUCTION W-BEAM	DIRECTION ALL	COMMENTS		
[ITEM 36D] RAIL END TREATMENT RATING: MEETS CURRENT STANDARDS-1 RATING : 05/23/2004		COMMENTS:			
Design_No = a4982					
Page 2					
This report contains information that is protected from disclosure by federal law, 23 USC Section 409 and the Missouri Open Records Law (Sunshine Act), Section 610.021 RSMo. Please review MoDOT's policy and procedure manual on the Sunshine Act before releasing any of the information contained herein.					

		Missouri Department of Transportation State Bridge Inspection Report		July 01, 2025 7:17:54AM
COUNTY: CALLAWAY		DISTRICT: CD	CLASS: STATBR	FED-ID: 30522
		BRIDGE: A4982		

GENERAL STRUCTURE INFORMATION			***BRIDGE INSPECTION INFORMATION***	
ROUTE: MO94E FEATURE: BIG TAVERN CR STATUS: A-OPEN LOG MILE: 30.132 DETOUR: 10.00 MILES NHS: NO BUILT: 2004 REHAB: LOCATION: S 27 T 46 R 7 W LATITUDE: 38 43 11.66 (DMS) LONGITUDE: 91 41 25.36 (DMS)	# SPANS: 3 LANES ON: 2 LANES UNDER: 0 COMPASS DIRECTION: WEST to EAST DIRECTION OF TRAFFIC: 2-WAY TRAF FUNCTIONAL CLASS: RL-MINOR ARTERIAL NBI OWNER: MODOT NBI MAINTAINED: MODOT MAINTENANCE DISTRICT: CD MAINTENANCE COUNTY: CALLAWAY SUB AREA: 7D36	PLACE CODE: 02656 AUXVASSE LENGTH: 243 FT 0 IN MAXIMUM SPAN: 110 FT 0 IN APPROACH ROADWAY: 40 FT 0 IN CURB TO CURB: 40 FT 0 IN OUT TO OUT: 42 FT 8 IN AADT: 630 AADT YEAR: 2024 AADT TRUCK: 6.0% FUTURE AADT: 1040 FUTURE AADT YEAR: 2044	DATE: 10/10/2024 FREQUENCY: 24 TEAM LEADER: DEREK LEPPER INSPECTOR 2: INSPECTOR 3: INSPECTOR 4:	RESPONSIBILITY: DISTRICT CALCULATED INTERVAL **: 24 ELEMENT: NO INSPECTOR 4:
** When calculated interval exceeds the frequency, a justification comment per BIRM is required.				
GENERAL INSPECTION COMMENTS (HOLZBJ, 01/28/2005)–THE LETTING DATE OF 10/15/2004 HAS BEEN USED AS A INITIAL DEFAULT INSPECTION DATE FOR NBI SUBMITTAL PURPOSES.				


FRACTURE CRITICAL INSPECTION INFORMATION				***INDEPTH INSPECTION INFORMATION***			
DATE:	RESPONSIBILITY:	CATEGORY:	NBI:	DATE:	RESPONSIBILITY:	CATEGORY:	NBI:
FREQUENCY:	CALCULATED INTERVAL **: 136		METHOD:	FREQUENCY:	CALCULATED INTERVAL **: 24		METHOD:
TEAM LEADER: DEREK LEPPER	INSPECTOR 3:			TEAM LEADER: DEREK LEPPER	INSPECTOR 3:		
INSPECTOR 2:	INSPECTOR 4:			INSPECTOR 2:	INSPECTOR 4:		
** When calculated interval exceeds the frequency, a justification comment per BIRM is required.				** When calculated interval exceeds the frequency, a justification comment per BIRM is required.			
FRACTURE CRITICAL INSPECTION COMMENTS				INDEPTH INSPECTION COMMENTS			


SPECIAL INSPECTION INFORMATION				***UNDERWATER INSPECTION INFORMATION***			
DATE: 10/10/2024	RESPONSIBILITY: DISTRICT	CATEGORY: CHANNEL CROSS SEC	NBI: NO	DATE: 10/10/2024	RESPONSIBILITY: DISTRICT	CATEGORY: DRY	NBI: NO
FREQUENCY: 120	CALCULATED INTERVAL **: 136		METHOD: WT TAPE	FREQUENCY: 60	CALCULATED INTERVAL **: 24		METHOD: VISUAL
TEAM LEADER: DEREK LEPPER	INSPECTOR 3:			TEAM LEADER: DEREK LEPPER	INSPECTOR 3:		
INSPECTOR 2:	INSPECTOR 4:			INSPECTOR 2:	INSPECTOR 4:		
** When calculated interval exceeds the frequency, a justification comment per BIRM is required.				** When calculated interval exceeds the frequency, a justification comment per BIRM is required.			
SPECIAL INSPECTION COMMENTS				UNDERWATER INSPECTION COMMENTS			

OTHER SPECIAL INSPECTIONS								OTHER UNDERWATER INSPECTIONS							
DATE	FREQUENCY	CATEGORY	NBI	CALCULATED INTERVAL	RESPONSIBILITY	METHOD		DATE	FREQUENCY	CATEGORY	NBI	CALCULATED INTERVAL	RESPONSIBILITY	METHOD	

Design_No = a4982

Page 1
This report contains information that is protected from disclosure by federal law, 23 USC Section 409 and the Missouri Open Records Law (Sunshine Act), Section 610.021 RSMo. Please review MoDOT's policy and procedure manual on the Sunshine Act before releasing any of the information contained herein.

<div>  <div> <div>Missouri Department of Transportation</div> <div>State Bridge Inspection Report</div> </div> <div> <div>July 01, 2025</div> <div>7:17:54AM</div> </div> </div>									
COUNTY: CALLAWAY		DISTRICT: CD		CLASS: STATBR		FED-ID: 30522		BRIDGE: A4982	
<u>MATERIAL</u>	<u>CONSTRUCTION</u>	<u>DIRECTION</u>	<u>COMMENTS</u>						
GALVANIZED STEEL	BREKAWAY SYSTEM	ALL							
APPROACH PAVEMENT: *Overall condition assigned for each approach pavement component is shown below.									
<u>MATERIAL</u>	<u>CONSTRUCTION</u>	<u>DIRECTION</u>	<u>CONDITION*</u>	<u>COMMENTS</u>					
ASPHALT/CONCRETE	MAT/TIESLAB	BOTH		(BOWDEN, 12/17/2008)--SETTLING @ SLEEPER SLAB					
<u>CONDITION</u>	<u>LOCATION 1</u>	<u>LOCATION 2</u>	<u>SEVERITY</u>	<u>COMMENT</u>					
SETTLEMENT	SLEEPER SLAB		MODERATE	(MARTEP, 12/21/2012)--EAST SLAB IN PARTICULAR HAS DIP IN IT.					
DRAINAGE, EXPANSION DEVICES, BANK/SLOPE, AND DECK PROTECTIVE COMPONENTS									
<u>DECK PROTECTIVE COMPONENTS:</u>									
<u>SERIES TYPE-#</u>	<u>COMPONENT</u>	<u>MATERIAL</u>	<u>CONSTRUCTION</u>	<u>THICKNESS</u>	<u>YEAR APPLIED</u>	<u>MANUFACTURE</u>	<u>OVERALL CONDITION</u>		
MAIN SERIES-1	WEARING SURFACE	PLAIN CONCRETE	MONOLITHIC				GOOD		
<u>COMMENT:</u>									
	DECK PROTECTION	EPOXY POLYMER	COATED REBAR						
<u>COMMENT:</u>									
	MEMBRANE	NOT APPLICABLE	NONE						
<u>COMMENT:</u>									
	SECONDARY DECK PROTECTION	LIQUID SEALANT	INTERNALLY SEALED		2023	SILANE			
<u>COMMENT:</u>									
<u>DRAINAGE COMPONENTS:</u>									
	<u>COMPONENT</u>	<u>MATERIAL</u>	<u>CONSTRUCTION</u>	<u>DIRECTION</u>	<u>COMMENTS</u>				
	DRAINAGE	GEOTEXTILE FABRIC	VERTICAL DRAIN-END BENT						
	DRAINAGE	GALVANIZED STEEL	FLOOR DRAIN						
<u>EXPANSION DEVICE COMPONENTS:</u>									
<u>SUB UNIT-#</u>	<u>SUB LABEL</u>	<u>COMPONENT</u>	<u>MATERIAL</u>	<u>CONSTRUCTION</u>	<u>GAP</u>	<u>YEAR APPLIED</u>	<u>MANUFACTURE</u>	<u>OVERALL CONDITION</u>	
<u>COMMENT:</u>									
<u>BANK/SLOPE PROTECTION COMPONENTS:</u>									
	<u>COMPONENT</u>	<u>MATERIAL</u>	<u>CONSTRUCTION</u>	<u>DIRECTION</u>	<u>COMMENTS</u>				
	BANK PROTECTION	ROCK	BLANKET	BOTH					
DECK COMPONENTS									
<u>SLAB TYPE-#</u>	<u>COMPONENT</u>	<u>MATERIAL</u>	<u>CONSTRUCTION</u>	<u>COMMENTS</u>					
MAIN SLABS-1	DECK	REINFORCED CONCRETE	CAST-IN-PLACE-F/C FORMS						
<u>CONDITION</u>	<u>LOCATION 1</u>	<u>LOCATION 2</u>	<u>SEVERITY</u>	<u>MEASUREMENT</u>	<u>COMMENT</u>				
LEACHING	OVERHANGS		LIGHT						
LEACHING	PRECAST PANELS		LIGHT						
LONGITUDINAL CRACKS	RANDOM		FEW						
REFLECTIVE CRACKS	THROUGHOUT		MANY						
TRANSVERSE CRACKS	OVERHANGS		FEW						
Design_No = a4982									
<div> <div>Page 3</div> <div>This report contains information that is protected from disclosure by federal law, 23 USC Section 409 and the Missouri Open Records Law (Sunshine Act), Section 610.021 RSMo. Please review MoDOT's policy and procedure manual on the Sunshine Act before releasing any of the information contained herein.</div> </div>									

	Missouri Department of Transportation State Bridge Inspection Report				July 01, 2025 7:17:54AM
COUNTY: CALLAWAY	DISTRICT: CD	CLASS: STATBR	FED-ID: 30522	BRIDGE: A4982	

<p style="text-align: center; margin: 0;">***COMPUTER GENERATED RATINGS AND DEFICIENCY ITEMS***</p> <p style="font-size: small; margin: 0;">NOTE: The items listed in this section are updated whenever computer edits are ran on a structure after the inspection updates have been entered in to TMS.</p> <table style="width: 100%; border-collapse: collapse;"> <thead> <tr> <th style="text-align: left; font-size: small;">Rated Item</th> <th style="text-align: left; font-size: small;">Rating</th> <th style="text-align: left; font-size: small;">Rating Date</th> </tr> </thead> <tbody> <tr> <td>[Item 67] Structure Evaluation Rating:</td> <td>8-EQ TO PRESENT DESIRAB</td> <td>11/26/2012</td> </tr> <tr> <td>[Item 68] Deck Geometry Rating:</td> <td>8-EQ TO PRESENT DESIRAB</td> <td>9/23/2004</td> </tr> <tr> <td>[Item 69] Underclearance:</td> <td>N-NOT APPLICABLE</td> <td>9/23/2004</td> </tr> <tr> <td>Sufficiency Rating:</td> <td>99.5%</td> <td>2/22/2022</td> </tr> <tr> <td>Deficiency:</td> <td>NOT DEFICIENT</td> <td>9/23/2004</td> </tr> <tr> <td>Funding Eligibility:</td> <td>---</td> <td>---</td> </tr> <tr> <td>Estimated New Structure Length:</td> <td>---</td> <td>---</td> </tr> <tr> <td>Estimated Structure Cost:</td> <td>---</td> <td>---</td> </tr> <tr> <td>Estimated Total Project Cost:</td> <td>---</td> <td>---</td> </tr> <tr> <td>Year of Cost Estimate:</td> <td>---</td> <td>---</td> </tr> </tbody> </table> <p style="font-size: x-small; margin-top: 5px;">NOTE: The above structure length and cost estimates are computer generated using algorithms in the TMS system. These algorithms are generalized to use NBI items to come up with a new structure length and width to calculate a new area which is taken times a representative cost per square foot. The actual structure size and cost may vary significantly from these numbers once site specific engineering is done.</p>	Rated Item	Rating	Rating Date	[Item 67] Structure Evaluation Rating:	8-EQ TO PRESENT DESIRAB	11/26/2012	[Item 68] Deck Geometry Rating:	8-EQ TO PRESENT DESIRAB	9/23/2004	[Item 69] Underclearance:	N-NOT APPLICABLE	9/23/2004	Sufficiency Rating:	99.5%	2/22/2022	Deficiency:	NOT DEFICIENT	9/23/2004	Funding Eligibility:	---	---	Estimated New Structure Length:	---	---	Estimated Structure Cost:	---	---	Estimated Total Project Cost:	---	---	Year of Cost Estimate:	---	---	<p style="text-align: center; margin: 0;">***ADVANCED SIGN INFORMATION***</p> <table style="width: 100%; border-collapse: collapse;"> <thead> <tr> <th style="text-align: left; font-size: small;">SIGN #</th> <th style="text-align: left; font-size: small;">SIGN TYPE</th> <th style="text-align: left; font-size: small;">PROBLEM</th> <th style="text-align: left; font-size: small;">PROBLEM DIRECTION</th> </tr> </thead> <tbody> <tr> <td style="text-align: center;">1</td> <td></td> <td></td> <td></td> </tr> </tbody> </table> <p style="text-align: center; margin: 10px 0;">***OUTFALL INSPECTION INFORMATION***</p> <table style="width: 100%; border-collapse: collapse;"> <tr> <td style="width: 50%; vertical-align: top;"> # OUTFALLS: STATUS: NOTES: </td> <td style="width: 50%; vertical-align: top;"> INSPECTOR: DATE: </td> </tr> </table>	SIGN #	SIGN TYPE	PROBLEM	PROBLEM DIRECTION	1				# OUTFALLS: STATUS: NOTES:	INSPECTOR: DATE:
Rated Item	Rating	Rating Date																																										
[Item 67] Structure Evaluation Rating:	8-EQ TO PRESENT DESIRAB	11/26/2012																																										
[Item 68] Deck Geometry Rating:	8-EQ TO PRESENT DESIRAB	9/23/2004																																										
[Item 69] Underclearance:	N-NOT APPLICABLE	9/23/2004																																										
Sufficiency Rating:	99.5%	2/22/2022																																										
Deficiency:	NOT DEFICIENT	9/23/2004																																										
Funding Eligibility:	---	---																																										
Estimated New Structure Length:	---	---																																										
Estimated Structure Cost:	---	---																																										
Estimated Total Project Cost:	---	---																																										
Year of Cost Estimate:	---	---																																										
SIGN #	SIGN TYPE	PROBLEM	PROBLEM DIRECTION																																									
1																																												
# OUTFALLS: STATUS: NOTES:	INSPECTOR: DATE:																																											



Missouri Department of Transportation
State Bridge Inspection Report

July 01, 2025
7:17:54AM

COUNTY: CALLAWAY

DISTRICT: CD

CLASS: STATBR

FED-ID: 30522

BRIDGE: A4982

CLEARANCES UNDER BRIDGE

**NOTE: Vertical clearances for permitting purposes are taken as 2 inches less than the actual field measured clearance.

<u>RECORD #</u>	<u>ROUTE</u>	<u># LANES</u>	<u>DIRECTION OF TRAFFIC</u>	<u>RIGHT LATERAL CLEARANCE</u>	<u>LEFT LATERAL CLEARANCE</u>	<u>UR-ID</u>
<u>VERTICAL CLEARANCE TYPE**</u>	<u>VALUE</u>	<u>DIRECTION</u>	<u>DATE</u>	<u>COMMENT</u>		

STRUCTURE PAINT INFORMATION

CONDITION: GOOD

RUST AMOUNT : 9=.03% OF SURFACE RUSTED

STEEL TONS : 113

ORIGINAL PAINT

CONTRACT REPAINT

DEPARTMENT REPAINT

PAINT TYPE : G SYSTEM
NAME : ZINC/EPOXY/ACRYLIC
PAINT COLOR : GRAY
PAINT YEAR : 2005
MILS : 7

PAINT TYPE :
NAME :
PAINT COLOR :
PAINT YEAR :
MILS :

PAINT TYPE :
NAME :
PAINT COLOR :
PAINT YEAR :
MILS :

MANUFACTURE :
SURFACE PREP :

REQUESTED WORK ITEMS

GENERAL WORK COMMENTS:

<u>RESPONSIBILITY</u>	<u>LOCATION</u>	<u>ITEM</u>	<u>CATEGORY</u>	<u>PRIORITY</u>	<u>DATE</u>	<u>WORK ITEM COMMENT</u>
DISTRICT SPECIAL	ROADWAY SURFACE	SEAL WITH SILANE	DECK	3	08/21/2029	

UTILITY ATTACHMENTS

<u>UTILITY</u>	<u>OWNER</u>	<u>METHOD</u>	<u>MEASUREMENT TYPE</u>	<u>VALUE</u>	<u>NUMBER</u>	<u>UTILITY ATTACHMENT COMMENT</u>
----------------	--------------	---------------	-------------------------	--------------	---------------	-----------------------------------


****PROGRAM NOTES INFORMATION****

<u>YEAR</u>	<u>PROJECT #</u>	<u>MONTH LET</u>	<u>YEAR LET</u>	<u>ITEMS</u>	<u>COMMENT</u>
-------------	------------------	------------------	-----------------	--------------	----------------

Design_No = s4982

Page 6

This report contains information that is protected from disclosure by federal law, 23 USC Section 409 and the Missouri Open Records Law (Sunshine Act), Section 610.021 RSMo. Please review MoDOT's policy and procedure manual on the Sunshine Act before releasing any of the information contained herein.

<div>  <div> <div>Missouri Department of Transportation</div> <div>State Bridge Inspection Report</div> </div> <div> <div>July 01, 2025</div> <div>7:17:54AM</div> </div> </div>										
COUNTY: CALLAWAY			DISTRICT: CD		CLASS: STATBR		FED-ID: 30522		BRIDGE: A4982	
TURNED BACK WINGS		REINFORCED CONCRETE		CAST-IN-PLACE						
<u>CONDITION</u>		<u>LOCATION 1</u>		<u>LOCATION 2</u>		<u>SEVERITY</u>		<u>MEASUREMENT</u> <u>COMMENT</u>		
BENT-2	RA-25 DEGREES	43 FT 4 IN	REINFORCED CONCRETE	MULTIPLE COLUMN						
<u>CONDITION</u>		<u>LOCATION 1</u>		<u>LOCATION 2</u>		<u>SEVERITY</u>		<u>MEASUREMENT</u> <u>COMMENT</u>		
<u>ASSOCIATED COMPONENT</u>		<u>MATERIAL</u>		<u>CONSTRUCTION</u>						
BEAM CAP		REINFORCED CONCRETE		CAST-IN-PLACE						
<u>CONDITION</u>		<u>LOCATION 1</u>		<u>LOCATION 2</u>		<u>SEVERITY</u>		<u>MEASUREMENT</u> <u>COMMENT</u>		
VERTICAL CRACKS		RANDOM				FEW				
<u>CONDITION</u>		<u>LOCATION 1</u>		<u>LOCATION 2</u>		<u>SEVERITY</u>		<u>MEASUREMENT</u> <u>COMMENT</u>		
COLUMN		REINFORCED CONCRETE		CAST-IN-PLACE						
<u>CONDITION</u>		<u>LOCATION 1</u>		<u>LOCATION 2</u>		<u>SEVERITY</u>		<u>MEASUREMENT</u> <u>COMMENT</u>		
DRILLED SHAFT		REINFORCED CONCRETE		CAST-IN-PLACE						
<u>CONDITION</u>		<u>LOCATION 1</u>		<u>LOCATION 2</u>		<u>SEVERITY</u>		<u>MEASUREMENT</u> <u>COMMENT</u>		
FIXED BEARING		ELASTOMERIC		LAMINATED NEOPRENE						
<u>CONDITION</u>		<u>LOCATION 1</u>		<u>LOCATION 2</u>		<u>SEVERITY</u>		<u>MEASUREMENT</u> <u>COMMENT</u>		
BENT-3		RA-25 DEGREES	43 FT 4 IN	REINFORCED CONCRETE	MULTIPLE COLUMN					
<u>CONDITION</u>		<u>LOCATION 1</u>		<u>LOCATION 2</u>		<u>SEVERITY</u>		<u>MEASUREMENT</u> <u>COMMENT</u>		
<u>ASSOCIATED COMPONENT</u>		<u>MATERIAL</u>		<u>CONSTRUCTION</u>						
BEAM CAP		REINFORCED CONCRETE		CAST-IN-PLACE						
<u>CONDITION</u>		<u>LOCATION 1</u>		<u>LOCATION 2</u>		<u>SEVERITY</u>		<u>MEASUREMENT</u> <u>COMMENT</u>		
VERTICAL CRACKS		RANDOM				FEW				
<u>CONDITION</u>		<u>LOCATION 1</u>		<u>LOCATION 2</u>		<u>SEVERITY</u>		<u>MEASUREMENT</u> <u>COMMENT</u>		
COLUMN		REINFORCED CONCRETE		CAST-IN-PLACE						
<u>CONDITION</u>		<u>LOCATION 1</u>		<u>LOCATION 2</u>		<u>SEVERITY</u>		<u>MEASUREMENT</u> <u>COMMENT</u>		
DRILLED SHAFT		REINFORCED CONCRETE		CAST-IN-PLACE						
<u>CONDITION</u>		<u>LOCATION 1</u>		<u>LOCATION 2</u>		<u>SEVERITY</u>		<u>MEASUREMENT</u> <u>COMMENT</u>		
FIXED BEARING		ELASTOMERIC		LAMINATED NEOPRENE						
<u>CONDITION</u>		<u>LOCATION 1</u>		<u>LOCATION 2</u>		<u>SEVERITY</u>		<u>MEASUREMENT</u> <u>COMMENT</u>		
ABUTMENT-4		RA-25 DEGREES	47 FT 1 IN	REINFORCED CONCRETE	INTEGRAL					
<u>CONDITION</u>		<u>LOCATION 1</u>		<u>LOCATION 2</u>		<u>SEVERITY</u>		<u>MEASUREMENT</u> <u>COMMENT</u>		
<u>ASSOCIATED COMPONENT</u>		<u>MATERIAL</u>		<u>CONSTRUCTION</u>						
BEAM CAP		REINFORCED CONCRETE		CAST-IN-PLACE						
<u>CONDITION</u>		<u>LOCATION 1</u>		<u>LOCATION 2</u>		<u>SEVERITY</u>		<u>MEASUREMENT</u> <u>COMMENT</u>		
VERTICAL CRACKS		RANDOM				FEW				
<u>CONDITION</u>		<u>LOCATION 1</u>		<u>LOCATION 2</u>		<u>SEVERITY</u>		<u>MEASUREMENT</u> <u>COMMENT</u>		
FIXED BEARING		STEEL		GIRDER CHAIRS						
<u>CONDITION</u>		<u>LOCATION 1</u>		<u>LOCATION 2</u>		<u>SEVERITY</u>		<u>MEASUREMENT</u> <u>COMMENT</u>		
PILING		STEEL		H-SHAPE						
<u>CONDITION</u>		<u>LOCATION 1</u>		<u>LOCATION 2</u>		<u>SEVERITY</u>		<u>MEASUREMENT</u> <u>COMMENT</u>		
TURNED BACK WINGS		REINFORCED CONCRETE		CAST-IN-PLACE						
<u>CONDITION</u>		<u>LOCATION 1</u>		<u>LOCATION 2</u>		<u>SEVERITY</u>		<u>MEASUREMENT</u> <u>COMMENT</u>		
OVER/UNDER ROUTES CLEARANCE INFORMATION										
<div> <div> <div>CLEARANCES OVER DECK</div> <div> <div>VERTICAL CLEARANCE TYPE**</div> <div>VALUE</div> <div>DIRECTION</div> <div>DATE</div> <div>COMMENT</div> </div> </div> <div> <div>**NOTE: Vertical clearances for permitting purposes are taken as 2 inches less than the actual field measured clearance.</div> </div> </div>										

Design_No = s4982



Missouri Department of Transportation
State Bridge Inspection Report

July 01, 2025
7:17:54AM

COUNTY: CALLAWAY

DISTRICT: CD

CLASS: STATBR

FED-ID: 30522

BRIDGE: A4982

TRANSVERSE CRACKS RANDOM MANY

MAIN SPANS-2	DECK	REINFORCED CONCRETE	CAST-IN-PLACE F/C FORMS			
<u>CONDITION</u>		<u>LOCATION 1</u>	<u>LOCATION 2</u>	<u>SEVERITY</u>	<u>MEASUREMENT</u>	<u>COMMENT</u>
LEACHING		OVERHANGS		MINOR		
LONGITUDINAL CRACKS		RANDOM		FEW		
REFLECTIVE CRACKS		THROUGHOUT		MANY		
TRANSVERSE CRACKS		OVERHANGS		FEW		
TRANSVERSE CRACKS		PRECAST PANELS		FEW		

MAIN SPANS-3	DECK	REINFORCED CONCRETE	CAST-IN-PLACE F/C FORMS			
<u>CONDITION</u>		<u>LOCATION 1</u>	<u>LOCATION 2</u>	<u>SEVERITY</u>	<u>MEASUREMENT</u>	<u>COMMENT</u>
LEACHING		OVERHANGS		LIGHT		
LEACHING		PRECAST PANELS		LIGHT		
LONGITUDINAL CRACKS		RANDOM		FEW		
REFLECTIVE CRACKS		THROUGHOUT		MANY		
TRANSVERSE CRACKS		OVERHANGS		FEW		
TRANSVERSE CRACKS		PRECAST PANELS		FEW		

SUPERSTRUCTURE COMPONENTS

<u>SERIES TYPE-H</u>	<u>SPAN TYPE</u>	<u>MATERIAL</u>	<u>CONSTRUCTION</u>	<u>LABEL</u>	<u>COMMENTS</u>
MAIN SERIES-1	CONTINUOUS SLAN	STEEL	PLATE GIRDERS		
<u>SPAN</u>	<u>COMPOSITE INDICATOR</u>	<u>LENGTH</u>	<u>WEATHERING STEEL</u>	<u>COMMENTS</u>	
MAIN SPANS-1	COMPOSITE	65 FT 0 IN	NO		
<u>CONDITION</u>		<u>LOCATION 1</u>	<u>LOCATION 2</u>	<u>SEVERITY</u>	<u>MEASUREMENT</u> <u>COMMENT</u>
LEACHING		GIRDER ENCASEMENT		MINOR	
VERTICAL CRACKS		DIAPHRAGMS		FEW	
MAIN SPANS-2	COMPOSITE	110 FT 0 IN	NO		
<u>CONDITION</u>		<u>LOCATION 1</u>	<u>LOCATION 2</u>	<u>SEVERITY</u>	<u>MEASUREMENT</u> <u>COMMENT</u>
DEADLOAD DEFLECTION		MID SPAN		MINOR	
MAIN SPANS-3	COMPOSITE	65 FT 0 IN	NO		
<u>CONDITION</u>		<u>LOCATION 1</u>	<u>LOCATION 2</u>	<u>SEVERITY</u>	<u>MEASUREMENT</u> <u>COMMENT</u>
OTHER		THROUGHOUT		NOT APPLICABLE	(MEYERM3, 01/04/2021)--DIAPHRAGM OVERHANGING ABUTMENT
VERTICAL CRACKS		DIAPHRAGMS		FEW	
VERTICAL CRACKS		GIRDER ENCASEMENT		MINOR	

SUBSTRUCTURE COMPONENTS

<u>SUBSTRUCTURE</u>	<u>SKEW</u>	<u>LENGTH</u>	<u>MATERIAL</u>	<u>CONSTRUCTION</u>	<u>LABEL</u>	<u>COMMENTS</u>
ABUTMENT-1	RA-25 DEGREES	47 FT 1 IN	REINFORCED CONCRETE	INTEGRAL		
<u>ASSOCIATED COMPONENT</u>	<u>CONDITION</u>	<u>LOCATION 1</u>	<u>LOCATION 2</u>	<u>SEVERITY</u>	<u>MEASUREMENT</u>	<u>COMMENT</u>
BEAM CAP		REINFORCED CONCRETE	CAST-IN-PLACE			
<u>CONDITION</u>		<u>LOCATION 1</u>	<u>LOCATION 2</u>	<u>SEVERITY</u>	<u>MEASUREMENT</u>	<u>COMMENT</u>
FIXED BEARING		STEEL	GIRDER CHAIRS			
<u>CONDITION</u>		<u>LOCATION 1</u>	<u>LOCATION 2</u>	<u>SEVERITY</u>	<u>MEASUREMENT</u>	<u>COMMENT</u>
PILING		STEEL	H-SHAPE			
<u>CONDITION</u>		<u>LOCATION 1</u>	<u>LOCATION 2</u>	<u>SEVERITY</u>	<u>MEASUREMENT</u>	<u>COMMENT</u>

Design_No = s4982

Page 4

This report contains information that is protected from disclosure by federal law, 23 USC Section 409 and the Missouri Open Records Law (Sunshine Act), Section 610.021 RSMo. Please review MoDOT's policy and procedure manual on the Sunshine Act before releasing any of the information contained herein.



Missouri Department of Transportation
State Bridge Inspection Report

July 01, 2025
7:17:54AM

COUNTY: CALLAWAY

DISTRICT: CD

CLASS: STATBR

FED-ID: 30522

BRIDGE: A4982

Design_No = s4982

Page 8

This report contains information that is protected from disclosure by federal law, 23 USC Section 409 and the Missouri Open Records Law (Sunshine Act), Section 610.021 RSMo. Please review MoDOT's policy and procedure manual on the Sunshine Act before releasing any of the information contained herein.

		Missouri Department of Transportation State Bridge Inspection Report		July 01, 2025 7:17:06AM
COUNTY: CALLAWAY		DISTRICT: CD	CLASS: STATBR	FED-ID: 30523
		BRIDGE: A4988		

GENERAL STRUCTURE INFORMATION			***BRIDGE INSPECTION INFORMATION***	
ROUTE: MO94E FEATURE: MAINT. RD, KATY TRAIL, STATUS: A-OPEN LOG MILE: 26.411 DETOUR: 22.00 MILES NHS: NO BUILT: 2004 REHAB: LOCATION: S 31 T 46 R 7 W LATITUDE: 38 42 31.21 (DMS) LONGITUDE: 91 44 35.24 (DMS)	# SPANS: 4 LANES ON: 2 LANES UNDER: 1 COMPASS DIRECTION: WEST to EAST DIRECTION OF TRAFFIC: 2-WAY TRAF FUNCTIONAL CLASS: RL-MINOR ARTERIAL NBI OWNER: MODOT NBI MAINTAINED: MODOT MAINTENANCE DISTRICT: CD MAINTENANCE COUNTY: CALLAWAY SUB AREA: 7D36	PLACE CODE: 02656 AUXVASSE LENGTH: 363 FT 0 IN MAXIMUM SPAN: 102 FT 0 IN APPROACH ROADWAY: 40 FT 0 IN CURB TO CURB: 40 FT 0 IN OUT TO OUT: 42 FT 8 IN AADT: 600 AADT YEAR: 2024 AADT TRUCK: 5.6% FUTURE AADT: 990 FUTURE AADT YEAR: 2044	DATE: 10/10/2024 FREQUENCY: 24 TEAM LEADER: DEREK LEPPER INSPECTOR 2: INSPECTOR 3: INSPECTOR 4:	RESPONSIBILITY: DISTRICT CALCULATED INTERVAL **: 24 ELEMENT: NO INSPECTOR 4:
** When calculated interval exceeds the frequency, a justification comment per BIRM is required.				
GENERAL INSPECTION COMMENTS (HOLZBJ, 01/28/2005)–THE LETTING DATE OF 10/15/2004 HAS BEEN USED AS A INITIAL DEFAULT INSPECTION DATE FOR NBI SUBMITTAL PURPOSES.				


FRACTURE CRITICAL INSPECTION INFORMATION				***INDEPTH INSPECTION INFORMATION***			
DATE:	RESPONSIBILITY:	CATEGORY:	NBI:	DATE:	RESPONSIBILITY:	CATEGORY:	NBI:
FREQUENCY:	CALCULATED INTERVAL **: 136		METHOD:	FREQUENCY:	CALCULATED INTERVAL **: 24		METHOD:
TEAM LEADER: DEREK LEPPER	INSPECTOR 3:			TEAM LEADER: DEREK LEPPER	INSPECTOR 3:		
INSPECTOR 2:	INSPECTOR 4:			INSPECTOR 2:	INSPECTOR 4:		
** When calculated interval exceeds the frequency, a justification comment per BIRM is required.				** When calculated interval exceeds the frequency, a justification comment per BIRM is required.			
FRACTURE CRITICAL INSPECTION COMMENTS				INDEPTH INSPECTION COMMENTS			


SPECIAL INSPECTION INFORMATION				***UNDERWATER INSPECTION INFORMATION***			
DATE: 10/10/2024	RESPONSIBILITY: DISTRICT	CATEGORY: CHANNEL CROSS SEC	NBI: NO	DATE: 10/10/2024	RESPONSIBILITY: DISTRICT	CATEGORY: DRY	NBI: NO
FREQUENCY: 120	CALCULATED INTERVAL **: 136		METHOD: WT TAPE	FREQUENCY: 60	CALCULATED INTERVAL **: 24		METHOD: VISUAL
TEAM LEADER: DEREK LEPPER	INSPECTOR 3:			TEAM LEADER: DEREK LEPPER	INSPECTOR 3:		
INSPECTOR 2:	INSPECTOR 4:			INSPECTOR 2:	INSPECTOR 4:		
** When calculated interval exceeds the frequency, a justification comment per BIRM is required.				** When calculated interval exceeds the frequency, a justification comment per BIRM is required.			
SPECIAL INSPECTION COMMENTS				UNDERWATER INSPECTION COMMENTS			


OTHER SPECIAL INSPECTIONS								OTHER UNDERWATER INSPECTIONS							
DATE	FREQUENCY	CATEGORY	NBI	CALCULATED INTERVAL	RESPONSIBILITY	METHOD		DATE	FREQUENCY	CATEGORY	NBI	CALCULATED INTERVAL	RESPONSIBILITY	METHOD	

Design_No = a4988

Page 1
This report contains information that is protected from disclosure by federal law, 23 USC Section 409 and the Missouri Open Records Law (Sunshine Act), Section 610.021 RSMo. Please review MoDOT's policy and procedure manual on the Sunshine Act before releasing any of the information contained herein.

	Missouri Department of Transportation State Bridge Inspection Report				July 01, 2025 7:17:06AM
COUNTY: CALLAWAY	DISTRICT: CD	CLASS: STATBR	FED-ID: 30523	BRIDGE: A4988	
STRUCTURE POSTING					
APPROVED CATEGORY: S-1 Ton 1:		NO POSTING REQUIRED Ton 2:		Ton 3:	
COMMENTS:					
FIELD CATEGORY: S-1 Ton 1:		NO POSTING REQUIRED Ton 2:		Ton 3:	
COMMENTS:		PROBLEM:		PROBLEM DIRECTION:	
GENERAL COMMENTS/MAJOR RATED ITEMS					
GENERAL COMMENTS: (BOWDEJ1, 03/01/2007)--(70'-102'-102'-85') CONT PL GDR SPANS					
[ITEM 58] DECK: 7-GOOD CONDITION RATING : 11/06/2014		COMMENTS: (TRAMPA, 01/03/2017)--CRACKING W/MINOR LEACH;			
[ITEM 59] SUPER: 8-VERY GOOD CONDITION RATING : 11/06/2014		COMMENTS: (TRAMPA, 01/03/2017)--V-CR & LE DIAPH E ABUT;			
[ITEM 60] SUB: 8-VERY GOOD CONDITION RATING : 02/27/2025		COMMENTS: (GREENA2, 02/23/2023)--NO DEFICIENCIES NOTED. (LEPPED1, 02/27/2025)--FEW CRACKS IN ABUT AND BENT			
[ITEM 61] BANK/CHANNEL: 7-MINOR DAMAGE RATING : 02/15/2017		COMMENTS: (STEGEC, 02/15/2017)--BIG SWEEPING CURVE UPSTREAM WITH SOME MINOR EROSION IN 2016			
[ITEM 113] SCOUR: 8-STABLE FOR CALCULATED RATING : 09/23/2004 EVALUATION TYPE :		COMMENTS:			
[ITEM 71] WATERWAY ADEQUACY: ABOVE FLOOD ELEVATIONS RATING : 09/23/2004		COMMENTS:			
[ITEM 72] APPRRDWY ALIGNMENT: 8-VERYGOOD RATING : 09/23/2004		COMMENTS:			
RAILING AND APPROACH PAVEMENT COMPONENTS AND RATINGS					
[ITEM 36A] BRIDGE RAILING RATING: MEETS CURRENT STANDARDS-1		RATING : 05/23/2004		COMMENTS:	
<u>MATERIAL</u>	<u>CONSTRUCTION</u>	<u>DIRECTION</u>	<u>COMMENTS</u>		
REINFORCED CONCRETE	SAFETY BARRIER CURB	BOTH			
[ITEM 36B] TRANSITION RAILING RATING: MEETS CURRENT STANDARDS-1		RATING : 05/23/2004		COMMENTS:	
<u>MATERIAL</u>	<u>CONSTRUCTION</u>	<u>DIRECTION</u>	<u>COMMENTS</u>		
GALVANIZED STEEL	THRIE BEAM TO W-BEAM	ALL			
[ITEM 36C] APPROACH RAILING RATING: MEETS CURRENT STANDARDS-1		RATING : 05/23/2004		COMMENTS:	
<u>MATERIAL</u>	<u>CONSTRUCTION</u>	<u>DIRECTION</u>	<u>COMMENTS</u>		
GALVANIZED STEEL	W-BEAM	ALL			
[ITEM 36D] RAIL END TREATMENT RATING: MEETS CURRENT STANDARDS-1		RATING : 05/23/2004		COMMENTS:	
Design_No = a4988 <div style="text-align: right;">Page 2</div>					
This report contains information that is protected from disclosure by federal law, 23 USC Section 409 and the Missouri Open Records Law (Sunshine Act), Section 610.021 RSMo. Please review MoDOT's policy and procedure manual on the Sunshine Act before releasing any of the information contained herein.					

	Missouri Department of Transportation State Bridge Inspection Report				July 01, 2025 7:17:06AM	
COUNTY: CALLAWAY	DISTRICT: CD	CLASS: STATBR	FED-ID: 30523	BRIDGE: A4988		
GENERAL WORK COMMENTS:						
RESPONSIBILITY DISTRICT SPECIAL	LOCATION ROADWAY SURFACE	ITEM SEAL DECK WITH IN DECK	CATEGORY DECK	PRIORITY 3	DATE 01/03/2017	WORK ITEM COMMENT
UTILITY ATTACHMENTS						
UTILITY	OWNER	METHOD	MEASUREMENT TYPE	VALUE	NUMBER	UTILITY ATTACHMENT COMMENT
PROGRAM NOTES INFORMATION						
YEAR	PROJECT #	MONTH LET	YEAR LET	ITEMS	COMMENT	
COMPUTER GENERATED RATINGS AND DEFICIENCY ITEMS						
NOTE: The items listed in this section are updated whenever computer edits are ran on a structure after the inspection updates have been entered in to TMS.			***ADVANCED SIGN INFORMATION***			
<u>Rated Item</u>	<u>Rating</u>	<u>Rating Date</u>	SIGN #	SIGN TYPE	PROBLEM	PROBLEM DIRECTION
[Item 67] Structure Evaluation Rating:	8-EQ TO PRESENT DESIRAB	1/26/2017	1			
[Item 68] Deck Geometry Rating:	8-EQ TO PRESENT DESIRAB	9/24/2004				
[Item 69] Underclearance:	6-EQ TO PRESENT MIN CRITR	9/24/2004				
Sufficiency Rating:	99.0%	1/16/2025				
Deficiency:	NOT DEFICIENT	9/24/2004				
Funding Eligibility:		---	***OUTFALL INSPECTION INFORMATION***			
Estimated New Structure Length:		---	# OUTFALLS: STATUS: NOTES:	INSPECTOR: DATE:		
Estimated Structure Cost:		---				
Estimated Total Project Cost:		---				
Year of Cost Estimate:		---				
NOTE: The above structure length and cost estimates are computer generated using algorithms in the TMS system. These algorithms are generalized to use NBI items to come up with a new structure length and width to calculate a new area which is taken times a representative cost per square foot. The actual structure size and cost may vary significantly from these numbers once site specific engineering is done.						

		Missouri Department of Transportation State Bridge Inspection Report				July 01, 2025 7:17:06AM			
COUNTY: CALLAWAY		DISTRICT: CD		CLASS: STATBR		FED-ID: 30523		BRIDGE: A4988	

ABUTMENT-5	RA-30 DEGREES	49 FT. 88 IN	REINFORCED CONCRETE	INTEGRAL					
	<u>CONDITION</u>		<u>LOCATION 1</u>	<u>LOCATION 2</u>	<u>SEVERITY</u>	<u>MEASUREMENT</u>	<u>COMMENT</u>		
<u>ASSOCIATED COMPONENT</u>		<u>MATERIAL</u>		<u>CONSTRUCTION</u>					
BEAM CAP		REINFORCED CONCRETE		CAST-IN-PLACE					
	<u>CONDITION</u>		<u>LOCATION 1</u>	<u>LOCATION 2</u>	<u>SEVERITY</u>	<u>MEASUREMENT</u>	<u>COMMENT</u>		
FIXED BEARING		ELASTOMERIC		PLAIN NEOPRENE					
	<u>CONDITION</u>		<u>LOCATION 1</u>	<u>LOCATION 2</u>	<u>SEVERITY</u>	<u>MEASUREMENT</u>	<u>COMMENT</u>		
PILING		STEEL		H-SHAPE					
	<u>CONDITION</u>		<u>LOCATION 1</u>	<u>LOCATION 2</u>	<u>SEVERITY</u>	<u>MEASUREMENT</u>	<u>COMMENT</u>		
TURNED BACK WINGS		REINFORCED CONCRETE		CAST-IN-PLACE					
	<u>CONDITION</u>		<u>LOCATION 1</u>	<u>LOCATION 2</u>	<u>SEVERITY</u>	<u>MEASUREMENT</u>	<u>COMMENT</u>		

OVER/UNDER ROUTES CLEARANCE INFORMATION				
CLEARANCES OVER DECK				
<small>**NOTE: Vertical clearances for permitting purposes are taken as 2 inches less than the actual field measured clearance.</small>				
<u>VERTICAL CLEARANCE TYPE**</u>	<u>VALUE</u>	<u>DIRECTION</u>	<u>DATE</u>	<u>COMMENT</u>

CLEARANCES UNDER BRIDGE						
<small>**NOTE: Vertical clearances for permitting purposes are taken as 2 inches less than the actual field measured clearance.</small>						
<u>RECORD #</u>	<u>ROUTE</u>	<u># LANES</u>	<u>DIRECTION OF TRAFFIC</u>	<u>RIGHT LATERAL CLEARANCE</u>	<u>LEFT LATERAL CLEARANCE</u>	<u>UR-ID</u>
1	MAINT. ROAD	1	1-WAY TRAF	10 FT 0 IN		95886
<u>VERTICAL CLEARANCE TYPE**</u>		<u>VALUE</u>	<u>DIRECTION</u>	<u>DATE</u>	<u>COMMENT</u>	
PLANNED		17 FT 0 IN				

STRUCTURE PAINT INFORMATION			
CONDITION:	GOOD	RUST AMOUNT : 9=.03% OF SURFACE RUSTED	STEEL TONS : 149
<u>ORIGINAL PAINT</u>		<u>CONTRACT REPAINT</u>	
<u>PAINT TYPE</u> : G SYSTEM		<u>PAINT TYPE</u> :	
<u>NAME</u> : ZINC/EPOXY/ACRYLIC		<u>NAME</u> :	
<u>PAINT COLOR</u> : GRAY		<u>PAINT COLOR</u> :	
<u>PAINT YEAR</u> : 2005		<u>PAINT YEAR</u> :	
<u>MILS</u> :		<u>MILS</u> :	
<u>MANUFACTURE</u> :		<u>MANUFACTURE</u> :	
<u>SURFACE PREP</u> :		<u>SURFACE PREP</u> :	

REQUESTED WORK ITEMS	
-----------------------------------	--

Design_No = a4988	Page 6	<small>This report contains information that is protected from disclosure by federal law, 23 USC Section 409 and the Missouri Open Records Law (Sunshine Act), Section 610.021 RSMo. Please review MoDOT's policy and procedure manual on the Sunshine Act before releasing any of the information contained herein.</small>
-------------------	--------	--



Missouri Department of Transportation
State Bridge Inspection Report

July 01, 2025
7:17:06AM

COUNTY: CALLAWAY

DISTRICT: CD

CLASS: STATBR

FED-ID: 30523

BRIDGE: A4988

<u>CONDITION</u>		<u>LOCATION 1</u>	<u>LOCATION 2</u>	<u>SEVERITY</u>	<u>MEASUREMENT</u>	<u>COMMENT</u>
<u>ASSOCIATED COMPONENT</u>		<u>MATERIAL</u>	<u>CONSTRUCTION</u>			
BEAM CAP		REINFORCED CONCRETE	CAST-IN-PLACE			
<u>CONDITION</u>		<u>LOCATION 1</u>	<u>LOCATION 2</u>	<u>SEVERITY</u>	<u>MEASUREMENT</u>	<u>COMMENT</u>
VERTICAL CRACKS		BACKWALL		FEW		
FIXED BEARING		ELASTOMERIC	LAMINATED NEOPRENE			
<u>CONDITION</u>		<u>LOCATION 1</u>	<u>LOCATION 2</u>	<u>SEVERITY</u>	<u>MEASUREMENT</u>	<u>COMMENT</u>
PILING		STEEL	H-SHAPE			
<u>CONDITION</u>		<u>LOCATION 1</u>	<u>LOCATION 2</u>	<u>SEVERITY</u>	<u>MEASUREMENT</u>	<u>COMMENT</u>
TURNED BACK WINGS		REINFORCED CONCRETE	CAST-IN-PLACE			
<u>CONDITION</u>		<u>LOCATION 1</u>	<u>LOCATION 2</u>	<u>SEVERITY</u>	<u>MEASUREMENT</u>	<u>COMMENT</u>
BENT-2	RA-30 DEGREES	45 FT 2 IN	REINFORCED CONCRETE	MULTIPLE COLUMN		
<u>CONDITION</u>		<u>LOCATION 1</u>	<u>LOCATION 2</u>	<u>SEVERITY</u>	<u>MEASUREMENT</u>	<u>COMMENT</u>
<u>ASSOCIATED COMPONENT</u>		<u>MATERIAL</u>	<u>CONSTRUCTION</u>			
BEAM CAP		REINFORCED CONCRETE	CAST-IN-PLACE			
<u>CONDITION</u>		<u>LOCATION 1</u>	<u>LOCATION 2</u>	<u>SEVERITY</u>	<u>MEASUREMENT</u>	<u>COMMENT</u>
VERTICAL CRACKS		AT BEAM CAP		FEW		
COLUMN		REINFORCED CONCRETE	CAST-IN-PLACE			
<u>CONDITION</u>		<u>LOCATION 1</u>	<u>LOCATION 2</u>	<u>SEVERITY</u>	<u>MEASUREMENT</u>	<u>COMMENT</u>
SCALING		WATERLINE		LIGHT		
FIXED BEARING		ELASTOMERIC	LAMINATED NEOPRENE			
<u>CONDITION</u>		<u>LOCATION 1</u>	<u>LOCATION 2</u>	<u>SEVERITY</u>	<u>MEASUREMENT</u>	<u>COMMENT</u>
FOOTING		REINFORCED CONCRETE	SPREAD			
<u>CONDITION</u>		<u>LOCATION 1</u>	<u>LOCATION 2</u>	<u>SEVERITY</u>	<u>MEASUREMENT</u>	<u>COMMENT</u>
BENT-3	RA-30 DEGREES	45 FT 2 IN	REINFORCED CONCRETE	MULTIPLE COLUMN		
<u>CONDITION</u>		<u>LOCATION 1</u>	<u>LOCATION 2</u>	<u>SEVERITY</u>	<u>MEASUREMENT</u>	<u>COMMENT</u>
<u>ASSOCIATED COMPONENT</u>		<u>MATERIAL</u>	<u>CONSTRUCTION</u>			
BEAM CAP		REINFORCED CONCRETE	CAST-IN-PLACE			
<u>CONDITION</u>		<u>LOCATION 1</u>	<u>LOCATION 2</u>	<u>SEVERITY</u>	<u>MEASUREMENT</u>	<u>COMMENT</u>
VERTICAL CRACKS		AT BEAM CAP		FEW		
COLUMN		REINFORCED CONCRETE	CAST-IN-PLACE			
<u>CONDITION</u>		<u>LOCATION 1</u>	<u>LOCATION 2</u>	<u>SEVERITY</u>	<u>MEASUREMENT</u>	<u>COMMENT</u>
SCALING		WATERLINE		LIGHT		
FIXED BEARING		ELASTOMERIC	LAMINATED NEOPRENE			
<u>CONDITION</u>		<u>LOCATION 1</u>	<u>LOCATION 2</u>	<u>SEVERITY</u>	<u>MEASUREMENT</u>	<u>COMMENT</u>
FOOTING		REINFORCED CONCRETE	SPREAD			
<u>CONDITION</u>		<u>LOCATION 1</u>	<u>LOCATION 2</u>	<u>SEVERITY</u>	<u>MEASUREMENT</u>	<u>COMMENT</u>
BENT-4	RA-30 DEGREES	45 FT 2 IN	REINFORCED CONCRETE	MULTIPLE COLUMN		
<u>CONDITION</u>		<u>LOCATION 1</u>	<u>LOCATION 2</u>	<u>SEVERITY</u>	<u>MEASUREMENT</u>	<u>COMMENT</u>
<u>ASSOCIATED COMPONENT</u>		<u>MATERIAL</u>	<u>CONSTRUCTION</u>			
BEAM CAP		REINFORCED CONCRETE	CAST-IN-PLACE			
<u>CONDITION</u>		<u>LOCATION 1</u>	<u>LOCATION 2</u>	<u>SEVERITY</u>	<u>MEASUREMENT</u>	<u>COMMENT</u>
COLUMN		REINFORCED CONCRETE	CAST-IN-PLACE			
<u>CONDITION</u>		<u>LOCATION 1</u>	<u>LOCATION 2</u>	<u>SEVERITY</u>	<u>MEASUREMENT</u>	<u>COMMENT</u>
EXPANSION BEARING		ELASTOMERIC	LAMINATED NEOPRENE			
<u>CONDITION</u>		<u>LOCATION 1</u>	<u>LOCATION 2</u>	<u>SEVERITY</u>	<u>MEASUREMENT</u>	<u>COMMENT</u>
FOOTING		REINFORCED CONCRETE	H-PILE			
<u>CONDITION</u>		<u>LOCATION 1</u>	<u>LOCATION 2</u>	<u>SEVERITY</u>	<u>MEASUREMENT</u>	<u>COMMENT</u>

Design_No = s4988

Page 5

This report contains information that is protected from disclosure by federal law, 23 USC Section 409 and the Missouri Open Records Law (Sunshine Act), Section 610.021 RSMo. Please review MoDOT's policy and procedure manual on the Sunshine Act before releasing any of the information contained herein.



Missouri Department of Transportation
State Bridge Inspection Report

July 01, 2025
7:17:06AM

COUNTY: CALLAWAY

DISTRICT: CD

CLASS: STATBR

FED-ID: 30523

BRIDGE: A4988

MAIN SPANS-2	DECK	REINFORCED CONCRETE	CAST-IN-PLACE-F/C FORMS			
<u>CONDITION</u>		<u>LOCATION 1</u>	<u>LOCATION 2</u>	<u>SEVERITY</u>	<u>MEASUREMENT</u>	<u>COMMENT</u>
LEACHING		OVERHANGS		MINOR		
LONGITUDINAL CRACKS		THROUGHOUT		FEW		
REFLECTIVE CRACKS		RANDOM		FEW		
TRANSVERSE CRACKS		OVERHANGS		FEW		
TRANSVERSE CRACKS		THROUGHOUT		RANDOM		

MAIN SPANS-3	DECK	REINFORCED CONCRETE	CAST-IN-PLACE-F/C FORMS			
<u>CONDITION</u>		<u>LOCATION 1</u>	<u>LOCATION 2</u>	<u>SEVERITY</u>	<u>MEASUREMENT</u>	<u>COMMENT</u>
LEACHING		OVERHANGS		MINOR		
LONGITUDINAL CRACKS		THROUGHOUT		FEW		
REFLECTIVE CRACKS		RANDOM		FEW		
TRANSVERSE CRACKS		OVERHANGS		FEW		
TRANSVERSE CRACKS		PRECAST PANELS		RANDOM		

MAIN SPANS-4	DECK	REINFORCED CONCRETE	CAST-IN-PLACE-F/C FORMS			
<u>CONDITION</u>		<u>LOCATION 1</u>	<u>LOCATION 2</u>	<u>SEVERITY</u>	<u>MEASUREMENT</u>	<u>COMMENT</u>
LEACHING		OVERHANGS		MINOR		
LEACHING		THROUGHOUT		MINOR		
LEAKING		PRECAST PANELS		MINOR		
LONGITUDINAL CRACKS		THROUGHOUT		FEW		
REFLECTIVE CRACKS		RANDOM		FEW		
TRANSVERSE CRACKS		OVERHANGS		FEW		
TRANSVERSE CRACKS		PRECAST PANELS		RANDOM		

SUPERSTRUCTURE COMPONENTS

<u>SERIES TYPE-#</u>	<u>SPAN TYPE</u>	<u>MATERIAL</u>	<u>CONSTRUCTION</u>	<u>LABEL</u>	<u>COMMENTS</u>	
MAIN SERIES-1	CONTINUOUS SLAB	STEEL	PLATE GIRDERS			
<u>SPAN</u>	<u>COMPOSITE INDICATOR</u>	<u>LENGTH</u>	<u>WEATHERING STEEL</u>	<u>COMMENTS</u>		
MAIN SPANS-1	COMPOSITE	70 FT 0 IN	NO			
<u>CONDITION</u>		<u>LOCATION 1</u>	<u>LOCATION 2</u>	<u>SEVERITY</u>	<u>MEASUREMENT</u>	<u>COMMENT</u>
MAIN SPANS-2	COMPOSITE	102 FT 0 IN	NO			
<u>CONDITION</u>		<u>LOCATION 1</u>	<u>LOCATION 2</u>	<u>SEVERITY</u>	<u>MEASUREMENT</u>	<u>COMMENT</u>
MAIN SPANS-3	COMPOSITE	102 FT 0 IN	NO			
<u>CONDITION</u>		<u>LOCATION 1</u>	<u>LOCATION 2</u>	<u>SEVERITY</u>	<u>MEASUREMENT</u>	<u>COMMENT</u>
MAIN SPANS-4	COMPOSITE	85 FT 0 IN	NO			
<u>CONDITION</u>		<u>LOCATION 1</u>	<u>LOCATION 2</u>	<u>SEVERITY</u>	<u>MEASUREMENT</u>	<u>COMMENT</u>
LEACHING		DIAPHRAGMS		MINOR		
VERTICAL CRACKS		DIAPHRAGMS		MINOR		


SUBSTRUCTURE COMPONENTS

<u>SUBSTRUCTURE</u>	<u>SKW</u>	<u>LENGTH</u>	<u>MATERIAL</u>	<u>CONSTRUCTION</u>	<u>LABEL</u>	<u>COMMENTS</u>
ABUTMENT-1	RA-30 DEGREES	49 FT 25 IN	REINFORCED CONCRETE	INTEGRAL		

Design No = s4988

Page 4

This report contains information that is protected from disclosure by federal law, 23 USC Section 409 and the Missouri Open Records Law (Sunshine Act), Section 610.021 RSMo. Please review MoDOT's policy and procedure manual on the Sunshine Act before releasing any of the information contained herein.

		Missouri Department of Transportation State Bridge Inspection Report				July 01, 2025 7:17:06AM	
COUNTY: CALLAWAY		DISTRICT: CD		CLASS: STATBR		FED-ID: 30523	
BRIDGE: A4988							
MATERIAL GALVANIZED STEEL		CONSTRUCTION BREKAWAY SYSTEM		DIRECTION ALL		COMMENTS	
APPROACH PAVEMENT: *Overall condition assigned for each approach pavement component is shown below.							
MATERIAL ASPHALT/CONCRETE		CONSTRUCTION MAT/TIESLAB		DIRECTION BOTH		CONDITION* FAIR	
COMMENTS (BOWDEN, 02/27/2009)--SETTLING @ SLEEPER SLAB		LOCATION 1 THROUGHOUT		LOCATION 2		SEVERITY HEAVY	
CONDITION SETTLEMENT		COMMENT (STEGEC, 02/15/2017)--OVERLAYED 2016					
DRAINAGE, EXPANSION DEVICES, BANK/SLOPE, AND DECK PROTECTIVE COMPONENTS							
DECK PROTECTIVE COMPONENTS:							
SERIES TYPE-# MAIN SERIES-1		COMPONENT WEARING SURFACE		MATERIAL FLAIN CONCRETE		CONSTRUCTION MONOLITHIC	
THICKNESS		YEAR APPLIED		MANUFACTURE		OVERALL CONDITION GOOD	
COMMENT:							
DECK PROTECTION		EPOXY POLYMER		COATED REBAR			
COMMENT:							
MEMBRANE		NOT APPLICABLE		NONE			
COMMENT:							
SECONDARY DECK PROTECTION		LIQUID SEALANT		INTERNALLY SEALED		2010 STAR MACRO	
COMMENT:							
DRAINAGE COMPONENTS:							
COMPONENT DRAINAGE		MATERIAL GEOTEXTILE FABRIC		CONSTRUCTION VERTICAL DRAIN-END BENT		DIRECTION 	
COMMENTS							
DRAINAGE		GALVANIZED STEEL		FLOOR DRAIN			
EXPANSION DEVICE COMPONENTS:							
SUB UNIT-#		SUB LABEL		COMPONENT		MATERIAL	
CONSTRUCTION		GAP		YEAR APPLIED		MANUFACTURE	
OVERALL CONDITION							
COMMENT:							
BANK/SLOPE PROTECTION COMPONENTS:							
COMPONENT BANK PROTECTION		MATERIAL ROCK		CONSTRUCTION BLANKET		DIRECTION BOTH	
COMMENTS							
DECK COMPONENTS							
SLAB TYPE-# MAIN SLABS-1		COMPONENT DECK		MATERIAL REINFORCED CONCRETE		CONSTRUCTION CAST-IN-PLACE-F/C FORMS	
COMMENTS		LOCATION 1		LOCATION 2		SEVERITY	
MEASUREMENT		COMMENT					
LEACHING		OVERHANGS		MINOR			
LEAKING		PRECAST PANELS		MODERATE			
REFLECTIVE CRACKS		THROUGHOUT		FEW			
TRANSVERSE CRACKS		OVERHANGS		FEW			
TRANSVERSE CRACKS		THROUGHOUT		FEW			
(MARTEP, 12/26/2012)--HEAVY BOTTOM SIDE EFFL THRU PANEL JOINTS							
Design_No = a4988							
Page 3							
This report contains information that is protected from disclosure by federal law, 23 USC Section 409 and the Missouri Open Records Law (Sunshine Act), Section 610.021 RSMo. Please review MoDOT's policy and procedure manual on the Sunshine Act before releasing any of the information contained herein.							



Missouri Department of Transportation
State Bridge Inspection Report

July 01, 2025
7:17:06AM

COUNTY: CALLAWAY

DISTRICT: CD

CLASS: STATBR


FED-ID: 30523

BRIDGE: A4988

Design_No = s4988

Page 8

This report contains information that is protected from disclosure by federal law, 23 USC Section 409 and the Missouri Open Records Law (Sunshine Act), Section 610.021 RSMo. Please review MoDOT's policy and procedure manual on the Sunshine Act before releasing any of the information contained herein.

		Missouri Department of Transportation State Bridge Inspection Report				July 01, 2025 7:19:01AM			
COUNTY: CALLAWAY		DISTRICT: CD		CLASS: STATBR		FED-ID: 2898		BRIDGE: A3450	

GENERAL STRUCTURE INFORMATION						***BRIDGE INSPECTION INFORMATION***					
ROUTE: US54W FEATURE: RT J STATUS: A-OPEN LOG MILE: 91.600 DETOUR: 1.00 MILES NHS: YES BUILT: 1992 REHAB: LOCATION: S 32 T 46 R 10 W LATITUDE: 38 43 10.73 (DMS) LONGITUDE: 92 4 34.23 (DMS)		# SPANS: 3 LANES ON: 2 LANES UNDER: 2 COMPASS DIRECTION: EAST to WEST DIRECTION OF TRAFFIC: 1-WAY TRAF FUNCTIONAL CLASS: RL-FREEWAY NBI OWNER: MODOT NBI MAINTAINED: MODOT MAINTENANCE DISTRICT: CD MAINTENANCE COUNTY: CALLAWAY SUB AREA: 7D25		PLACE CODE: 12142 CEDAR LENGTH: 196 FT 0 IN MAXIMUM SPAN: 78 FT 0 IN APPROACH ROADWAY: 44 FT 0 IN CURB TO CURB: 38 FT 10 IN OUT TO OUT: 41 FT 6 IN AADT: 7660 AADT YEAR: 2024 AADT TRUCK: 10.0% FUTURE AADT: 14171 FUTURE AADT YEAR: 2044		DATE: 11/08/2024 FREQUENCY: 24 TEAM LEADER: DEREK LEPPER INSPECTOR 2: INSPECTOR 3: INSPECTOR 4: RESPONSIBILITY: DISTRICT CALCULATED INTERVAL **: 25 ELEMENT: YES ** When calculated interval exceeds the frequency, a justification comment per BIRM is required.		GENERAL INSPECTION COMMENTS (LEPPER1, 01/31/2025)--STAFF LIMITATIONS			


FRACTURE CRITICAL INSPECTION INFORMATION						***INDEPTH INSPECTION INFORMATION***					
DATE: FREQUENCY: TEAM LEADER: INSPECTOR 2:		RESPONSIBILITY: CALCULATED INTERVAL **: INSPECTOR 3: INSPECTOR 4:		CATEGORY: NBI: METHOD:		DATE: FREQUENCY: TEAM LEADER: INSPECTOR 2:		RESPONSIBILITY: CALCULATED INTERVAL **: INSPECTOR 3: INSPECTOR 4:		CATEGORY: NBI: METHOD:	
** When calculated interval exceeds the frequency, a justification comment per BIRM is required.						** When calculated interval exceeds the frequency, a justification comment per BIRM is required.					
FRACTURE CRITICAL INSPECTION COMMENTS						INDEPTH INSPECTION COMMENTS					


SPECIAL INSPECTION INFORMATION						***UNDERWATER INSPECTION INFORMATION***					
DATE: FREQUENCY: TEAM LEADER: INSPECTOR 2:		RESPONSIBILITY: CALCULATED INTERVAL **: INSPECTOR 3: INSPECTOR 4:		CATEGORY: NBI: METHOD:		DATE: FREQUENCY: TEAM LEADER: INSPECTOR 2:		RESPONSIBILITY: CALCULATED INTERVAL **: INSPECTOR 3: INSPECTOR 4:		CATEGORY: NBI: METHOD:	
** When calculated interval exceeds the frequency, a justification comment per BIRM is required.						** When calculated interval exceeds the frequency, a justification comment per BIRM is required.					
SPECIAL INSPECTION COMMENTS						UNDERWATER INSPECTION COMMENTS					

OTHER SPECIAL INSPECTIONS						OTHER UNDERWATER INSPECTIONS					
<u>DATE</u> <u>FREQUENCY</u> <u>CATEGORY</u> <u>NBI</u> <u>CALCULATED INTERVAL</u> <u>RESPONSIBILITY</u> <u>METHOD</u>						<u>DATE</u> <u>FREQUENCY</u> <u>CATEGORY</u> <u>NBI</u> <u>CALCULATED INTERVAL</u> <u>RESPONSIBILITY</u> <u>METHOD</u>					

Design_No = a3450

Page 1
This report contains information that is protected from disclosure by federal law, 23 USC Section 409 and the Missouri Open Records Law (Sunshine Act), Section 610.021 RSMo. Please review MoDOT's policy and procedure manual on the Sunshine Act before releasing any of the information contained herein.

	Missouri Department of Transportation State Bridge Inspection Report				July 01, 2025 7:19:01AM																
COUNTY: CALLAWAY	DISTRICT: CD	CLASS: STATBR	FED-ID: 2898	BRIDGE: A3450																	
STRUCTURE POSTING																					
APPROVED CATEGORY: SW-1 NO POSTING REQUIRED Ton 1: Ton 2: Ton 3: COMMENTS: (HAWCRC1, 05/13/2025)--LOAD POSTING LETTER, 5/13/2025, MODOT.																					
FIELD CATEGORY: SW-1 NO POSTING REQUIRED Ton 1: Ton 2: Ton 3: PROBLEM: PROBLEM DIRECTION: COMMENTS:																					
GENERAL COMMENTS/MAJOR RATED ITEMS																					
GENERAL COMMENTS: (BOWDEJ1, 06/03/2008)--(59'-78'-59') P/S CONC I-GDR SPANS																					
[ITEM 58] DECK: 7-GOOD CONDITION COMMENTS: (TRAMPA, 01/03/2017)--TRANS CRACK AND MINOR SPALL AT JTS; RATING : 05/18/2001																					
[ITEM 59] SUPER: 7-GOOD CONDITION COMMENTS: (OTTINM, 11/04/2014)--GIRDER CRACKS, 3 LOCATIONS. RATING : 12/16/2008																					
[ITEM 60] SUB: 7-GOOD CONDITION COMMENTS: (TRAMPA, 12/26/2018)--VERTICAL CRACKS IN ABUTS; MINOR DELAMS IN BT 3 DIAPH; RATING : 05/18/2001																					
[ITEM 61] BANK/CHANNEL: N-NOT APPLIC NO WATERWAY COMMENTS: RATING : 05/18/2001																					
[ITEM 113] SCOUR: N-NOT APPLIC NOT WATERW COMMENTS: RATING : 05/18/2001 EVALUATION TYPE :																					
[ITEM 71] WATERWAY ADEQUACY: NOT APPLICABLE COMMENTS: RATING : 05/18/2001																					
[ITEM 72] APPRRDWY ALIGNMENT: 8-VERYGOOD COMMENTS: RATING : 05/18/2001																					
RAILING AND APPROACH PAVEMENT COMPONENTS AND RATINGS																					
[ITEM 36A] BRIDGE RAILING RATING: MEETS CURRENT STANDARDS-1 RATING : 05/18/2001 COMMENTS: <table style="width:100%; border-collapse: collapse;"> <tr> <td style="width:25%;"><u>MATERIAL</u></td> <td style="width:25%;"><u>CONSTRUCTION</u></td> <td style="width:25%;"><u>DIRECTION</u></td> <td style="width:25%;"><u>COMMENTS</u></td> </tr> <tr> <td>REINFORCED CONCRETE</td> <td>SAFETY BARRIER CURB</td> <td>BOTH</td> <td></td> </tr> </table>						<u>MATERIAL</u>	<u>CONSTRUCTION</u>	<u>DIRECTION</u>	<u>COMMENTS</u>	REINFORCED CONCRETE	SAFETY BARRIER CURB	BOTH									
<u>MATERIAL</u>	<u>CONSTRUCTION</u>	<u>DIRECTION</u>	<u>COMMENTS</u>																		
REINFORCED CONCRETE	SAFETY BARRIER CURB	BOTH																			
[ITEM 36B] TRANSITION RAILING RATING: MEETS CURRENT STANDARDS-1 RATING : 05/18/2001 COMMENTS: <table style="width:100%; border-collapse: collapse;"> <tr> <td style="width:25%;"><u>MATERIAL</u></td> <td style="width:25%;"><u>CONSTRUCTION</u></td> <td style="width:25%;"><u>DIRECTION</u></td> <td style="width:25%;"><u>COMMENTS</u></td> </tr> <tr> <td>GALVANIZED STEEL</td> <td>THREE BEAM TO W-BEAM</td> <td>BOTH-NORTH</td> <td></td> </tr> </table>						<u>MATERIAL</u>	<u>CONSTRUCTION</u>	<u>DIRECTION</u>	<u>COMMENTS</u>	GALVANIZED STEEL	THREE BEAM TO W-BEAM	BOTH-NORTH									
<u>MATERIAL</u>	<u>CONSTRUCTION</u>	<u>DIRECTION</u>	<u>COMMENTS</u>																		
GALVANIZED STEEL	THREE BEAM TO W-BEAM	BOTH-NORTH																			
[ITEM 36C] APPROACH RAILING RATING: MEETS CURRENT STANDARDS-1 RATING : 05/18/2001 COMMENTS: <table style="width:100%; border-collapse: collapse;"> <tr> <td style="width:25%;"><u>MATERIAL</u></td> <td style="width:25%;"><u>CONSTRUCTION</u></td> <td style="width:25%;"><u>DIRECTION</u></td> <td style="width:25%;"><u>COMMENTS</u></td> </tr> <tr> <td>GALVANIZED STEEL</td> <td>W-BEAM</td> <td>BOTH-NORTH</td> <td></td> </tr> <tr> <td><u>CONDITION</u></td> <td><u>LOCATION1</u></td> <td><u>LOCATION2</u></td> <td><u>SEVERITY</u> <u>COMMENT</u></td> </tr> <tr> <td>OTHER</td> <td>GROUND LINE</td> <td></td> <td>NOT APPLICABLE (EICHHR, 04/25/2002)--SLOPE EROSION AT EAST BANK AT GR POST</td> </tr> </table>						<u>MATERIAL</u>	<u>CONSTRUCTION</u>	<u>DIRECTION</u>	<u>COMMENTS</u>	GALVANIZED STEEL	W-BEAM	BOTH-NORTH		<u>CONDITION</u>	<u>LOCATION1</u>	<u>LOCATION2</u>	<u>SEVERITY</u> <u>COMMENT</u>	OTHER	GROUND LINE		NOT APPLICABLE (EICHHR, 04/25/2002)--SLOPE EROSION AT EAST BANK AT GR POST
<u>MATERIAL</u>	<u>CONSTRUCTION</u>	<u>DIRECTION</u>	<u>COMMENTS</u>																		
GALVANIZED STEEL	W-BEAM	BOTH-NORTH																			
<u>CONDITION</u>	<u>LOCATION1</u>	<u>LOCATION2</u>	<u>SEVERITY</u> <u>COMMENT</u>																		
OTHER	GROUND LINE		NOT APPLICABLE (EICHHR, 04/25/2002)--SLOPE EROSION AT EAST BANK AT GR POST																		
[ITEM 36D] RAIL END TREATMENT RATING: MEETS CURRENT STANDARDS-1 RATING : 11/04/2014 COMMENTS:																					
Design_No = a3450																					

	Missouri Department of Transportation State Bridge Inspection Report	July 01, 2025 7:19:01AM
COUNTY: CALLAWAY	DISTRICT: CD	CLASS: STATBR FED-ID: 2898 BRIDGE: A3450

CLEARANCES OVER DECK **NOTE: Vertical clearances for permitting purposes are taken as 2 inches less than the actual field measured clearance.						
<u>VERTICAL CLEARANCE TYPE**</u>	<u>VALUE</u>	<u>DIRECTION</u>	<u>DATE</u>	<u>COMMENT</u>		

CLEARANCES UNDER BRIDGE **NOTE: Vertical clearances for permitting purposes are taken as 2 inches less than the actual field measured clearance.						
<u>RECORD #</u>	<u>ROUTE</u>	<u># LANES</u>	<u>DIRECTION OF TRAFFIC</u>	<u>RIGHT LATERAL CLEARANCE</u>	<u>LEFT LATERAL CLEARANCE</u>	<u>UR ID</u>
1	RT JS	2	1-WAY TRAF			6716
<u>VERTICAL CLEARANCE TYPE**</u>	<u>VALUE</u>	<u>DIRECTION</u>	<u>DATE</u>	<u>COMMENT</u>		
ACTUAL	16 FT 10 IN					

STRUCTURE PAINT INFORMATION			
CONDITION:	RUST AMOUNT :	STEEL TONS :	
<u>ORIGINAL PAINT</u>	<u>CONTRACT REPAINT</u>	<u>DEPARTMENT REPAINT</u>	
PAINT TYPE :	PAINT TYPE :	PAINT TYPE :	MANUFACTURE :
NAME :	NAME :	NAME :	SURFACE PREP :
PAINT COLOR :	PAINT COLOR :	PAINT COLOR :	
PAINT YEAR :	PAINT YEAR :	PAINT YEAR :	
MILS :	MILS :	MILS :	

REQUESTED WORK ITEMS						
GENERAL WORK COMMENTS:						
<u>RESPONSIBILITY</u>	<u>LOCATION</u>	<u>ITEM</u>	<u>CATEGORY</u>	<u>PRIORITY</u>	<u>DATE</u>	<u>WORK ITEM COMMENT</u>
DISTRICT SPECIAL	ROADWAY SURFACE	SEAL DECK WITH IN DECK	DECK	3	01/03/2017	

UTILITY ATTACHMENTS						
<u>UTILITY</u>	<u>OWNER</u>	<u>METHOD</u>	<u>MEASUREMENT TYPE</u>	<u>VALUE</u>	<u>NUMBER</u>	<u>UTILITY ATTACHMENT COMMENT</u>

PROGRAM NOTES INFORMATION						
Design_No = a3450 <div style="text-align: center;">Page 6</div> This report contains information that is protected from disclosure by federal law, 23 USC Section 409 and the Missouri Open Records Law (Sunshine Act), Section 610.021 RSMo. Please review MoDOT's policy and procedure manual on the Sunshine Act before releasing any of the information contained herein.						



Missouri Department of Transportation
State Bridge Inspection Report

July 01, 2025
7:19:01AM

COUNTY: CALLAWAY

DISTRICT: CD

CLASS: STATBR

FED-ID: 2898

BRIDGE: A3450

BENT-2	RA-35 DEGREES <u>CONDITION</u>	47 FT 9 IN	REINFORCED CONCRETE <u>LOCATION 1</u>	MULTIPLE COLUMN <u>LOCATION 2</u>	<u>SEVERITY</u>	<u>MEASUREMENT</u>	<u>COMMENT</u>
	<u>ASSOCIATED COMPONENT</u>		<u>MATERIAL</u>	<u>CONSTRUCTION</u>			
BEAM CAP	<u>CONDITION</u>		REINFORCED CONCRETE <u>LOCATION 1</u>	CAST-IN-PLACE <u>LOCATION 2</u>	<u>SEVERITY</u>	<u>MEASUREMENT</u>	<u>COMMENT</u>
	DELAMINATION VERTICAL CRACKS		CAP FACE AT BEAM CAP		MINOR FINE		(LEPPED1, 01/31/2025)--BETWEEN COLUMNS
COLUMN	<u>CONDITION</u>		REINFORCED CONCRETE <u>LOCATION 1</u>	CAST-IN-PLACE <u>LOCATION 2</u>	<u>SEVERITY</u>	<u>MEASUREMENT</u>	<u>COMMENT</u>
FOOTING	<u>CONDITION</u>		REINFORCED CONCRETE <u>LOCATION 1</u>	SPREAD <u>LOCATION 2</u>	<u>SEVERITY</u>	<u>MEASUREMENT</u>	<u>COMMENT</u>
FIXED BEARING	<u>CONDITION</u>		ELASTOMERIC <u>LOCATION 1</u>	PLAIN NEOPRENE <u>LOCATION 2</u>	<u>SEVERITY</u>	<u>MEASUREMENT</u>	<u>COMMENT</u>
BENT-3	RA-35 DEGREES <u>CONDITION</u>	47 FT 9 IN	REINFORCED CONCRETE <u>LOCATION 1</u>	MULTIPLE COLUMN <u>LOCATION 2</u>	<u>SEVERITY</u>	<u>MEASUREMENT</u>	<u>COMMENT</u>
	<u>ASSOCIATED COMPONENT</u>		<u>MATERIAL</u>	<u>CONSTRUCTION</u>			
BEAM CAP	<u>CONDITION</u>		REINFORCED CONCRETE <u>LOCATION 1</u>	CAST-IN-PLACE <u>LOCATION 2</u>	<u>SEVERITY</u>	<u>MEASUREMENT</u>	<u>COMMENT</u>
	VERTICAL CRACKS		AT BEAM CAP		FINE		(LEPPED1, 01/31/2025)--BETWEEN COLUMNS
COLUMN	<u>CONDITION</u>		REINFORCED CONCRETE <u>LOCATION 1</u>	CAST-IN-PLACE <u>LOCATION 2</u>	<u>SEVERITY</u>	<u>MEASUREMENT</u>	<u>COMMENT</u>
	PATCHES RUST STAINS		RANDOM RANDOM		FEW MINOR		
FOOTING	<u>CONDITION</u>		REINFORCED CONCRETE <u>LOCATION 1</u>	SPREAD <u>LOCATION 2</u>	<u>SEVERITY</u>	<u>MEASUREMENT</u>	<u>COMMENT</u>
FIXED BEARING	<u>CONDITION</u>		ELASTOMERIC <u>LOCATION 1</u>	PLAIN NEOPRENE <u>LOCATION 2</u>	<u>SEVERITY</u>	<u>MEASUREMENT</u>	<u>COMMENT</u>
ABUTMENT-4	RA-35 DEGREES <u>CONDITION</u>	50 FT 0 IN	REINFORCED CONCRETE <u>LOCATION 1</u>	NON-INTEGRAL <u>LOCATION 2</u>	<u>SEVERITY</u>	<u>MEASUREMENT</u>	<u>COMMENT</u>
	<u>ASSOCIATED COMPONENT</u>		<u>MATERIAL</u>	<u>CONSTRUCTION</u>			
BEAM CAP	<u>CONDITION</u>		REINFORCED CONCRETE <u>LOCATION 1</u>	CAST-IN-PLACE <u>LOCATION 2</u>	<u>SEVERITY</u>	<u>MEASUREMENT</u>	<u>COMMENT</u>
	VERTICAL CRACKS		THROUGHOUT		MINOR		
PILING	<u>CONDITION</u>		STEEL <u>LOCATION 1</u>	H-SHAPE <u>LOCATION 2</u>	<u>SEVERITY</u>	<u>MEASUREMENT</u>	<u>COMMENT</u>
TURNED BACK WINGS	<u>CONDITION</u>		REINFORCED CONCRETE <u>LOCATION 1</u>	CAST-IN-PLACE <u>LOCATION 2</u>	<u>SEVERITY</u>	<u>MEASUREMENT</u>	<u>COMMENT</u>
WING PILES	<u>CONDITION</u>		STEEL <u>LOCATION 1</u>	H-SHAPE <u>LOCATION 2</u>	<u>SEVERITY</u>	<u>MEASUREMENT</u>	<u>COMMENT</u>
BACKWALL	<u>CONDITION</u>		REINFORCED CONCRETE <u>LOCATION 1</u>	CAST-IN-PLACE <u>LOCATION 2</u>	<u>SEVERITY</u>	<u>MEASUREMENT</u>	<u>COMMENT</u>
	VERTICAL CRACKS		THROUGHOUT		MINOR		
EXPANSION BEARING	<u>CONDITION</u>		ELASTOMERIC <u>LOCATION 1</u>	LAMINATED NEOPRENE <u>LOCATION 2</u>	<u>SEVERITY</u>	<u>MEASUREMENT</u>	<u>COMMENT</u>
	RUSTING RUSTING		ANCHOR BOLTS THROUGHOUT		MINOR MINOR		

OVER/UNDER ROUTES CLEARANCE INFORMATION

Design_No = a3450

Page 5

This report contains information that is protected from disclosure by federal law, 23 USC Section 409 and the Missouri Open Records Law (Sunshine Act), Section 610.021 RSMo. Please review MoDOT's policy and procedure manual on the Sunshine Act before releasing any of the information contained herein.



Missouri Department of Transportation
State Bridge Inspection Report

July 01, 2025
7:19:01AM

COUNTY: CALLAWAY

DISTRICT: CD

CLASS: STATBR

FED-ID: 2898

BRIDGE: A3450

MAIN SPANS-2	DECK	REINFORCED CONCRETE	CAST-IN-PLACE F/C FORMS
<u>CONDITION</u>	<u>LOCATION 1</u>	<u>LOCATION 2</u>	<u>SEVERITY</u>
TRANSVERSE CRACKS	RANDOM		FEW

MAIN SPANS-3	DECK	REINFORCED CONCRETE	CAST-IN-PLACE F/C FORMS
<u>CONDITION</u>	<u>LOCATION 1</u>	<u>LOCATION 2</u>	<u>SEVERITY</u>
SEALLS	AT JOINTS		MINOR
TRANSVERSE CRACKS	RANDOM		FEW

SUPERSTRUCTURE COMPONENTS

SERIES TYPE-#	SPAN TYPE	MATERIAL	CONSTRUCTION	LABEL	COMMENTS
MAIN SERIES-1	CONTINUOUS SPAN	PRESTRESSED CONCRETE	I-GIRDERS		
<u>SPAN</u>	<u>COMPOSITE INDICATOR</u>	<u>LENGTH</u>	<u>WEATHERING STEEL</u>	<u>COMMENTS</u>	
MAIN SPANS-1	COMPOSITE	59 FT 2 IN	NO		
<u>CONDITION</u>	<u>LOCATION 1</u>	<u>LOCATION 2</u>	<u>SEVERITY</u>	<u>MEASUREMENT</u>	<u>COMMENT</u>
DIAGONAL CRACKS	GDR5		MINOR		(MARTEP, 12/24/2012)--AT BENT 2
MAIN SPANS-2	COMPOSITE	78 FT 0 IN	NO		
<u>CONDITION</u>	<u>LOCATION 1</u>	<u>LOCATION 2</u>	<u>SEVERITY</u>	<u>MEASUREMENT</u>	<u>COMMENT</u>
MAIN SPANS-3	COMPOSITE	59 FT 2 IN	NO		
<u>CONDITION</u>	<u>LOCATION 1</u>	<u>LOCATION 2</u>	<u>SEVERITY</u>	<u>MEASUREMENT</u>	<u>COMMENT</u>
DELAMINATION	DIAPHRAGMS		MINOR		(STEGEC, 02/14/2017)--AT GIRDER 2 - BENT 3
VERTICAL CRACKS	GDR5		MINOR		(STEGEC, 02/14/2017)--AT BENT 3

SUBSTRUCTURE COMPONENTS

SUBSTRUCTURE	SKREW	LENGTH	MATERIAL	CONSTRUCTION	LABEL	COMMENTS
ABUTMENT-1	RA-35 DEGREES	50 FT 0 IN	REINFORCED CONCRETE	NON-INTEGRAL		
<u>CONDITION</u>	<u>LOCATION 1</u>	<u>LOCATION 2</u>	<u>SEVERITY</u>	<u>MEASUREMENT</u>	<u>COMMENT</u>	
DETERIORATION	BACKWALL		MODERATE			(EICHHR, 04/25/2002)--CRACKING
<u>ASSOCIATED COMPONENT</u>	<u>MATERIAL</u>	<u>CONSTRUCTION</u>				
BEAM CAP	REINFORCED CONCRETE	CAST-IN-PLACE				
<u>CONDITION</u>	<u>LOCATION 1</u>	<u>LOCATION 2</u>	<u>SEVERITY</u>	<u>MEASUREMENT</u>	<u>COMMENT</u>	
VERTICAL CRACKS	RANDOM		FEW			(MEYERM3, 01/14/2021)--AT ANCHOR BOLTS
PILING	STEEL	H-SHAPE				
<u>CONDITION</u>	<u>LOCATION 1</u>	<u>LOCATION 2</u>	<u>SEVERITY</u>	<u>MEASUREMENT</u>	<u>COMMENT</u>	
TURNED BACK WINGS	REINFORCED CONCRETE	CAST-IN-PLACE				
<u>CONDITION</u>	<u>LOCATION 1</u>	<u>LOCATION 2</u>	<u>SEVERITY</u>	<u>MEASUREMENT</u>	<u>COMMENT</u>	
WING PILES	STEEL	H-SHAPE				
<u>CONDITION</u>	<u>LOCATION 1</u>	<u>LOCATION 2</u>	<u>SEVERITY</u>	<u>MEASUREMENT</u>	<u>COMMENT</u>	
BACKWALL	REINFORCED CONCRETE	CAST-IN-PLACE				
<u>CONDITION</u>	<u>LOCATION 1</u>	<u>LOCATION 2</u>	<u>SEVERITY</u>	<u>MEASUREMENT</u>	<u>COMMENT</u>	
LEACHING	THROUGHOUT		MINOR			
VERTICAL CRACKS	RANDOM		FEW			
EXPANSION BEARING	ELASTOMERIC	LAMINATED NEOPRENE				
<u>CONDITION</u>	<u>LOCATION 1</u>	<u>LOCATION 2</u>	<u>SEVERITY</u>	<u>MEASUREMENT</u>	<u>COMMENT</u>	
RUSTING	RANDOM		MINOR			

Design_No = a3450

Page 4

This report contains information that is protected from disclosure by federal law, 23 USC Section 409 and the Missouri Open Records Law (Sunshine Act), Section 610.021 RSMo. Please review MoDOT's policy and procedure manual on the Sunshine Act before releasing any of the information contained herein.

MoDOT		Missouri Department of Transportation				July 01, 2025 7:19:01AM	
COUNTY: CALLAWAY		DISTRICT: CD		CLASS: STATBR		FED-ID: 2898	
BRIDGE: A3450							
<u>MATERIAL</u>	<u>CONSTRUCTION</u>	<u>DIRECTION</u>	<u>COMMENTS</u>				
GALVANIZED STEEL	BREKAWAY SYSTEM	BOTH-NORTH	(EICHHR, 04/25/2002)--BCT				
APPROACH PAVEMENT: *Overall condition assigned for each approach pavement component is shown below.							
<u>MATERIAL</u>	<u>CONSTRUCTION</u>	<u>DIRECTION</u>	<u>CONDITION*</u>	<u>COMMENTS</u>			
REINFORCED CONCRETE	TIED SLAB	BOTH	GOOD				
DRAINAGE, EXPANSION DEVICES, BANK/SLOPE, AND DECK PROTECTIVE COMPONENTS							
<u>DECK PROTECTIVE COMPONENTS:</u>							
<u>SERIES TYPE-#</u>	<u>COMPONENT</u>	<u>MATERIAL</u>	<u>CONSTRUCTION</u>	<u>THICKNESS</u>	<u>YEAR APPLIED</u>	<u>MANUFACTURE</u>	<u>OVERALL CONDITION</u>
MAIN SERIES-1	WEARING SURFACE	PLAIN CONCRETE	MONOLITHIC				GOOD
<u>COMMENT:</u>							
	DECK PROTECTION	EPOXY POLYMER	COATED REBAR				
<u>COMMENT:</u>							
	MEMBRANE	NOT APPLICABLE	NONE				
<u>COMMENT:</u>							
	SECONDARY DECK PROTECTION	LIQUID SEALANT	INTERNALLY SEALED		2010	STAR MACRO	
<u>COMMENT:</u>							
<u>DRAINAGE COMPONENTS:</u>							
	<u>COMPONENT</u>	<u>MATERIAL</u>	<u>CONSTRUCTION</u>	<u>DIRECTION</u>	<u>COMMENTS</u>		
	DRAINAGE	GALVANIZED STEEL	FLOOR DRAIN				
	DRAINAGE	GEOTEXTILE FABRIC	VERTICAL DRAIN-END BENT				
<u>EXPANSION DEVICE COMPONENTS:</u>							
<u>SUB UNIT-#</u>	<u>SUB LABEL</u>	<u>COMPONENT</u>	<u>MATERIAL</u>	<u>CONSTRUCTION</u>	<u>GAP</u>	<u>YEAR APPLIED</u>	<u>MANUFACTURE</u>
ABUTMENT-1		CLOSED EXPANSION JOINT	ELASTOMERIC	STRIP SEAL			GOOD
<u>COMMENT:</u>							
ABUTMENT-4		CLOSED EXPANSION JOINT	ELASTOMERIC	STRIP SEAL			GOOD
<u>COMMENT:</u>							
<u>BANK/SLOPE PROTECTION COMPONENTS:</u>							
	<u>COMPONENT</u>	<u>MATERIAL</u>	<u>CONSTRUCTION</u>	<u>DIRECTION</u>	<u>COMMENTS</u>		
	SLOPE PROTECTION	PLAIN CONCRETE	FLARED SLOPE				
DECK COMPONENTS							
<u>SEAN TYPE-#</u>	<u>COMPONENT</u>	<u>MATERIAL</u>	<u>CONSTRUCTION</u>	<u>COMMENTS</u>			
MAIN SLABS-1	DECK	REINFORCED CONCRETE	CAST-IN-PLACE F/C FORMS				
	<u>CONDITION</u>	<u>LOCATION 1</u>	<u>LOCATION 2</u>	<u>SEVERITY</u>	<u>MEASUREMENT</u>	<u>COMMENT</u>	
	SEALLS	AT JOINTS		MINOR			
	TRANSVERSE CRACKS	PRECAST PANELS		FEW			
	TRANSVERSE CRACKS	RANDOM		FEW			
Design_No = a3450							
Page 3							
This report contains information that is protected from disclosure by federal law, 23 USC Section 409 and the Missouri Open Records Law (Sunshine Act), Section 610.021 RSMo. Please review MoDOT's policy and procedure manual on the Sunshine Act before releasing any of the information contained herein.							

		Missouri Department of Transportation State Bridge Inspection Report				July 01, 2025 7:19:01AM																																	
		COUNTY: CALLAWAY DISTRICT: CD CLASS: STATBR FED-ID: 2898 BRIDGE: A3450																																					
<u>YEAR</u>	<u>PROJECT #</u>	<u>MONTH LET</u>	<u>YEAR LET</u>	<u>ITEMS</u>	<u>COMMENT</u>																																		
COMPUTER GENERATED RATINGS AND DEFICIENCY ITEMS					***ADVANCED SIGN INFORMATION***																																		
NOTE: The items listed in this section are updated whenever computer edits are ran on a structure after the inspection updates have been entered in to TMS.					SIGN #	SIGN TYPE																																	
<table style="width:100%; border-collapse: collapse;"> <tr> <td style="text-align: left; width: 30%;"><u>Rated Item</u></td> <td style="text-align: left; width: 30%;"><u>Rating</u></td> <td style="text-align: left; width: 40%;"><u>Rating Date</u></td> </tr> <tr> <td>[Item 67] Structure Evaluation Rating:</td> <td>7-BETTER THAN PRESENT MIN</td> <td>1/13/2009</td> </tr> <tr> <td>[Item 68] Deck Geometry Rating:</td> <td>7-BETTER THAN PRESENT MIN</td> <td>5/18/2001</td> </tr> <tr> <td>[Item 69] Underclearance:</td> <td>N-NOT APPLICABLE</td> <td>5/18/2001</td> </tr> <tr> <td>Sufficiency Rating:</td> <td>94.6%</td> <td>2/22/2022</td> </tr> <tr> <td>Deficiency:</td> <td>NOT DEFICIENT</td> <td>5/18/2001</td> </tr> <tr> <td>Funding Eligibility:</td> <td colspan="2">---</td> </tr> <tr> <td>Estimated New Structure Length:</td> <td colspan="2">---</td> </tr> <tr> <td>Estimated Structure Cost:</td> <td colspan="2">---</td> </tr> <tr> <td>Estimated Total Project Cost:</td> <td colspan="2">---</td> </tr> <tr> <td>Year of Cost Estimate:</td> <td colspan="2">---</td> </tr> </table>					<u>Rated Item</u>	<u>Rating</u>	<u>Rating Date</u>	[Item 67] Structure Evaluation Rating:	7-BETTER THAN PRESENT MIN	1/13/2009	[Item 68] Deck Geometry Rating:	7-BETTER THAN PRESENT MIN	5/18/2001	[Item 69] Underclearance:	N-NOT APPLICABLE	5/18/2001	Sufficiency Rating:	94.6%	2/22/2022	Deficiency:	NOT DEFICIENT	5/18/2001	Funding Eligibility:	---		Estimated New Structure Length:	---		Estimated Structure Cost:	---		Estimated Total Project Cost:	---		Year of Cost Estimate:	---		1	
<u>Rated Item</u>	<u>Rating</u>	<u>Rating Date</u>																																					
[Item 67] Structure Evaluation Rating:	7-BETTER THAN PRESENT MIN	1/13/2009																																					
[Item 68] Deck Geometry Rating:	7-BETTER THAN PRESENT MIN	5/18/2001																																					
[Item 69] Underclearance:	N-NOT APPLICABLE	5/18/2001																																					
Sufficiency Rating:	94.6%	2/22/2022																																					
Deficiency:	NOT DEFICIENT	5/18/2001																																					
Funding Eligibility:	---																																						
Estimated New Structure Length:	---																																						
Estimated Structure Cost:	---																																						
Estimated Total Project Cost:	---																																						
Year of Cost Estimate:	---																																						
					PROBLEM																																		
					PROBLEM DIRECTION																																		
					OUTFALL INSPECTION INFORMATION																																		
					# OUTFALLS:	INSPECTOR:																																	
					STATUS:	DATE:																																	
					NOTES:																																		
NOTE: The above structure length and cost estimates are computer generated using algorithms in the TMS system. These algorithms are generalized to use NBI items to come up with a new structure length and width to calculate a new area which is taken times a representative cost per square foot. The actual structure size and cost may vary significantly from these numbers once site specific engineering is done.																																							



Missouri Department of Transportation
State Bridge Inspection Report

July 01, 2025
7:19:01AM

COUNTY: CALLAWAY

DISTRICT: CD

CLASS: STATBR

FED-ID: 2898

BRIDGE: A3450

Design_No = a3450

Page 8

This report contains information that is protected from disclosure by federal law, 23 USC Section 409 and the Missouri Open Records Law (Sunshine Act), Section 610.021 RSMo. Please review MoDOT's policy and procedure manual on the Sunshine Act before releasing any of the information contained herein.





APPENDIX B: EXCERPT OF THE 2019 MANUAL FOR BRIDGE ELEMENT INSPECTION

To make this report self-contained, the guidelines and referenced photos (AASHTO, 2019) used to help assign the condition state of bridge elements are excerpted. They are not the outcome of this study and presented here for information purposes only.


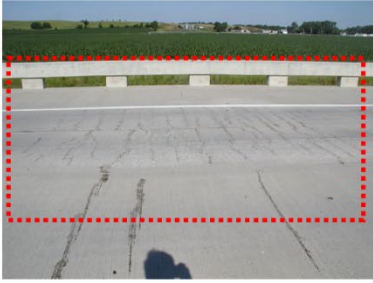


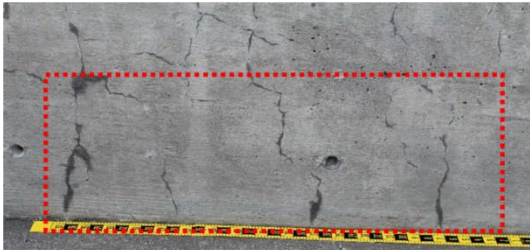
Defects for Reinforced Concrete

Defects	CS 1	CS 2	CS 3	CS 4
	GOOD	FAIR	POOR	SEVERE
Delamination/Spall/ Patched Area (1080)	None.	Delaminated. Spall 1 in. or less deep or 6 in. or less in diameter. Patched area that is sound.	Spall greater than 1 in. deep or greater than 6 in. diameter. Patched area that is unsound or showing distress. Does not warrant structural review.	The condition warrants a structural review to determine the effect on strength or serviceability of the element or bridge; OR a structural review has been completed and the defects impact strength or serviceability of the element or bridge.
Exposed Rebar (1090)	None.	Present without measurable section loss.	Present with measurable section loss but does not warrant structural review.	
Efflorescence/Rust Staining (1120)	None.	Surface white without build-up or leaching without rust staining.	Heavy build-up with rust staining.	
Cracking (RC) (1130)	Insignificant cracks or moderate-width cracks that have been sealed.	Unsealed moderate-width cracks, or unsealed moderate pattern (map) cracking.	Wide cracks or heavy pattern (map) cracking.	
Abrasion/Wear (PSC/RC) (1190)	No abrasion or wearing.	Abrasion or wearing has exposed coarse aggregate but the aggregate remains secure in the concrete.	Coarse aggregate is loose or has popped out of the concrete matrix due to abrasion or wear.	
Settlement (4000)	None.	Exists within tolerable limits or arrested with no observed structural distress.	Exceeds tolerable limits but does not warrant structural review.	
Scour (6000)	None.	Exists within tolerable limits or has been arrested with effective countermeasures.	Exceeds tolerable limits but is less than the critical limits determined by scour evaluation and does not warrant structural review.	
Damage (7000)	Not applicable.	The element has impact damage. The specific damage caused by the impact has been captured in CS 2 under the appropriate material defect entry.	The element has impact damage. The specific damage caused by the impact has been captured in CS 3 under the appropriate material defect entry.	The element has impact damage. The specific damage caused by the impact has been captured in CS 4 under the appropriate material defect entry.

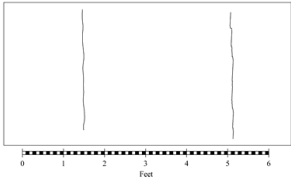
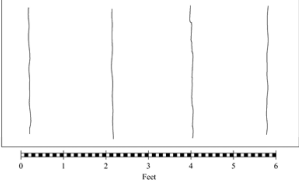
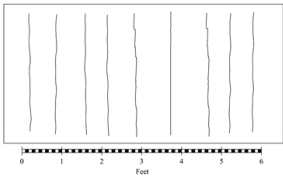
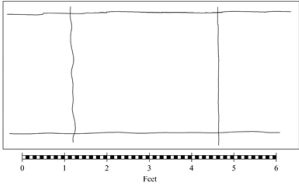
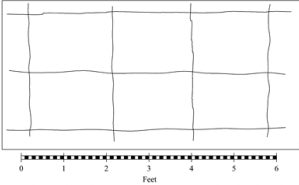
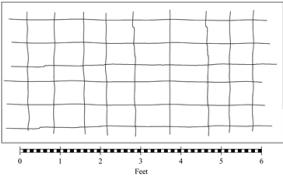
Defect 1120—Efflorescence/Rust Staining

Condition State 1	Condition State 2	Condition State 3
None.	Surface white without build-up or leaching without rust staining.	Heavy build-up with rust staining.
		
Boundary Image CS 1–2		Boundary Image CS 2–3
		

Defect 1130—Cracking (RC and Other)

Condition State 1	Condition State 2	Condition State 3
Insignificant cracks or moderate-width cracks that have been sealed.	Unsealed moderate width cracks or unsealed moderate pattern (map) cracking.	Wide cracks or heavy pattern (map) cracking.
<i>Spacing greater than 3.0 ft.</i>	<i>Spacing of 1.0—3.0 ft.</i>	<i>Spacing of less than 1 ft.</i>
		
Boundary Image CS 1–2		Boundary Image CS 2–3
		

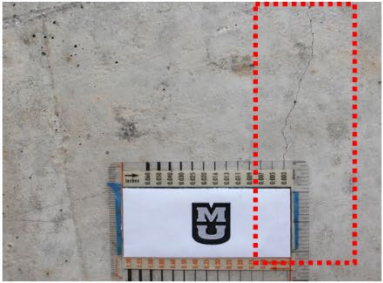
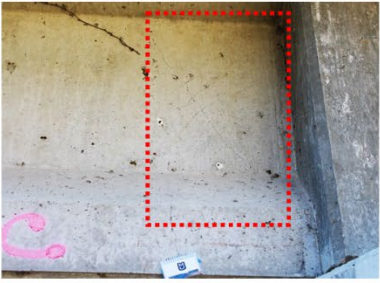
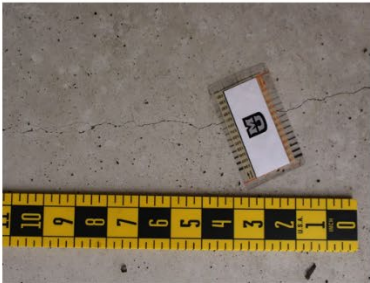
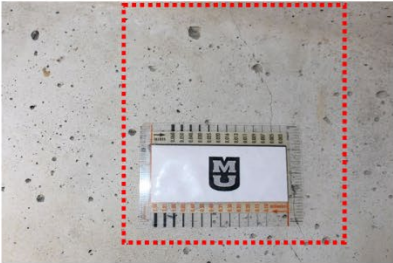

Crack Pattern Guide

Condition State 1	Condition State 2	Condition State 3
Spacing >3 ft.	Moderate pattern (map) cracking, spacing 1–3 ft.	Heavy pattern (map) cracking, spacing less than 1 ft.
		
		

Defects for Prestressed Concrete Elements

Defects	CS 1	CS 2	CS 3	CS 4
	GOOD	FAIR	POOR	SEVERE
Delamination/Spalls/ Patch Areas (1080)	None.	Delaminated. Spall 1 in. or less deep or 6 in. or less in diameter. Patched area that is sound.	Spall greater than 1 in. deep or greater than 6 in. diameter. Patched area that is unsound or showing distress. Does not warrant structural review.	The condition warrants a structural review to determine the effect on strength or serviceability of the element or bridge; OR a structural review has been completed and the defects impact strength or serviceability of the element or bridge.
Exposed Rebar (1090)	None.	Present without measurable section loss.	Present with measurable section loss but does not warrant structural review.	
Exposed Prestressing (1100)	None.	Present without section loss.	Present with section loss but does not warrant structural review.	
Efflorescence/Rust Staining (1120)	None.	Surface white without build-up or leaching without rust staining	Heavy build-up with rust staining.	
Cracking (PSC) (1110)	Insignificant cracks or moderate-width cracks that have been sealed.	Unsealed moderate-width cracks or unsealed moderate pattern (map) cracking.	Wide cracks or heavy pattern (map) cracking.	
Abrasion/Wear (PSC/RC) (1190)	No abrasion or wearing.	Abrasion or wearing has exposed coarse aggregate but the aggregate remains secure in the concrete.	Coarse aggregate is loose or has popped out of the concrete matrix due to abrasion or wear.	
Distortion (1900)	None.	Distortion not requiring mitigation or mitigated distortion.	Distortion that requires mitigation that has not been addressed but does not warrant structural review.	
Settlement (4000)	None.	Exists within tolerable limits or no observed structural distress.	Exceeds tolerable limits but does not warrant structural review.	The element has impact damage. The specific damage caused by the impact has been captured in CS 4 under the appropriate material defect entry.
Scour (6000)	None.	Exists within tolerable limits or has been arrested with effective countermeasures.	Exceeds tolerable limits but is less than the critical limits determined by scour evaluation and does not warrant structural review.	
Damage (7000)	Not applicable.	The element has impact damage. The specific damage caused by the impact has been captured in CS 2 under the appropriate material defect entry.	The element has impact damage. The specific damage caused by the impact has been captured in CS 3 under the appropriate material defect entry.	



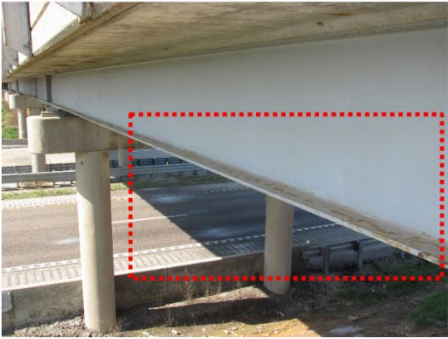

Defect 1110—Cracking (PSC)

Condition State 1	Condition State 2	Condition State 3
Insignificant cracks or moderate-width cracks that have been sealed.	Unsealed moderate width cracks or unsealed moderate pattern (map) cracking.	Wide cracks or heavy pattern (map) cracking.
Width less than 0.004 in. or spacing greater than 3 ft.	Width 0.004–0.009 in. or spacing 1.0–3.0 ft.	Width greater than 0.009 in. or spacing less than 1 ft.
		
Boundary Image CS 1–2		Boundary Image CS 2–3
		


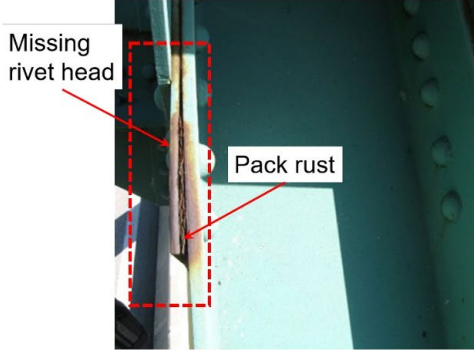



Defects for Steel Elements

Defects	CS 1	CS 2	CS 3	CS 4
	GOOD	FAIR	POOR	SEVERE
Corrosion (1000)	None.	Freckled rust. Corrosion of the steel has initiated.	Section loss is evident or pack rust is present but does not warrant structural review.	The condition warrants a structural review to determine the effect on strength or serviceability of the element or bridge; OR a structural review has been completed and the defects impact strength or serviceability of the element or bridge.
Cracking (1010)	None.	Crack that has self-arrested or has been arrested with effective arrest holes, doubling plates, or similar.	Identified crack that is not arrested but does not warrant structural review.	
Connection (1020)	Connection is in place and functioning as intended.	Loose fasteners or pack rust without distortion is present but the connection is in place and functioning as intended.	Missing bolts, rivets, or fasteners; broken welds; or pack rust with distortion but does not warrant a structural review.	
Distortion (1900)	None.	Distortion not requiring mitigation or mitigated distortion.	Distortion that requires mitigation that has not been addressed but does not warrant structural review.	
Settlement (4000)	None.	Exists within tolerable limits or arrested with no observed structural distress.	Exceeds tolerable limits but does not warrant structural review.	
Scour (6000)	None.	Exists within tolerable limits or has been arrested with effective countermeasures.	Exceeds tolerable limits but is less than the critical limits determined by scour evaluation and does not warrant structural review.	The element has impact damage. The specific damage caused by the impact has been captured in CS 4 under the appropriate material defect entry.
Damage (7000)	Not applicable.	The element has impact damage. The specific damage caused by the impact has been captured in CS 2 under the appropriate material defect entry.	The element has impact damage. The specific damage caused by the impact has been captured in CS 3 under the appropriate material defect entry.	

Defect 1000—Corrosion

Condition State 1	Condition State 2	Condition State 3
None.	Freckled rust. Corrosion of steel has initiated.	Section loss is evident or pack rust is present but does not warrant structural review.
		
Boundary Image CS 1–2		Boundary Image CS 2–3
		


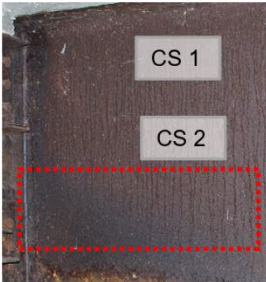





Defect 1020—Connection

Condition State 1	Condition State 2	Condition State 3
	Loose fasteners or pack rust without distortion is present but the connection is in place and functioning as intended.	Missing bolts, rivets, or fasteners; broken welds; or pack rust with distortion but does not warrant a structural review.
		
Boundary Image CS 1–2	Boundary Image CS 2–3	Boundary Image CS 3–4
		





Defects for Steel Protective Coating

Defects	CS 1	CS 2	CS 3	CS 4
	GOOD	FAIR	POOR	SEVERE
Chalking (Steel Protective Coatings) (3410)	None.	Surface dulling.	Loss of pigment.	Not applicable.
Peeling/Bubbling/Cracking (Steel Protective Coatings) (3420)	None.	Finish coats only.	Finish and primer coats.	Exposure of bare metal.
Oxide Film Degradation Color/Texture Adherence (Steel Protective Coatings) (3430)	Yellow-orange or light brown for early development. Chocolate-brown to purple-brown for fully developed. Tightly adhered, capable of withstanding hammering or vigorous wire brushing.	Granular texture.	Small flakes, less than 1/2-in. diameter.	Dark black color. Large flakes, 1/2-in. diameter or greater, or laminar sheets or nodules.
Effectiveness (Steel Protective Coatings) (3440)	Fully effective.	Substantially effective.	Limited effectiveness.	Failed; no protection of the underlying metal.
Damage (7000)	Not applicable.	The element has impact damage. The specific damage caused by the impact has been captured in Condition State 2 under the appropriate material defect entry.	The element has impact damage. The specific damage caused by the impact has been captured in Condition State 3 under the appropriate material defect entry.	The element has impact damage. The specific damage caused by the impact has been captured in Condition State 4 under the appropriate material defect entry.

Defect 3430—Oxide Film Degradation

Condition State 1	Condition State 2	Condition State 3	Condition State 4
Yellow-orange or light brown for early development. Chocolate-brown to purple-brown for fully developed. Tightly adhered, capable of withstanding hammering or vigorous wire brushing.	Granular texture.	Small flakes, less than ½ in. diameter.	Dark black color. Large flakes ½ in. diameter or greater, or laminar sheets of nodules.
			
Boundary Image CS 1–2	Boundary Image CS 2–3	Boundary Image CS 3–4	
			

Defect 3440—Effectiveness (Steel Protective Coating)

Condition State 1	Condition State 2	Condition State 3	Condition State 4
Fully effective.	Substantially effective.	Limited effectiveness.	Failed, no protection of underlying steel.
			
Boundary Image CS 1–2		Boundary Image CS 2–3	Boundary Image CS 3–4
